SYNTHESIS AND EVALUATION OF LIGHT TRIGGERABLE REDOX-ACTIVE SPECIES GENERATORS

A THESIS

SUBMITTED IN PARTIAL FULFILMENT OF THE

REQUIREMENTS

OF THE DEGREE OF

DOCTOR OF PHILOSOPHY

BY

AJAY KUMAR SHARMA

20143332

INDIAN INSTITUTE OF SCIENCE EDUCATION AND

RESEARCH PUNE – 411 008

2019

Dedicated to…

My Parents

भारतीय विज्ञान शिक्षा एवं अनुसंधान संस्थान, पुणे
INDIAN INSTITUTE OF SCIENCE EDUCATION AND RESEARCH (IISER), PUNE
(An Autonomous Institution, Ministry of Human Resource Development, Govt. of India)
900 NCL Innovation Park Dr Homi Bhabha Road Pune 411008

Harinath Chakrapani, Ph.D.
Associate Professor – Chemistry
www.iiserpune.ac.in/~harinath/

CERTIFICATE

Certified that, the work incorporated in the thesis entitled, "***Synthesis and Evaluation of Light Triggerable Redox-Active Species Generators***" submitted by ***Ajay Kumar Sharma*** was carried out by the candidate, under my supervision. The work presented here or any part of it has not been included in any other thesis submitted previously for the award of any degree or diploma from any other University or institution.

Date: 29th July 2019 **Dr. Harinath Chakrapani**

Pune (MH), India.

DECLARATION

I declare that this written submission represents my ideas in my own words and where others' ideas have been included; I have adequately cited and referenced the original sources. I also declare that I have adhered to all principles of academic honesty and integrity and have not misrepresented or fabricated or falsified any idea/data/fact/source in my submission. I understand that violation of the above will be cause for disciplinary action by the Institute and can also evoke penal action from the sources which have thus not been properly cited or from whom proper permission has not been taken when needed.

Date: 29th July 2019 **Ajay Kumar Sharma**

Pune (MH), India. **20143332**

Table of Contents

Chapter 2. UV Light Triggerable ROS Generators

Chapter 3.1. Synthesis and Evaluation of a Triggerable Hydroquinone Based ROS Releasing Molecule

Chapter 3.2. Synthesis and Evaluation of Visible Light Triggerable ROS Generator

Chapter 4. Visible Light Triggered Uncaging of COS/H_2S

General remarks

- ^{1}H spectra were recorded on a JEOL ECX 400 MHz or a Bruker 400 MHz spectrometer unless otherwise specified using as an internal tetramethylsilane (δ_H = 0.00). Chemical shifts are expressed in ppm units downfield to TMS.
- ^{13}C spectra were recorded on a JEOL 100 MHz or a Bruker 100 MHz spectrometer unless otherwise specified using as an internal tetramethylsilane (δ_C = 0.0).
- Chemical shifts (δ) are reported in ppm and coupling constants (*J*) in Hz.
- Mass spectra were obtained using HRMS-ESI-Q-Time of Flight LC-MS (Synapt G2, Waters) or MALDI TOF/TOF Analyser (Applied Biosystems 4800 Plus).
- FT-IR spectra were obtained using Bruker Alpha-FT-IR spectrometer and reported in cm^{-1}.
- All reactions were monitored by Thin-Layer Chromatography carried out on precoated Merck silica plates (F254, 0.25 mm thickness); compounds were visualized by UV light.
- All reactions were carried out under nitrogen or argon atmosphere with dried solvents under anhydrous conditions and yields refer to chromatographically homogenous materials unless otherwise stated.
- All evaporations were carried out under reduced pressure on Büchi and Heildoph rotary evaporator below 45 °C unless otherwise specified.
- Silica gel (60-120) and (100-200) mesh were used for column chromatography.
- Materials were obtained from commercial suppliers and were used without further purification.
- Preparative HPLC purification was performed using high performance liquid chromatography (HPLC) with C-18 preparative column (21.2 mm × 250 mm, 10 μm; Kromasil®C-18).
- HPLC analysis data was obtained using Agilent Technologies 1260 Infinity, C18 reversed phase column (4.6 mm × 250 mm, 5 μm).
- Irradiation was done using 365 nm UV-LED flashlight-3W or HI-LITE Blue COB LED-3W and intensity was calibrated using GENTEC-EO-UNO laser power meter.
- Spectrophotometric and fluorimetric measurements were performed using Thermo Scientific Varioscan microwell plate reader.

Abbreviations

Ac – Acetyl

ACN – Acetonitrile

AcOH – Acetic acid

Ac_2O – Acetic anhydride

Ag_2O – Silver(I) oxide

$AlCl_3$ – Aluminium chloride

au – Arbitrary unit

AR – Amplex Red

ARE – Antioxidant response elements

BODIPY – Boron-dipyrromethene

bs – Broad singlet

CA – Carbonic anhydrase

Calcd – Calculated

CBS – Cystathionine-β-synthase

$CDCl_3$ – Chloroform-D

$CHCl_3$ – Chloroform

CNS – Central nervous system

COS – Carbonyl sulfide

COX – Cyclooxygenase

CSE – Cystathionine-γ-lyase

Ctrl – Control

$CuSO_4.5H_2O$ – Copper sulfate pentahydrate

Cys – Cysteine

DAD – Diode array detector

DCF – 2′,7′-dichlorodihydrofluorescein

dd – Doublet of doublet

DCM – Dichloromethane

DMAP – *N*, *N*-Dimethylaminopyridine

DMEM – Dulbecco's Modified Eagle's Medium

DMF – *N*, *N*-Dimethylformamide

DMSO – Dimethylsulfoxide

DHE – Dihydroethidium

DNA – Deoxyribonucleic acid

DPBS – Dulbecco's Phosphate-Buffered Saline

dt – Doublet of triplet

DTPA – Diethylenetriaminepentaacetic acid

δ – Delta (in ppm)

E^+ – Ethidium

EDG – Electron donating group

eq. – Equivalent

ER – Estrogen-receptor

ERK – Extracellular signal-regulated kinase

ES – Esterase

ESIPT – Excited state intramolecular proton transfer

ESI – Electron spray ionization

ETC – Electron transport chain

Et_3N – Triethylamine

EtOH – Ethanol

EtOAc – Ethyl acetate

Et_2O – Diethyl ether

EWG – Electron withdrawing group

FAD – Flavin adenine dinucleotide

FBS – Fetal bovine serum

FLD – Fluorescence detector

g – Gram

GABA – Gamma-aminobutyric acid

GFP – Green fluorescence protein

GSH – Glutathione

h – Hour

HCl – Hydrochloric acid

HNO – Nitroxyl

HNO_3 – Nitric acid

HPLC – High performance liquid chromatography

HRMS – High-resolution mass spectrometry

HRP – Horseradish peroxidase

Hz – Hertz

H_2DCF-DA – 2',7'-dichlorodihydrofluorescein diacetate

H_2O – Water

H_2O_2 – Hydrogen peroxide

H_2S – Hydrogen sulfide

IC_{50} – Half maximal inhibitory concentration

IR – Infrared

J – Coupling constant

JNK – c-JunNH_2-terminal kinase

Keap1 – Kelch-like ECH-associated protein 1

K_2CO_3 – Potassium carbonate

$LiAlH_4$ – Lithium aluminium hydride

λ_{ex} – Excitation wavelength

λ_{em} – Emission wavelength

m – Multiplet

MAPK – Mitogen-activated protein kinase

MB – Methylene blue

MALDI – Matrix-Assisted Laser Desorption Ionization

Me – Methyl

MeOH – Methanol

mg – Milligram

min – Minute

MHz – Megahertz

mL – Millilitre

mM – Millimolar

mmol – Millimole

MS – Mass spectrum

mTOR – Mechanistic target of rapamycin

MTT – 3-(4,5-Dimethylthiazol-2-yl)-2,5-diphenyltetrazolium bromide

MW – Molecular weight

m/*z* – Mass to Charge ratio

$NaBH_4$ – Sodium borohydride

NADPH – Reduced nicotinamide-adenine-dinucleotide phosphate

$NaHCO_3$ – Sodium bicarbonate

NaHS – Sodium hydrosulfide

NaI – Sodium iodide

$NaNO_2$ – Sodium nitrite

NaOCl – Sodium hypochlorite

Na_2SO_4 – Sodium sulfate

Na_2S – Sodium sulfide

NF-κB – Nuclear factor-kappa beta

NH_4Cl – Ammonium chloride

NMR – Nuclear magnetic resonance

NO – Nitric oxide

NO^+– Nitrosonium cation

NOS – Nitric oxide synthase

Nrf2 – Nuclear factor erythroid 2-related factor 2

nM – Nanomolar

NTR – Nitroreductase

OD – Optical density

$^{\bullet}OH$ – Hydroxyl radical

$O_2^{\bullet-}$ – Superoxide radical anion

$ONOO^-$ – Peroxynitrite

PBr_3 – Phosphorous tribromide

PBS – Phosphate buffered saline

*p*HP – *para*-hydroxypehnyl acetyl

PI3K – Phosphoinositide-3-kinase

PKC – Protein kinase C

Pd – Palladium

$Pd(PPh_3)_4$ – Tetrakis(triphenylphosphine)palladium(0)

PDT – Photodynamic therapy

PET – Photo-induced electron transfer

pH – Potential of hydrogen

Ph – Phenyl

PPh_3 – Triphenylphosphine

Py – Pyridine

ppm – Parts per million

% – Percent

RFI – Relative fluorescence intensity

R_f – Retention factor

RNS − Reactive nitrogen species

ROS – Reactive oxygen species

RPMI Medium – Roswell Park Memorial Institute Medium

RT – Room temperature

RSS – Reactive sulfur species

s – Singlet

SOD – Superoxide dismutase

SiO_2 – Silica

t – Triplet

TBHP – *tert*-butyl hydroperoxide

TEA – Triethylamine

TFA – Trifluoroacetic acid

THF – Tetrahydrofuran

TLC – Thin layer chromatography

TMS – Tetramethylsilane

TrX – Thioredoxin

UPS – Ubiquitination/Proteasome System

UV – ultraviolet

VSR – Vascular structural remodeling

µg – Microgram

µM- micromolar

µmol– Micromole

µL – Microlitre

µm – Micrometre

Zn – Zinc

1,4-HQ – 1,4-hydroquinone

2-OH-E^+ – 2-hydroxyethidium

3-MST – 3-mercaptopyruvate-sulfur-transferase

Acknowledgements

This is most important part of my thesis. First, I would like to express my gratitude to my thesis Supervisor, Dr. Harinath Chakrapani for his constant support and guidance throughout my Ph.D. tenure. He always motivated me in my professionally and personally tough situations. He has set the high slandered research environment in lab and I have learned so many things from him.

I would like to thank the former director of IISER Pune Prof. K. N. Ganesh and current director Prof. Jayant B. Udgaonkar for providing excellent infrastructure and facilities at IISER Pune. I would like to thank Prof. M. Jayakannan (Former chair of chemistry department) and Prof. H.N. Gopi (IISER Pune, chair of chemistry) for providing very good facilities.

I would like to thank IISER pune for facilities and CSIR for fellowship during Ph.D.

I would like to thank to my RAC members Dr. D. Srinivasa Reddy (NCL Pune), Prof. H.N. Gopi (IISER Pune, chair of chemistry) for their valuable suggestions and feedback during RAC meeting. I wish to extend my thank to our collaborator Dr. Deepak Saini kumar (IISc) for his support. I thank all the IISER Pune chemistry faculty members for their support and encouragement.

Further, I thank all my colleagues. I thank to Dr. Dharmaraja, he is a very good person and a great researcher and mentored me in starting of my Ph.D. and I learned several techniques from him which help me in my Ph.D. Dr. Satish is a very good researcher. I thank Dr. Kavita, she is a cheerful, calm and cool person and also a great researcher and taught me several things. I also thank Dr. Vinayak, he is great researcher and very helpful person who taught me setting up some sensitive reactions. I thank Dr. Kundan, who is very good personality, a cheerful person and very good in synthesis. I and Kundan sometimes used to go for dinner at different places and we also used to go for movies, trekking etc. He is a very good at planning the lab trip. I thank Dr. Ravikumar, he is a very helpful highly organized person and has high dedication towards the research. His presentation skill and organization skills are so good and I have learned so many things from him in the regards of research and other things. I thank Dr. Viraj, she is very helpful person and very good friend of mine and I learned so many things regarding microbiology. Dr. Ritu is a very good person and she taught me so many things regarding synthesis.

I would like to thank my other colleagues who made the lab environment cheerful and constantly helped me during Ph.d. I thank Amogh, he is a very good friend of mine, very helpful and highly talented personality. He taught me several things regarding synthesis and instrumentations during my early days of Ph.D. I thank Preeti, my very good friend and lunch-mate. She helped me in several aspects during Ph.D. I thank Prerona, she is a talented personality, I learned several things from her. I thank Anand, who is highly organized and punctual. He has done excellent job in organizing chemicals and made process easy for ordering chemicals which help all of us to find chemicals easily and getting chemicals from vendors was also became easy. He also helped me during writing thesis and presentations. I thank Pooja, for her help during synthesis. I thank Laxman, for his support. I thank Suman, who is very helpful and a highly motivated person towards research and had helpful discussion regarding synthesis. I thank Gaurav, who is a calm and cool person and very good in presentation and writing and he helped me and also taught me several things during thesis writing. I thank for Farhan for his help and support during thesis writing. I thank Minhaj, for making cheerful environment in lab and Dr. Amol for helpful discussion regarding synthesis. I thank Harshit for help and support in synthesis and during thesis writing. I thank Mrutyunjay, he is highly motivated and great talent and he helped me during synthesis. I also thank project student Isha for her help in synthesis and report writing. I thank Aswin for his help in synthesis. I would also like to thank R. Sankar, Komal, Mrs. Beula for their support and I thank Sharath, Charu, Sushma, Abhishek, Shreyas, Swetha, Sourav, Harsha, Bhakti, Bandana, Suraj, Amal, Jishnu, Manjima for their help and in making cheerful environment in lab.

I would further extend my thanks to IISER Friends, Shatruhan, "Chomu", Kamal "Panditji", Ashok lal, Vinay Lal, Chandan "Sahukar", Madan "Veer" Sanjit "Confused", Bappa, Saddham, for their help in making environment lively.

I also thank IISER friend: Reman (trek-mate), Shammi Rana, Dinesh Mullangi, Anindita, Prachi, Sachin batar, S. Balamurugan, Aamod V. Desai, Mahesh Neralkar, Yashwant Kumar, Manisha, Pavan, Mohan, Ganesh, Rahul for their help.

My special thanks to NCL and CURAJ friends: Farsa ram, Priyanka, Ambrish, Joy, Suman D. Dr. Suresh ji, Dr. Sushil ji, Achal, Surbhi, who always make the environment enjoyable.

I also thank my SVNIT friends: Ravalika, Neelam, Vishal, Soujanaya, Pratyush, Saurav, Lokesh for their help and support.

A special thanks to Mayuresh, Mahesh, Yathish, Nayna, Tushar, Mrs. Sayalee and Prabhas for their administrative help throughout my doctoral study and also Dr. V.S. Rao for figuring out fellowship related issues. Swati (MALDI-TOF), Swati, Nayna and Sandip (HRMS), Deepali, Chinmay and Nitin (NMR), Ganesh (IR).

I wish to thank my B.Sc. professors, Mr. Chetram, Mr. Prahald, Dr. Goswami (Govt. college Karauli, Raj.) and M.Sc. professors Dr. Raghu Chitta, Late Dr. Sunil Naik, Dr. Easwar Srinivasan, Dr. Yaragorla (Central university of Rajasthan) for their support at the various stages and they always motivated me for doing science.

Finally, I would like to acknowledge the most important people in my life- my mother Smt. Asha devi, my father Shree Banwari Lal and my Brother Deepak and my love Sibani for their continuous support in everything.

Ajay

****

ABSTRACT

A majority of essential biomolecules or scaffolds are based upon carbon, oxygen, sulfur and nitrogen. These molecules exist in a flux and are constantly broken down and resynthesized. Some derivatives of O, S and N form highly reactive species, which can undergo redox processes in cells and are termed as redox-active species. Based on the reactive atom(s), these species are classified as reactive oxygen species (ROS), reactive sulfur species (RSS) and reactive nitrogen species (RNS). Amongst these, ROS are oxygen-derived species, primarily generated by NAD(P)H oxidase and the leakage of electrons in electron transport chain (ETC) during oxidative phosphorylation in mitochondria. When present in an optimum concentration, ROS are known to regulate several essential signaling pathways. However, at elevated levels, ROS damage essential biomolecules which, in turn, leads to cell death. To counter ROS-mediated damage, cells have evolved antioxidant machinery (which regulates ROS levels), such as superoxide dismutase (SOD), catalases, thiols *etc.* Apart from ROS, RSS such as glutathione (GSH), cysteine, sulfur dioxide (SO_2) and hydrogen sulfide (H_2S) are also important redox species in cellular metabolism. For instance, they play vital roles in signaling and antioxidant mechanisms. In addition, RNS – nitric oxide-based molecules – are endogenously synthesized and perform important modulation for certain signaling mechanisms. Therefore, it becomes essential to have tools to probe into redox-mediated cellular pathways. In this attempt, several molecules have been developed which are either triggered by one of several metabolic stimuli (such as cellular thiols, hydrogen peroxide and enzymes) to generate the aforementioned reactive species or are spontaneous generators of the same. Here, the triggerable approach provides control over the release of these reactive species. However, due to the wide prevalence of the metabolic stimuli, reactive species are produced in nearly all cells and achieving spatio-temporal control over release becomes challenging. Alternatively, light was sought as a stimulus to attain spatio-temporally controlled release of reactive species. As an external stimulus, it can provide better handle over localization and rate of cleavage can be tuned by varying intensity of light. To this end, a masked ROS generator was synthesized wherein the Diels-Alder adduct of 1,3-cyclohexadiene and juglone was attached with a 2-nitrobenzyl-based photo-responsive linker. The designed molecule released ROS only upon UV light irradiation, and was highly potent in inhibiting cancer cell growth which was not observed in absence of light. However, few limitations associated with UV light

as stimulus include marginal increase in cellular ROS levels and low tissue penetration which may hinder the usefulness of this strategy in studying cellular processes.

To address the above shortcomings, a linker was to be chosen such that it would cleave upon visible light irradiation. Herein, the visible light activatable group in the form of BODIPY was linked with a hydroquinone-based ROS generator. This molecule cleaved upon visible light irradiation to release ROS. BODIPY-based photo-responsive group was further utilized to mask hydrogen sulfide (H_2S), a gasotransmitter, in the form of COS which was subsequently hydrolyzed by carbonic anhydrase to generate H_2S. This molecule was further evaluated for cytoprotection against ROS-induced damage. In this thesis, the presented light-triggered tools may find an application to study redox-mediated signaling pathways in a spatio-temporally controlled manner.

Chapter 1. Introduction

1.1 Redox Chemistry and Biology

In living organisms, several molecules undergo oxidation-reduction reactions to facilitate cellular processes. These molecules play crucial roles in metabolic pathways which are mediated by several enzymatic and non-enzymatic mechanisms that may exploit either an intracellular redox-sensitive metal or a redox-active organic molecule. Among redox-active organic molecules, the quinone functionality is commonly found. In the electron transport chain (ETC), an array of quinones act as electron carriers from one complex to another by oxidation-reduction reactions.[1,2] Redox chemistry is also central to the $NADP^+/NADPH^+$ system, which act as a hydride carrier in the cell.[3] In addition, there are a number of cellular thiols, such as glutathione and cysteine that also participate in redox processes, owing to the variable oxidation states of sulfur. In addition to these small organic molecules, trace amounts of metals such as Cu(I) and Fe(II)[4,5] can also function as redox-active centers in the conversion of H_2O_2 to the hydroxyl radical. Furthermore, there are certain short-lived species form during normal metabolism, which are also known to participate in redox processes of cells. These species are collectively termed *reactive species*. These species are majorly classified to three categories based on the participating reactive atom (Figure 1.1).

1. Reactive oxygen species (ROS)
2. Reactive sulfur species (RSS)
3. Reactive nitrogen species (RNS)

1.1.1 Reactive Oxygen Species (ROS)

Oxygen (O_2) is a stable gaseous molecule which is essential for the survival of nearly all living beings on earth. The occurrence of this molecule in the atmosphere is 20.9%. In the presence of an electron donor, this molecule forms different short-lived species such as the superoxide radical anion ($O_2^{\bullet-}$), hydrogen peroxide (H_2O_2), the hydroxyl radical (ȮH) and singlet oxygen ($^1O_2$), which are collectively termed reactive oxygen species (ROS) (Figure 1.2). In general, ROS were considered toxic and deleterious substances due to their highly reactive nature and the detrimental effects caused to essential biomolecules. But in the last 20-30 years, these molecules have gained interest after it was found that, at subtoxic concentrations, they play a critical role in signaling mechanisms which are essential for cellular survival.[6–9] However, during oxidative stress, where ROS levels exceed normal levels, they can irreversibly oxidize

essential biomolecules like proteins, lipids and nucleic acids. This, in turn, can result in the dysfunction of the cellular machinery, ultimately leading to cell death.[8,9] ROS levels are balanced by cellular antioxidants such as glutathione (GSH),[10–13] superoxide dismutase (SOD),[14] catalase[14] etc., which maintain redox homeostasis within the cell.

Figure 1.1. Classification of redox active species

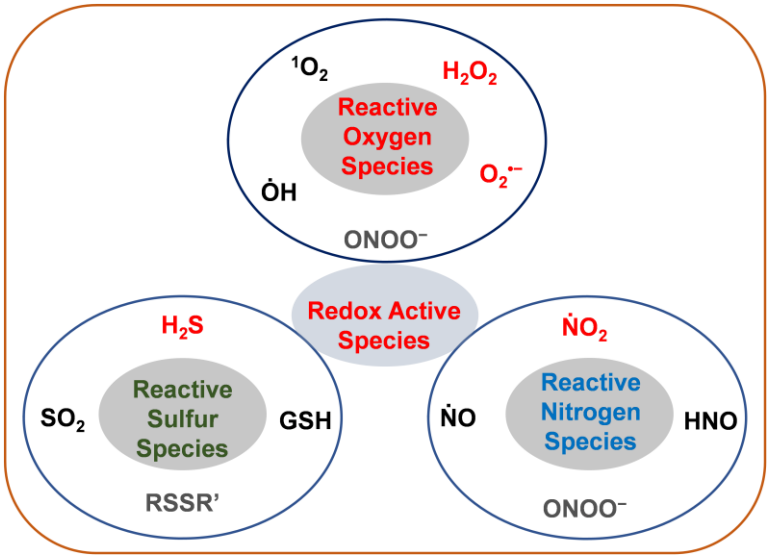

Figure 1.2. Generations of different types of ROS (SOD: Superoxide dismutase; Cat.: Catalase)

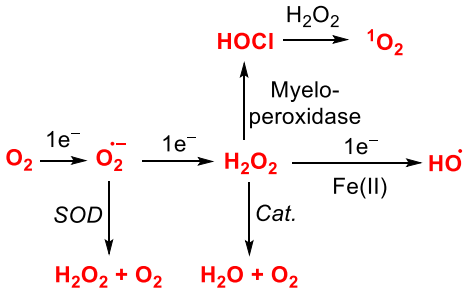

1.1.1.1 Endogenous Generation of ROS

Reactive oxygen species are produced in cells by several mechanisms. Some of these mechanisms are initiated by cellular exposure to external elements such as, low wavelength UV-radiation, which can generate hydrogen peroxide in cells[15]; also, during substrate hydroxylation processes, when lipid soluble substrates such as steroids, drugs, carcinogens *etc.* are converted into a water-soluble form for easy excretion, the cytochrome P450 can generate

$O_2^{\bullet-}$.[16] In addition to these mechanisms, exogeneous elements such as pathogens or foreign particles can also initiate inflammatory processes[17] where polymorphonuclear cells, eosinophils, monocytes, Kupffer cells and macrophages generate a burst of $O_2^{\bullet-}$ and H_2O_2 by highly specialized NADPH-dependent oxidase; this enzyme is present in the outer surface of the cell membrane and is coupled with the action of superoxide dismutase (SOD). Furthermore, ROS are also produced during ATP synthesis, where, 1-2% of electrons may leak from the ETC, which end up reducing molecular oxygen to $O_2^{\bullet-}$.[18] Apart from these, a large amount of hydrogen peroxide is produced during the deamination of biogenic amines by monoamine oxidase, which is present in the outer membrane of mitochondria.[19] In addition to these, xanthine oxidase generates $O_2^{\bullet-}$ using hypoxanthine as a substrate[20] and $O_2^{\bullet-}$ is also generated by cyclooxygenase (COX) and lipoxygenase during eicosanoid biosynthesis.[21]

1.1.1.2 ROS Regulation in the Cell

Multiple enzymatic and non-enzymatic systems have evolved to counter redox stress. One such mechanism is superoxide dismutase (SOD) catalyzing the conversion of $O_2^{\bullet-}$ to a more stable species, H_2O_2. This further undergoes degradation into water by several other enzymes such as catalases and peroxidases.[22] In the series of H_2O_2-degrading enzymes, an important one is glutathione peroxidase, which utilizes glutathione as a substrate in order to quench H_2O_2.[12] Here, glutathione (GSH) is converted to oxidized glutathione (GSSG) in the presence of H_2O_2 and the GSSG is subsequently reduced back to GSH by GSH reductase.[23] In addition to these, another key enzyme is thioredoxin (TRX),[24] having two cysteine residues in its catalytic site which undergo reversible oxidation to form a disulfide bridge in the presence of H_2O_2 and this is reduced back in the presence of TRX reductase (Figure 1.3).[22]

Figure 1.3. Major pathways of endogenous ROS generation and regulation

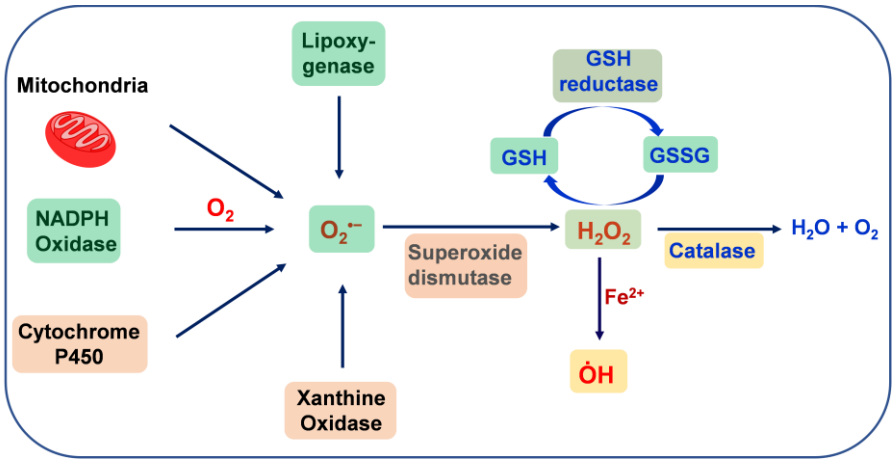

1.1.1.3 Physiology of ROS

ROS essay important physiological roles in biology; however, the beneficial and harmful effects are dependent upon their concentration. At homeostatic levels of ROS, where antioxidants and ROS generation are balanced, they regulate several pathways which are crucial for important cellular processes such as immune response,[25] inflammatory response,[17] differentiation,[26,27] proliferation,[28,29] protein folding,[30,31] angiogenesis,[32–34] metabolism[35–37] and cell signaling[9] (Figure 1.4). However, at low levels of ROS, some of these signaling pathways are inhibited[38–40] whereas elevated levels of ROS are associated with several pathophysiological conditions such as cancer,[41,42] Alzheimer's disease,[43,44] Parkinson's disease,[45–47] aging,[48–51] diabetes[52–55] *etc.* (Figure 1.5).

Figure 1.4. Physiological role of ROS

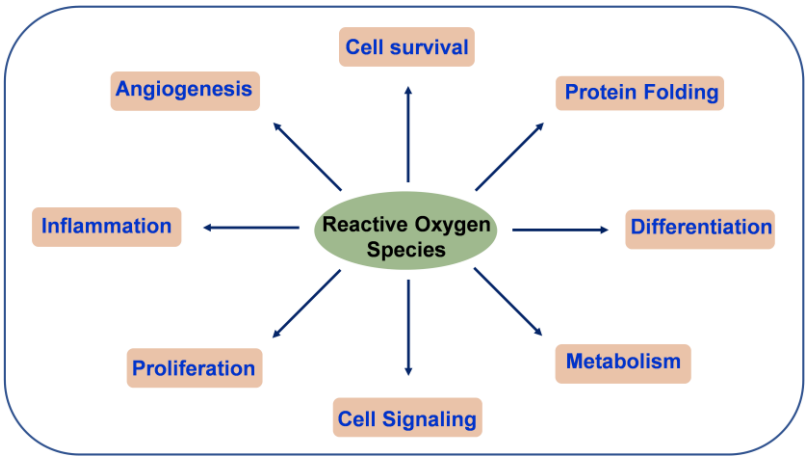

Figure 1.5. Concentration dependent effects of ROS

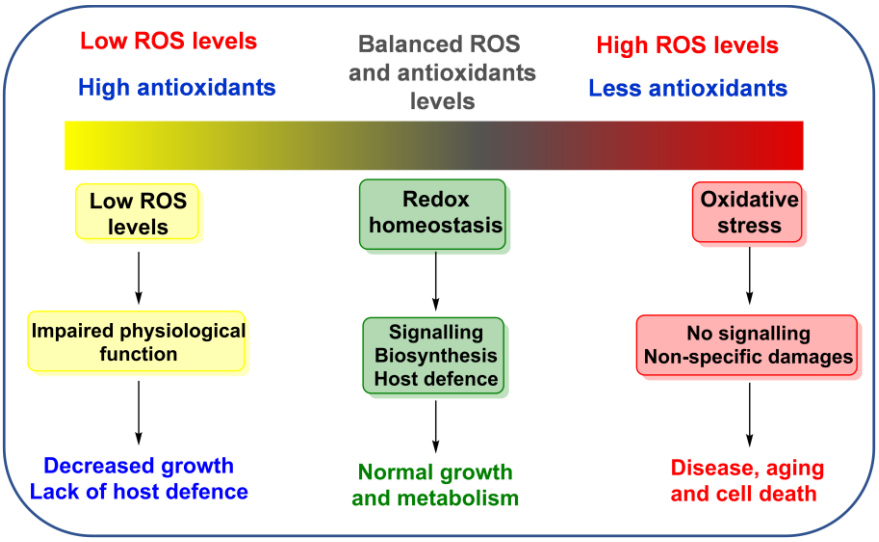

1.1.1.4 ROS Generators

As discussed, ROS are endogenously synthesized and play crucial roles for cell survival. These species are generated from molecular oxygen after it reacts with compounds having a greater reduction potential than itself. In the list of compounds which have a greater reduction potential than oxygen, hydroquinone and its derivatives are one such class of molecule; these are electron rich in nature and can readily reduce molecular oxygen to generate ROS and their quinone counterpart (Scheme 1.1). Therefore, these hydroquinone derivatives are considered viable scaffolds for ROS generation. Using this idea, several small organic molecules were developed which generate ROS spontaneously[56] or after activation by a particular trigger.[57–59] These ROS generators can then be classified into the following categories on the basis of their mode of activation to generate ROS:

1. Spontaneous ROS generators
2. Thiol-mediated ROS generators
3. Enzyme activated ROS generators

1.1.1.4.1 Spontaneous ROS Generators

Among reported ROS generators, juglone, a 1,4-naphthoquinone-based natural product, is known to generate ROS in cellular systems after activation with bioreductive enzymes (Scheme 1.2). However, reaction of juglone with 1,3-cyclohexadiene results in a derivative which has a reduced quinone moiety. This molecule can enolize in buffer to form a diolate intermediate. This diolate intermediate is an electron rich unit and subsequently reacts with molecular oxygen to generate ROS (Scheme 1.3).[56] As this molecule does not require any activation for ROS

generation, it is considered a spontaneous ROS generator. This molecule is an excellent ROS generator but does not provide us control over ROS generation.

Scheme 1.1. ROS generation by hydroquinone derivative

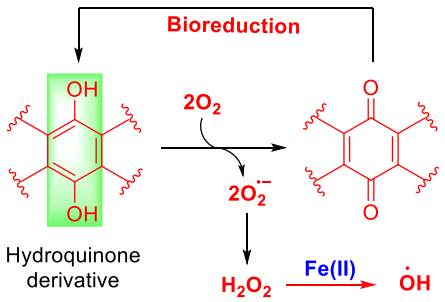

Scheme 1.2. ROS generation from juglone

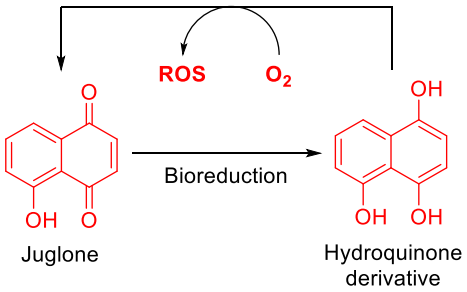

Scheme 1.3. Mechanism of ROS generation from 1,3 cyclohexadiene adduct of juglone

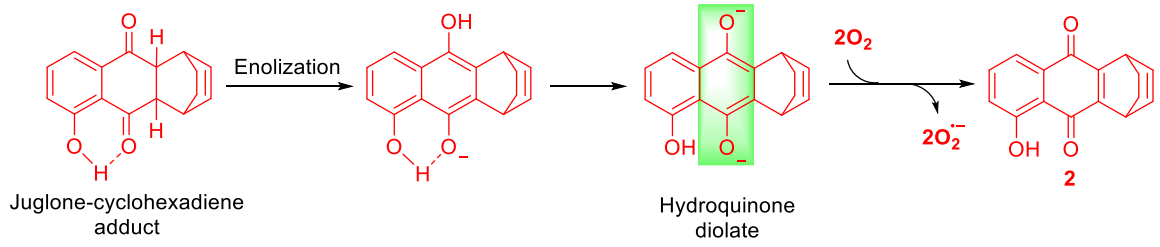

1.1.1.4.2 Thiol-Mediated ROS Generators

In the series of ROS generators, another category is 2,3-epoxy-1,4-naphthoquinone-based compounds, which are candidates for thiol attack, due to the presence of a strained epoxide ring. These molecules react with thiols to open up the epoxide ring, resulting in the formation of a hydroquinone derivative which reacts with molecular oxygen to produce ROS, and a naphthoquinone derivative as a by-product (Scheme 1.4).[58] Apart from this, piperlongumine, a

natural product, exhibits potent antiproliferative activity against cancer. This anticancer activity is believed to be due to thiol depletion and ROS enhancement. However, the exact molecular mechanism of ROS generation is not known (Figure 1.6).[60–65]

Scheme 1.4. Plausible mechanism of thiol mediated ROS generation from 2,3-epoxy-1,4-naphthoquinone

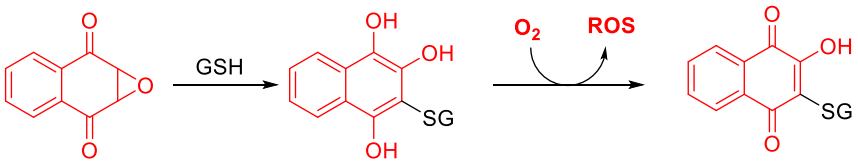

Figure 1.6. Reactive sites of piperlongumine for thiol attack and ROS generation

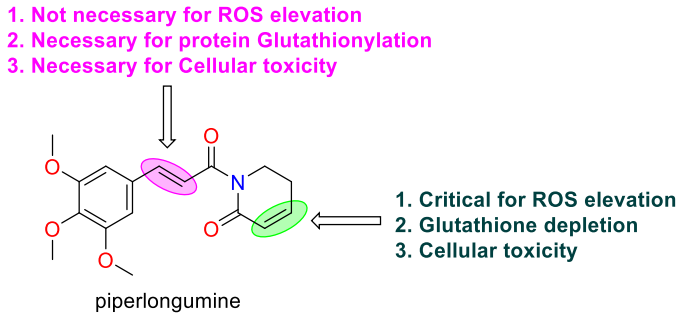

1.1.1.4.3 Enzyme Activated ROS Generators

In cells, a number of enzymes regulate different metabolic pathways which are essential for cellular homeostasis. Most of these enzymes are highly substrate specific; however, some of these can also metabolize unnatural substrates to carry out different processes. This property of enzyme can be utilizing in prodrug strategy where, an active molecule can be masked with appropriate functionality and released by a suitable enzyme. Using this, a number of ROS generators were developed which can be triggered by enzymatic reactions.

1.1.1.4.3.1 Bioreductively Activated ROS Generator

An efficient bioreductive machinery is present in cells for the detoxification of quinones, where quinones are converted to their respective hydroquinones which are more water-soluble and can be excreted from cellular systems. However, some quinones and their hydroquinone counterparts are not highly water-soluble; these can subsequently react with molecular oxygen to produce ROS. Using this idea, several molecules have been developed. In the list of these

molecules, β-lapachone[66–69] is one such example which is a type of 1,2-quinone that gets reduce by the NAD(P)H:quinone oxidoreductase 1 (NQO1) enzyme to form a 1,2-hydroquinone (Scheme 1.5). This hydroquinone further oxidizes to form β-lapachone and concomitantly generates ROS. In addition to this, anthraquinone derivatives are also triggered by bioreductive enzymes to form a hydroquinone derivative, which can reduce oxygen to form ROS, and quinone as a byproduct (Scheme 1.6).[59] Apart from quinone derivatives, paraquat,[70–75] a quaternary ammonium derivative, also gets reduced by bioreductive enzymes to form paraquat radical cation, which reacts with molecular oxygen to generate ROS (Scheme 1.7).

Scheme 1.5. Bioreductively ROS generation from β-lapachone

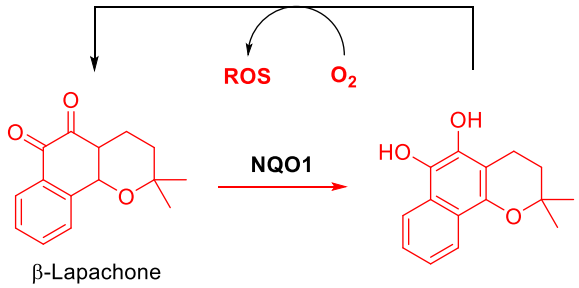

Scheme 1.6. Mechanism of ROS generation from anthraquinone derivative after bioreduction

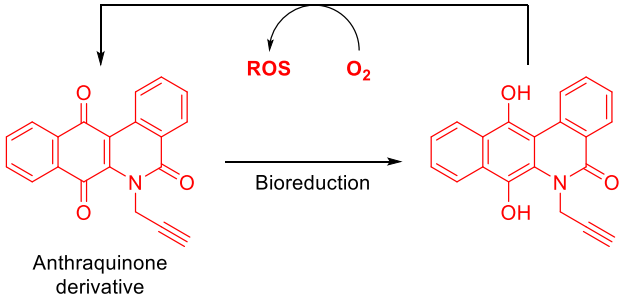

Scheme 1.7. Bioreductive activation of paraquat to generate ROS

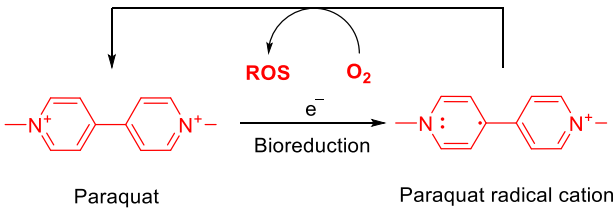

Thiol-mediated and bioreductively activated ROS generators are activated by a trigger and thus, offer us a better control over ROS generation compared to compounds that produce

ROS spontaneously in buffer. However, these molecules undergo redox cycles to produce a large amount of ROS. Apart from redox cycling by these molecules, ROS generation to a specific cell type may not be achieved due to the ubiquitous nature of the triggers: thiols and bioreductive enzymes; hence, these activation methods may not be very suitable for studying ROS-mediated biology.

1.1.1.4.3.2 Esterase Activated ROS Generators

Apart from cellular thiols and bioreductive activation, in an alternative strategy, an ROS generator can be masked with a specific linker such that the linker can be cleaved upon activation with a *specific stimulus* to release the active ROS generator. In order to do this, the cyclohexadiene adduct of juglone (which generates ROS spontaneously) has a free –OH (which is essential for ROS production[76]), which can be protected with methyl pivalate and thus, used in an esterase activation strategy; methyl pivalate is a substrate of esterase. Esterase is a serine-based enzyme, known to hydrolyze the ester functionality and is present in nearly all cells. This enzyme hydrolyzes pivalate, which further rearranges to release juglone derivative. This juglone derivative reacts with molecular oxygen to generate ROS (Scheme 1.8). But due to the wide prevalence of esterase, selective delivery of ROS cannot be achieved.

Scheme 1.8. Mechanism of ROS generation by esterase activation approach

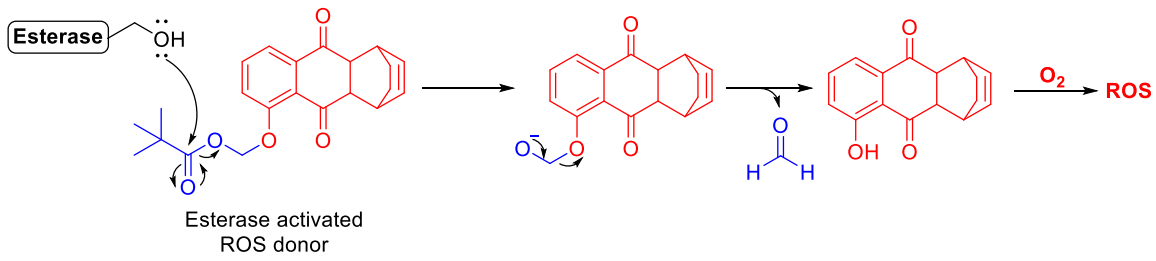

1.1.1.4.3.3 Nitroreductase Activated ROS Generators

In addition to the esterase activation approach, nitroreductase (NTR) triggered release of ROS is also known where the enzyme NTR, present in bacterial cells and in hypoxic regions of mammalian cells, can reduce nitro- groups to hydroxylamines or amines. To release the ROS generator using NTR-mediated activation, the –OH of juglone derivative can be protected with a 4-nitrobenzyl group, a well-established substrate of NTR. When the ROS generator is coupled with this 4-nitrobenzyl group and is then treated *in vitro* with NTR, the nitro group is reduced to form an amine or hydroxylamine, which release a juglone derivative upon molecular

rearrangement. As previously discussed, this juglone derivative subsequently reacts with molecular oxygen to generate ROS (Scheme 1.9).[57] ROS enhancement was also observed in bacterial cells. However, this scaffold was not effective in inhibiting the growth of bacterial cells, which could either be due to the slow reduction of the nitro group, resulting in slow generation of ROS or due to poor permeability. This slow and gradual increase in ROS levels can be perhaps countered by antioxidant machinery of the bacterial cells to prevent ROS-mediated damage.

Scheme 1.9. ROS generation by nitroreductase activation

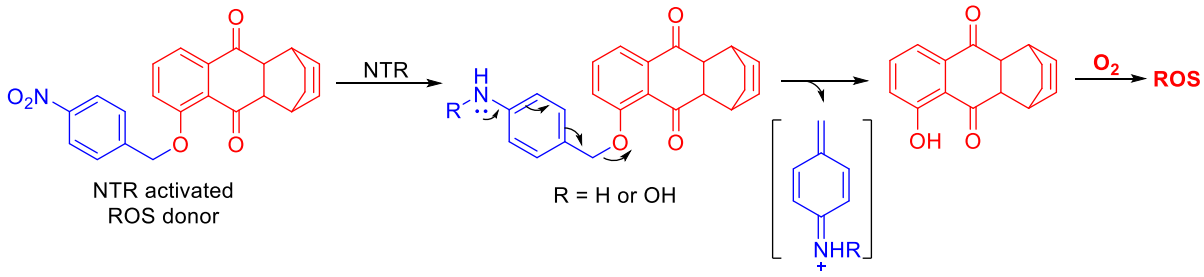

1.1.2 Reactive Sulfur Species (RSS)

Thiol-containing molecules are known to play important roles in redox biology because of the variable oxidation states of sulfur and major endogenous RSS are glutathione (GSH), cysteine (Cys), sulfur dioxide (SO_2) and hydrogen sulfide (H_2S).

Among these, glutathione is a major thiol, present in cells in the free form and plays key roles in redox homeostasis.[77,78] This is also an important player in the detoxification of quinone-based xenobiotics,[79,80] where the GSH forms a covalent bond with quinones to form an adduct, which is eventually be effluxed from the cell.

Another RSS is cysteine, which is an important motif of proteins in cellular systems. Several enzymes with active cysteine residues are known to be crucial for cellular metabolism.[81,82] The free thiol of cysteine can be reversibly oxidized with H_2O_2 to form a sulfenic acid, which is a crucial cellular signaling intermediate. Apart from sulfenic acid formation, cysteine can also undergo irreversible oxidation to form sulfinic or sulfonic acids, when excess H_2O_2 is present in cells. Such transformations may result in diminishing the protein activity. In addition to this, active cysteine can also act as a nucleophile to covalently react with electrophiles to form an adduct. If the adduct formation is irreversible, this might lead to a loss in the activity of protein.

Another RSS, sulfur dioxide (SO_2), an oxidized form of sulfur, is a gaseous molecule and known typically as an air-pollutant. In recent years, several studies have shown that SO_2 is produced endogenously in the cardiovascular tissues of rats[83,84] and exhibits physiological roles including vasodilation[84,85] and regulation of lipid metabolism.[86,87] It also plays a role in pathophysiological conditions such as vascular structural remodeling (VSR),[88,89] oxidative response [89,90] and inflammatory responses.[90]

Among the redox sulfur species, H_2S, a gaseous molecule, has attracted the attention of the research fraternity after the discovery of its crucial role in signaling mechanisms of the central nervous system (CNS),[91,92] aside from its antioxidant properties.[93–95] This molecule also facilitates posttranslational modification of proteins.

1.1.2.1 Biosynthesis of H_2S

Biosynthesis of H_2S is mainly mediated by three enzymes; cystathionine-β-synthase (CBS), cystathionine-γ-lyase (CSE) and 3-mercaptopyruvate-sulfur-transferase (3-MST) using cysteine as a substrate.[96–98]

1.1.2.2 Role of H_2S in Biology

H_2S is known to mediate several signaling pathways which play important roles in cytoprotection,[99–104] inflammation,[105–108] vascular function,[109–111] neurological systems,[112] tissue repair and healing.[113–118] It is also known to mediate apoptosis, cell cycle regulation,[119,120] mitochondrial function, energy metabolism and biogenesis,[121–132] obesity,[133–137] and aging.[138–144]

All the above mentioned phenotypes of H_2S are a result of its unique properties, such as its antioxidant nature by virtue of which elevated levels of ROS are scavenged.[145,146] Apart from this, H_2S also takes part in *S*-sulfhydration of proteins; this is a posttranslation modification to initiate several signaling pathways.[147,148] However, the signaling mechanisms are more complicated due to the cross talk of H_2S with other reactive species like, NO and ROS.[149–151]

1.1.2.3 H_2S Generators

The exact effects shown by H_2S are concentration- and location-dependent and hence, studying H_2S-mediated processes are challenging due to its highly diffusible nature and reactivity towards multiple sites in cells.[152] Thus, to study the physiology of H_2S, a tool is needed to

deliver this gaseous species in cells. There are several tools reported in literature for H_2S delivery.

1.1.2.3.1 Hydrolysis Based H_2S Generators

To generate H_2S, inorganic salts like, Na_2S and NaHS have been used for long, because of their property of producing a burst of H_2S under physiological conditions. These are an excellent source of H_2S; however, again, controlled generation of H_2S cannot be achieved. In addition to this, Lawesson's reagent-based derivatives such as GYY4137 and FW1256 have been developed for slow generation of H_2S.[153] Apart from these, dithiolethione derivatives, such as ADT and AP39, can also produce H_2S in a slow manner after hydrolysis. Furthermore, thioamino acid derivatives can also generate H_2S after hydrolysis in carbonated buffer (Figure 1.7). However, all of these methods produce H_2S after buffer hydrolysis and lack control over release, which may hinder the use of these molecules for studying H_2S-mediated cellular effects in a localized manner.

Figure 1.7. Hydrolysis-based H_2S generators

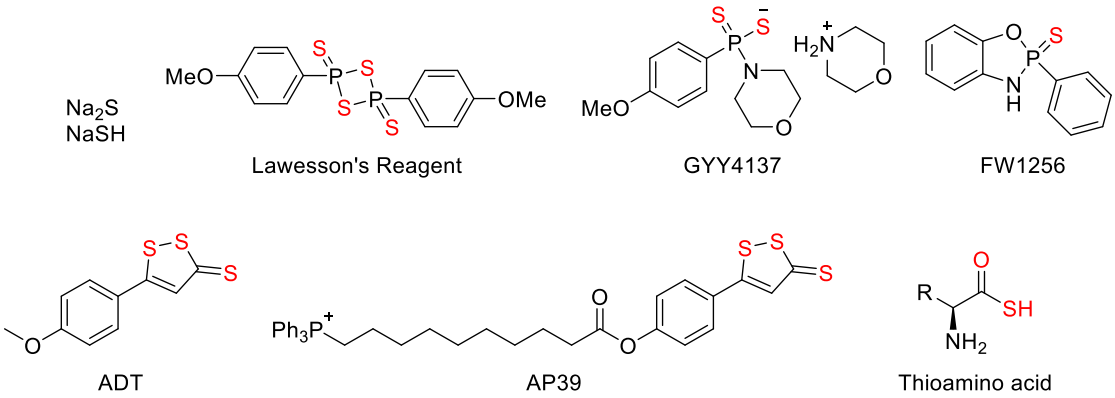

1.1.2.3.2 Triggerable H_2S Generators

To overcome the problems associated with spontaneous H_2S generation, controllable H_2S donors were developed such that they are triggered by different chemical and metabolic stimuli. Examples of these molecules are discussed under.

1.1.2.3.2.1 Thiol Activated H_2S Generators

Thiols are a part of important physiological processes and can also be used as a trigger to release bioactive molecules. Using this, a number of molecules have been reported which, upon reaction with thiol, release H_2S; for example, diallyl trisulfide, *N*-(acylthio)-benzamide derivative, persulfides, dithioperoxyanhydrides derivatives (Figure 1.8). These donors offer a great control over the release of H_2S; however, due to the ubiquitous nature of thiols, localized delivery towards a specific site cannot be achieved.

Figure 1.8. Thiol activated H_2S generators

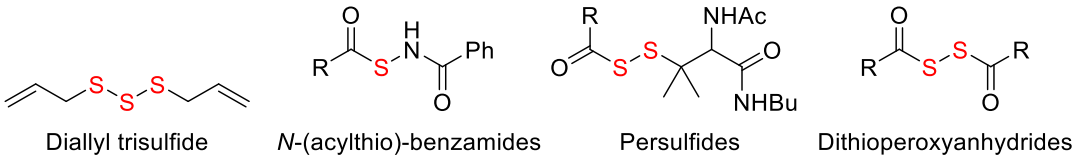

1.1.2.3.2.2 H_2O_2 Activated H_2S Generators

H_2O_2 is one of the reduced forms of ROS and can also be used as a stimulus to release bioactive molecules. In order to release H_2S using H_2O_2 mediated approaches, COS, a gaseous molecule, is masked in the form of thiocarbamate or carbamothioate[154,155] which is connected with a benzyl linker having a boronate ester at the *para*- position (Scheme 1.10). In the presence of H_2O_2, the boronate ester gets oxidized to form a phenolate intermediate; this self-immolates to release thiocarbamate or cabamothioate, which further rearranges to generate COS. This COS can be hydrolyzed in the presence of carbonic anhydrase, an enzyme widely used to release H_2S.

Scheme 1.10. H_2O_2 activated COS/H_2S generators

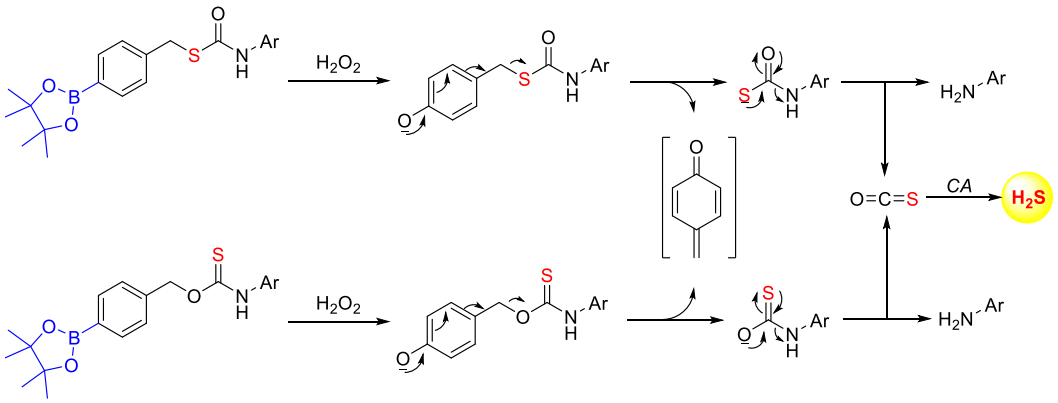

1.1.2.3.2.3 Enzyme Activated H_2S Release

As described before, enzymes can also be used as a trigger to release bioactive molecules. Using this idea, a number of approaches have been developed to release H_2S. In one of the methods, esterase is utilized to release H_2S using an ester-protected trimethyl lock derivative of a thioacid (Scheme 1.11). Apart from this, COS can also be masked with an esterase cleavable moiety which ultimately releases H_2S (Scheme 1.12). In addition to this, an NTR activation strategy is also used where, a *gem*-dithiol is protected with the 4-nitrobenzyl group, a well-established substrate of NTR[156] (Scheme 1.13). When a *gem*-dithiol coupled with the 4-nitrobenzyl group is treated with NTR, the nitro group reduces to form an amine or hydroxylamine, which rearranges to release a *gem*-dithiol; this further hydrolyzes to generate H_2S.

Scheme 1.11. Esterase activated H_2S generation

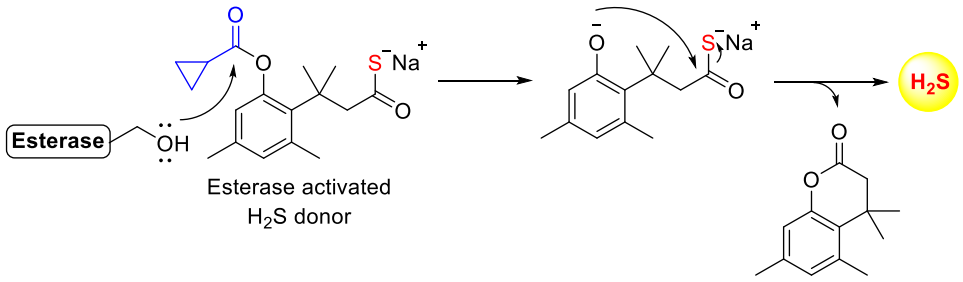

Scheme 1.12. Esterase activate COS/H_2S generation

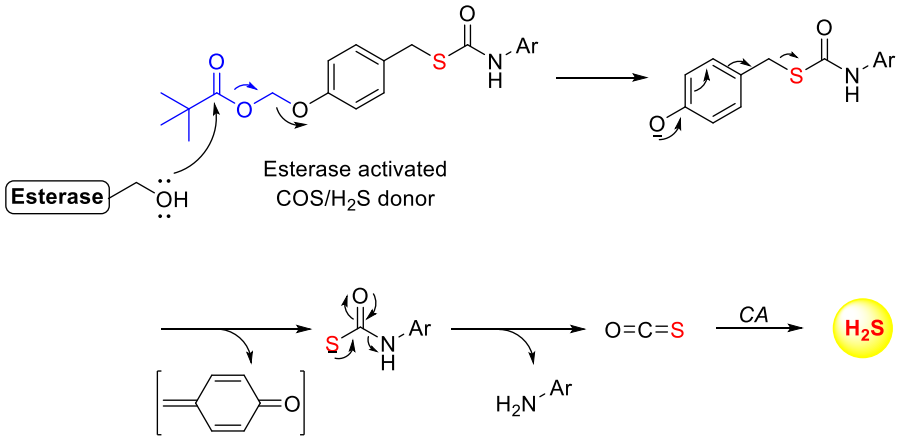

Scheme 1.13. NTR activated H_2S generator

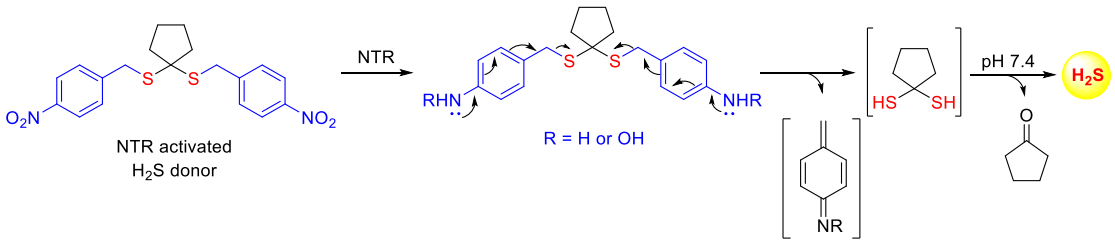

1.1.3 Reactive Nitrogen Species (RNS)

Reactive nitrogen species (RNS) are derivatives of nitric oxide (NO) such as nitroxyl (HNO), nitrosonium cation (NO^+), higher oxides of nitrogen, *S*-nitrosothiols and the peroxynitrite anion ($ONOO^-$). RNS play a crucial role in the regulation of different physiological functions in certain living cells, such as smooth muscle cells, cardiomyocytes, platelets, and nerve cells.[157–164] Their properties undergo a change after their interaction with reactive oxygen species and thiols. Apart from this, they also take part in posttranslational modifications of proteins. As with other reactive species, RNS also exhibit concentration-dependent properties where elevated levels can cause nitrosative stress, that might lead to cell injury and death. However, at subtoxic levels, several signaling pathways can be stimulated. Hence, to modulate RNS in cells, a number of compounds have been developed, which are also being evaluated for the involvement of RNS-mediated therapeutic effects of drugs used to treat cancer, neurodegenerative, metabolic, inflammatory and cardiovascular diseases.[165]

1.2 Light as a Tool to Study Biology

It may be stated that all species that are highly reactive may indiscriminately interact with several biomolecules and this may lead to the activation of non-specific cellular processes. For instance, NO interacts with $O_2^{\bullet-}$ to form $ONOO^-$ which differs from NO and $O_2^{\bullet-}$ alone. Likewise, H_2S also interacts with ROS to form polysulfides or sulfite. Further, RNS interact with thiols to form *S*-nitrosothiols.[166–173] In order to reduce the cross talk and off-site reactivity of the generated reactive species, one needs to develop molecules which can be activated under highly specific conditions to produce the desired species without any complications to cellular metabolic pathways. As discussed previously in this chapter that using metabolic stimuli such as, thiols, H_2O_2 and enzymatic triggers may not provide selectivity over the release of reactive species because of some inherent limitations. These limitations either could be due to ubiquity or slow metabolism with these triggers. Here, to overcome the problem of non-specific

delivery, light may be used as a stimulus, since the localization and intensity of light can be controlled externally thus providing spatio-temporal control over the delivery of reactive species. This photo-triggered approach may minimize any off-site generation of reactive species and may, further, be utilized for gaining valuable insights into understanding redox-mediated signaling pathways.

1.2.1 Strategies Towards Photo-Controlled Generation of Metabolites

Light is an external stimulus and can provide spatio-temporal delivery of reactive species. Based on the wavelength used, several light-activated approaches have been reported in recent literature.

1.2.1.1 Selected UV Light Triggered Approaches

There have been several approaches used for the release of different metabolites using UV light as a stimulus. Among them, the 2-nitrobenzyl group is commonly used as a caging group (Figure 1.9).[174–180] However, the uncaging process produces a nitrosoaldehyde as a by-product upon photolysis; this nitrosoaldehyde can affect cellular processes by reacting with different cellular nucleophiles. Apart from this, another commonly used caging group is based on the coumarin system as it is highly efficient in releasing its attached active compound.[181] In addition to these, the analogue of brominated hydroxyquinoline is also used for the release of carboxylate derivatives.[182] Another well-studied caging group is the *para*-hydroxyphenylacetyl (*p*HP) group, used to release γ-aminobutyric acid (GABA), a neurotransmitter.[183] In addition to these, the drug ibuprofen was released using a ketoprofen-derived caging group.[184] Apart from the above mentioned approaches, *S*-Pixyl derivatives were also utilized for the delivery of nucleosides[185] whereas anthraquinone derivatives[186] were used to mask alcohol as their carbonates; these are uncaged upon activation with UV light. Furthermore, there are different caging groups such as, 7-nitroindoline,[187] benzophenone,[188] 2-nitronaphthalene,[189] 2-acetylphenyl[190] and 2-dimethylamino-5-nitrophenoxy[191] derivatives; these are also used to deliver different alcohol- and carboxylate-derivatives.

The caging-uncaging approach provides a very good handle over the release of active motifs; however, it also has some limitations such as, the formation of stoichiometric amounts of by-products which might influence biological processes. Apart from this, a major drawback of the UV-triggered approach is the formation of radicals in cells because of the radiation-

biomolecule interaction, which can cause macromolecular damage. In addition to these limitations, performing *in vivo* studies is even more challenging due to low tissue penetration of UV light and hence, such a UV-based activation approach may not be very useful to study biological processes.

Figure 1.9. Different approaches for UV light triggered activation

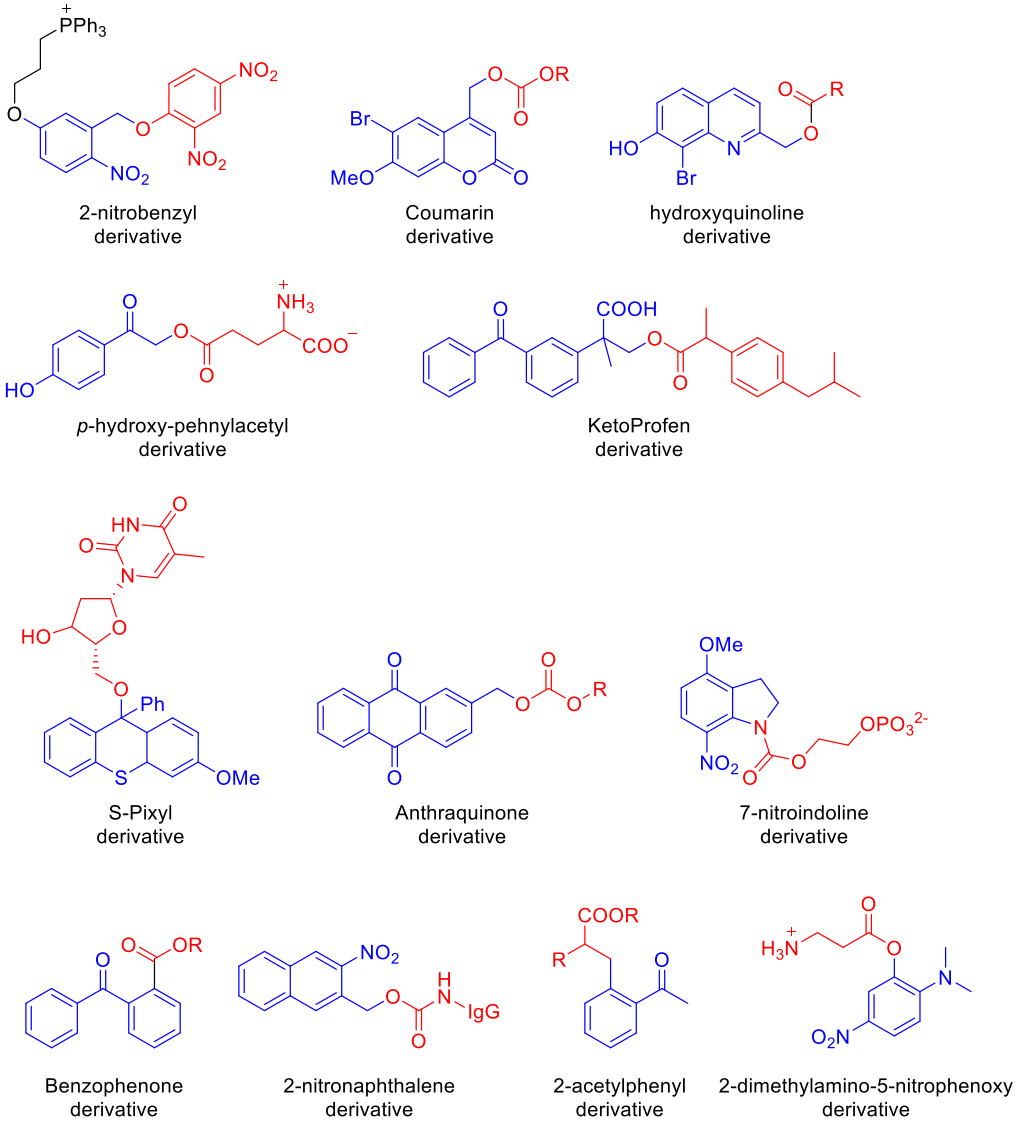

1.2.1.2 UV Light Activated ROS and H_2S Generation

In order to release ROS and H_2S using the light activation approach, there have been only a few methods that have been adopted for such uncaging. Chang and co-workers had reported a method to release ROS (Scheme 1.14), where the 2-nitrobenzyl derivative is used as a

photosensitive group and hydroxyquinol is the ROS donor. This molecule was shown to photo-cleave upon irradiation with 304 nm UV light to release hydroxyquinol, which further reacts with molecular oxygen to produce ROS.

Scheme 1.14. UV light activated ROS release

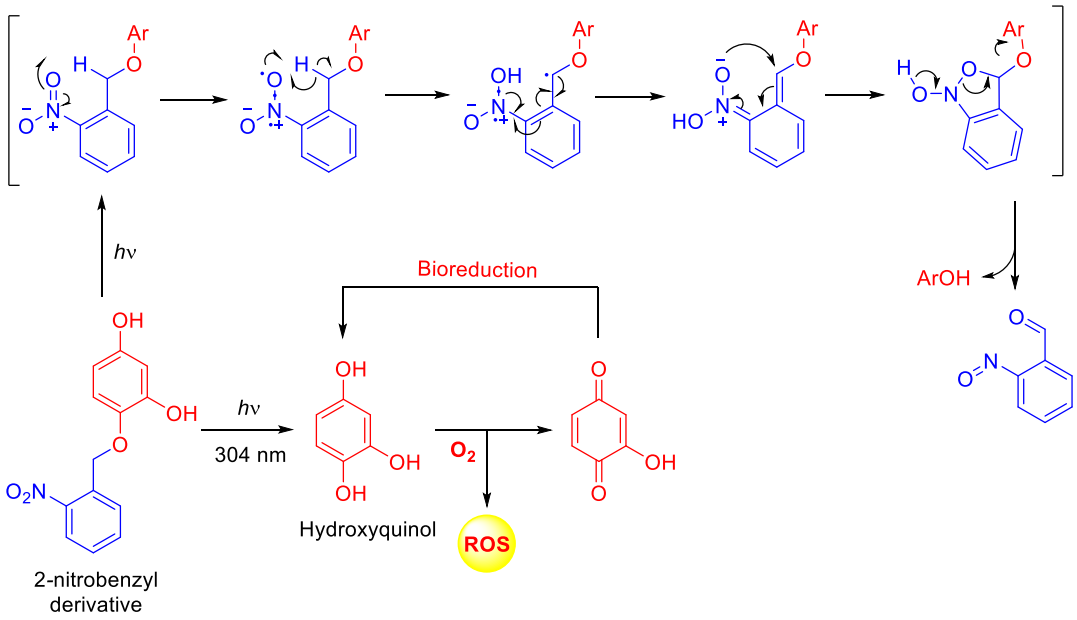

Apart from ROS generation, a number of UV light activated H_2S donors have been also developed. In one of the approaches, a *gem*-dithiol is caged with the 2-nitrobenzyl scaffold and is seen to uncage upon irradiation with UV light (Scheme 1.15). This *gem*-dithiol hydrolyzes in buffer to produce H_2S.[192]

Scheme 1.15. H_2S release by 2-nitrobenzyl thiol-based scaffold

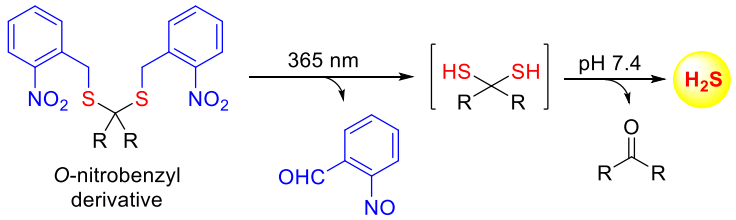

In addition, a ketoprofen scaffold is utilized to mask sulfur in a thioether form; this, upon irradiation, undergoes decarboxylation to form a carbanion. This carbanion further rearranges to release H_2S (Scheme 1.16).[175,178]

Scheme 1.16. Release of H_2S using ketoprofen derivative

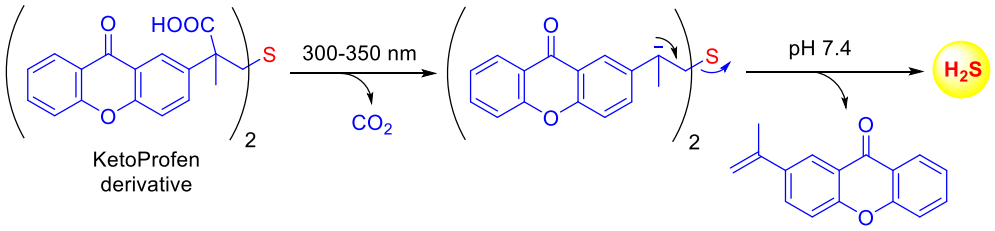

Apart from these methods, another method takes advantage of a phenylacetyl-based scaffold to mask a thioether which undergoes a Norrish type II photo-cleavage to release a thioaldehyde (Scheme 1.17). This thioaldehyde reacts with cellular amines to generate H_2S.[193] Furthermore, a thiocarbamate derivative is masked with the 2-nitrobenzyl based photo-sensitive group; this leads to the uncaging of the thiocarbamate derivative upon UV irrdiataion.[176] This derivative undergoes a rearrangement to produce carbonyl sulfide (COS), a gaseous molecule which is known to be hydrolyzed by carbonic anhydrase (CA) to produce H_2S (Scheme 1.18). While all these methods offer localized delivery of H_2S, the phototoxicity associated[194–198] with UV light is a major limitation. Therefore, a potential visible-light triggered generation of ROS and H_2S can be said to have distinct advantages over these methods.

Scheme 1.17. Release of thioaldehyde *via* Norrish type II photo-cleavage

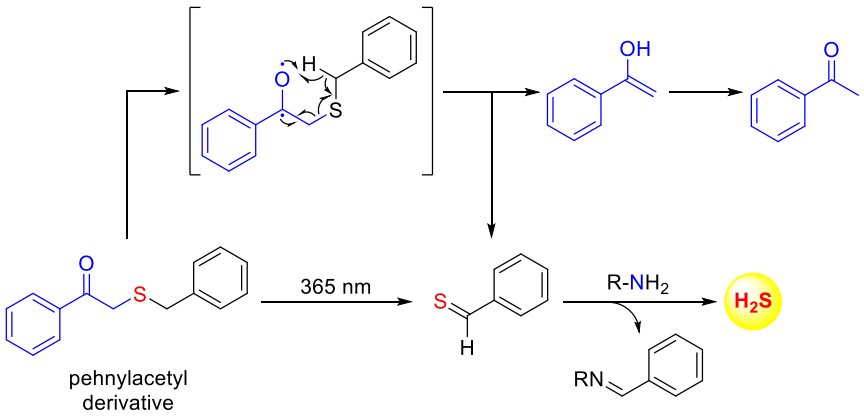

Scheme 1.18. Generation of COS/H_2S using 2-nitrobenzyl moiety

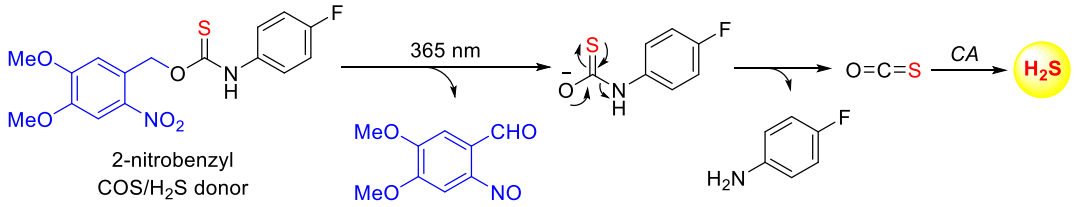

1.2.1.3 Visible Light Triggered Approaches

As a result of the problems associated with UV light activation methods, there is a demand for developing a molecule which can get activated under visible light to produce reactive species.

To this end, numerous strategies using a visible light uncaging group to release different functional groups have been reported in literature. One such method takes advantage of the *N*-methylpicolinium moiety as a photo sensitive group for the release of carboxylates (Scheme 1.19). Uncaging of this carboxylate is initiated by a ruthenium complex, which is a photosensitizer that, upon light irradiation, goes to its triplet excited state and transfers one electron to the aforementioned *N*-methylpicolinium moiety to form a radical. This radical rearranges to release a carboxylate. In this process, the ruthenium complex gets oxidized and is reduced back by ascorbic acid.[199,200] This is an excellent method to release carboxylate; however, use of the metal center and ascorbic acid may change the redox environment of cells and hence, cannot be used for the delivery of redox-active species.

Scheme 1.19. Release of carboxylate using *N*-Methylpicolinium moiety

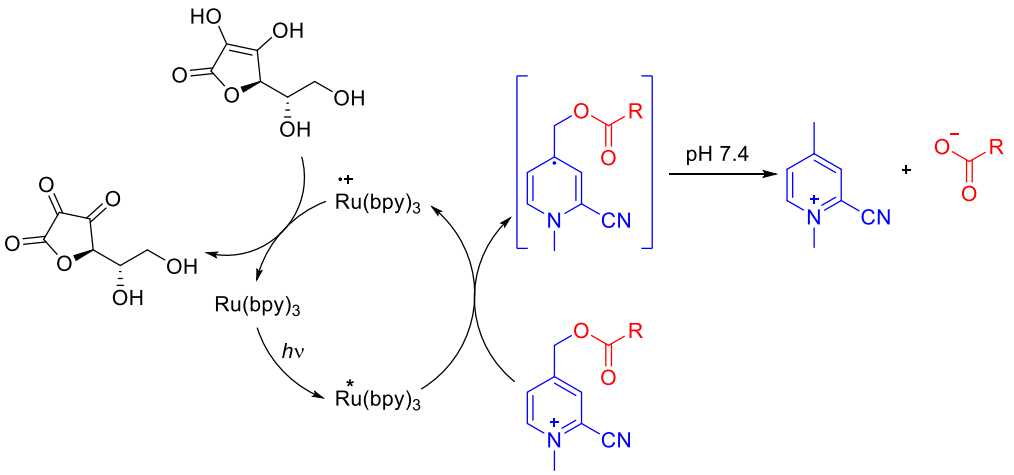

In another method, a fluorescein analogue was utilized as a photo-removable group[215] where carbon monoxide (CO) was unmasked in the presence of visible light without using any additives (Scheme 1.20), but lack of evidence for using this moiety in living systems may affect its usefulness.

Scheme 1.20. CO release using fluorescein analogue

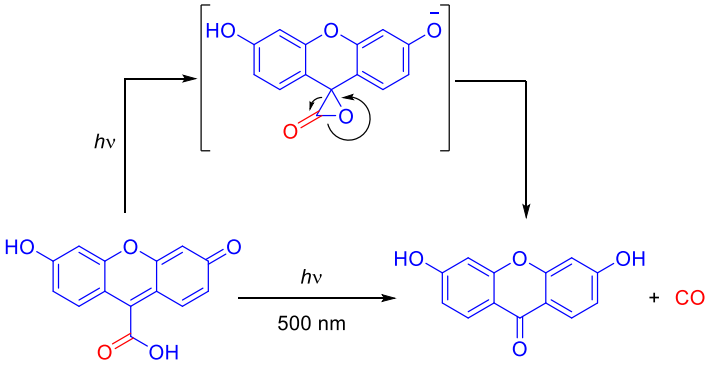

Furthermore, a ruthenium bipyridyl system was also used to deliver the γ-aminobutyric acid (GABA),[202–204] an important neurotransmitter in mammals, which was uncaged with visible light (Scheme 1.21). This system can provide the spatiotemporal delivery of GABA; however, a ruthenium bipyridyl system may act as a photosensitizer to produce singlet oxygen,[205] which would not be desirable for the purpose of uncaging redox-active species.

Scheme 1.21. Release of GABA using ruthenium complex

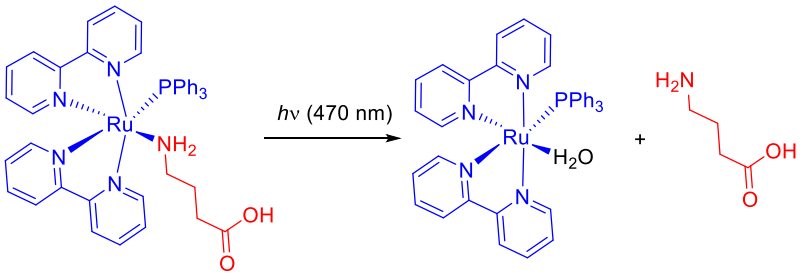

In addition to these reports on visible light activation release of biologically active molecules, a coumarin derivative has also been utilized for releasing cyclofen-OH, a ligand of the estrogen-receptor (ER)-binding domain, under visible light (Scheme 1.22).[206,207] All above described methods provide the spatio-temporal release of an active moiety under mild visible

light. However, the above-mentioned drawbacks limit the use of these molecules for a photoactivatable approach to release ROS.

Scheme 1.22. Release of an amine derivative using a coumarin analogue

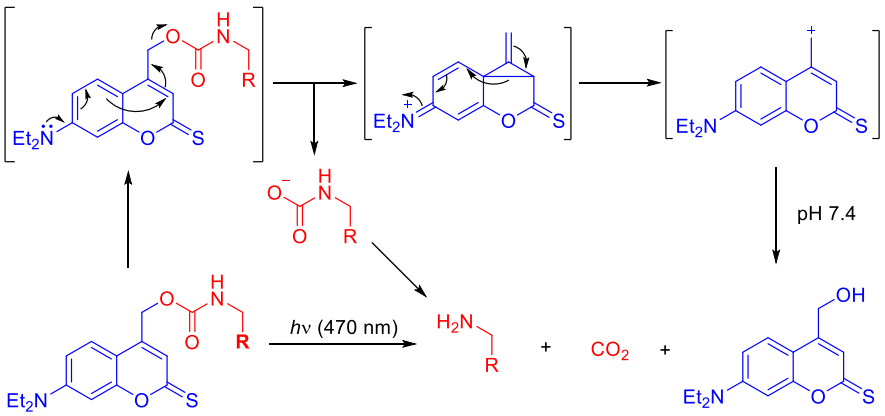

1.2.1.4 Visible Light Activated Release of ROS and H_2S

To the best of our knowledge, there are no reports available in literature where an $O_2^{\bullet-}$ releasing moiety was uncaged upon visible light activation. However, photodynamic (PDT) therapy has been developed for cancer treatment where $^1O_2$ is generated using visible light.[208] $^1O_2$ generation may not be relevant in the study of ROS-mediated pathways because of its typically low endogenous generation, which is not known to contribute much to ROS physiology.[208] Whereas endogenous generation of ROS via $O_2^{\bullet-}$ is the major pathway which contributes to ROS physiology. Hence, the generation of $O_2^{\bullet-}$ is desired.

There are a few methods reported in literature for visible light triggered release of H_2S. One such report employed a 1,3-diarylisobenzothiophene (DBTP) as an H_2S delivery system[209] where singlet oxygen is necessary to initiate the uncaging process of H_2S (Scheme 1.23). To release singlet oxygen, a photosensitizer is irradiated with visible light, which subsequently reacts with DBTP to form an endo-peroxide intermediate. This intermediate further rearranges to release H_2S. This molecule is a very good generator of H_2S upon activation with visible light; however, the generation of $^1O_2$ is not desirable because it can oxidize H_2S to polysulfides and may, thus, complicate the H_2S mediated pathways.[210]

Scheme 1.23. Plausible mechanism of H_2S generation from DBTP (PS: Photosensitizer)

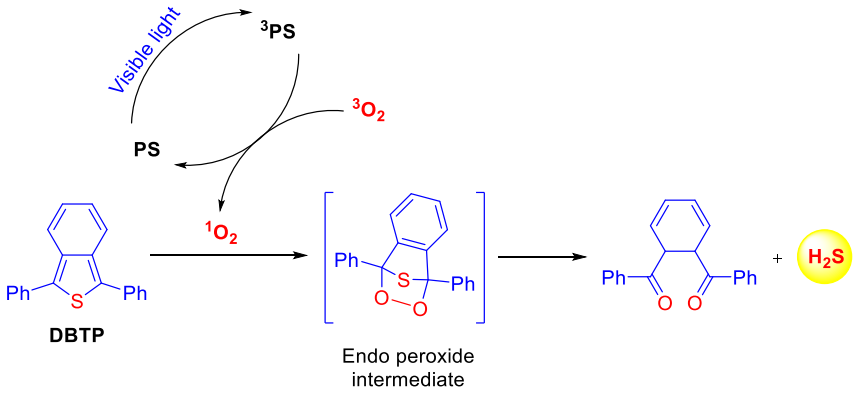

Another report is based on the ESIPT (excited state intramolecular proton transfer) process, where intramolecular proton transfer occurs in an excited state. This excited state further rearranges to uncage H_2S[211] (Scheme 1.24). Further, another report utilizes transition metal chemistry to cage GYY4137, an H_2S releasing molecule. This GYY4137 is uncaged upon irradiation with light, whereupon it subsequently hydrolyzes in buffer to produce H_2S[212] (Scheme 1.25).

Scheme 1.24. Plausible mechanism of H_2S release by the ESIPT-based method

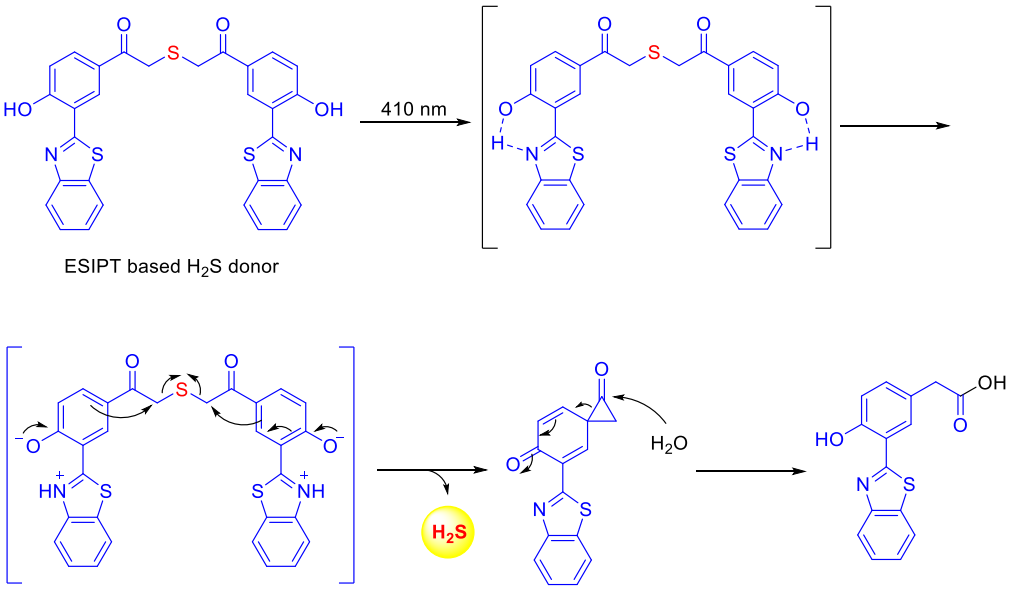

Scheme 1.25. Transition metal-based H_2S generation

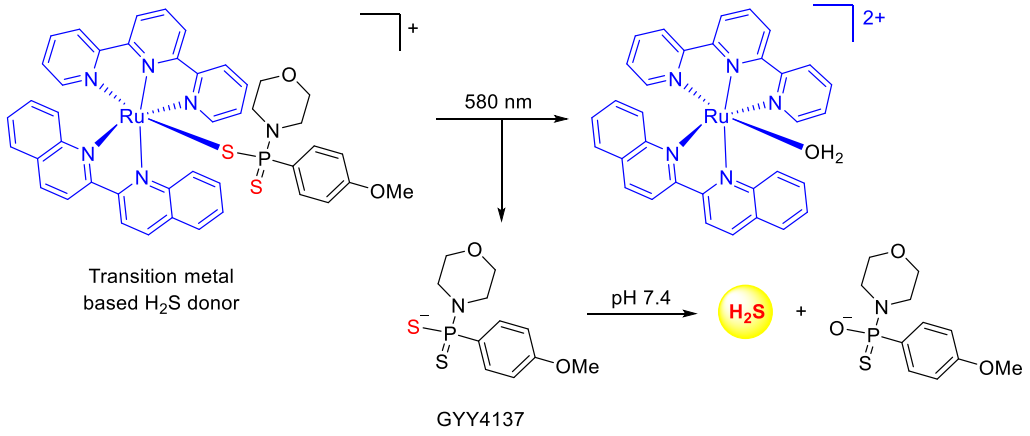

Apart from these reports, a BODIPY-based scaffold is also used for masking a COS moiety in the form of carbamothioate. This carbamothioate is released upon visible light activation to release COS, which can hydrolyze in the presence of carbonic anhydrase to produce H_2S[213] (Scheme 1.26). This strategy offers several advantages over the other methods, such as activation under longer wavelength light, and also, any metal or $^1O_2$ are not required for activation. However, the formation of the electrophilic by-product might affect the cellular machinery by reacting with biological nucleophiles.

Scheme 1.26. BODIPY-based COS/H_2S generation

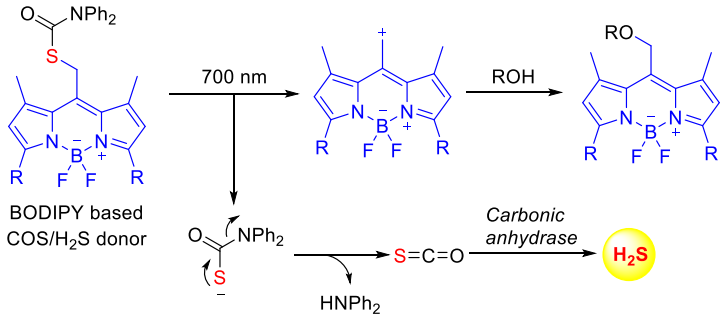

1.2.2 Limitations with Existing Visible Light Activation Methods

The above described methods to release ROS and H_2S upon activation with UV and visible light have certain limitations. As described, UV light can cause oxidative stress in cellular systems, which can result in the damage of essential biomolecules, rendering it unsuitable for studying the effects of reactive species; also, performing *in vivo* experiments is more challenging due to the low tissue penetration of UV light. To overcome these problems, a

number of methods have been developed where a molecule can be activated with visible light to generate reactive species. However, a major limitation is the photosensitizer-mediated generation of $^1O_2$ which can damage essential biomolecule and may present cytotoxicity. Hence, such activation with $^1O_2$ is not desirable. In another method, where a transition metal-based complex was deployed, the limitation arises from the variable oxidation states of transition metals, which can affect the cellular redox processes. In the method where an ESIPT process was utilized to uncage H_2S using 410 nm light, a marginal increase of the ROS levels was found in cells, leading to cytotoxicity.[214] Thus, this method is also not recommended for studying cell signaling. In the BODIPY-based method, the produced electrophilic by-product may react with different biological nucleophiles, which may create unnecessary complications with the cellular machinery. Hence, there is a need to develop a visible light activatable scaffold which does not require any metal or photosensitizer and also one that generates non-toxic photo-cleavage products. Such a scaffold should be versatile such that it can offer a scope for releasing different redox active species.

1.3 Aim

Our aim is to design, synthesize and evaluate molecules which can produce reactive species in a localized manner. To do this, since light is an external stimulus, spatio-temporal control over the generation of reactive species is possible. Here, in this thesis, light triggered strategies are presented to release ROS and H_2S.

In **Chapter 2**, an ROS generator coupled with 2-nitrobenzyl as a photo-responsive moiety is proposed, which may release the ROS generator upon UV light irradiation. Such a UV light activatable ROS generator can also be examined for being a potential candidate for a cancer-targeted approach, since ROS can inhibit the growth of cancer cells. As it is known that UV light-based methods have several drawbacks, rendering them unsuitable in studying ROS-mediated biological processes. To overcome these problems, in **Chapter 3**, a visible light triggered release of an ROS generator is developed, while making use of a BODIPY-based photo-responsive group. Finally, in **Chapter 4**, the selfsame BODIPY-based photo-cleavable linker is utilized to release H_2S upon visible light activation.

The different types of reactive species present in a cell which can cross-talk with each other and complicate the interpretation of results. These species can interact with different sites in cells, which may further complicate the system's study. As it is known that cellular processes themselves are highly involved. Due to all these reasons, results might be obtained because of

non-specific processes. Hence, the development of light activatable tools may find application in delivering these highly reactive species to a particular site in a localized manner, followed by the study of the effect(s) of these species. The proposed tools might be activated under mild conditions, which may not be responsible for any non-specific results.

1.4 References

(1) Minteer, S. D.; Giroud, F.; Milton, R. D.; Tan, B. Quinone Electrochemistry: From the Electron Transport Chain to Electron Mediators and Orientational Moieites. *Meet. Abstr.* **2015**, *01* (45), 2307–2307.

(2) Ziegler, d. M. The role of quinones in the Mitochondrial Electron Transport System. *Am. J. Clin. Nutr.* **1961**, *9* (4), 43–49.

(3) Hubbard, P. A.; Shen, A. L.; Paschke, R.; Kasper, C. B.; Kim, J. J. NADPH-Cytochrome P450 Oxidoreductase. Structural Basis for Hydride and Electron Transfer. *J. Biol. Chem.* **2001**, *276* (31), 29163–29170.

(4) Leonard, S. S.; Harris, G. K.; Shi, X. Metal-Induced Oxidative Stress and Signal Transduction. *Free Radic. Biol. Med.* **2004**, *37* (12), 1921–1942.

(5) Dizdaroglu, M.; Rao, G.; Halliwell, B.; Gajewski, E. Damage to the DNA Bases in Mammalian Chromatin by Hydrogen Peroxide in the Presence of Ferric and Cupric Ions. *Arch. Biochem. Biophys.* **1991**, *285* (2), 317–324.

(6) D'Autréaux, B.; Toledano, M. B. ROS as Signalling Molecules: Mechanisms That Generate Specificity in ROS Homeostasis. *Nat. Rev. Mol. Cell Biol.* **2007**, *8* (10), 813–824.

(7) Finkel, T. Signal Transduction by Reactive Oxygen Species. *J. Cell Biol.* **2011**, *194* (1), 7–15.

(8) Fruehauf, J. P.; Meyskens, F. L. Reactive Oxygen Species: A Breath of Life or Death? *Clin. Cancer Res.* **2007**, *13* (3), 789–794.

(9) Schieber, M.; Chandel, N. S. ROS Function in Redox Signaling and Oxidative Stress. *Curr. Biol.* **2014**, *24* (10), R453–R462.

(10) Jahngen-Hodge, J.; Obin, M. S.; Gong, X.; Shang, F.; Nowell, T. R.; Gong, J.; Abasi, H.; Blumberg, J.; Taylor, A. Regulation of Ubiquitin-Conjugating Enzymes by Glutathione Following Oxidative Stress. *J. Biol. Chem.* **1997**, *272* (45), 28218–28226.

(11) Dickinson, D. A.; Forman, H. J. A. Y. Glutathione in Defense and Signaling. *Ann. N. Y. Acad. Sci.* **2006**, *973* (1), 488–504.

(12) Meister, A. Glutathione, Ascorbate, and Cellular Protection. *Cancer Res.* **1994**, *54* (7), 1969s-1975s.

(13) Lu, J.; Holmgren, A. The Thioredoxin Antioxidant System. *Free Radic. Biol. Med.* **2014**, *66*, 75–87.

(14) Melov, S. Extension of Life-Span with Superoxide Dismutase/Catalase Mimetics. *Science.* **2000**, *289* (5484), 1567–1569.

(15) Tyrrell, R. M. Ultraviolet Radiation and Free Radical Damage to Skin. *Biochem. Soc. Symp.* **1995**, *61*, 47 LP – 53.

(16) Schenkman, J. B.; Jansson, I. The Many Roles of Cytochrome B5. *Pharmacol. Ther.* **2003**, *97* (2), 139–152.

(17) Mittal, M.; Siddiqui, M. R.; Tran, K.; Reddy, S. P.; Malik, A. B. Reactive Oxygen Species in Inflammation and Tissue Injury. *Antioxid. Redox Signal.* **2014**, *20* (7), 1126–1167.

(18) Lenaz, G.; Bovina, C.; D'Aurelio, M.; Fato, R.; Formiggini, G.; Genova, M. L.; Giuliano, G.; Pich, M. M.; Paolucci, U. G. O.; Castelli, G. P.; et al. Role of Mitochondria in Oxidative Stress and Aging. *Ann. N. Y. Acad. Sci.* **2002**, *959* (1), 199–213.

(19) Hauptmann, N.; Grimsby, J.; Shih, J. C.; Cadenas, E. The Metabolism of Tyramine by Monoamine Oxidase A/B Causes Oxidative Damage to Mitochondrial DNA. *Arch. Biochem. Biophys.* **1996**, *335* (2), 295–304.

(20) Harrison, R. Structure and Function of Xanthine Oxidoreductase: Where Are We Now? *Free Radic. Biol. Med.* **2002**, *33* (6), 774–797.

(21) Kukreja, R. C.; Kontos, H. A.; Hess, M. L.; Ellis, E. F. PGH Synthase and Lipoxygenase Generate Superoxide in the Presence of NADH or NADPH. *Circ. Res.* **1986**, *59* (6), 612.

(22) Hofmann, B.; Hecht, H. J.; Flohe, L. Peroxiredoxins. *Biol. Chem.* **2002**, *383* (3–4), 347–364.

(23) Dickinson, D. A.; Forman, H. J. Glutathione in Defense and Signaling: Lessons from a Small Thiol. *Ann. N. Y. Acad. Sci.* **2002**, *973*, 488–504.

(24) Mitsui, A.; Hirakawa, T.; Yodoi, J. Reactive Oxygen-Reducing and Protein-Refolding Activities of Adult t Cell Leukemia-Derived Factor /Human Thioredoxin. *Biochem. Biophys. Res. Commun.* **1992**, *186* (3), 1220–1226.

(25) Yang, Y.; Bazhin, A. V.; Werner, J.; Karakhanova, S. Reactive Oxygen Species in the Immune System. *Int. Rev. Immunol.* **2013**, *32* (3), 249–270.

(26) Ji, A.-R.; Ku, S.-Y.; Cho, M. S.; Kim, Y. Y.; Kim, Y. J.; Oh, S. K.; Kim, S. H.; Moon, S. Y.; Choi, Y. M. Reactive Oxygen Species Enhance Differentiation of Human Embryonic Stem Cells into Mesendodermal Lineage. *Exp. Mol. Med.* **2010**, *42* (3), 175–186.

(27) de Villiers, D.; Potgieter, M.; Ambele, M. A.; Adam, L.; Durandt, C.; Pepper, M. S. The Role of Reactive Oxygen Species in Adipogenic Differentiation. In *Advances in experimental medicine and biology*; **2017**, *1083*, 125–144.

(28) Manivannan, A.; Soundararajan, P.; Jeong, B. R. Role of Reactive Oxygen Species

Signaling in Cell Proliferation and Differentiation. In *Reactive Oxygen Species in Plants*; John Wiley & Sons, Ltd: Chichester, UK, **2017**, 319–329.

(29) Han, M.-J.; Kim, B.-Y.; Yoon, S.-O.; Chung, A.-S. Cell Proliferation Induced by Reactive Oxygen Species Is Mediated via Mitogen-Activated Protein Kinase in Chinese Hamster Lung Fibroblast (V79) Cells. *Mol. Cells* **2003**, *15* (1), 94–101.

(30) Gregersen, N.; Bross, P. Protein Misfolding and Cellular Stress: An Overview. In *Methods in molecular biology.* **2010**, *648*, 3–23.

(31) Ali, I.; Shah, S. Z. A.; Jin, Y.; Li, Z.-S.; Ullah, O.; Fang, N.-Z. Reactive Oxygen Species-Mediated Unfolded Protein Response Pathways in Preimplantation Embryos. *J. Vet. Sci.* **2017**, *18* (1), 1–9.

(32) Kim, Y.-W.; Byzova, T. V. Oxidative Stress in Angiogenesis and Vascular Disease. *Blood* **2014**, *123* (5), 625–631.

(33) Ushio-Fukai, M.; Nakamura, Y. Reactive Oxygen Species and Angiogenesis: NADPH Oxidase as Target for Cancer Therapy. *Cancer Lett.* **2008**, *266* (1), 37–52.

(34) Ushio-Fukai, M.; Alexander, R. W. Reactive Oxygen Species as Mediators of Angiogenesis Signaling: Role of NAD(P)H Oxidase. *Mol. Cell. Biochem.* **2004**, *264* (1–2), 85–97.

(35) Costa, A.; Scholer-Dahirel, A.; Mechta-Grigoriou, F. The Role of Reactive Oxygen Species and Metabolism on Cancer Cells and Their Microenvironment. *Semin. Cancer Biol.* **2014**, *25*, 23–32.

(36) Kim, J.; Kim, J.; Bae, J.-S. ROS Homeostasis and Metabolism: A Critical Liaison for Cancer Therapy. *Exp. Mol. Med.* **2016**, *48* (11), e269.

(37) Apel, K.; Hirt, h. Reactive oxygen species: Metabolism, Oxidative Stress, and Signal Transduction. *Annu. Rev. Plant Biol.* **2004**, *55* (1), 373–399.

(38) Michiels, C. Physiological and Pathological Responses to Hypoxia. *Am. J. Pathol.* **2004**, *164* (6), 1875–1882.

(39) Hoshikawa, Y.; Nana-Sinkam, P.; Moore, M. D.; Sotto-Santiago, S.; Phang, T.; Keith, R. L.; Morris, K. G.; Kondo, T.; Tuder, R. M.; Voelkel, N. F.; et al. Hypoxia Induces Different Genes in the Lungs of Rats Compared with Mice. *Physiol. Genomics* **2003**, *12* (3), 209–219.

(40) Lando, D.; Peet, D. J.; Whelan, D. A.; Gorman, J. J.; Whitelaw, M. L. Asparagine Hydroxylation of the HIF Transactivation Domain: A Hypoxic Switch. *Science (80-.).* **2002**, *295* (5556), 858–861.

(41) Liou, G.-Y.; Storz, P. Reactive Oxygen Species in Cancer. *Free Radic. Res.* **2010**, *44*

(5), 479–496.

(42) Kumari, S.; Badana, A. K.; G, M. M.; G, S.; Malla, R. Reactive Oxygen Species: A Key Constituent in Cancer Survival. *Biomark. Insights* **2018**, *13*.

(43) Tönnies, E.; Trushina, E. Oxidative Stress, Synaptic Dysfunction, and Alzheimer's Disease. *J. Alzheimers. Dis.* **2017**, *57* (4), 1105–1121.

(44) Huang, W.-J.; Zhang, X.; Chen, W.-W. Role of Oxidative Stress in Alzheimer's Disease. *Biomed. Reports* **2016**, *4* (5), 519.

(45) Dias, V.; Junn, E.; Mouradian, M. M. The Role of Oxidative Stress in Parkinson's Disease. *J. Parkinsons. Dis.* **2013**, *3* (4), 461–491.

(46) Hwang, O. Role of Oxidative Stress in Parkinson's Disease. *Exp. Neurobiol.* **2013**, *22* (1), 11–17.

(47) Weng, M.; Xie, X.; Liu, C.; Lim, K.-L.; Zhang, C.; Li, L. The Sources of Reactive Oxygen Species and Its Possible Role in the Pathogenesis of Parkinson's Disease. *Parkinsons. Dis.* **2018**, *2018*, 1–9.

(48) Piotrowska, A.; Bartnik, E. [The Role of Reactive Oxygen Species and Mitochondria in Aging]. *Postepy Biochem.* **2014**, *60* (2), 240–247.

(49) Davalli, P.; Mitic, T.; Caporali, A.; Lauriola, A.; D'Arca, D. ROS, Cell Senescence, and Novel Molecular Mechanisms in Aging and Age-Related Diseases. *Oxid. Med. Cell. Longev.* **2016**, *2016*, 3565127.

(50) Stefanatos, R.; Sanz, A. The Role of Mitochondrial ROS in the Aging Brain. *FEBS Lett.* **2018**, *592* (5), 743–758.

(51) Cui, H.; Kong, Y.; Zhang, H. Oxidative Stress, Mitochondrial Dysfunction, and Aging. *J. Signal Transduct.* **2012**, *2012*, 646354.

(52) Kaneto, H.; Katakami, N.; Matsuhisa, M.; Matsuoka, T. Role of Reactive Oxygen Species in the Progression of Type 2 Diabetes and Atherosclerosis. *Mediators Inflamm.* **2010**, *2010*, 453892.

(53) Fakhruddin, S.; Alanazi, W.; Jackson, K. E. Diabetes-Induced Reactive Oxygen Species: Mechanism of Their Generation and Role in Renal Injury. *J. Diabetes Res.* **2017**, *2017*, 1–30.

(54) Ha, H.; Hwang, I.-A.; Park, J. H.; Lee, H. B. Role of Reactive Oxygen Species in the Pathogenesis of Diabetic Nephropathy. *Diabetes Res. Clin. Pract.* **2008**, *82*, S42–S45.

(55) Volpe, C. M. O.; Villar-Delfino, P. H.; Dos Anjos, P. M. F.; Nogueira-Machado, J. A. Cellular Death, Reactive Oxygen Species (ROS) and Diabetic Complications. *Cell Death Dis.* **2018**, *9* (2), 119.

(56) Dharmaraja, A. T.; Alvala, M.; Sriram, D.; Yogeeswari, P.; Chakrapani, H. Design, Synthesis and Evaluation of Small Molecule Reactive Oxygen Species Generators as Selective Mycobacterium Tuberculosis Inhibitors. *Chem. Commun.* **2012**, *48* (83), 10325–10327.

(57) Dharmaraja, A. T.; Chakrapani, H. A Small Molecule for Controlled Generation of Reactive Oxygen Species (ROS). *Org. Lett.* **2014**, *16* (2), 398–401.

(58) Dharmaraja, A. T.; Dash, T. K.; Konkimalla, V. B.; Chakrapani, H. Synthesis, Thiol-Mediated Reactive Oxygen Species Generation Profiles and Anti-Proliferative Activities of 2,3-Epoxy-1,4-Naphthoquinones. *Medchemcomm* **2012**, *3* (2), 219–224.

(59) Khodade, V. S.; Sharath Chandra, M.; Banerjee, A.; Lahiri, S.; Pulipeta, M.; Rangarajan, R.; Chakrapani, H. Bioreductively Activated Reactive Oxygen Species (ROS) Generators as MRSA Inhibitors. *ACS Med. Chem. Lett.* **2014**, *5* (7), 777–781.

(60) Roh, J.-L.; Kim, E. H.; Park, J. Y.; Kim, J. W.; Kwon, M.; Lee, B.-H. Piperlongumine Selectively Kills Cancer Cells and Increases Cisplatin Antitumor Activity in Head and Neck Cancer. *Oncotarget* **2014**, *5* (19), 9227–9238.

(61) Karki, K.; Hedrick, E.; Kasiappan, R.; Jin, U.-H.; Safe, S. Piperlongumine Induces Reactive Oxygen Species (ROS)-Dependent Downregulation of Specificity Protein Transcription Factors. *Cancer Prev. Res.* **2017**, *10* (8), 467–477.

(62) Dhillon, H.; Chikara, S.; Reindl, K. M. Piperlongumine Induces Pancreatic Cancer Cell Death by Enhancing Reactive Oxygen Species and DNA Damage. *Toxicol. Reports* **2014**, *1*, 309–318.

(63) Xu, X.; Fang, X.; Wang, J.; Zhu, H. Identification of Novel ROS Inducer by Merging the Fragments of Piperlongumine and Dicoumarol. *Bioorg. Med. Chem. Lett.* **2017**, *27* (5), 1325–1328.

(64) Yan, W.-J.; Wang, Q.; Yuan, C.-H.; Wang, F.; Ji, Y.; Dai, F.; Jin, X.-L.; Zhou, B. Designing Piperlongumine-Directed Anticancer Agents by an Electrophilicity-Based Prooxidant Strategy: A Mechanistic Investigation. *Free Radic. Biol. Med.* **2016**, *97*, 109–123.

(65) Gong, L.-H.; Chen, X.-X.; Wang, H.; Jiang, Q.-W.; Pan, S.-S.; Qiu, J.-G.; Mei, X.-L.; Xue, Y.-Q.; Qin, W.-M.; Zheng, F.-Y.; et al. Piperlongumine Induces Apoptosis and Synergizes with Cisplatin or Paclitaxel in Human Ovarian Cancer Cells. *Oxid. Med. Cell. Longev.* **2014**, *2014*, 906804.

(66) Beg, M. S.; Huang, X.; Silvers, M. A.; Gerber, D. E.; Bolluyt, J.; Sarode, V.; Fattah, F.; Deberardinis, R. J.; Merritt, M. E.; Xie, X.-J.; et al. Using a Novel NQO1 Bioactivatable

Drug, Beta-Lapachone (ARQ761), to Enhance Chemotherapeutic Effects by Metabolic Modulation in Pancreatic Cancer. *J. Surg. Oncol.* **2017**, *116* (1), 83–88.

(67) Yang, Y.; Zhou, X.; Xu, M.; Piao, J.; Zhang, Y.; Lin, Z.; Chen, L. β-Lapachone Suppresses Tumour Progression by Inhibiting Epithelial-to-Mesenchymal Transition in NQO1-Positive Breast Cancers. *Sci. Rep.* **2017**, *7* (1), 2681.

(68) Silvers, M. A.; Deja, S.; Singh, N.; Egnatchik, R. A.; Sudderth, J.; Luo, X.; Beg, M. S.; Burgess, S. C.; DeBerardinis, R. J.; Boothman, D. A.; et al. The NQO1 Bioactivatable Drug, β-Lapachone, Alters the Redox State of NQO1+ Pancreatic Cancer Cells, Causing Perturbation in Central Carbon Metabolism. *J. Biol. Chem.* **2017**, *292* (44), 18203–18216.

(69) Ough, M.; Lewis, A.; Bey, E. A.; Gao, J.; Ritchie, J. M.; Bornmann, W.; Boothman, D. A.; Oberley, L. W.; Cullen, J. J. Efficacy of Beta-Lapachone in Pancreatic Cancer Treatment: Exploiting the Novel, Therapeutic Target NQO1. *Cancer Biol. Ther.* **2005**, *4* (1), 102–109.

(70) Wang, X.; Luo, F.; Zhao, H. Paraquat-Induced Reactive Oxygen Species Inhibit Neutrophil Apoptosis via a P38 MAPK/NF-KB–IL-6/TNF-α Positive-Feedback Circuit. *PLoS One* **2014**, *9* (4), e93837.

(71) Kim, H.; Lee, S. W.; Baek, K. M.; Park, J. S.; Min, J. H. Continuous Hypoxia Attenuates Paraquat-Induced Cytotoxicity in the Human A549 Lung Carcinoma Cell Line. *Exp. Mol. Med.* **2011**, *43* (9), 494–500.

(72) Castello, P. R.; Drechsel, D. A.; Patel, M. Mitochondria Are a Major Source of Paraquat-Induced Reactive Oxygen Species Production in the Brain. *J. Biol. Chem.* **2007**, *282* (19), 14186–14193.

(73) Frank, D. M.; Arora, P. K.; Blumer, J. L.; Sayre, L. M. Model Study on the Bioreduction of Paraquat, MPP+, and Analogs. Evidence against a “Redox Cycling” Mechanism in MPTP Neurotoxicity. *Biochem. Biophys. Res. Commun.* **1987**, *147* (3), 1095–1104.

(74) DeGray, J. A.; Rao, D. N. R.; Mason, R. P. Reduction of Paraquat and Related Bipyridylium Compounds to Free Radical Metabolites by Rat Hepatocytes. *Arch. Biochem. Biophys.* **1991**, *289* (1), 145–152.

(75) Robb, E. L.; Gawel, J. M.; Aksentijević, D.; Cochemé, H. M.; Stewart, T. S.; Shchepinova, M. M.; Qiang, H.; Prime, T. A.; Bright, T. P.; James, A. M.; et al. Selective Superoxide Generation within Mitochondria by the Targeted Redox Cycler MitoParaquat. *Free Radic. Biol. Med.* **2015**, *89*, 883–894.

(76) Kelkar, D. S.; Ravikumar, G.; Mehendale, N.; Singh, S.; Joshi, A.; Sharma, A. K.;

Mhetre, A.; Rajendran, A.; Chakrapani, H.; Kamat, S. S. A Chemical–Genetic Screen Identifies ABHD12 as an Oxidized-Phosphatidylserine Lipase. *Nat. Chem. Biol.* **2019**, *15* (2), 169–178.

(77) Aquilano, K.; Baldelli, S.; Ciriolo, M. R. Glutathione: New Roles in Redox Signaling for an Old Antioxidant. *Front. Pharmacol.* **2014**, *5*, 196.

(78) Mohanasundaram, K. A.; Haworth, N. L.; Grover, M. P.; Crowley, T. M.; Goscinski, A.; Wouters, M. A. Potential Role of Glutathione in Evolution of Thiol-Based Redox Signaling Sites in Proteins. *Front. Pharmacol.* **2015**, *6*, 1.

(79) Chandrasena, R. E. P.; Edirisinghe, P. D.; Bolton, J. L.; Thatcher, G. R. J. Problematic Detoxification of Estrogen Quinones by NAD(P)H-Dependent Quinone Oxidoreductase and Glutathione- *S*- Transferase. *Chem. Res. Toxicol.* **2008**, *21* (7), 1324–1329.

(80) Li, J.; Wang, W.; Zhang, H.; Le, X. C.; Li, X.-F. Glutathione-Mediated Detoxification of Halobenzoquinone Drinking Water Disinfection Byproducts in T24 Cells. *Toxicol. Sci.* **2014**, *141* (2), 335–343.

(81) Nagahara, N. Catalytic Site Cysteines of Thiol Enzyme: Sulfurtransferases. *J. Amino Acids* **2011**, *2011*, 709404.

(82) Marino, S. M.; Gladyshev, V. N. Analysis and Functional Prediction of Reactive Cysteine Residues. *J. Biol. Chem.* **2012**, *287* (7), 4419–4425.

(83) Luo, L.; Chen, S.; Jin, H.; Tang, C.; Du, J. Endogenous Generation of Sulfur Dioxide in Rat Tissues. *Biochem. Biophys. Res. Commun.* **2011**, *415* (1), 61–67.

(84) DU, S.; JIN, H.; BU, D.; ZHAO, X.; GENG, B.; TANG, C.; DU, J. Endogenously Generated Sulfur Dioxide and Its Vasorelaxant Effect in Rats [1]. *Acta Pharmacol. Sin.* **2008**, *29* (8), 923–930.

(85) Meng, Z.; Zhang, H. The Vasodilator Effect and Its Mechanism of Sulfur Dioxide-Derivatives on Isolated Aortic Rings of Rats. *Inhal. Toxicol.* **2007**, *19* (11), 979–986.

(86) Lovati, M. R.; Manzoni, C.; Daldossi, M.; Spolti, S.; Sirtori, C. R. Effects of Sub-Chronic Exposure to SO2 on Lipid and Carbohydrate Metabolism in Rats. *Arch. Toxicol.* **1996**, *70* (3–4), 164–173.

(87) Li, W.; Tang, C.; Jin, H.; Du, J. Regulatory Effects of Sulfur Dioxide on the Development of Atherosclerotic Lesions and Vascular Hydrogen Sulfide in Atherosclerotic Rats. *Atherosclerosis* **2011**, *215* (2), 323–330.

(88) Sun, Y.; Tian, Y.; Prabha, M.; Liu, D.; Chen, S.; Zhang, R.; Liu, X.; Tang, C.; Tang, X.; Jin, H.; et al. Effects of Sulfur Dioxide on Hypoxic Pulmonary Vascular Structural Remodeling. *Lab. Investig.* **2010**, *90* (1), 68–82.

(89) JIN, H.; DU, S.; ZHAO, X.; WEI, H.; WANG, Y.; LIANG, Y.; TANG, C.; DU, J. Effects of Endogenous Sulfur Dioxide on Monocrotaline-Induced Pulmonary Hypertension in Rats [1]. *Acta Pharmacol. Sin.* **2008**, *29* (10), 1157–1166.

(90) Chen, S.; Zheng, S.; Liu, Z.; Tang, C.; Zhao, B.; Du, J.; Jin, H. Endogeous Sulfur Dioxide Protects against Oleic Acid-Induced Acute Lung Injury in Association with Inhibition of Oxidative Stress in Rats. *Lab. Investig.* **2015**, *95* (2), 142–156.

(91) Qu, K.; Lee, S. W.; Bian, J. S.; Low, C.-M.; Wong, P. T.-H. Hydrogen Sulfide: Neurochemistry and Neurobiology. *Neurochem. Int.* **2008**, *52* (1–2), 155–165.

(92) Ishigami, M.; Hiraki, K.; Umemura, K.; Ogasawara, Y.; Ishii, K.; Kimura, H. A Source of Hydrogen Sulfide and a Mechanism of Its Release in the Brain. *Antioxid. Redox Signal.* **2009**, *11* (2), 205–214.

(93) Chang, L.; Geng, B.; Yu, F.; Zhao, J.; Jiang, H.; Du, J.; Tang, C. Hydrogen Sulfide Inhibits Myocardial Injury Induced by Homocysteine in Rats. *Amino Acids* **2008**, *34* (4), 573–585.

(94) Whiteman, M.; Armstrong, J. S.; Chu, S. H.; Jia-Ling, S.; Wong, B.-S.; Cheung, N. S.; Halliwell, B.; Moore, P. K. The Novel Neuromodulator Hydrogen Sulfide: An Endogenous Peroxynitrite "Scavenger"? *J. Neurochem.* **2004**, *90* (3), 765–768.

(95) Geng, B.; Yang, J.; Qi, Y.; Zhao, J.; Pang, Y.; Du, J.; Tang, C. H2S Generated by Heart in Rat and Its Effects on Cardiac Function. *Biochem. Biophys. Res. Commun.* **2004**, *313* (2), 362–368.

(96) Rose, P.; Moore, P. K.; Zhu, Y. Z. H2S Biosynthesis and Catabolism: New Insights from Molecular Studies. *Cell. Mol. Life Sci.* **2017**, *74* (8), 1391–1412.

(97) Kabil, O.; Banerjee, R. Enzymology of H_2S Biogenesis, Decay and Signaling. *Antioxid. Redox Signal.* **2014**, *20* (5), 770–782.

(98) Huang, C. W.; Moore, P. K. H2S Synthesizing Enzymes: Biochemistry and Molecular Aspects. In *Handbook of experimental pharmacology*. **2015**, *230*, 3–25.

(99) Meng, J.-L.; Mei, W.-Y.; Dong, Y.-F.; Wang, J.-H.; Zhao, C.-M.; Lan, A.-P.; Yang, C.-T.; Chen, P.-X.; Feng, J.-Q.; Hu, C.-H. Heat Shock Protein 90 Mediates Cytoprotection by H2S against Chemical Hypoxia-Induced Injury in PC12 Cells. *Clin. Exp. Pharmacol. Physiol.* **2011**, *38* (1), 42–49.

(100) Yang, C.; Yang, Z.; Zhang, M.; Dong, Q.; Wang, X.; Lan, A.; Zeng, F.; Chen, P.; Wang, C.; Feng, J. Hydrogen Sulfide Protects against Chemical Hypoxia-Induced Cytotoxicity and Inflammation in HaCaT Cells through Inhibition of ROS/NF-KB/COX-2 Pathway. *PLoS One* **2011**, *6* (7), e21971.

(101) Yang, M.; Huang, Y.; Chen, J.; Chen, Y.; Ma, J.; Shi, P. Activation of AMPK Participates Hydrogen Sulfide-Induced Cyto-Protective Effect against Dexamethasone in Osteoblastic MC3T3-E1 Cells. *Biochem. Biophys. Res. Commun.* **2014**, *454* (1), 42–47.

(102) Calvert, J. W.; Jha, S.; Gundewar, S.; Elrod, J. W.; Ramachandran, A.; Pattillo, C. B.; Kevil, C. G.; Lefer, D. J. Hydrogen Sulfide Mediates Cardioprotection Through Nrf2 Signaling. *Circ. Res.* **2009**, *105* (4), 365–374.

(103) Zayachkivska, O.; Havryluk, O.; Hrycevych, N.; Bula, N.; Grushka, O.; Wallace, J. L. Cytoprotective Effects of Hydrogen Sulfide in Novel Rat Models of Non-Erosive Esophagitis. *PLoS One* **2014**, *9* (10), e110688.

(104) Szabo, C. Hydrogen Sulphide and Its Therapeutic Potential. *Nat. Rev. Drug. Discov.* **2007**, *6* (11), 917–935.

(105) Gemici, B.; Wallace, J. L. Anti-Inflammatory and Cytoprotective Properties of Hydrogen Sulfide. In *Methods in enzymology*. **2015**, 555, 169–193.

(106) Whiteman, M.; Li, L.; Rose, P.; Tan, C.-H.; Parkinson, D. B.; Moore, P. K. The Effect of Hydrogen Sulfide Donors on Lipopolysaccharide-Induced Formation of Inflammatory Mediators in Macrophages. *Antioxid. Redox Signal.* **2010**, *12* (10), 1147–1154.

(107) Zanardo, R. C. O.; Brancaleone, V.; Distrutti, E.; Fiorucci, S.; Cirino, G.; Wallace, J. L. Hydrogen Sulfide Is an Endogenous Modulator of Leukocyte-Mediated Inflammation. *FASEB J.* **2006**, *20* (12), 2118–2120.

(108) Li, L.; Bhatia, M.; Zhu, Y. Z.; Zhu, Y. C.; Ramnath, R. D.; Wang, Z. J.; Anuar, F. B. M.; Whiteman, M.; Salto-Tellez, M.; Moore, P. K. Hydrogen Sulfide Is a Novel Mediator of Lipopolysaccharide-Induced Inflammation in the Mouse. *FASEB J.* **2005**, *19* (9), 1196–1198.

(109) Yang, R.; Teng, X.; Li, H.; Xue, H.-M.; Guo, Q.; Xiao, L.; Wu, Y.-M. Hydrogen Sulfide Improves Vascular Calcification in Rats by Inhibiting Endoplasmic Reticulum Stress. *Oxid. Med. Cell. Longev.* **2016**, *2016*, 1–9.

(110) Zhao, W.; Zhang, J.; Lu, Y.; Wang, R. The Vasorelaxant Effect of H2S as a Novel Endogenous Gaseous KATP Channel Opener. *EMBO J.* **2001**, *20* (21), 6008–6016.

(111) Köhn, C.; Schleifenbaum, J.; Szijártó, I. A.; Markó, L.; Dubrovska, G.; Huang, Y.; Gollasch, M. Differential Effects of Cystathionine-γ-Lyase–Dependent Vasodilatory H2S in Periadventitial Vasoregulation of Rat and Mouse Aortas. *PLoS One* **2012**, *7* (8), e41951.

(112) Wang, Z.; Liu, D.-X.; Wang, F.-W.; Zhang, Q.; Du, Z.-X.; Zhan, J.-M.; Yuan, Q.-H.; Ling, E.-A.; Hao, A.-J. L-Cysteine Promotes the Proliferation and Differentiation of Neural Stem Cells via the CBS/H2S Pathway. *Neuroscience* **2013**, *237*, 106–117.

(113) CAI, W.; WANG, M.; MOORE, P.; JIN, H.; YAO, T.; ZHU, Y. The Novel Proangiogenic Effect of Hydrogen Sulfide Is Dependent on Akt Phosphorylation. *Cardiovasc. Res.* **2007**, *76* (1), 29–40.

(114) Wallace, J. L.; Dicay, M.; McKnight, W.; Martin, G. R. Hydrogen Sulfide Enhances Ulcer Healing in Rats. *FASEB J.* **2007**, *21* (14), 4070–4076.

(115) Papapetropoulos, A.; Pyriochou, A.; Altaany, Z.; Yang, G.; Marazioti, A.; Zhou, Z.; Jeschke, M. G.; Branski, L. K.; Herndon, D. N.; Wang, R.; et al. Hydrogen Sulfide Is an Endogenous Stimulator of Angiogenesis. *Proc. Natl. Acad. Sci.* **2009**, *106* (51), 21972–21977.

(116) Liu, W.; Liu, K.; Ma, C.; Yu, J.; Peng, Z.; Huang, G.; Cai, Z.; Li, R.; Xu, W.; Sun, X.; et al. Protective Effect of Hydrogen Sulfide on Hyperbaric Hyperoxia-Induced Lung Injury in a Rat Model. *Undersea Hyperb. Med. 41* (6), 573–578.

(117) Wang, G.; Li, W.; Chen, Q.; Jiang, Y.; Lu, X.; Zhao, X. Hydrogen Sulfide Accelerates Wound Healing in Diabetic Rats. *Int. J. Clin. Exp. Pathol.* **2015**, *8* (5), 5097–5104.

(118) Jang, H.; Oh, M.-Y.; Kim, Y.-J.; Choi, I.-Y.; Yang, H. sung; Ryu, W.-S.; Lee, S.-H.; Yoon, B.-W. Hydrogen Sulfide Treatment Induces Angiogenesis after Cerebral Ischemia. *J. Neurosci. Res.* **2014**, *92* (11), 1520–1528.

(119) Yang, G.-D.; Wang, R. H(2)S and Cellular Proliferation and Apoptosis. *Sheng Li Xue Bao* **2007**, *59* (2), 133–140.

(120) Baskar, R.; Bian, J. Hydrogen Sulfide Gas Has Cell Growth Regulatory Role. *Eur. J. Pharmacol.* **2011**, *656* (1–3), 5–9.

(121) Vicente, J. B.; Malagrinò, F.; Arese, M.; Forte, E.; Sarti, P.; Giuffrè, A. Bioenergetic Relevance of Hydrogen Sulfide and the Interplay between Gasotransmitters at Human Cystathionine β-Synthase. *Biochim. Biophys. Acta - Bioenerg.* **2016**, *1857* (8), 1127–1138.

(122) Zhao, F.; Fang, F.; Qiao, P.; Yan, N.; Gao, D.; Yan, Y. AP39, a Mitochondria-Targeted Hydrogen Sulfide Donor, Supports Cellular Bioenergetics and Protects against Alzheimer's Disease by Preserving Mitochondrial Function in APP/PS1 Mice and Neurons. *Oxid. Med. Cell. Longev.* **2016**, *2016*, 1–19.

(123) Goubern, M.; Andriamihaja, M.; Nübel, T.; Blachier, F.; Bouillaud, F. Sulfide, the First Inorganic Substrate for Human Cells. *FASEB J.* **2007**, *21* (8), 1699–1706.

(124) Elrod, J. W.; Calvert, J. W.; Morrison, J.; Doeller, J. E.; Kraus, D. W.; Tao, L.; Jiao, X.; Scalia, R.; Kiss, L.; Szabo, C.; et al. Hydrogen Sulfide Attenuates Myocardial Ischemia-Reperfusion Injury by Preservation of Mitochondrial Function. *Proc. Natl. Acad. Sci.* **2007**, *104* (39), 15560–15565.

(125) Sun, A.; Wang, Y.; Liu, J.; Yu, X.; Sun, Y.; Yang, F.; Dong, S.; Wu, J.; Zhao, Y.; Xu, C.; et al. Exogenous H2S Modulates Mitochondrial Fusion–Fission to Inhibit Vascular Smooth Muscle Cell Proliferation in a Hyperglycemic State. *Cell Biosci.* **2016**, *6* (1), 36.

(126) Miao, L.; Shen, X.; Whiteman, M.; Xin, H.; Shen, Y.; Xin, X.; Moore, P. K.; Zhu, Y.-Z. Hydrogen Sulfide Mitigates Myocardial Infarction *via* Promotion of Mitochondrial Biogenesis-Dependent M2 Polarization of Macrophages. *Antioxid. Redox Signal.* **2016**, *25* (5), 268–281.

(127) Coletta, C.; Módis, K.; Szczesny, B.; Brunyánszki, A.; Oláh, G.; Rios, E. C. S.; Yanagi, K.; Ahmad, A.; Papapetropoulos, A.; Szabo, C. Regulation of Vascular Tone, Angiogenesis and Cellular Bioenergetics by the 3-Mercaptopyruvate Sulfurtransferase/H2S Pathway: Functional Impairment by Hyperglycemia and Restoration by Dl-α-Lipoic Acid. *Mol. Med.* **2015**, *21* (1), 1–14.

(128) Szczesny, B.; Módis, K.; Yanagi, K.; Coletta, C.; Le Trionnaire, S.; Perry, A.; Wood, M. E.; Whiteman, M.; Szabo, C. AP39, a Novel Mitochondria-Targeted Hydrogen Sulfide Donor, Stimulates Cellular Bioenergetics, Exerts Cytoprotective Effects and Protects against the Loss of Mitochondrial DNA Integrity in Oxidatively Stressed Endothelial Cells in Vitro. *Nitric Oxide* **2014**, *41*, 120–130.

(129) Banu, S. A.; Ravindran, S.; Kurian, G. A. Hydrogen Sulfide Post-Conditioning Preserves Interfibrillar Mitochondria of Rat Heart during Ischemia Reperfusion Injury. *Cell Stress Chaperones* **2016**, *21* (4), 571–582.

(130) GUO, Z.; LI, C. S.; WANG, C. M.; XIE, Y. J.; WANG, A. L. CSE/H2S System Protects Mesenchymal Stem Cells from Hypoxia and Serum Deprivation-Induced Apoptosis via Mitochondrial Injury, Endoplasmic Reticulum Stress and PI3K/Akt Activation Pathways. *Mol. Med. Rep.* **2015**, *12* (2), 2128–2134.

(131) Módis, K.; Asimakopoulou, A.; Coletta, C.; Papapetropoulos, A.; Szabo, C. Oxidative Stress Suppresses the Cellular Bioenergetic Effect of the 3-Mercaptopyruvate Sulfurtransferase/Hydrogen Sulfide Pathway. *Biochem. Biophys. Res. Commun.* **2013**, *433* (4), 401–407.

(132) Módis, K.; Coletta, C.; Erdélyi, K.; Papapetropoulos, A.; Szabo, C. Intramitochondrial

Hydrogen Sulfide Production by 3-Mercaptopyruvate Sulfurtransferase Maintains Mitochondrial Electron Flow and Supports Cellular Bioenergetics. *FASEB J.* **2013**, *27* (2), 601–611.

(133) Jamroz-Wiśniewska, A.; Gertler, A.; Solomon, G.; Wood, M. E.; Whiteman, M.; Bełtowski, J. Leptin-Induced Endothelium-Dependent Vasorelaxation of Peripheral Arteries in Lean and Obese Rats: Role of Nitric Oxide and Hydrogen Sulfide. *PLoS One* **2014**, *9* (1), e86744.

(134) Candela, J.; Velmurugan, G. V.; White, C. Hydrogen Sulfide Depletion Contributes to Microvascular Remodeling in Obesity. *Am. J. Physiol. Circ. Physiol.* **2016**, *310* (9), H1071–H1080.

(135) Velmurugan, G. V.; Huang, H.; Sun, H.; Candela, J.; Jaiswal, M. K.; Beaman, K. D.; Yamashita, M.; Prakriya, M.; White, C. Depletion of H_2S during Obesity Enhances Store-Operated Ca^{2+} Entry in Adipose Tissue Macrophages to Increase Cytokine Production. *Sci. Signal.* **2015**, *8* (407), ra128–ra128.

(136) Geng, B.; Cai, B.; Liao, F.; Zheng, Y.; Zeng, Q.; Fan, X.; Gong, Y.; Yang, J.; Cui, Q. hua; Tang, C.; et al. Increase or Decrease Hydrogen Sulfide Exert Opposite Lipolysis, but Reduce Global Insulin Resistance in High Fatty Diet Induced Obese Mice. *PLoS One* **2013**, *8* (9), e73892.

(137) Whiteman, M.; Gooding, K. M.; Whatmore, J. L.; Ball, C. I.; Mawson, D.; Skinner, K.; Tooke, J. E.; Shore, A. C. Adiposity Is a Major Determinant of Plasma Levels of the Novel Vasodilator Hydrogen Sulphide. *Diabetologia* **2010**, *53* (8), 1722–1726.

(138) Wei, Y.; Kenyon, C. Roles for ROS and Hydrogen Sulfide in the Longevity Response to Germline Loss in *Caenorhabditis Elegans*. *Proc. Natl. Acad. Sci.* **2016**, *113* (20), E2832–E2841.

(139) Li, L.; Li, M.; Li, Y.; Sun, W.; Wang, Y.; Bai, S.; Li, H.; Wu, B.; Yang, G.; Wang, R.; et al. Exogenous H2S Contributes to Recovery of Ischemic Post-Conditioning-Induced Cardioprotection by Decrease of ROS Level via down-Regulation of NF-KB and JAK2-STAT3 Pathways in the Aging Cardiomyocytes. *Cell Biosci.* **2016**, *6* (1), 26.

(140) Jin, S.; Pu, S.-X.; Hou, C.-L.; Ma, F.-F.; Li, N.; Li, X.-H.; Tan, B.; Tao, B.-B.; Wang, M.-J.; Zhu, Y.-C. Cardiac H_2S Generation Is Reduced in Ageing Diabetic Mice. *Oxid. Med. Cell. Longev.* **2015**, *2015*, 1–14.

(141) Yang, G.; An, S. S.; Ji, Y.; Zhang, W.; Pei, Y. Hydrogen Sulfide Signaling in Oxidative Stress and Aging Development. *Oxid. Med. Cell. Longev.* **2015**, *2015*, 1–2.

(142) Krejcova, T.; Smelcova, M.; Petr, J.; Bodart, J.-F.; Sedmikova, M.; Nevoral, J.;

Dvorakova, M.; Vyskocilova, A.; Weingartova, I.; Kucerova-Chrpova, V.; et al. Hydrogen Sulfide Donor Protects Porcine Oocytes against Aging and Improves the Developmental Potential of Aged Porcine Oocytes. *PLoS One* **2015**, *10* (1), e0116964.

(143) Qabazard, B.; Ahmed, S.; Li, L.; Arlt, V. M.; Moore, P. K.; Stürzenbaum, S. R. C. Elegans Aging Is Modulated by Hydrogen Sulfide and the Sulfhydrylase/Cysteine Synthase Cysl-2. *PLoS One* **2013**, *8* (11), e80135.

(144) Qabazard, B.; Li, L.; Gruber, J.; Peh, M. T.; Ng, L. F.; Kumar, S. D.; Rose, P.; Tan, C.-H.; Dymock, B. W.; Wei, F.; et al. Hydrogen Sulfide Is an Endogenous Regulator of Aging in *Caenorhabditis Elegans*. *Antioxid. Redox Signal.* **2014**, *20* (16), 2621–2630.

(145) Whiteman, M.; Armstrong, J. S.; Chu, S. H.; Jia-Ling, S.; Wong, B.-S.; Cheung, N. S.; Halliwell, B.; Moore, P. K. The Novel Neuromodulator Hydrogen Sulfide: An Endogenous Peroxynitrite "Scavenger"? *J. Neurochem.* **2004**, *90* (3), 765–768.

(146) Whiteman, M.; Cheung, N. S.; Zhu, Y.-Z.; Chu, S. H.; Siau, J. L.; Wong, B. S.; Armstrong, J. S.; Moore, P. K. Hydrogen Sulphide: A Novel Inhibitor of Hypochlorous Acid-Mediated Oxidative Damage in the Brain? *Biochem. Biophys. Res. Commun.* **2005**, *326* (4), 794–798.

(147) Filipovic, M. R. Persulfidation (S-Sulfhydration) and H2S; 2015; pp 29–59.

(148) Mustafa, A. K.; Gadalla, M. M.; Sen, N.; Kim, S.; Mu, W.; Gazi, S. K.; Barrow, R. K.; Yang, G.; Wang, R.; Snyder, S. H. H2S Signals Through Protein S-Sulfhydration. *Sci. Signal.* **2009**, *2* (96), ra72–ra72.

(149) Cortese-Krott, M. M.; Kuhnle, G. G. C.; Dyson, A.; Fernandez, B. O.; Grman, M.; DuMond, J. F.; Barrow, M. P.; McLeod, G.; Nakagawa, H.; Ondrias, K.; et al. Key Bioactive Reaction Products of the NO/H $_2$ S Interaction Are S/N-Hybrid Species, Polysulfides, and Nitroxyl. *Proc. Natl. Acad. Sci.* **2015**, *112* (34), E4651–E4660.

(150) Whiteman, M.; Li, L.; Kostetski, I.; Chu, S. H.; Siau, J. L.; Bhatia, M.; Moore, P. K. Evidence for the Formation of a Novel Nitrosothiol from the Gaseous Mediators Nitric Oxide and Hydrogen Sulphide. *Biochem. Biophys. Res. Commun.* **2006**, *343* (1), 303–310.

(151) Pryor, W. A.; Houk, K. N.; Foote, C. S.; Fukuto, J. M.; Ignarro, L. J.; Squadrito, G. L.; Davies, K. J. A. Free Radical Biology and Medicine: It's a Gas, Man! *Am. J. Physiol. Integr. Comp. Physiol.* **2006**, *291* (3), R491–R511.

(152) Li, L.; Rose, P.; Moore, P. K. Hydrogen Sulfide and Cell Signaling. *Annu. Rev. Pharmacol. Toxicol.* **2011**, *51* (1), 169–187.

(153) Kang, J.; Neill, D. L.; Xian, M. Phosphonothioate-Based Hydrogen Sulfide Releasing

Reagents: Chemistry and Biological Applications. *Front. Pharmacol.* **2017**, *8*, 457.

(154) Zhao, Y.; Pluth, M. D. Hydrogen Sulfide Donors Activated by Reactive Oxygen Species. *Angew. Chemie Int. Ed.* **2016**, *55* (47), 14638–14642.

(155) Chauhan, P.; Jos, S.; Chakrapani, H. Reactive Oxygen Species-Triggered Tunable Hydrogen Sulfide Release. *Org. Lett.* **2018**, *20* (13), 3766–3770.

(156) Shukla, P.; Khodade, V. S.; SharathChandra, M.; Chauhan, P.; Mishra, S.; Siddaramappa, S.; Pradeep, B. E.; Singh, A.; Chakrapani, H. "On Demand" Redox Buffering by H_2S Contributes to Antibiotic Resistance Revealed by a Bacteria-Specific H_2S Donor. *Chem. Sci.* **2017**, *8* (7), 4967–4972.

(157) Landar, A.; Darley-Usmar, V. M. Nitric Oxide and Cell Signaling; Modulation of Redox Tone and Protein Modification. *Amino Acids* **2003**, *25* (3–4), 313–321.

(158) Shen, H.-M.; Liu, Z. JNK Signaling Pathway Is a Key Modulator in Cell Death Mediated by Reactive Oxygen and Nitrogen Species. *Free Radic. Biol. Med.* **2006**, *40* (6), 928–939.

(159) Mikkelsen, R. B.; Wardman, P. Biological Chemistry of Reactive Oxygen and Nitrogen and Radiation-Induced Signal Transduction Mechanisms. *Oncogene* **2003**, *22* (37), 5734–5754.

(160) Forman, H. J.; Fukuto, J. M.; Torres, M. Redox Signaling: Thiol Chemistry Defines Which Reactive Oxygen and Nitrogen Species Can Act as Second Messengers. *Am. J. Physiol. Physiol.* **2004**, *287* (2), C246–C256.

(161) Vaváková, M.; Ďuračková, Z.; Trebatická, J. Markers of Oxidative Stress and Neuroprogression in Depression Disorder. *Oxid. Med. Cell. Longev.* **2015**, *2015*, 898393.

(162) Olas, B.; Wachowicz, B. Role of Reactive Nitrogen Species in Blood Platelet Functions. *Platelets* **2007**, *18* (8), 555–565.

(163) Singh, P. P.; Mahadi, F.; Roy, A.; Sharma, p. Reactive oxygen species, reactive nitrogen species and antioxidants in etiopathogenesis of diabetes mellitus type-2, **2009**, 24.

(164) Eiserich, J. P.; Patel, R. P.; O'Donnell, V. B. Pathophysiology of Nitric Oxide and Related Species: Free Radical Reactions and Modification of Biomolecules. *Mol. Aspects Med. 19* (4–5), 221–357.

(165) Martínez, M. C.; Andriantsitohaina, R. Reactive Nitrogen Species: Molecular Mechanisms and Potential Significance in Health and Disease. *Antioxid. Redox Signal.* **2009**, *11* (3), 669–702.

(166) Di Simplicio, P.; Franconi, F.; Frosalí, S.; Di Giuseppe, D. Thiolation and Nitrosation

of Cysteines in Biological Fluids and Cells. *Amino Acids* **2003**, *25* (3–4), 323–339.

(167) Winterbourn, C. C.; Hampton, M. B. Thiol Chemistry and Specificity in Redox Signaling. *Free Radic. Biol. Med.* **2008**, *45* (5), 549–561.

(168) Zheng, N.; Liu, L.; Liu, W.; Li, F.; Hayashi, T.; Tashiro, S.; Onodera, S.; Ikejima, T. Crosstalk of ROS/RNS and Autophagy in Silibinin-Induced Apoptosis of MCF-7 Human Breast Cancer Cells in Vitro. *Acta Pharmacol. Sin.* **2017**, *38* (2), 277–289.

(169) Bubici, C.; Papa, S.; Dean, K.; Franzoso, G. Mutual Cross-Talk between Reactive Oxygen Species and Nuclear Factor-Kappa B: Molecular Basis and Biological Significance. *Oncogene* **2006**, *25* (51), 6731–6748.

(170) Gordeeva, A. V; Zvyagilskaya, R. A.; Labas, Y. A. Cross-Talk between Reactive Oxygen Species and Calcium in Living Cells. *Biochemistry. (Mosc).* **2003**, *68* (10), 1077–1080.

(171) Lindermayr, C. Crosstalk between Reactive Oxygen Species and Nitric Oxide in Plants: Key Role of *S*-Nitrosoglutathione Reductase. *Free Radic. Biol. Med.* **2018**, *122*, 110–115.

(172) Kolbert, Z.; Feigl, G. Cross-Talk of Reactive Oxygen Species and Nitric Oxide in Various Processes of Plant Development. In *Reactive Oxygen Species in Plants*; John Wiley & Sons, Ltd: Chichester, UK, **2017**, 261–289.

(173) Zhao, J. Interplay among Nitric Oxide and Reactive Oxygen Species: A Complex Network Determining Cell Survival or Death. *Plant Signal. Behav.* **2007**, *2* (6), 544–547.

(174) Il'ichev, Y. V; Schwö, M. A.; Wirz, J. Photochemical Reaction Mechanisms of 2-Nitrobenzyl Compounds: Methyl Ethers and Caged ATP. *J. Am. Chem. Soc.* **2004**, *126* (14), 4581–4595.

(175) Fukushima, N.; Ieda, N.; Kawaguchi, M.; Sasakura, K.; Nagano, T.; Hanaoka, K.; Miyata, N.; Nakagawa, H. Development of Photo-Controllable Hydrogen Sulfide Donor Applicable in Live Cells. *Bioorg. Med. Chem. Lett.* **2015**, *25* (2), 175–178.

(176) Zhao, Y.; Bolton, S. G.; Pluth, M. D. Light-Activated COS/H2S Donation from Photocaged Thiocarbamates. *Org. Lett.* **2017**, *19* (9), 2278–2281.

(177) Linsley, C. S.; Wu, B. M. Recent Advances in Light-Responsive on-Demand Drug-Delivery Systems. *Ther. Deliv.* **2017**, *8* (2), 89–107.

(178) Fukushima, N.; Ieda, N.; Sasakura, K.; Nagano, T.; Hanaoka, K.; Suzuki, T.; Miyata, N.; Nakagawa, H. Synthesis of a Photocontrollable Hydrogen Sulfide Donor Using Ketoprofenate Photocages. *Chem. Commun.* **2014**, *50* (5), 587–589.

(179) Hansen, M. J.; Velema, W. A.; Lerch, M. M.; Szymanski, W.; Feringa, B. L. Wavelength-Selective Cleavage of Photoprotecting Groups: Strategies and Applications in Dynamic Systems. *Chem. Soc. Rev.* **2015**, *44*, 3358.

(180) Chalmers, S.; Caldwell, S. T.; Quin, C.; Prime, T. A.; James, A. M.; Cairns, A. G.; Murphy, M. P.; McCarron, J. G.; Hartley, R. C. Selective Uncoupling of Individual Mitochondria within a Cell Using a Mitochondria-Targeted Photoactivated Protonophore. *J. Am. Chem. Soc.* **2012**, *134* (2), 758–761.

(181) Akinobu Z. Suzuki; Takayoshi Watanabe; Mika Kawamoto; Keiko Nishiyama; Hirotaka Yamashita; Megumi Ishii; Michiko Iwamura, and; Furuta*, T. Coumarin-4-Ylmethoxycarbonyls as Phototriggers for Alcohols and Phenols. *Oragani Lett.* **2003**, *5* (25), 4867–4870.

(182) and, O. D. F.; Dore, T. M. Brominated Hydroxyquinoline as a Photolabile Protecting Group with Sensitivity to Multiphoton Excitation. *Org. Lett.* **2002**, *4* (20), 3419–3422.

(183) Peter G. Conrad II; Richard S. Givens, *; Jörg F. W. Weber, and; Kandler†, K. New Phototriggers:1 Extending the p-Hydroxyphenacyl Π−π* Absorption Range. *Org. Lett.* **2000**, *2* (11), 1545–1547.

(184) and, M. L.; Scaiano*, J. C. Carbanion-Mediated Photocages: Rapid and Efficient Photorelease with Aqueous Compatibility. *J. Am. Chem. Soc.* **2005**, *127* (21), 7698–7699.

(185) and, M. P. C.; Boyd, M. K. S-Pixyl Analogues as Photocleavable Protecting Groups for Nucleosides. *J. Org. Chem.* **2002**, *67* (22), 7641–7648.

(186) Toshiaki Furuta, Yuuki Hirayama, M. I. Anthraquinon-2-Ylmethoxycarbonyl (Aqmoc): A New Photochemically Removable Protecting Group for Alcohols. *Org. Lett.* **2001**, *3* (12), 1809–1812.

(187) Papageorgiou, G.; Barth, A.; Corrie, J. E. T. Flash Photolytic Release of Alcohols from Photolabile Carbamates or Carbonates Is Rate-Limited by Decarboxylation of the Photoproduct. *Photochem. Photobiol. Sci.* **2005**, *4* (2), 216.

(188) Jana Pika, Armands Konosonoks, Rachel M. Robinson, Pradeep N. D. Singh, and Anna D. Gudmundsdottir, Photoenolization as a Means To Release Alcohols. *J. Org. Chem.* **2003**, *68* (5), 1964–1972.

(189) A. K. S.; Khade, P. K. Synthesis and Photochemical Properties of Nitro-Naphthyl Chromophore and the Corresponding Immunoglobulin Bioconjugate. *Bioconjug. Chem.* **2002**, *13* (6), 1286–1291.

(190) Walters N. Atemnkeng; Larry D. Louisiana II; Promise K. Yong; Breanne Vottero, and;

Banerjee*, A. 1-[2-(2-Hydroxyalkyl)Phenyl]Ethanone: A New Photoremovable Protecting Group for Carboxylic Acids. *Org. Lett.* **2003**, *5* (23), 4469–4471.

(191) Anamitro Banerjee, Christof Grewer, Latha Ramakrishnan, Jürgen Jäger, Armanda Gameiro, Hans-Georg A. Breitinger, Kyle R. Gee, Barry K. Carpenter, and George P. Hess. Toward the Development of New Photolabile Protecting Groups That Can Rapidly Release Bioactive Compounds upon Photolysis with Visible Light. *J. Org. Chem.* **2003**, *68* (22), 8361–8367.

(192) Devarie-Baez, N. O.; Bagdon, P. E.; Peng, B.; Zhao, Y.; Park, C.-M.; Xian, M. Light-Induced Hydrogen Sulfide Release from "Caged" Gem-Dithiols. *Org. Lett.* **2013**, *15* (11), 2786–2789.

(193) Xiao, Z.; Bonnard, T.; Shakouri-Motlagh, A.; Wylie, R. A. L.; Collins, J.; White, J.; Heath, D. E.; Hagemeyer, C. E.; Connal, L. A. Triggered and Tunable Hydrogen Sulfide Release from Photogenerated Thiobenzaldehydes. *Chem. - A Eur. J.* **2017**, *23* (47), 11294–11300.

(194) Jackson, D. A.; Hassan, A. B.; Errington, R. J.; Cook, P. R. Oxidative Stress Is Involved in the UV Activation of P53. *J. Cell Sci.* **1996**, *107* (7), 1753–1760.

(195) Zhang, X.; Rosenstein, B. S.; Wang, Y.; Lebwohl, M.; Wei, H. Identification of Possible Reactive Oxygen Species Involved in Ultraviolet Radiation-Induced Oxidative DNA Damage. *Free Radic. Biol. Med.* **1997**, *23* (7), 980–985.

(196) Heck, D. E.; Vetrano, A. M.; Mariano, T. M.; Laskin, J. D. UVB Light Stimulates Production of Reactive Oxygen Species. *J. Biol. Chem.* **2003**, *278* (25), 22432–22436.

(197) Bossi, O.; Gartsbein, M.; Leitges, M.; Kuroki, T.; Grossman, S.; Tennenbaum, T. UV Irradiation Increases ROS Production via PKCδ Signaling in Primary Murine Fibroblasts. *J. Cell. Biochem.* **2008**, *105* (1), 194–207.

(198) de Jager, T. L.; Cockrell, A. E.; Du Plessis, S. S. Ultraviolet Light Induced Generation of Reactive Oxygen Species; Springer, Cham, 2017; pp 15–23.

(199) J. Brian Borak; Susana López-Sola, A.; Falvey, D. E. Photorelease of Carboxylic Acids Mediated by Visible-Light-Absorbing Gold-Nanoparticles. *Org. Lett.* **2007**, *10* (3), 457–460.

(200) Borak, J. B.; Falvey, D. E. A New Photolabile Protecting Group for Release of Carboxylic Acids by Visible-Light-Induced Direct and Mediated Electron Transfer. *J. Org. Chem.* **2009**, *74* (10), 3894–3899.

(201) Antony, L. A. P.; Slanina, T.; Šebej, P.; Šolomek, T.; Klán, P. Fluorescein Analogue Xanthene-9-Carboxylic Acid: A Transition-Metal-Free CO Releasing Molecule

Activated by Green Light. *Org. Lett.* **2013**, *15* (17), 4552–4555.

(202) Filevich, O.; Etchenique, R. RuBiGABA-2: A Hydrophilic Caged GABA with Long Wavelength Sensitivity. *Photochem. Photobiol. Sci.* **2013**, *12* (9), 1565.

(203) Zayat, L.; Noval, M. G.; Campi, J.; Calero, C. I.; Calvo, D. J.; Etchenique, R. A New Inorganic Photolabile Protecting Group for Highly Efficient Visible Light GABA Uncaging. *ChemBioChem* **2007**, *8* (17), 2035–2038.

(204) Rial Verde, E. M.; Zayat, L.; Etchenique, R.; Yuste, R. Photorelease of GABA with Visible Light Using an Inorganic Caging Group. *Front. Neural Circuits* **2008**, *2*, 2.

(205) DeRosa, M. C.; Crutchley, R. J. Photosensitized Singlet Oxygen and Its Applications. *Coord. Chem. Rev.* **2002**, *233–234*, 351–371.

(206) Olson, J. P.; Banghart, M. R.; Sabatini, B. L.; Ellis-Davies, G. C. R. Spectral Evolution of a Photochemical Protecting Group for Orthogonal Two-Color Uncaging with Visible Light. *J. Am. Chem. Soc.* **2013**, *135* (42), 15948–15954.

(207) Fournier, L.; Gauron, C.; Xu, L.; Aujard, I.; Le Saux, T.; Gagey-Eilstein, N.; Maurin, S.; Dubruille, S.; Baudin, J.-B.; Bensimon, D.; et al. A Blue-Absorbing Photolabile Protecting Group for *in Vivo* Chromatically Orthogonal Photoactivation. *ACS Chem. Biol.* **2013**, *8* (7), 1528–1536.

(208) Agostinis, P.; Berg, K.; Cengel, K. A.; Foster, T. H.; Girotti, A. W.; Gollnick, S. O.; Hahn, S. M.; Hamblin, M. R.; Juzeniene, A.; Kessel, D.; et al. Photodynamic Therapy of Cancer: An Update. *CA. Cancer J. Clin.* **2011**, *61* (4), 250–281.

(209) Yi, S. Y.; Moon, Y. K.; Kim, S.; Kim, S.; Park, G.; Kim, J. J.; You, Y. Visible Light-Driven Photogeneration of Hydrogen Sulfide. *Chem. Commun.* **2017**, *53* (86), 11830–11833.

(210) Benchoam, D.; Cuevasanta, E.; Möller, M.; Alvarez, B. Hydrogen Sulfide and Persulfides Oxidation by Biologically Relevant Oxidizing Species. *Antioxidants* **2019**, *8* (2), 48.

(211) Venkatesh, Y.; Das, J.; Chaudhuri, A.; Karmakar, A.; Maiti, T. K.; Singh, N. D. P. Light Triggered Uncaging of Hydrogen Sulfide (H_2S) with Real-Time Monitoring. *Chem. Commun.* **2018**, *54* (25), 3106–3109.

(212) Woods, J. J.; Cao, J.; Lippert, A. R.; Wilson, J. J. Characterization and Biological Activity of a Hydrogen Sulfide-Releasing Red Light-Activated Ruthenium(II) Complex. *J. Am. Chem. Soc.* **2018**, *140* (39), 12383–12387.

(213) Štacko, P.; Muchová, L.; Vítek, L.; Klán, P. Visible to NIR Light Photoactivation of Hydrogen Sulfide for Biological Targeting. *Org. Lett.* **2018**, *20* (16), 4907–4911.

(214) Nakashima, Y.; Ohta, S.; Wolf, A. M. Blue Light-Induced Oxidative Stress in Live Skin. *Free Radic. Biol. Med.* **2017**, *108*, 300–310.

Chapter 2. UV Light Triggerable ROS Generators

2.1 Introduction

Reactive oxygen species (ROS) such as superoxide radical anion ($O_2^{\bullet-}$) are majorly produced in mitochondria during the aerobic metabolism by leakage of an electron from the electron transport chain (ETC).[1,2] This ROS diffuses to the cytoplasm and regulates several signaling pathways[3] in cells and maintains its integrity at the homeostatic level; this state is termed redox homeostasis. During episodes of disease or cellular dysfunction, levels of ROS escalate. This situation induces stress in the cell and is frequently referred to as oxidative stress.[3–7] Oxidative stress is also stimulated when cells are treated with exogenous ROS generators such as juglone,[8] menadione,[9,10] β-lapachone,[11–14] paraquat,[15–20] etc. This, in turn, can lead to protein oxidation, lipid peroxidation and double strand breaks in DNA, thereby resulting in cell death.

In pursuit of cancer therapeutics, there is a growing demand for developing new interventional strategies. Perturbing the oxidative species levels in tumor[5,21,22] is one of the emerging strategies to inhibit proliferation. For instance, photodynamic therapy (PDT)[23–25] is one such method where oxidative species is elevated leading to cell apoptosis. In PDT, a photosensitizer that produces singlet oxygen upon irradiation is used thereby leading to an increase in the ROS levels which damages essential biomolecules in cellular system and thereupon resulting in cell death. Herein, we propose to explore the concept of enhancing ROS in cells by generating superoxide ($O_2^{\bullet-}$) which dismutase to hydrogen peroxide (H_2O_2) followed by hydroxyl radical (ȮH) which may lead to cell death. These ROS can be generated by several methods using various metabolic stimuli such as bioreductive,[26] thiols,[27] esterase enzyme,[28] *etc*. Alternatively, we plan to generate ROS employing light as a stimulus to gain improved handle over localization and intensity of light which governs the rate of release for a molecule. These approach has gained a lot of interest in drug delivery systems where spatiotemporally controlled delivery can be achieved by a photoactivatable prodrug concept.[29–35]

The efforts of releasing $O_2^{\bullet-}$ using light as a trigger, have been initiated by Chang and co-workers[36]. They used the 2-nitrobenzyl group as a photoactivable moiety and 1,2,4-trihydroxybenzene as ROS generator (Scheme 2.1). Moreover, formation of cofilin/actin rod which is symptomatic of increased level of ROS within cells has also been shown by the same group. But there are certain drawbacks to this approach:

1. Deployment of 304 nm UV light can cause oxidative stress[37–41] because of radiation-biomolecule interaction, which is undesirable in biological applications
2. This strategy cannot be used to target cancers since the ROS generator used is not efficient in ROS generation hence does not result in inhibition of cell proliferation
3. The end product formed after ROS generation can react with cellular thiols which complicates interpretations.[42]

Here, a molecule needs to be designed which would release ROS generator upon irradiation and possess following properties:
1. Stable in buffer
2. Efficient in generating ROS
3. ROS donor or its end product should not react with thiols

Scheme 2.1. UV light activated H_2O_2 release where trihydroxybenzene was used as ROS generator and 2-nitro benzyl as a photo-cleavable linker

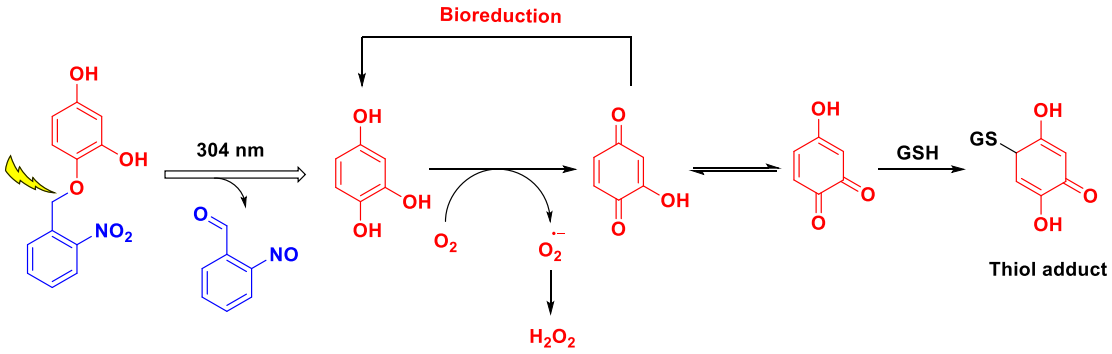

In most ROS generators, either a 1,4- or 1,2-quinone functional group is bioreductively converted to its hydroquinone counterpart.[43–46] These electron rich hydroquinones react with molecular oxygen and are revert back to quinones, concomitantly generating ROS. These quinones, for example, juglone and menadione have an α,β-unsaturated site where thiols can react in a 1,4-Michael fashion to form thiol adducts.[42] These thiol adducts can either be effluxed out of the cells as a detoxification mechanism[42] or can further generate ROS. Furthermore, important cysteine residues can be covalently modified by quinones and crucial pathways can eventually be affected *in situ*.[42] In such scenario, the observed phenotype may not be due to ROS generation alone. Therefore, to overcome the problems due to off-site reactivity of ROS generators, an ROS releasing molecule need to be chosen which would not react with cellular thiols thereby obtained results may only be due to the ROS generation.

Thiol reactivity with juglone and menadione could be due to easy accessibility to the less hindered α, β-unsaturated site. Here, rationale is to design a ROS donor having relatively more hindered α, β-unsaturated site which may not be accessible by thiols. As known in the literature that compound **1**, a Diels-Alder adduct of juglone[47] converts to compound **2,** a quinone derivative after ROS generation. In compound **2,** α,β-unsaturated site of quinone is more hindered and hence may not accessible to thiols while, compound **1** is not a candidate for thiol attack in the absence of α, β-unsaturated site [28] (Scheme 2.2).

Scheme 2.2. Representative scheme for thiol reaction with known ROS generators

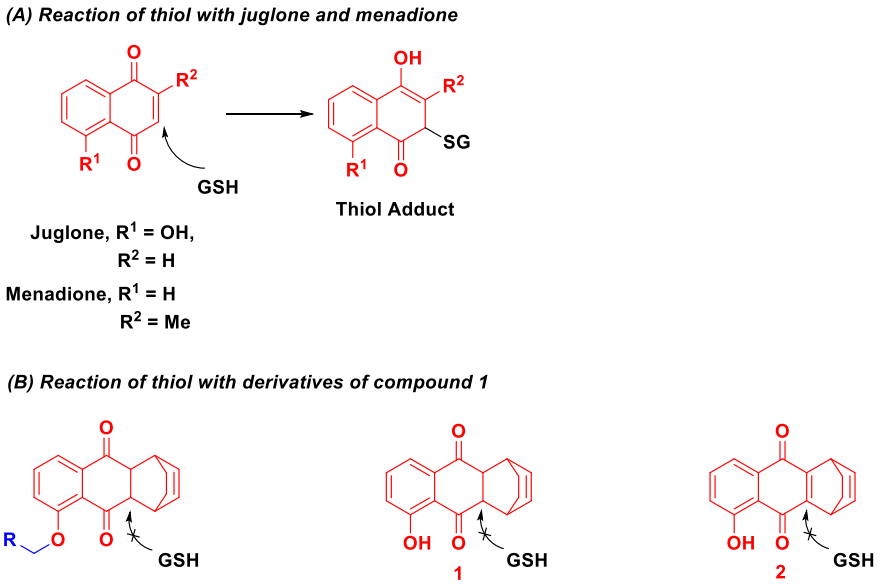

As it is known that compound **1** generates ROS in buffer, only when its hydroxyl group is in free from, if this hydroxy is protected, the resulting scaffold shows diminished ROS generating capacity.[47] Using this concept, the phenolic group of compound **1** can be protected with a suitable trigger for selective activation to generate ROS in order to reduce its off-site activity. The efforts of selective activation to release compound **1** as ROS generating molecule were made in our lab where 4-nitro benzyl moiety, a substrate of nitroreductase (NTR) enzyme was used to protect hydroxyl group of compound **1** (Scheme 2.3). Nitro group of the protected compound metabolizes in the presence of NTR to produce amine/hydroxylamine derivative as intermediates, which upon self-immolation releases compound **1**.[48] Further, this compound **1** reacts with oxygen to produce ROS.

Scheme 2.3. Activation methods to release compound **1**

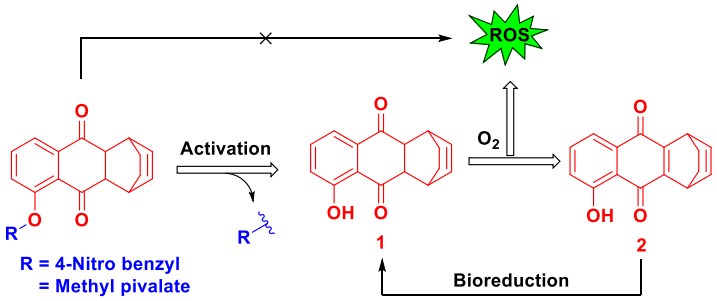

Recently, an ester was used to protect hydroxyl group of compound **1**, which hydrolyses in the presence of an esterase to release compound **1**, which further produces ROS[28] (Scheme 2.3). These studies suggest that compound **1** and its quinone counterpart **2** have diminished reactivity with thiol and also can be released in a selective manner if phenolic group is masked with a suitable trigger. Inspired by these approaches, phenolic group of compound **1** can be protected with light triggerable linker, 2-nitrobenzyl which may release compound **1** in the presence of light to generate ROS.

2.2 Design

To design a photo responsive ROS generator, the free phenolic group of **1** can be protected by a functional group that can be cleaved under light conditions. To carry out this, the phenolic group of compound **1** can be attach with 2-nitrobenzyl moiety which is known to cleave under light conditions and can release a phenolate.[33,34,49–52] Apart from this, the biotin moiety can also be incorporated in this ROS generator to facilitate the accumulation of the molecule in the cancer cells over normal cells[53–56] (Scheme 2.4). As it is known that cancer cells rapidly multiply and need nutrition in higher amount than the normal cells. To meet this criteria, cancer cells have evolved with overexpressed vitamin receptors that facilitate enhanced accumulation of vitamin molecules in cancer cells than the normal cells.[53] Thus, attaching a biotin molecule to ROS donor might enhance the uptake as well as increases the buffer solubility of this compound up to several folds.

Scheme 2.4. Design of Light activatable ROS Generator

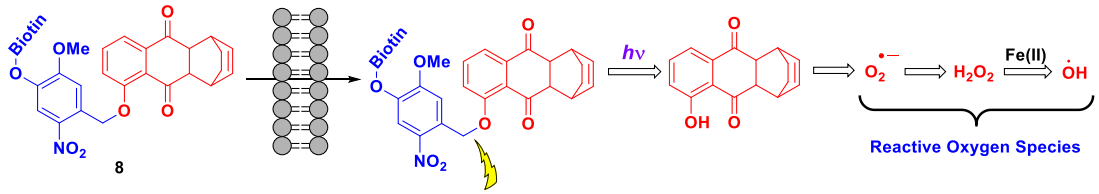

The designed compound must be stable in cell growth media and should not produce ROS under the dark condition while the attached biotin moiety might help the compound to localized intracellularly. When compound treated cells will be irradiated under 365 nm light it might release compound **1** which should react with oxygen to produce $O_2^{\bullet-}$. This $O_2^{\bullet-}$ either reacts with SOD or disproportionate to produce H_2O_2. In the cellular system trace metal ions, *i.e.*, Fe(II) and Cu(I) are present which can react with H_2O_2 to form a highly reactive ROS, hydroxyl radical (ȮH). This ȮH can damage essential biomolecules of cell that might result into the cell death.

2.3 Results and Discussion

2.3.1 Synthesis

Synthesis of the designed molecules were done in the multiple steps. Bromides **10** and **11** are commercially available and were used without any further purification. To synthesize compounds **4** and **5**, substitution reactions on bromides **10** and **11** with compound **1** were performed in the presence of Ag_2O, as it interacts with bromide to make it a better leaving group and hydroxyl group of compound **1** attacks on the carbon bearing bromide to get *O*-alkylated compounds **4** and **5**. However, the *C*-alkylated product **9** was observed when the bromide **11** was reacted with **1** (Scheme 2.5). Friedel-Crafts *C*-alkylation with phenols is known. Here, both *ortho*- as well as *para*- substituted products are formed. In our hands, the *ortho*- substituted product was only observed (Scheme 2.6). This is likely due to the 4- position (*para* position) is in the resonance with the carbonyl, an electron withdrawing group hence has lesser electron density. However, the 2-position is resonating with hydroxyl group and hence is more electron rich which could resulting in the nucleophilic attack at the carbon bearing bromide to give the *C*-alkylated product.

Scheme 2.5. Reaction of bromides **10** and **11** with compound **1**

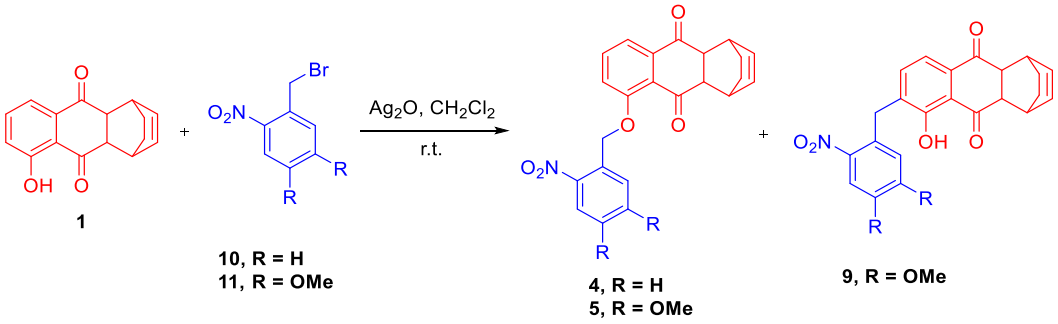

Scheme 2.6. Plausible mechanism of formation of *C* and *O*- Alkylated products

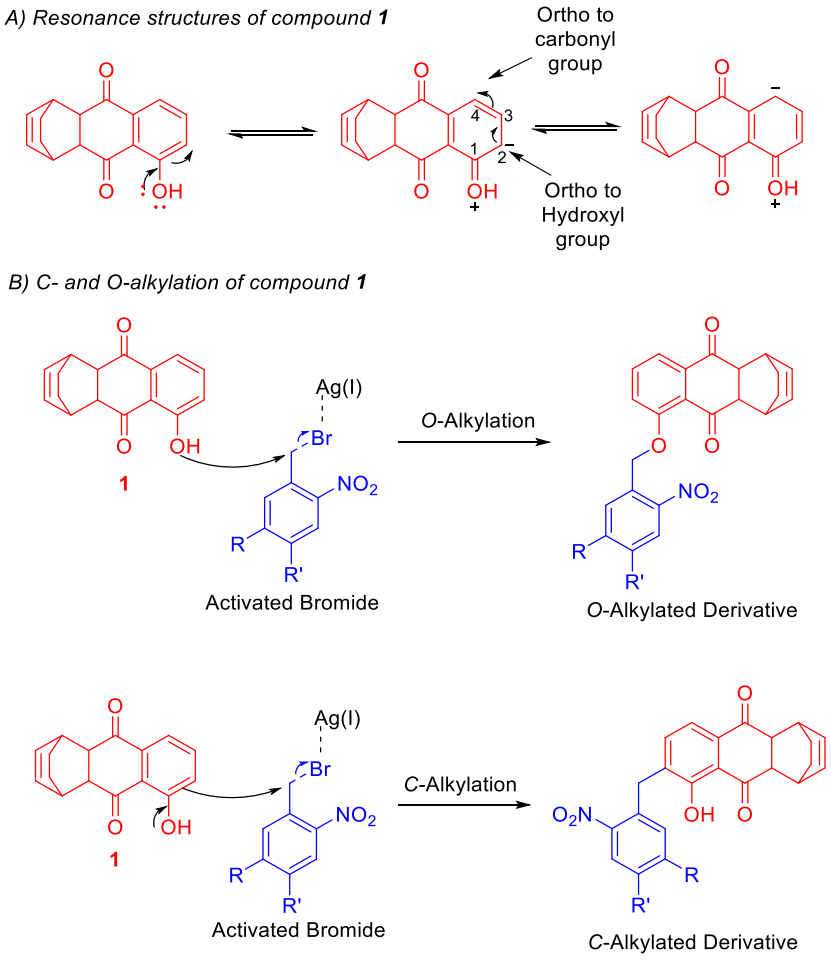

Next, a bromide with an alkyne functionality appended was synthesized, which may provide a handle for alkyne-azide click reaction to attach a biotin moiety. In order to synthesize an alkyne appended bromide **12**,[57] synthesis was started from commercially available vanillin **14**, which was reacted with propargyl bromide to get propargylated-vanillin **15** in 82% yield.

This compound **15** was further nitrated with nitric acid to obtained **16** in 84% yield. The sodium borohydride mediated reduction of compound **16** gave alcohol **17** in 94% yield. Further, the alcohol **17** was brominated in the presence of PBr_3 to obtain compound **12** as a white solid (Scheme 2.7). In order to synthesize compound **6**, bromide **12** was reacted with compound **1** in the presence of Ag_2O with dichloromethane as solvent, but did not yield the desired compound **6** (Scheme 2.8). The possible reason being the interaction of alkyne with Ag_2O,[58] resulting in the formation of a complex that was insoluble in dichloromethane which may result in decreased reactivity of compound **1** with bromide **12**.

Scheme 2.7. Synthesis of bromide **12**

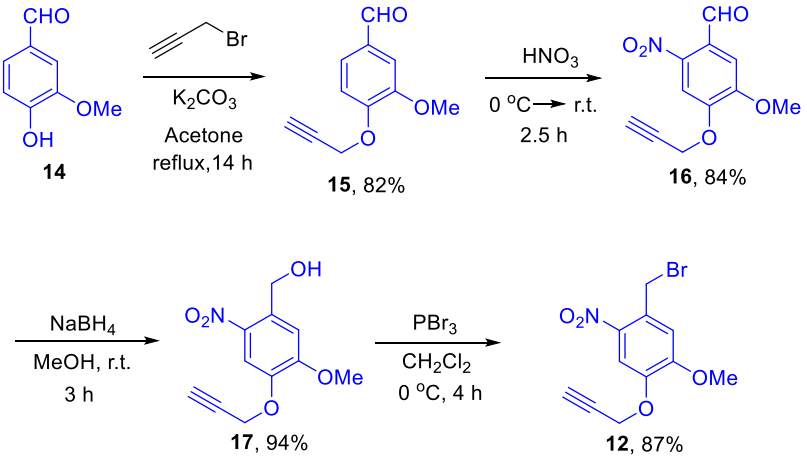

Scheme 2.8. Reaction of bromide **12** with compound **1**

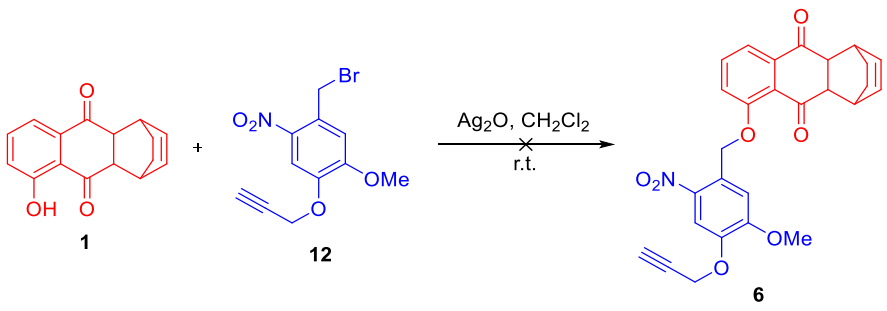

Unfortunately, an attempt of synthesizing compound **6** was failed and therefore as an alternative, a bromide **13** having an azide functionality which may be further utilized in the azide-alkyne click reaction to attach a biotin moiety, was synthesized in five linear steps (Scheme 2.9). The synthesis of **13** was started from commercially available vanillin **14**, which was reacted with 2-bromoethanol to get **18** as a white solid in moderate yield, which was further nitrated with the mixture of nitric acid, sulfuric acid and acetic acid to obtained compound **19**.

The compound **19** was then reacted with sodium azide to get **20**. Further, compound **20** was reduced in the presence of sodium borohydride to form an alcohol **21** in good yield. Next, alcohol **21** was brominated in the presence of PBr_3 to obtained bromide **13** as a white solid. Furthermore, bromide **13** was reacted with compound **1** in the presence of Ag_2O in dichloromethane at room temperature to obtained compound **7** in moderate yield (Scheme 2.10).

Scheme 2.9. Synthesis of bromide **13**

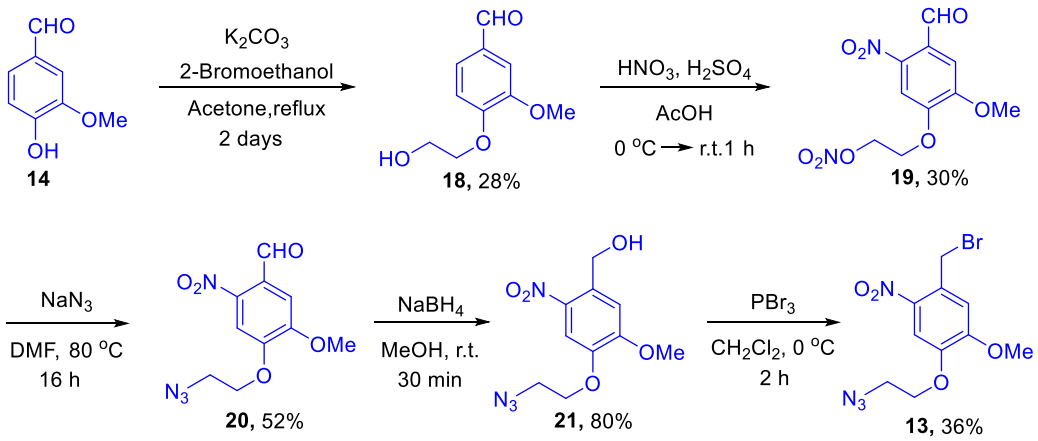

Scheme 2.10. Reaction of bromide **13** with compound **1**

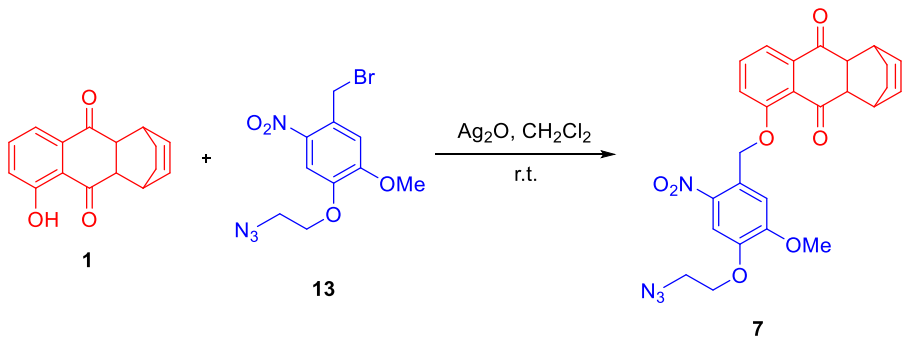

After synthesizing compound **7** bearing an azide moiety, a copper catalyzed alkyne-azide click reaction was carried out with propargylated-biotin **22** in the presence of sodium ascorbate and $CuSO_4$ to afford biotinylated compound **8** (Scheme 2.11). All the new compounds were fully characterized using ^{1}H-NMR, ^{13}C NMR, HRMS and IR techniques.

Scheme 2.11. Click reaction of Propargyl-biotin **22** with **7** to synthesize biotinylated photo-clevable ROS generator

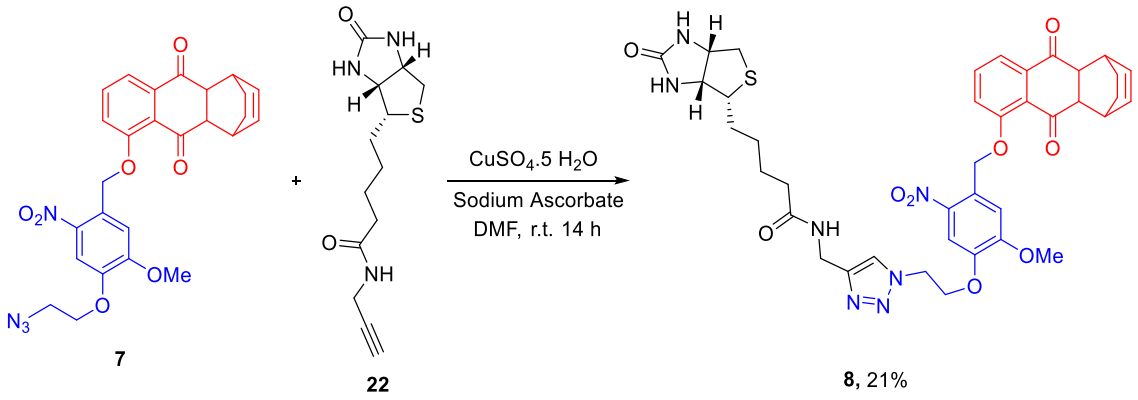

2.3.2 *In Vitro* Photolysis Study

To test the hypothesis of the release of compound **1** upon UV irradiation, compounds **4**, **5** and **8** were independently diluted in buffer:acetonitrile mixture and irradiated using 365 nm for 15 min and analyzed by reverse phase HPLC. As expected, it was found that compound **1** was released from 2-nitrobenzyl derivatives only after irradiation (Figure 2.1, Figure 2.2 and Figure **2.3**). However, all the compounds were stable and remain in their caged form under dark conditions. This study suggests that compounds were stable in dark and produce compound **1**, a ROS donor only in the presence of light.

Scheme 2.12. Mechanism of photolysis and ROS generation

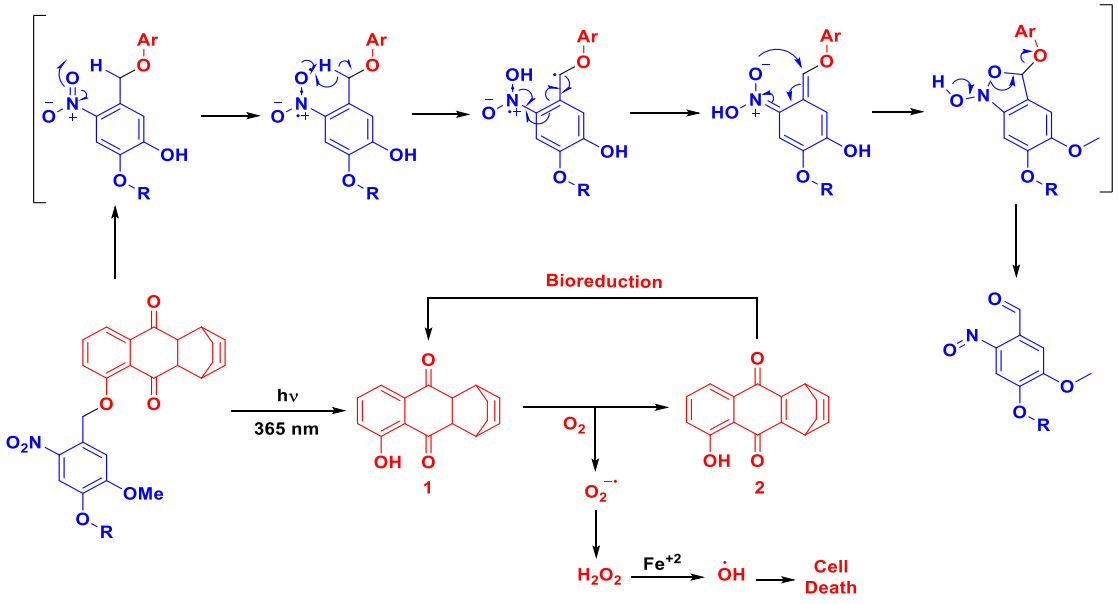

Figure 2.1. HPLC traces of photolysis study with compound **4** (50 µM) in the presence and absence of light

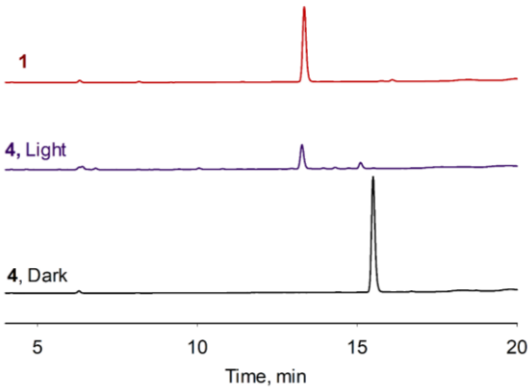

Figure 2.2. HPLC traces of photolysis study with compound **5** (50 µM) in the presence and absence of light

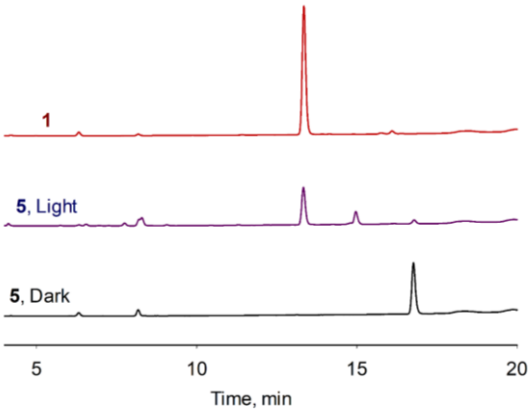

Figure 2.3. HPLC traces of photolysis study with compound **8** (50 µM) in the presence and absence of light

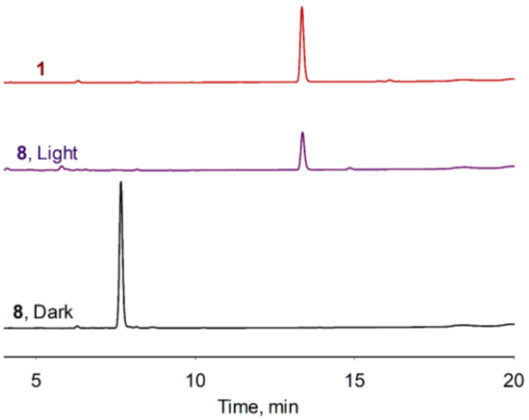

2.3.3 *In Vitro* ROS Detection

After performing the photolysis studies of **4, 5** and **8**, it was found that these compounds undergo cleavage upon irradiation with 365 nm UV light and release compound **1** which should react with oxygen to produce $O_2^{\bullet-}$. This $O_2^{\bullet-}$ should than be converted to H_2O_2. To detect these reactive species following assays have been performed.

2.3.3.1 Superoxide Detection Using DHE Assay

Dihydroethidium (DHE) is a dye which reacts with $O_2^{\bullet-}$ and other ROS species to form 2-hydroxyethidium (2-OH-E^+) and ethidium (E^+) respectively (Scheme 2.13).[47,48,59–64] These 2-OH-E^+ and E^+ species are fluorescent in nature and can be separated in HPLC and gives two distinct peaks. This assay has been performed with compounds **4**, **5** and **8** in the presence of light and an intense peak for 2-OH-E^+ was observed at 29.5 min only in the irradiated samples of these compounds. This signal was diminished when reaction mixture was treated with superoxide dismutase (SOD), a known quencher of $O_2^{\bullet-}$ which suggests that the signal which was observed in HPLC trace corresponds to $O_2^{\bullet-}$ (Figure 2.4, Figure 2.5 and Figure 2.6). The same experiment was also performed with these compounds in the absence of light and peaks for 2-OH-E^+ and E^+ were not observed. As a positive control, compound **1** was used which result in the formation of a peak that corresponds to 2-OH-E^+. However, in the irradiated samples an intense peak for E^+ at 30.5 min was observed, which remain even in the presence of SOD, suggests that there is some non-specific oxidation occurred by the light. Taken together, these results corroborate that these molecules photolyzed and produce $O_2^{\bullet-}$ only in the presence of light.

Scheme 2.13. Reaction of dihydroethidium (DHE) with superoxide and other ROS (H_2O_2, ȮH etc.) to form 2-hydroxyethidium (2-OH-E^+) and ethidium (E^+) respectively.

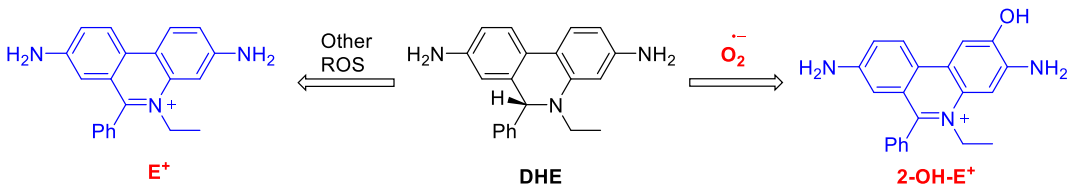

Figure 2.4. HPLC traces of DHE assay for $O_2^{\bullet-}$ detection with compound **4**

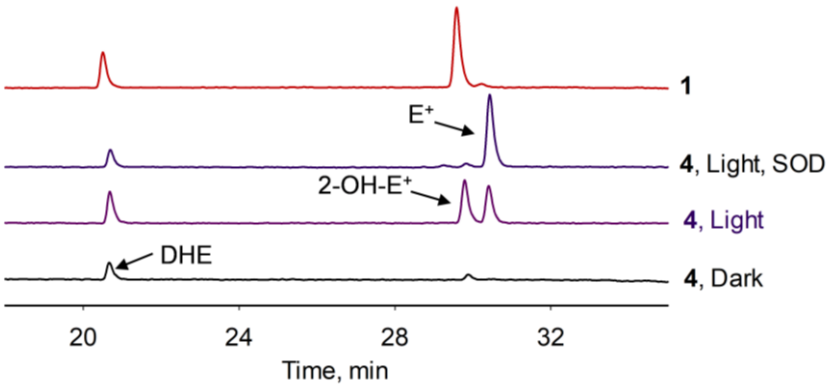

Figure 2.5. HPLC traces of DHE assay for $O_2^{\bullet-}$ detection with compound **5**

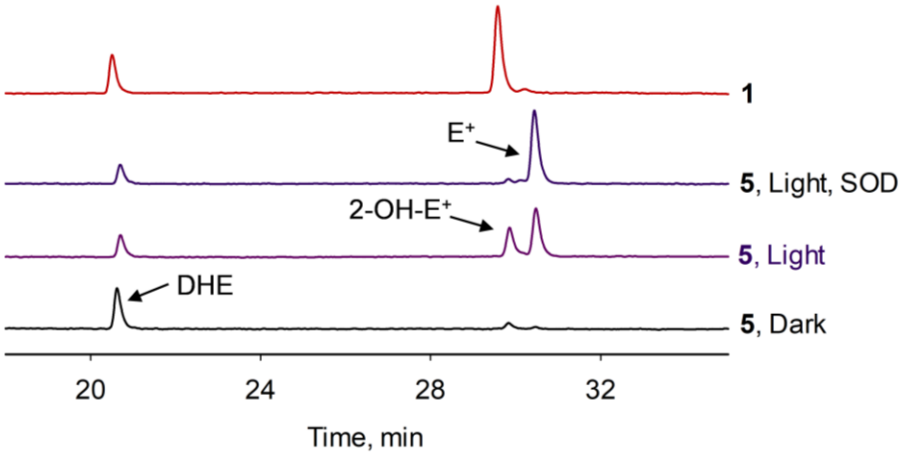

Figure 2.6. HPLC traces of DHE assay for $O_2^{\bullet-}$ detection with biotinylated compound **8**

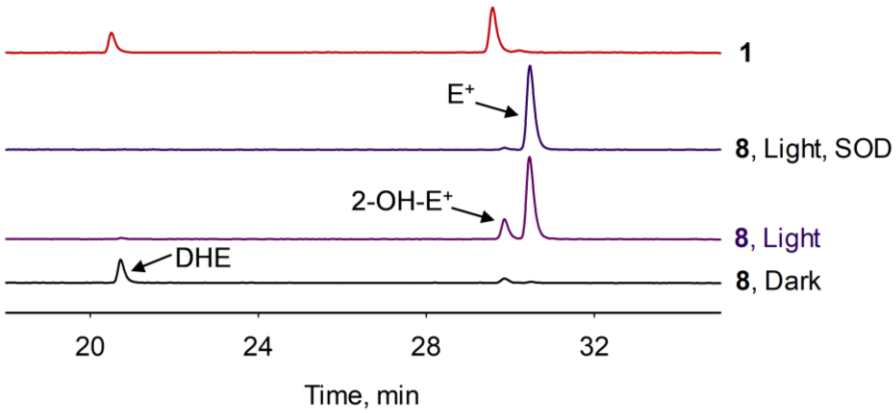

2.3.3.2 Hydrogen Peroxide Detection

As it was illustrated by DHE assay that these compounds produce $O_2^{\bullet-}$ which should disproportionate to form H_2O_2, another ROS species. Here, two independent assays were conducted to detect H_2O_2.

2.3.3.2.1 H_2O_2 Detection Using Boro-Umb Dye 23

H_2O_2 is a stable form of ROS which reacts with aryl boronate esters and boronic acids to form corresponding phenols.[65,66] Utilizing this strategy, boronate-ester of umelliferone derivative **23**, was used as H_2O_2 probe, which is weakly-fluorescent. Upon oxidation of the boronate-ester with H_2O_2, a highly fluorescent umbelliferone derivative (**24)** is formed (Scheme 2.14) and the increase in the fluorescence signal can be measured by fluorimeter. H_2O_2 detection was performed using **23** and enhanced fluorescence signal in the irradiated samples was observed. However, the fluorescence signal was diminished when the irradiated mixture was treated with the catalase, an enzyme which catalyzes the decomposition of H_2O_2 to water and oxygen, confirming that the signal was due to H_2O_2 (Figure 2.7). The same experiment was also performed with the non-irradiated sample and any significant increase in the fluorescence signal was not observed. This study suggests that these compounds produce H_2O_2 only in the presence of light.

Scheme 2.14. Reaction of Dye **23** with H_2O_2

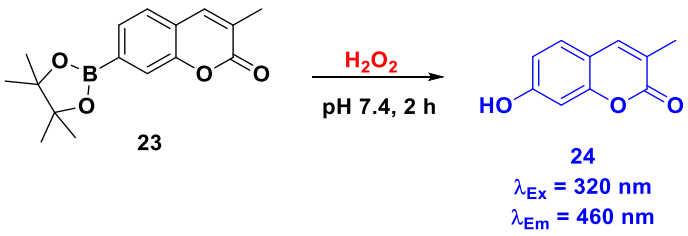

Figure 2.7. Hydrogen peroxide detection using dye **23** as a probe; Data represent the mean ± s.d. for 3 technical replicates per group.

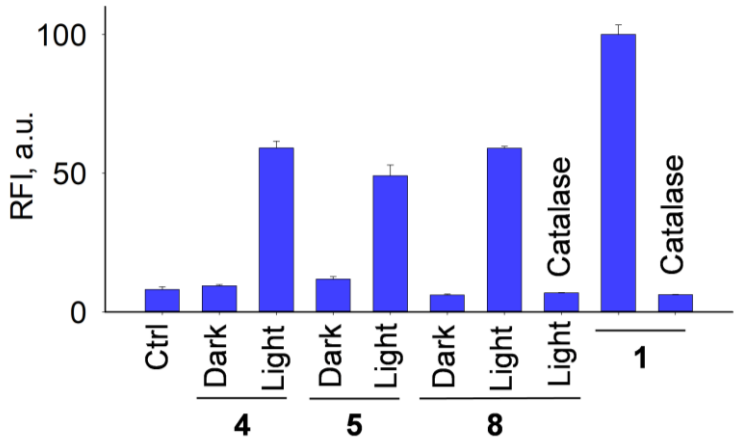

2.3.3.2.2 Hydrogen Peroxide Detection Using Amplex Red Assay

The reactivity of H_2O_2 with metal ions like, Fe(II) and Cu(I) is well known which results in the formation of hydroxyl radical, a highly reactive form of ROS. Apart from the reactivity with these metals, horseradish peroxidase (HRP) can convert H_2O_2 to hydroxyl radical (ȮH). Amplex Red (AR) is a non-fluorescent dye, a resorufin molecule is masked with an acetyl group to form a non-conjugate double bond system resulting in non-fluorescent nature of this molecule. ȮH can function as deacetylating agent followed by oxidation of AR which can result in the formation of Resorufin,[67,68] a highly fluorescent molecule that can be detected by fluorimeter (Scheme 2.15). Compound **8** was irradiated, incubated for 2 h and further incubated with AR reagents, which contained AR dye and HRP. It was found that enhanced fluorescence signal was observed in the irradiated samples. However, the fluorescence signal was diminished when the irradiated mixture was treated with the catalase, an enzyme which convert H_2O_2 to water and oxygen, confirming that the enhanced signal was due to H_2O_2 (Figure 2.8). The same experiment was also performed with the non-irradiated sample and no enhanced fluorescence signal was observed. Taken together, this study suggests that the compound **8** was stable in dark and produce H_2O_2 only in the presence of light.

Scheme 2.15. Reaction of hydrogen peroxide with Amplex red in the presence of Horseradish peroxidase enzyme to form a highly fluorescent molecule, resorufin

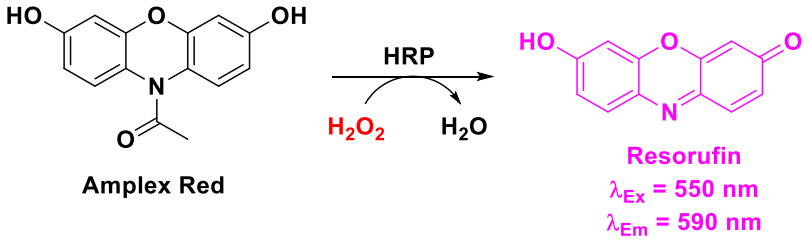

Figure 2.8. Hydrogen peroxide detection using Amplex Red dye; Data represent the mean ± s.d. for 3 technical replicates per group.

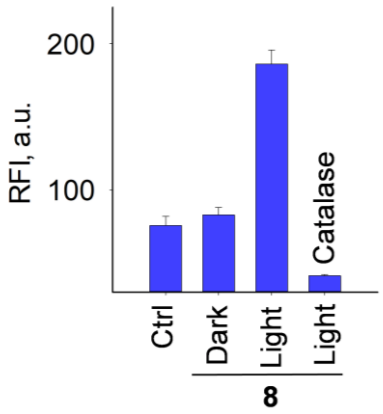

2.3.4 *In Vitro* Thiol Reactivity with Known ROS Generators

As described in the introduction part of this chapter that most of the ROS donors are quinone based and suffer with the thiol reactivity which eventually may lead to the interference in the obtained results due to off-site reactivity. Here, to test the thiol reactivity, known ROS donors; juglone, menadione, compound **1** and compound **2,** an oxidized form of compound **1**, were chosen. These compounds were reacted with glutathione (GSH), a most abundant cellular thiol and did not find reactivity with compound **1** and **2** (Figure 2.9). However, significant reaction of thiol with juglone and menadione was observed (Figure 2.10). The possible reason of high reactivity of thiol with juglone and menadione is easy accessibility to the less hindered α, β-unsaturated site whereas In the compound **2,** α, β-unsaturated site of quinone is more hindered and hence may not be accessible to thiols while compound **1** is not a candidate for thiol attack because of the absence of α, β-unsaturated site. [28]

Figure 2.9. HPLC traces of glutathione reaction with compound **1** and **2**

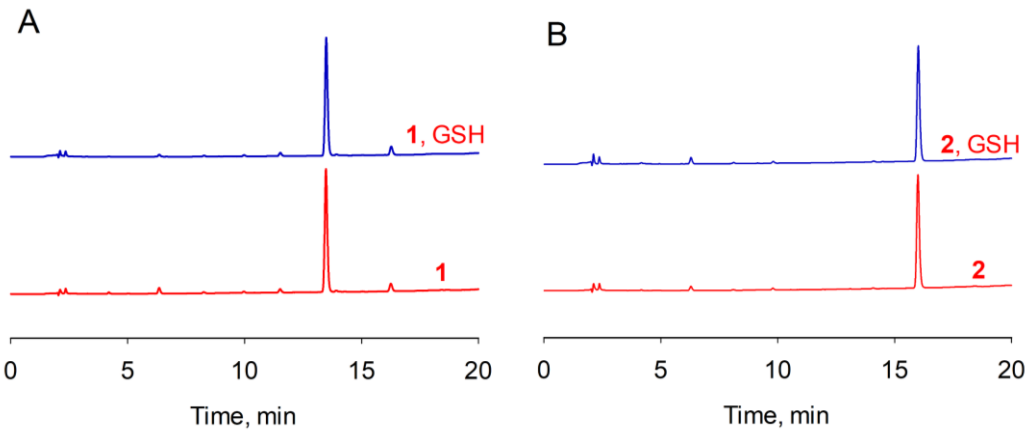

Figure 2.10. HPLC traces of glutathione reaction with juglone and menadione

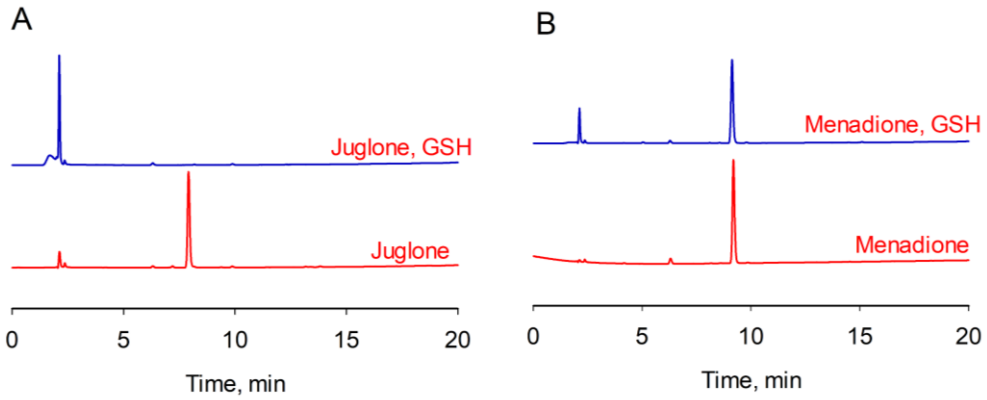

2.3.5 Cellular Studies

In-vitro studies suggested that all the three compounds (**4**, **5** and **8**) photo-cleaved to produce compound **1** which reacts with oxygen to produce ROS. In order to test the hypothesis of ROS generation in cellular system, two independent assays for extracellular H_2O_2 detection and one assay for intracellular detection of ROS were carried out.

2.3.5.1 Extracellular Hydrogen Peroxide Detection

For cellular studies, only the biotinylated compound **8** was chosen, because it has better aqueous solubility than other two compounds. It might also have a better permeability because of the presence of biotin moiety. In order to test the extracellular hydrogen peroxide release, Lung carcinoma cells, A549 were used which were treated with compound **8**, irradiated for 5 min and incubated for 2 h at 37 ºC. After irradiation, compound **8** should release compound **1** which should produce $O_2^{\bullet-}$ followed by H_2O_2. To detect H_2O_2, an aliquot of extracellular media

was incubated with H_2O_2 responsive dye **23** and fluorescence was measured after 1 h. As expected, enhanced fluorescence signal was observed only in the irradiated and compound treated wells, however no enhanced signal was observed in dark and in cells which were irradiated without compound (Figure 2.11 A). This study suggested that compound **8** produces hydrogen peroxide only in the presence of light and UV light alone does not cause an increase in ROS level extracellularly in the conditions used for irradiation.

Extracellular H_2O_2 was also detected by Amplex red assay where the enhanced fluorescence signal was observed only in the presence of light and again, UV light alone does not cause an increase in the level of H_2O_2 extracellularly (Figure 2.11 B). Taken together, both these studies suggested that compound **8** is stable in media under dark conditions and hence does not produce H_2O_2. However, when compound treated wells were irradiated it results in the release of H_2O_2 in the extracellular media.

Figure 2.11. Extracellular Hydrogen peroxide detection; A) using dye **23** as a probe and D) using Amplex Red dye; Data represent the mean ± s.e.m. for 3 technical replicates per group.

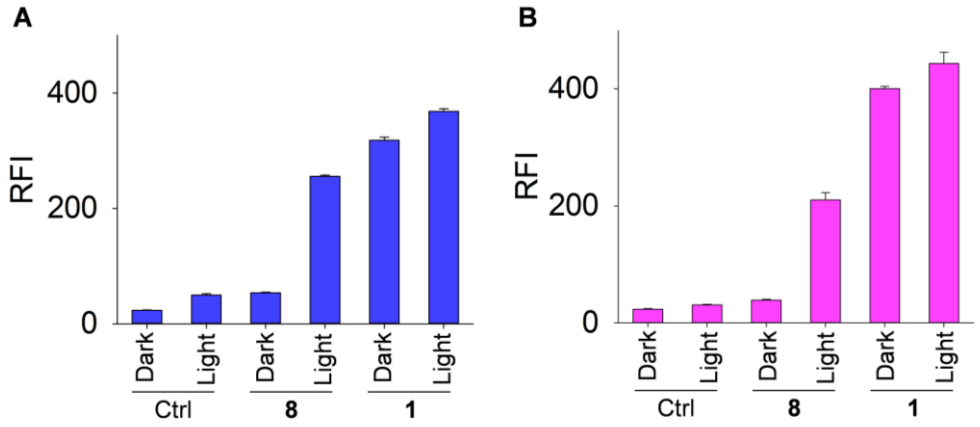

2.3.5.2 Intracellular ROS Detection Using H_2DCF-DA Dye

After having established that compound **8** undergoes photocleavage and produce ROS *in vitro* and extracellularly. This compound may permeate through the cellular membrane and accumulate intracellularly. If these cells are exposed to light then, compound **1** should be released intracellularly and can increase the ROS level. Whereas, if these cells are incubated in dark, should not increase the ROS level. To evaluate the intracellular ROS generation from compound **8**, a cell permeable weakly fluorescent ROS responsive dye, 2',7'-dichlorodihydrofluorescein diacetate (H_2DCF-DA) was used which reacts with hydroxyl

radical to form a highly fluorescent molecule, 2',7'-dichlorodihydrofluorescein (DCF)[69,70] (Scheme 2.16). Cells having DCF molecule can be imaged using fluorescence microscopy and also the fluorescence intensity of these cells can be measured using well plate reader. This assay was performed using A549 cells and found that cells treated with compound **8** showed enhanced fluorescence signal after irradiation. However, cells which were treated with compound **8** but not irradiated and cells which were irradiated but not treated with compound **8**, did not show intense fluorescence signal (Figure 2.12 A & B). This study reveals that compound **8** is cells permeable and photo-cleaved to release compound **1.** The released compound **1** generate $O_2^{\bullet-}$ which then converts to H_2O_2 by SOD. This H_2O_2 can react with trace metal ion like Fe(II) to form hydroxyl radical. This hydroxyl radical can deacetylate H_2DCF-DA and further oxidize it to form a highly fluorescent molecule, DCF. This study also suggested that conditions used for irradiation, 365 nm UV light for 5 min, alone does not enhance the ROS level in cells.

Scheme 2.16. Reaction of H_2DCF-DA with ROS to form DCF, a highly fluorescent molecule

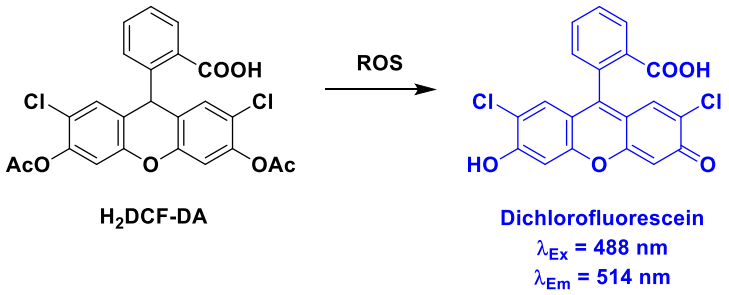

H_2DCF-DA

Dichlorofluorescein
λ_{Ex} = 488 nm
λ_{Em} = 514 nm

Figure 2.12. Intracellular ROS detection using H_2DCF-DA dye; A) Cellular images and B) Relative intensity graph of intracellular ROS level; Data represent the mean ± s.e.m. for 3 technical replicates per group.

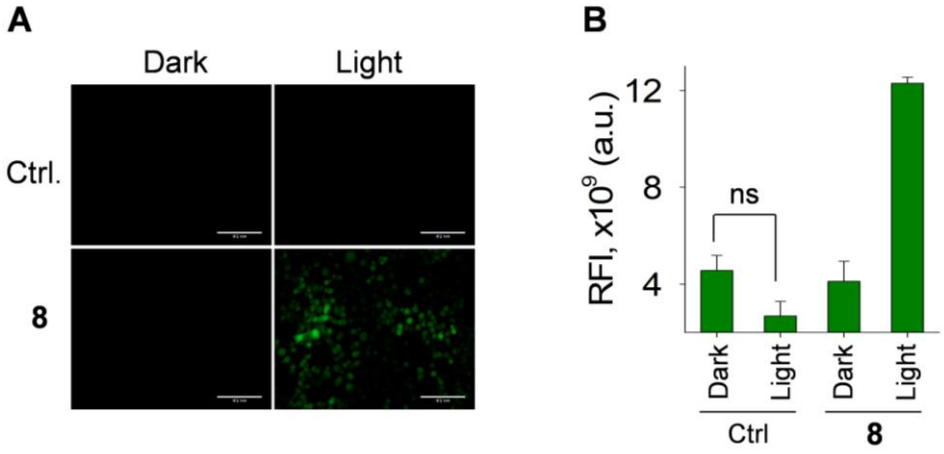

2.3.5.3 Effect on Cellular Proliferation

Generation of burst amount of ROS endogenously may damage essential bio-molecules which may result into the cell death. As described by the experiments that compound **8** produces intracellular ROS in the presence of light. Here, the potency of these compounds to inhibit the growth of cancer cells was assayed. For this experiment A549, lung cancer cells have been chosen and cellular growth inhibition assay was performed using MTT dye in the presence and absence of light irradiation. Nearly complete inhibition in growth was observed, only in the presence of light at 10 µM of compound **8** (Figure 2.13). This assay was performed with different concentration of compound **8** and the inhibition of cellular growth was found in the dose depended manner (Figure 2.15). The IC_{50} of compound **8** in the presence of light, were calculated and found to be 5.8 µM (Figure 2.14). However, in the dark, no cell growth inhibition was observed up to 25 µM of compound **8**.

Figure 2.13. Cell growth inhibition assay using MTT dye using A549 with 10 µM of compounds; Data represent the mean ± s.e.m. for 3 technical replicates per group.

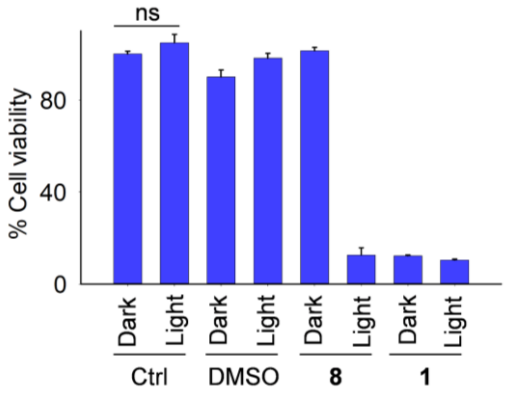

Figure 2.14. Growth inhibition curve using A549 cells with compound **8** after irradiation; Data represent the mean ± s.e.m. for 3 technical replicates per group.

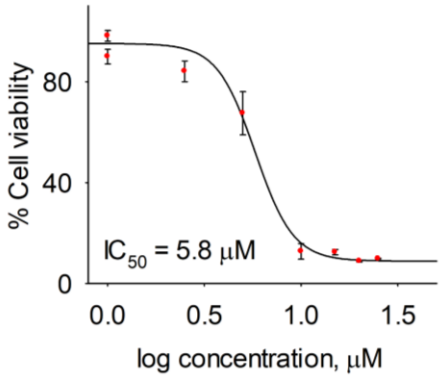

Figure 2.15. Cell viability assay using A549 cells varying the concentration of **8**; Data represent the mean ± s.e.m. for 3 technical replicates per group.

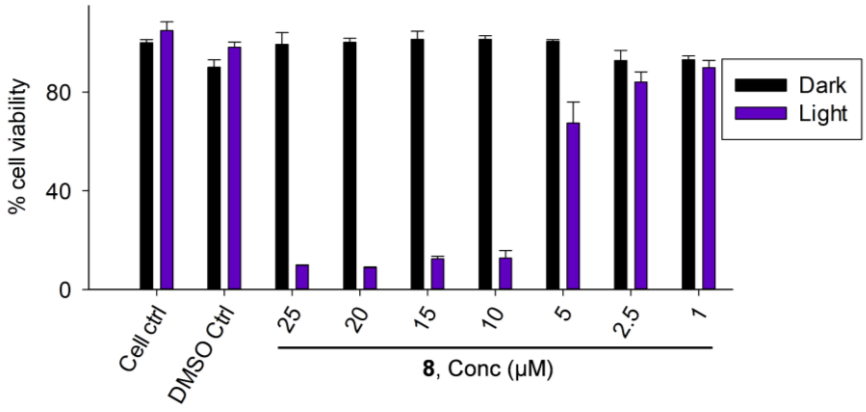

The cell growth inhibitory activity of compound **8** was also performed using DLD-1, colon cancer cell and as expected, a nearly complete growth inhibition was found at 10 μM concentration in the irradiated cells (Scheme 2.16). This assay was also performed varying the concentration of compound **8** (Figure 2.18) and found dose dependent inhibition in cellular growth. The IC_{50} of the compound **8** in the presence of light, were calculated and found to be 5.3 μM (Figure 2.17). However, no effect on cellular growth was observed in the dark up to 50 μM of compound **8**. This suggests that compound **8** remains in the caged form in the dark and did not affect the cellular growth, exposing to light uncaged the compound **1** producing burst of ROS, resulting in damage of the essential bio-macromolecules which eventually leads to inhibition of cellular growth.

As it is known that alone UV light can cause the damage of essential biomolecules and hence it can result in the inhibition of the cellular growth. When this experiment was performed, the irradiation condition which was used in cellular experiments is not affecting the cellular growth, suggested that 365 nm UV light for 5 min was well tolerated by cells and can be used for cellular experiments.

Figure 2.16. Cell growth inhibition assay using MTT dye using DLD-1 cells with 10 μM of compounds; Data represent the mean ± s.e.m. for 3 technical replicates per group.

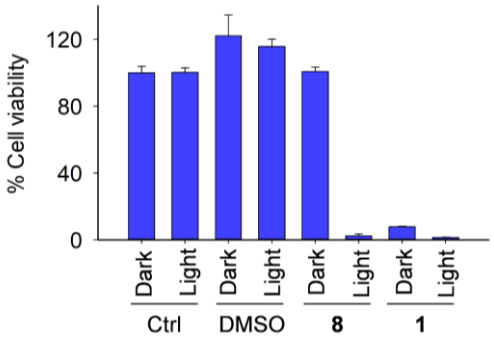

Figure 2.17. Growth inhibition curve using DLD-1 cells with compound **8** after irradiation; Data represent the mean ± s.e.m. for 3 technical replicates per group.

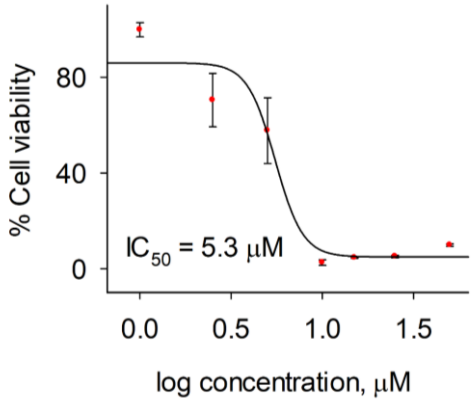

Figure 2.18. Cell viability assay using DLD-1 cells varying the concentration of **8**; Data represent the mean ± s.e.m. for 3 technical replicates per group.

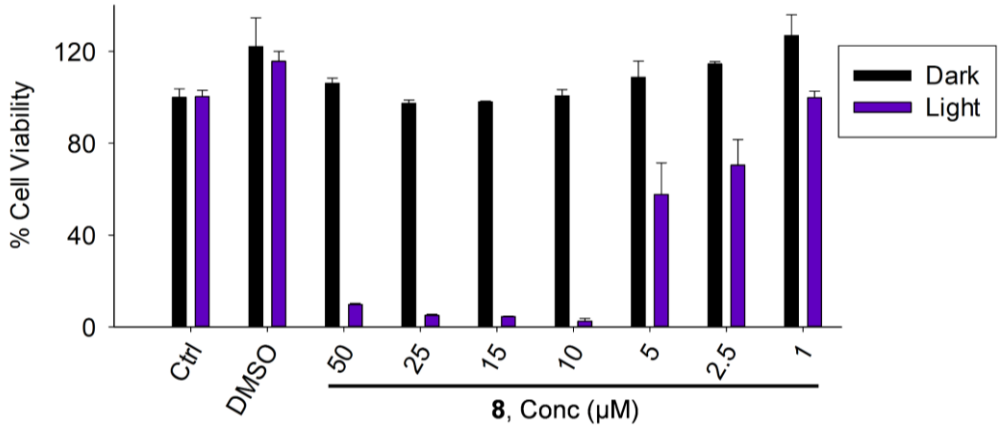

2.4 Conclusion

In this chapter, photoactivable ROS donors has been designed and synthesized. To achieve the selectivity towards the cancer cells over normal cells, unique overexpression of vitamin receptors was attempted to exploit, where vitamin molecules or vitamin moiety containing molecules might have a better uptake in cancer cells. Using this feature of cancer cells, a biotin moiety was attached, which only results in improving buffer solubility and enhanced uptake by cancer cells over normal cells was not observed. These molecules contain a ROS generating moiety which was caged with a photo-clevable linker. Upon irradiation with 365 nm UV light, all these molecules photo-cleaved to release an active ROS generating molecule which generate $O_2^{\bullet-}$ followed by H_2O_2. $O_2^{\bullet-}$ was detected using DHE assay while H_2O_2 detection was carried out using Boronate-umbelliferone dye **23** and Amplex Red assays. Compound **8** was also evaluated as an extracellular and intracellular ROS generator where it was found that compound **8** produces H_2O_2 extracellularly in the presence of light. Compound **8** is cell permeable and produce ROS intracellularly which was confirmed using H_2DCF-DA dye. Finally, compound **8** was tested for cellular growth inhibitory activity with cancer cell lines and it was found that compound **8** is highly potent only in the presence of light. However, no toxicity was found in the absence of light. These studies suggest that compound **8** can be a potential candidate for understanding the ROS mediated pathways of cellular system in spatiotemporally controlled manner using light as a stimulus.

The unique photoactivable ROS generators were developed which produce ROS only in the presence of light and might be used as cancer therapeutics. However, there are few shortcomings associated with the UV triggered approach e.g., UV light induced oxidative stress[37–41] and its lower tissue penetration. Owing to such limitations, *in vivo* experiments are more challenging to perform with the compound **8**. To overcome these drawbacks, there is need to develop a molecule which can get activated under visible light to produce ROS.

2.5 Experimental Protocols and Characterization Data

2.5.1 General Methods

All the chemicals and solvents were purchased from commercial sources and used as received unless stated otherwise. Column chromatography was performed using Silica gel Spectrochem (100-200 mesh) as stationary phase. Preparative high-performance liquid chromatography (HPLC) was done using Combiflash EZ prep UV using a Kromasil®C-18 preparative column (250 mm × 21.2 mm, 5 µm). ^{1}H and ^{13}C spectra were recorded on a JEOL 400 MHz (or 100 MHz for ^{13}C) or a Bruker 400 MHz (or 100 MHz for ^{13}C) spectrometer unless otherwise specified using as an internal tetramethylsilane (δ_H = 0.00, δ_C = 0.0). Chemical shifts (δ) are reported in ppm and coupling constants (*J*) in Hz. The following abbreviations are used: br (broad signal), m (multiplet), s (singlet), d (doublet), t (triplet) and dd (doublet of doublets). High-resolution mass spectra were obtained from HRMS-ESI-Q-Time of Flight LC/MS. FT-IR spectra were recorded using BRUKER-ALPHA FT-IR spectrometer. Analytical HPLC was performed on an Agilent1260-infinity with Phenomenex® C-18 reverse phase column (250 mm × 4.6 mm, 5 µm). Irradiation was done using 365 nm UV-LED flashlight-3W and intensity was calibrated using GENTEC-EO-UNO laser power meter. Photometric and fluorometric measurements were performed using a Thermo Scientific Varioskan microtiter plate reader.

2.5.2 Synthesis Protocols

Compounds **1**[47], **2**[47], **12**[57], **18**[71], **22**[72] and **23**[66] were synthesized using previously reported procedures and analytical data were consistent with reported values.

Synthesis of 2-(4-formyl-2-methoxy-5-nitrophenoxy)ethyl nitrate (19): To a solution of 4-

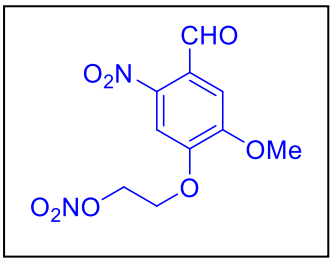

(2-hydroxyethoxy)-3-methoxybenzaldehyde (3.4 g, 17.33 mmol) in glacial acetic acid (10 mL) with continuous stirring at ice cold condition was added a mixture of conc. HNO_3 (10 mL) and conc. H_2SO_4. This reaction mixture was stirred additionally for 1 h at r.t. After completion of reaction as monitored by TLC analysis, reaction was quenched with ice water and extracted with dichloromethane. This dichloromethane layers were dried over anhydrous sodium sulphate and concentrated under reduced pressure to get crude, which was purified by silica gel column chromatography to obtain yellowish solid (1.5 g, 30 %); FT-IR (ν_{max}, cm^{-1}): 2921, 1691, 1521, 1338; ^{1}H NMR (400

MHz, $CDCl_3$): δ 10.46 (s, 1H), 7.63 (s, 1H), 7.43 (s, 1H), 4.94 – 4.90 (m, 2H), 4.47 – 4.42 (m, 2H), 4.02 (s, 3H); HRMS (ESI-TOF) for $[C_{10}H_{10}N_2O_8 + H]^+$ calcd: 287.0515; found: 287.0507.

Synthesis of 4-(2-azidoethoxy)-5-methoxy-2-nitrobenzaldehyde (20): To a solution of **19**

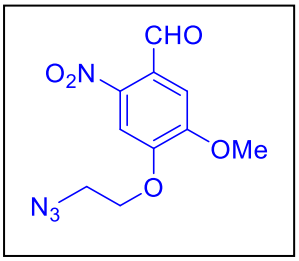

(2.5 g, 8.74 mmol) in anhydrous DMF (20 mL) with continuous stirring, sodium azide (1.00 g, 15.38 mmol) was added. This reaction mixture was stirred at 80 °C for 16 h in inert atmosphere. After completion of reaction as monitored by TLC analysis, DMF was evaporated under reduced pressure to get crude, which was purified by silica gel column chromatography to obtain yellowish solid (1.2 g, 52 %); FT-IR (ν_{max}, cm^{-1}): 2109, 1691, 1520, 1337; ^1H NMR (400 MHz, $CDCl_3$): δ 10.45 (s, 1H), 7.63 (s, 1H), 7.43 (s, 1H), 4.32 (t, *J* = 5.0 Hz, 2 H), 4.02 (s, 3H), 3.74 (t, *J* = 5.0 Hz, 2H); ^{13}C NMR (100 MHz, $CDCl_3$): δ 187.7, 153.7, 151.1, 143.4, 126.3, 110.2, 108.5, 68.6, 56.7, 49.8; HRMS (ESI-TOF) for $[C_{10}H_{10}N_4O_5 + H]^+$ calcd: 267.0729; found: 267.0724.

Synthesis of (4-(2-azidoethoxy)-5-methoxy-2-nitrophenyl)methanol (21): To a solution of

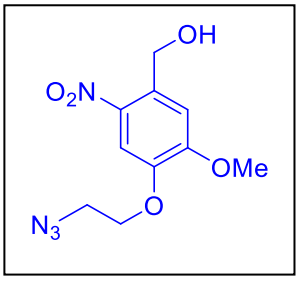

20 (936 mg, 3.52 mmol) in anhydrous methanol (20 mL) with continuous stirring, $NaBH_4$ (410 mg, 10.84 mmol) was added portion wise. This reaction mixture was stirred at r.t. for 30 min in inert atmosphere. After completion of reaction as monitored by TLC analysis, reaction was quenched with saturated NH_4Cl solution and extracted with ethyl acetate. The organic fractions were combined, dried over anhydrous sodium sulphate and concentrated under reduced pressure to get crude. The crude was purified by silica gel column chromatography to obtain yellowish solid (750 mg, 80 %); FT-IR (ν_{max}, cm^{-1}): 3264, 2921, 2108, 1516, 1329; ^1H NMR (400 MHz, $CDCl_3$): δ 7.73 (s, 1H), 7.21 (s, 1H), 4.98 (s, 2H), 4.25 (t, *J* = 5.0 Hz, 2H), 4.00 (s, 3H), 3.70 (t, *J* = 5.0 Hz, 2H), 2.20 – 2.20 (br, 1H); ^{13}C NMR (100 MHz, $CDCl_3$): δ 154.6, 146.7, 139.5, 133.2, 111.4, 110.2, 68.4, 62.8, 56.5, 50.0; HRMS (ESI-TOF) for $[C_{10}H_{12}N_4O_5 + Na]^+$ calcd: 291.0705 ; found: 291.0702.

Synthesis of 1-(2-azidoethoxy)-4-(bromomethyl)-2-methoxy-5-nitrobenzene (13): To a solution of **21** (1.00 g, 3.73 mmol) in anhydrous dichloromethane (40 mL) kept at ice bath, PBr_3 (1.06 mL, 11.16 mmol) was added. This reaction mixture was stirred at ice cold condition for 2 h in inert atmosphere. After completion of reaction as monitored by TLC analysis,

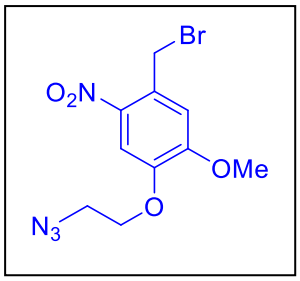

reaction was quenched with saturated $NaHCO_3$ solution and extracted with dichloromethane. The organic layers were combined. dried over anhydrous sodium sulphate and concentrated under reduced pressure to get crude. The crude was purified by silica gel column chromatography to afford a white solid (450 mg, 36 %); FT-IR (ν_{max}, cm^{-1}): 2920, 2103, 1517, 1338; ^1H NMR (400 MHz, $CDCl_3$): δ 7.69 (s, 1H), 6.97 (s, 1H), 4.87 (s, 2H), 4.25 (t, *J* = 5.0 Hz, 2H), 3.99 (s, 3H), 3.70 (t, *J* = 5.0 Hz, 2H); ^{13}C NMR (100 MHz, $CDCl_3$): δ 153.8, 147.6, 140.0, 128.3, 114.1, 110.4, 68.4, 56.5, 49.9, 30.0; HRMS (ESI-TOF) for $[C_{10}H_{11}BrN_4O_4 + Na]^+$ calcd: 352.9861; found: 352.9860.

Synthesis of 5-((2-nitrobenzyl)oxy)-1,4,4a,9a-tetrahydro-1,4-ethanoanthracene-9,10-dione (4): A solution of **10** (128 mg, 0.592 mmol), **1** (100 mg, 0.393 mmol) and Ag_2O (274 mg, 1.18 mmol) in anhydrous dichloromethane (5 mL) was kept at continuous stirring for 3 days at room temperature in inert atmosphere. After complete consumption of starting material which was confirmed by TLC analysis, reaction mixture was subjected to normal silica gel column chromatography using hexane: ethyl acetate (100:0 to 70:30) as a eluent to afford white solid which was further washed with acetonitrile to obtain pure compound **4** (85 mg, 55 %); FT-IR (ν_{max}, cm^{-1}): 2924, 1682, 1526, 1342; ^1H NMR (400 MHz, $CDCl_3$): δ 8.40 (d, *J* = 7.8 Hz, 1H), 8.21 (d, *J* = 8.0 Hz, 1H), 7.83 (t, *J* = 7.5 Hz, 1H), 7.67 – 7.56 (m, 2H), 7.53 (t, *J* = 7.8 Hz, 1H), 7.34 (d, *J* = 7.8 Hz, 1H), 6.26 – 6.11 (m, 2H), 5.63 – 5.51 (m, 2H), 3.41 – 3.30 (m, 2H), 3.29 – 3.20 (m, 2H), 1.80 – 1.69 (m, 2H), 1.49 – 1.35 (m, 2H); ^{13}C NMR (100 MHz, $CDCl_3$): δ 197.9, 196.3, 156.7, 146.3, 138.7, 134.7, 134.6, 134.0, 133.5, 133.2, 129.1, 128.4, 125.6, 124.9, 119.4, 118.0, 67.9, 52.1, 50.9, 34.5, 34.0, 24.8, 24.6; HRMS (ESI-TOF) for $[C_{23}H_{19}NO_5 + H]^+$ calcd: 390.1341; found: 390.1345.

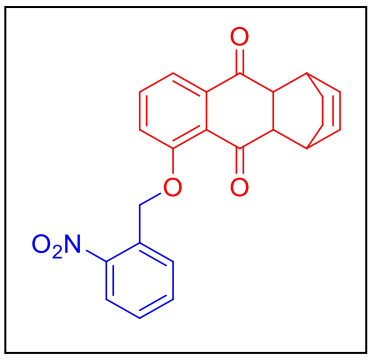

Synthesis of 5-((4,5-dimethoxy-2-nitrobenzyl)oxy)-1,4,4a,9a-tetrahydro-1,4-ethanoanthracene-9,10-dione (5) and 6-(4,5-dimethoxy-2-nitrobenzyl)-5-hydroxy-1,4,4a,9a-tetrahydro-1,4-ethanoanthracene-9,10-dione (9): A solution of 11 (114 mg, 0.413 mmol), 1 (149 mg, 0.586 mmol) and Ag_2O (270 mg, 1.17 mmol) in anhydrous dichloromethane (5 mL) was kept at continuous stirring for 3 days at room temperature in inert atmosphere. After complete consumption of starting material which was confirmed by TLC analysis,

reaction mixture was subjected to normal silica gel column chromatography using hexane: ethylacetate (100:0 to 85:15) as a eluent to afford compound **5** (55 mg, 30 %) and **9** (20 mg, 11 %); Characterization of 4b; FT-IR (ν_{max}, cm^{-1}): 2923, 1737, 1682, 1517, 1376; ^{1}H NMR (400 MHz, $CDCl_3$): δ 8.25 (s, 1H), 7.80 (s, 1H), 7.69 – 7.62 (m, 1H), 7.62 – 7.55 (m, 1H), 7.44 – 7.36 (m, 1H), 6.22 – 6.11 (m, 2H), 5.56 (s, 2H), 4.26 (s, 3H), 3.99 (s, 3H), 3.35 – 3.26 (m, 2H), 3.23 (s, 2H), 1.78 – 1.70 (m, 2H), 1.45 – 1.36 (m, 2H); ^{13}C NMR (100 MHz, $CDCl_3$): δ 198.0, 196.2, 156.6, 154.7, 147.8, 138.6, 138.3, 134.8, 133.9, 133.6, 129.0, 125.2, 119.2, 117.7, 110.7, 107.7, 67.9, 57.2, 56.4, 52.1, 50.8, 34.6, 34.3, 24.8, 24.7; HRMS (ESI-TOF) for $[C_{25}H_{23}NO_7 + Na]^+$ calcd: 472.1372; found: 472.1374.

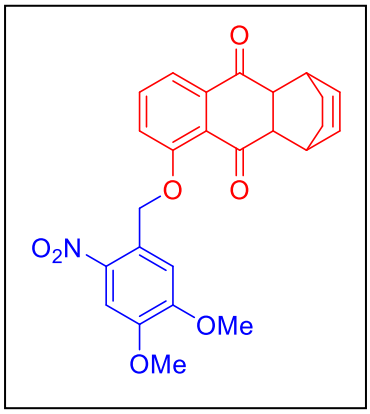

Characterization data of 6-(4,5-dimethoxy-2-nitrobenzyl)-5-hydroxy-1,4,4a,9a-tetrahydro-1,4-ethanoanthracene-9,10-dione (9): FT-IR (ν_{max}, cm^{-1}): 2929, 1734, 1681, 1520; ^{1}H NMR (400 MHz, $CDCl_3$): δ 13.10 (s, 1H), 7.66 (s, 1H), 7.46 (d, J = 7.8 Hz, 1H), 7.29 (s, 1H), 6.78 (s, 1H), 6.23-6.13(m, 2H), 4.46-4.32 (m, 2H), 3.95 (s, 3H), 3.89 (s, 3H), 3.43-3.30 (m, 2H), 3.27 (m, 1H), 3.18 (m, 1H), 1.85 – 1.76 (m, 2H), 1.42 (dd, J = 6.5, 4.7 Hz, 2H); ^{13}C NMR (100 MHz, $CDCl_3$): δ 205.1, 197.0, 159.8, 153.1, 147.7, 141.5, 136.5, 134.6, 134.1, 133.8, 133.3, 128.7, 117.9, 117.5, 114.2, 108.3, 56.4, 50.3, 49.9, 36.2, 35.9, 33.2, 25.0, 24.8; HRMS (ESI-TOF) for $[C_{25}H_{23}NO_7 + H]^+$ calcd: 450.1553; found: 450.1550.

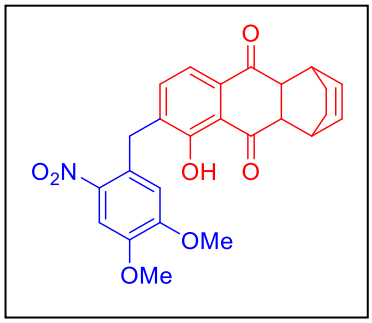

Synthesis of 5-((4-(2-azidoethoxy)-5-methoxy-2-nitrobenzyl)oxy)-1,4,4a,9a-tetrahydro-1,4-ethanoanthracene-9,10-dione (7): A solution of **13** (400 mg, 1.21 mmol), **1** (460 mg, 1.81 mmol) and Ag_2O (1.95 g, 8.41 mmol) in anhydrous dichloromethane (30 mL) was kept at continuous stirring for 4 days at room temperature in nitrogen atmosphere. After complete consumption of starting material which was confirmed by TLC analysis, reaction mixture was subjected to normal silica gel column chromatography using hexane: ethylacetate (100:0 to 50:50) as a eluent to afford pale yellow solid as compound **7** (150 mg, 25 %); FT-IR (ν_{max}, cm^{-1}):

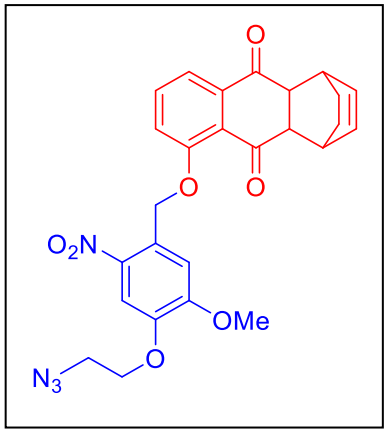

2922, 2103, 1682, 1520; ^{1}H NMR (400 MHz, $CDCl_3$): δ 8.26 (s, 1H), 7.82 (s, 1H), 7.66 (t, *J* = 7.9 Hz, 1H), 7.61 – 7.57 (m, 1H), 7.40 (d, *J* = 8.0 Hz, 1H), 6.21 – 6.11 (m, 2H), 5.56 (s, 2H), 4.28 (t, *J* = 5.0 Hz, 2H), 4.24 (s, 3H), 3.73 (t, *J* = 5.0 Hz, 2H), 3.35 – 3.26 (m, 2H), 3.24 (s, 2H), 1.77 - 1.73 (m, 2H), 1.44 - 1.37 (m, 2H); ^{13}C NMR (100 MHz, $CDCl_3$): δ 198.0, 196.2, 156.5, 155.3, 146.4, 138.6, 138.0, 134.8, 133.9, 133.6, 129.9, 125.2, 119.2, 117.7, 111.2, 109.7, 68.3, 67.8, 57.2, 52.0, 50.8, 50.0, 34.6, 34.3, 24.8, 24.7; HRMS (ESI-TOF) for $[C_{26}H_{24}N_4O_7 + Na]^+$ calcd: 527.1543; found: 527.1542.

Synthesis of N-((1-(2-(4-(((9,10-dioxo-1,4,4a,9,9a,10-hexahydro-1,4-ethanoanthracen-5-yl)oxy)methyl)-2-methoxy-5-nitrophenoxy)ethyl)-1H-1,2,3-triazol-4-yl)methyl)-5-((3aR,4R,6aS)-2-oxohexahydro-1H-thieno[3,4-d]imidazol-4-yl)pentanamide (8): A

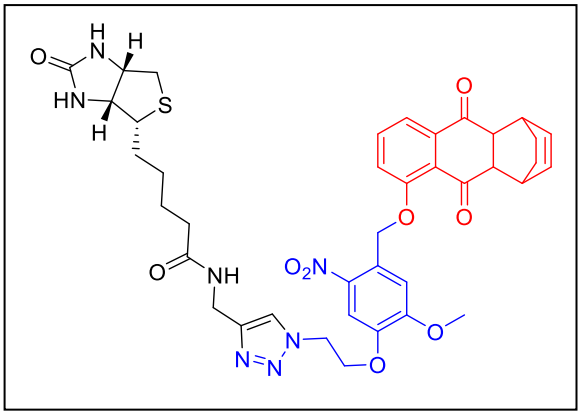

solution of **7** (105 mg, 0.208 mmol), **22** (50 mg, 0.178 mmol), $CuSO_4.5H_20$ (88 mg, 0.352 mmol) and sodium ascorbate (71 mg, 0.358 mmol) in anhydrous DMF (7 mL) was kept at continuous stirring for 14 h at room temperature in inert atmosphere. After complete consumption of starting material which was confirmed by TLC analysis, reaction mixture was subjected to normal silica gel column chromatography using chloroform: methanol (100:0 to 90:10) as a eluent to give pale yellow solid, which was further purified by preparative HPLC using MeOH:Acetonitrle (30:70): water as mobile phase to afford white solid as compound **8** (30 mg, 21 %); FT-IR (ν_{max}, cm^{-1}): 3230, 2924, 1684, 1523, 1329; ^{1}H NMR (400 MHz, DMSO-d_6): δ 8.31 (t, *J* = 5.7 Hz, 1H), 8.04 (s, 1H), 7.99 (s, 1H), 7.80 (s, 1H), 7.75 (t, *J* = 8.0 Hz, 1H), 7.53 (d, *J* = 8.3 Hz, 1H), 7.44 (d, *J* = 7.6 Hz, 1H), 6.40 (s, 1H), 6.35 (s, 1H), 6.19 - 6.07 (m, 2H), 5.62 - 5.48 (m, 2H), 4.78 (t, *J* = 4.8 Hz, 2H), 4.55 (t, *J* = 4.9 Hz, 2H), 4.35 - 4.24 (m, 3H), 4.15 - 4.03 (m, 4H), 3.21 - 3.13 (m, 2H), 3.11 - 2.01 (m, 1H), 2.79 (dd, *J* = 12.4, 4.9 Hz, 1H), 2.56 (d, *J* = 12.7 Hz, 1H), 2.14 - 2.06 (m, 2H), 1.76 - 1.66 (m, 2H), 1.64 - 1.38 (m, 4H), 1.34 – 1.22 (m, 4H); ^{13}C NMR (100 MHz, DMSO-d_6): δ 197.4, 195.6, 171.8, 162.6, 156.0, 154.0, 145.8, 145.1, 138.3, 137.9, 134.9, 134.0, 133.4, 128.9, 124.7, 123.1, 118.4, 118.2, 111.1, 110.0, 67.6, 67.2, 60.9, 59.1, 56.4, 55.3, 51.3, 50.1, 48.7, 34.9, 34.0, 33.5, 33.1, 28.1, 27.9, 25.1, 24.0; HRMS (ESI-TOF) for $[C_{39}H_{43}N_7O_9S + H]^+$ calcd: 786.2921; found: 786.2916.

2.5.3 General Preparation

10 mM stocks of all the compounds **4**, **5** and **8** were independently prepared in DMSO and stored in the dark at -4 °C. 10 mM stocks of Boronate ester probe **23** and dihydroethidium (DHE) and Amplex® red were prepared in DMSO and stored at -4 °C. 100 U/mL stocks of Superoxide dismutase (SOD) enzyme, 100 U/mL stocks of horseradish peroxidase (HRP) and 10000 U/mL stocks of catalase enzyme were prepared in phosphate buffer (50 mM) of pH 7.4 and stored at -4 °C. For making working solution for Amplex-red assay, HRP (100 µL of 100 U/mL) and Amplex® Red (50 µL of 10 mM) were mixed in phosphate buffer of pH 7.4 (4850 µL) and stored in dark at 0 °C until its use. (Working solution of Amplex® Red needs to be freshly prepared)

2.5.4 Procedure for Irradiation

A quartz cuvette containing compounds **4**, **5** and **8** in phosphate buffer or phosphate buffer: acetonitrile mixture (60: 40) was irradiated at 365 nm (30 mW/cm^2) using 365 nm LED flashlight at room temperature in a closed chamber. This solution was used for further analysis as described below.

2.5.5 Photo-Cleavage Study by HPLC After Irradiation

A quartz cuvette containing compounds **4**, **5** and **8** (2.5 µL of 10 mM) in 60: 40 mixture of phosphate buffer:Acetonitrile of pH 7.4 (497 µL) was irradiated. Similarly, compounds **4**, **5** and **8** (2.5 µL of 10 mM) in 60: 40 mixture of phosphate buffer: Acetonitrile of pH 7.4 (497 µL) was kept in dark for 40 min. 25 µL of aliquot from each Sample of these irradiated and non-irradiated samples were injected in HPLC and analysis was conducted using a diode array detector (DAD) operating at 250 nm. A mobile phase of water: acetonitrile was used with a run time of 25 min. A multistep gradient was used with a flow rate of 1 mL/min starting with 50: 50 →0 to 2 min, 50:50 to 10: 90 → 2 - 17 min, 10: 90 → 17 – 20 min, 10: 90 to 50: 50 → 20 - 22 min, 50:50 → 22 - 25 min.

2.5.6 Superoxide Detection Using DHE Assay

A quartz cuvette containing compounds **4**, **5** and **8** (1.25 µL of 10 mM) in phosphate buffer of pH 8.0 (496 µL) was irradiated. Similarly, compounds **4**, **5** and **8** (1.25 µL of 10 mM) in phosphate buffer of pH 8.0 (496 µL) was kept in dark. In the non-irradiated and irradiated samples, DHE (2.5 µL of 10 mM) was added and incubated for 1 h at 37 °C. The reaction

mixture was filtered (0.45 µm) and injected (50 µL) in an Agilent high performance liquid chromatograph (HPLC) attached with a fluorescence detector (excitation at 480 nm; emission at 580 nm). The column used was Agilent1260-infinity with Phenomenex®C-18 reverse phase column (250 mm × 4.6 mm, 5 µm), the mobile phase was water: acetonitrile containing 0.1% trifluoroacetic acid and a gradient starting with 90: 10 % → 0 min, 10: 90 to 44: 56 → 0 – 35 min, 0: 100 → 35 – 37 min, 0: 100 → 37 – 40 min, 10: 90 → 40 – 42 min, 10: 90 → 42 – 45 min was used with a flow rate of 0.5 mL/min. Compound **1**, a known superoxide generator (1.25 µL of 10 mM) were mixed in phosphate buffer (pH 8.0, 50 mM) along with DHE (2.5 µL of 10 mM) for 1 h and served as a positive control. Known scavenger of superoxide, Superoxide dismutase enzyme (5 µL of 100 U/mL) was also used as a control with the irradiated sample. Signal for $O_2^{\bullet-}$ was not observed in SOD treated samples.

2.5.7 H_2O_2 Detection Using Probe 23

A quartz cuvette containing compounds **4**, **5** and **8** (2.0 µL of 10 mM) in phosphate buffer of pH 7.4 (790 µL) was irradiated. Similarly, compounds **4**, **5** and **8** (2.0 µL of 10 mM) in phosphate buffer of pH 7.4 (790 µL) was kept in dark. In the non-irradiated and irradiated samples, Boro-umb **23** (8 µL of 10 mM) was added and incubated for 2 h at 37 °C. A compound **1** (2.0 µL of 10 mM) in phosphate buffer of pH 7.4 (790 µL) followed by addition of Boro-Umb probe **23**(8 µL of 10 mM) and incubated for 2 h at 37 °C, was used as a positive control. In another control experiment, **4**, **5** and **8** (2.0 µL of 10 mM) in phosphate buffer of pH 7.4 (782 µL) was irradiated, followed by addition of catalase enzyme (8 µL of 10000 U/mL), which treated with Boro-Umb probe (8 µL of 10 mM) and incubated for 2 h at 37 °C. All these irradiation experiments were done in duplicates. Further aliquots (200 µL) of these solutions were transferred to the 96 well-plate in triplicates and the fluorescence was measured using Thermo Scientific Varioskan microtiter plate reader (λ_{ex} = 320 nm and λ_{em} = 460 nm).

2.5.8 H_2O_2 Detection Using Amplex® Red

A quartz cuvette containing compounds **8** (1.25 µL of 10 mM) in phosphate buffer of pH 7.4 (499 µL) was irradiated. Similarly, compounds **8** (1.25 µL of 10 mM) in phosphate buffer of pH 7.4 (499 µL) was kept in dark. As a positive control, **1** (1.25 µL of 10 mM) in phosphate buffer of pH 7.4 (499 µL) was used in dark. In a separate control experiment, **8** (1.25 µL of 10 mM) in phosphate buffer of pH 7.4 (494 µL) was irradiated, followed by addition of catalase enzyme (5 µL of 10,000 U/mL). Aliquots (100 µL) of these solutions were transferred to the

96 well-plate in triplicates and incubated for 2 h at 37 °C. The working solution of Amplex® Red (100 μL) was added in each well and further incubated for 30 min at 37 °C. Fluorescence measurement was done using Thermo Scientific Varioskan microtiter plate reader (λ_{ex} = 550 nm and λ_{em} = 590 nm).

2.5.9 Thiol Reactivity of ROS Generators

Compound **1**, **2,** Juglone and Menadione (5 μL of 10 mM stock in DMSO) in the 1:1 mixture of pH 7.4 phosphate buffer:Acetonitrile (945 μL) were independently reacted with glutathione (50 μL of 10 mM) for 4 h at 37 °C. Reaction mixtures were filtered (0.45 μm) and injected (25 μL) in an Agilent high performance liquid chromatograph (HPLC) attached with a Diode array detector operating at 250 nm. A mobile phase of water: acetonitrile was used with a run time of 20 min. A multistep gradient was used with a flow rate of 1 mL/min starting with 50: 50 →0 to 2 min, 50:50 to 10: 90 → 2 - 17 min, 10: 90 to 50:50 →17 – 19 min, 50:50 → 19 - 20 min.

2.5.10 Extracellular H_2O_2 Detection Using Boronate-Ester Probe 23

Human adenocarcinomic alveolar basal epithelial cells, A549 cells were seeded at a concentration of 1×10^4 cells/well overnight in a 96-well plate in complete RPMI media. Cells were treated with 50 μM concentrations of the compound **8** and **1**. Cells were first exposed to 365 nm light for 5 min and as a control other section of plate was covered with aluminum foil kept in dark then incubated for 2 h at 37 ºC. In the non-irradiated and irradiated part of the plate, **23** (100 μM) was added and incubated for 2 h at 37 °C. All these experiments were done in triplicate. Further aliquots (200 μL) from these wells were transferred to another 96 well-plate and the fluorescence was measured using Thermo Scientific Varioskan microtiter plate reader (λ_{ex} = 320 nm and λ_{em} = 460 nm).

2.5.11 Extracellular H_2O_2 Detection Using Amplex® Red

Human adenocarcinomic alveolar basal epithelial cells, A549 cells were seeded at a concentration of 1×10^4 cells/well overnight in a 96-well plate in complete RPMI media. Cells were treated with 50 μM concentrations of the compound **8** and **1**. Cells were first exposed to 365 nm light for 5 min and other as a control other section of plate was covered with aluminum foil kept in dark then incubated for 4 h at 37 ºC. Further aliquots (50 μL) from these wells were transferred to another 96 well-plate. The working solution of Amplex® Red (50 μL) was added

in each well and further incubated for 30 min at 37 °C. Fluorescence measurement was done using Thermo Scientific Varioskan microtiter plate reader (λ_{ex} = 550 nm and λ_{em} = 590 nm).

2.5.12 Intracellular ROS Detection Using H_2DCFDA Dye by Fluorescence Measurement

Human adenocarcinomic alveolar basal epithelial cells, A549 cells were seeded at a concentration of 2×10^4 cells/well overnight in two parts of 96-well plate in complete RPMI media. Cells in both parts were exposed to 50 µM of the compound **8.** After 2 h incubation at 37 ºC, old media of each wells was replaced with fresh media and one part of the plate was exposed to 365 nm light for 5 min and other part of plate was covered with aluminum foil then incubated for 1 h at 37 ºC. A 10 µM solution of 2',7'-dichlorodihydrofluorescein diacetate (H_2DCFDA) was prepared in RPMI media and 300 µL of this solution was added to each well. After 10 min incubation, the excess dye was removed and washed twice with PBS and finally 200 µL of PBS was added. Intensity of all the wells were measured in Operetta CLS™ high-content analysis system by PerkinElmer in the GFP channel (excitation 488 nm; emission 514 nm).

2.5.13 Intracellular ROS Detection by H_2DCFDA Dye by Fluorescence Imaging

Human adenocarcinomic alveolar basal epithelial cells, A549 cells were seeded at a concentration of 1×10^5 cells/well in two parts of 12-well plate in complete RPMI media and incubated for 48 h at 37 ºC. Cells were treated with 50 µM of the compound **8** and further incubated for 2 h at 37 ºC. Old media of each wells were removed and washed twice with PBS. At this point, fresh media was added and one part of the plate was exposed to 365 nm light for 5 min and other part of plate was covered with aluminum foil then incubated for 1 h at 37 ºC. A 10 µM solution of 2',7'-dichlorodihydrofluorescein diacetate (H_2DCFDA) was prepared in RPMI media and 1 mL of this solution was added to each well. After 10 min incubation, the excess dye was removed and washed twice with PBS and finally 1 mL of PBS was added. All the wells were Imaged in EVOS® FL Auto Imaging System in the GFP channel (excitation 488 nm; emission 514 nm).

2.5.14 Cell Viability Assay Using MTT Dye

Human adenocarcinomic alveolar basal epithelial cells, A549 and human colon adenocarcinoma cells, DLD-1 were seeded independently at a concentration of 1×10^3 cells/well overnight in a 96-well plate in complete RPMI media. Cells were exposed to varying

concentrations of the compound **1** and **8** prepared as a 10 mM DMSO stock solution so that the final concentration of DMSO was 0.5%. Cells were first exposed to 365 nm light for 5 min and then incubated for 72 h at 37 ºC. Similar plate was also kept in dark as a control. A solution of 3-(4, 5-dimethylthiazol-2-yl)-2, 5-diphenyl tetrazolium bromide (MTT) was prepared by dissolving MTT reagent (3.5 mg) in 7 mL RPMI media. 100 μL of this solution was added to each well. After 4 h incubation, the media was removed carefully and 100 μL of DMSO was added. Spectrophotometric analysis of each well was carried out at 570 nm using a Thermo Scientific Varioskan microplate reader to estimate cell viability.

2.6 Spectral Charts

^{1}H NMR spectrum ($CDCl_3$, 400 MHz) of **12**

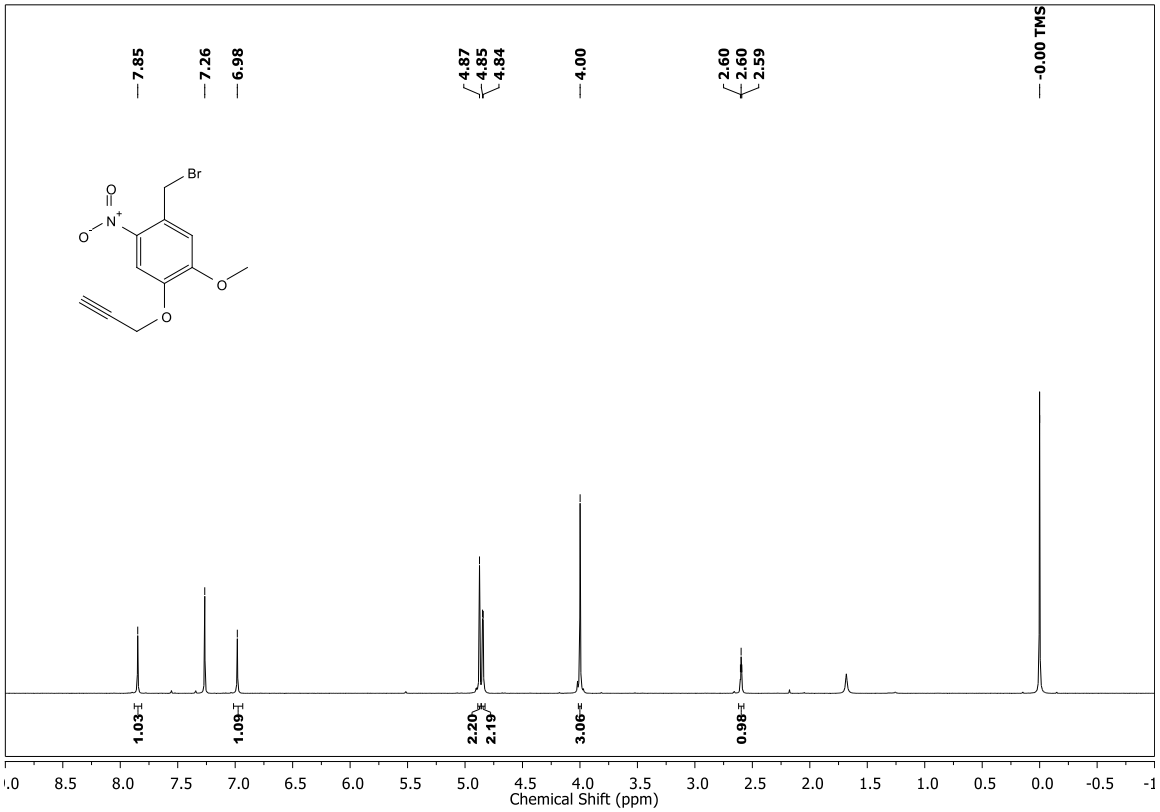

^{1}H NMR spectrum ($CDCl_3$, 400 MHz) of **19**

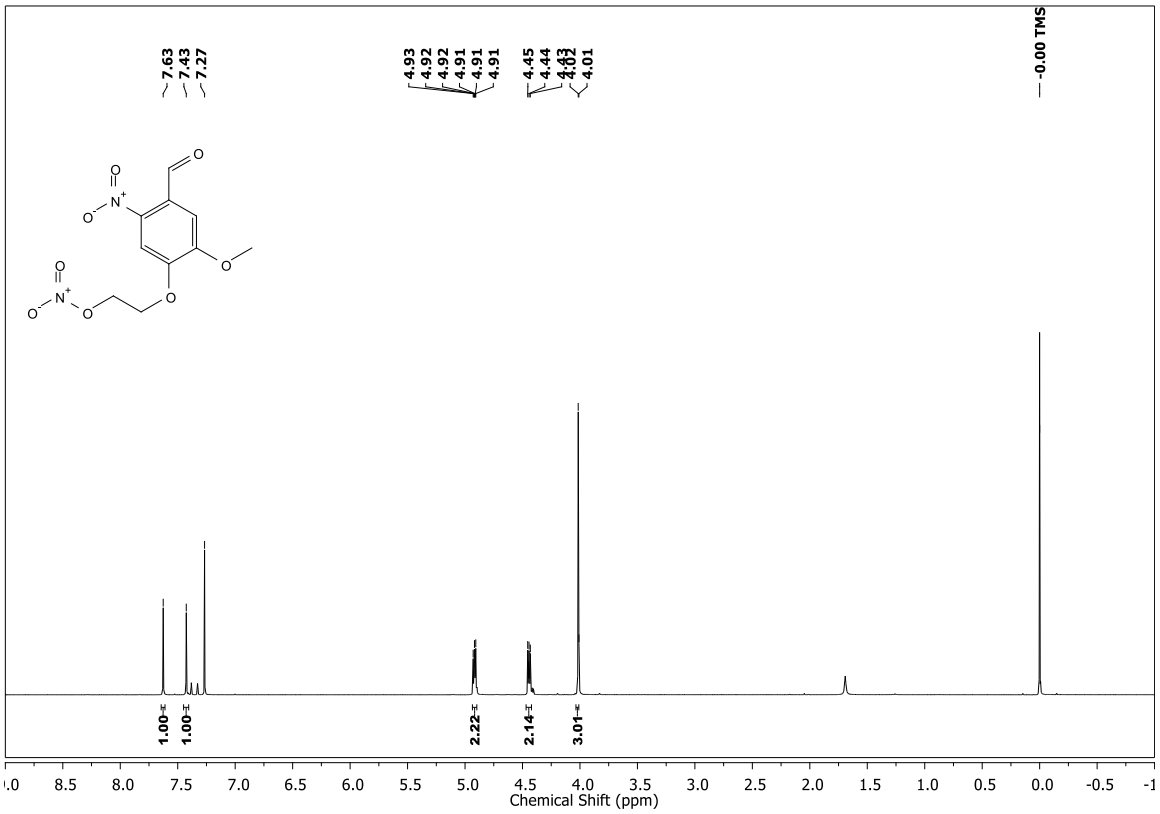

^{1}H NMR spectrum ($CDCl_3$, 400 MHz) of **20**

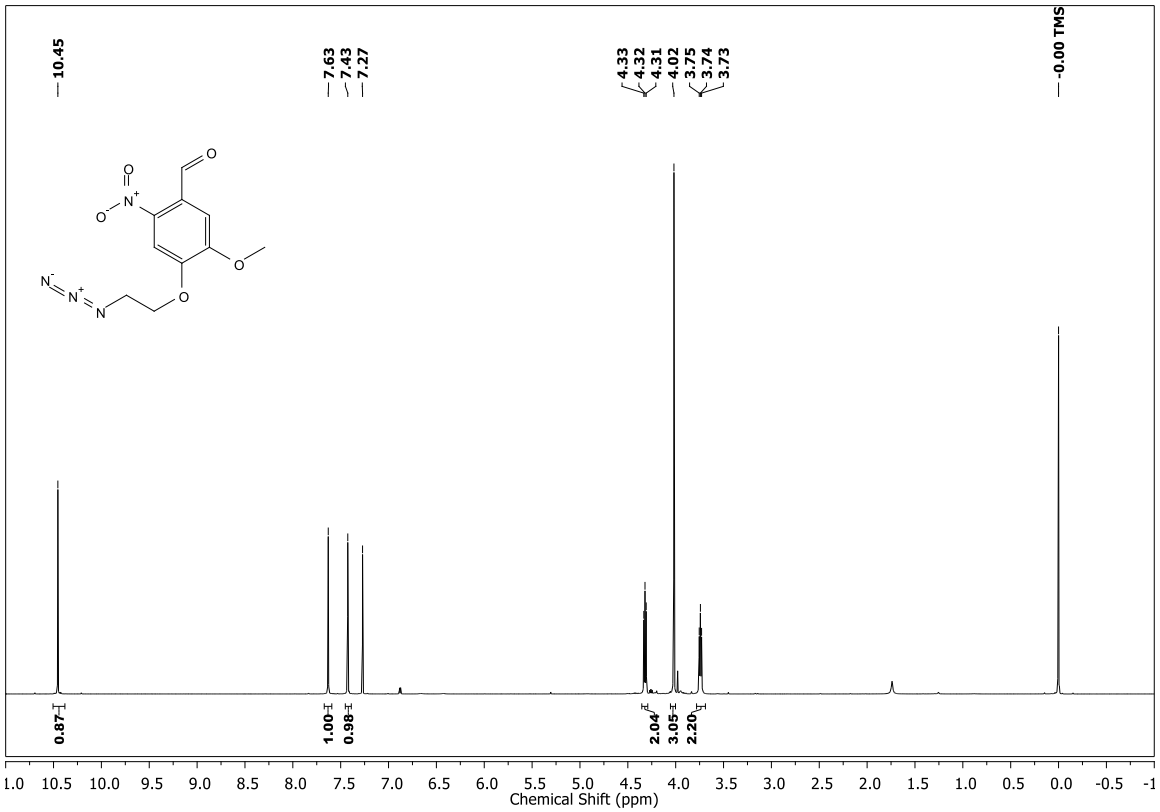

^{13}C-NMR spectrum ($CDCl_3$, 100 MHz) of **20**

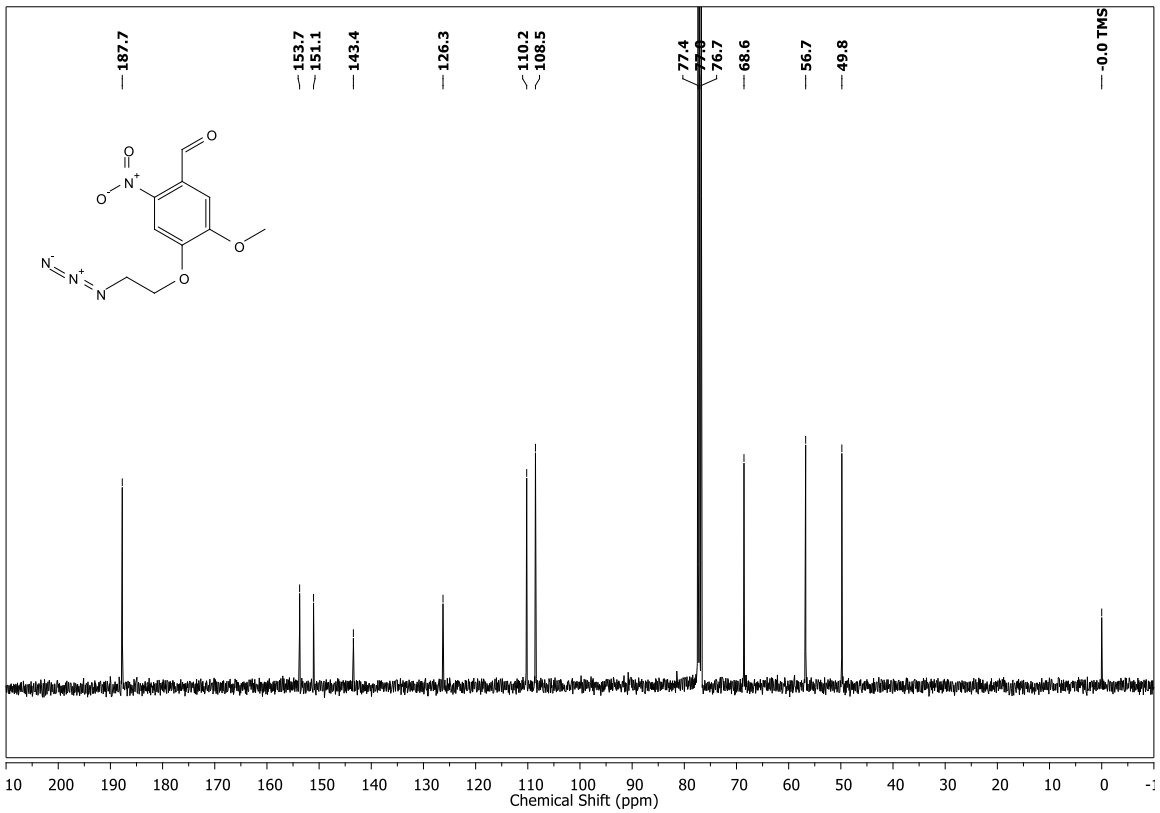

^{1}H NMR spectrum ($CDCl_3$, 400 MHz) of **21**

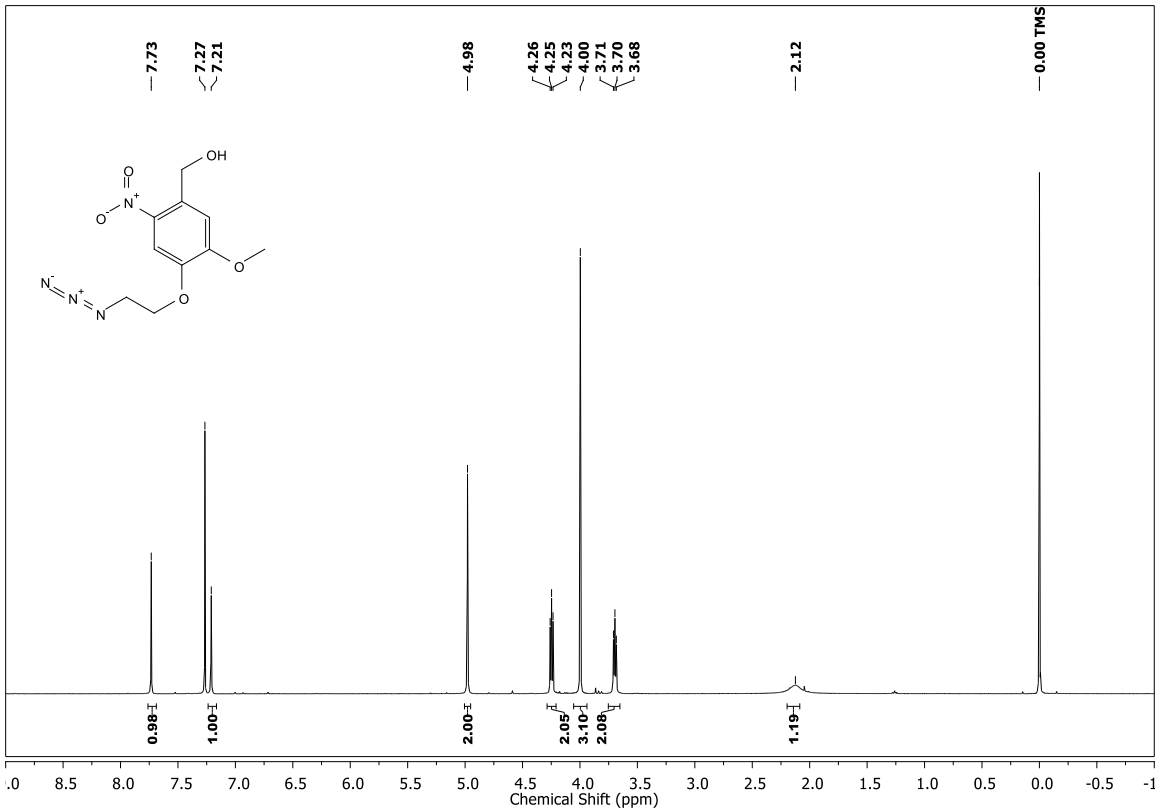

^{13}C NMR spectrum ($CDCl_3$, 100 MHz) of **21**

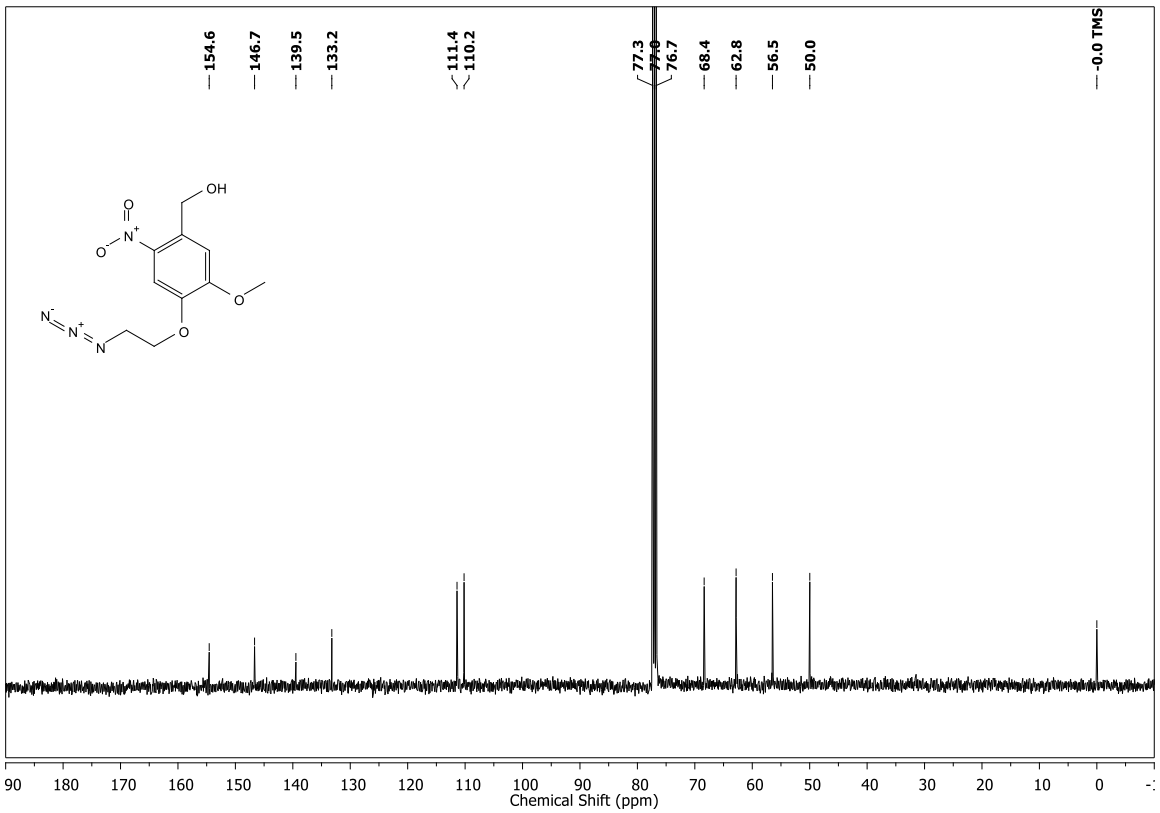

^{1}H NMR spectrum ($CDCl_3$, 400 MHz) of **13**

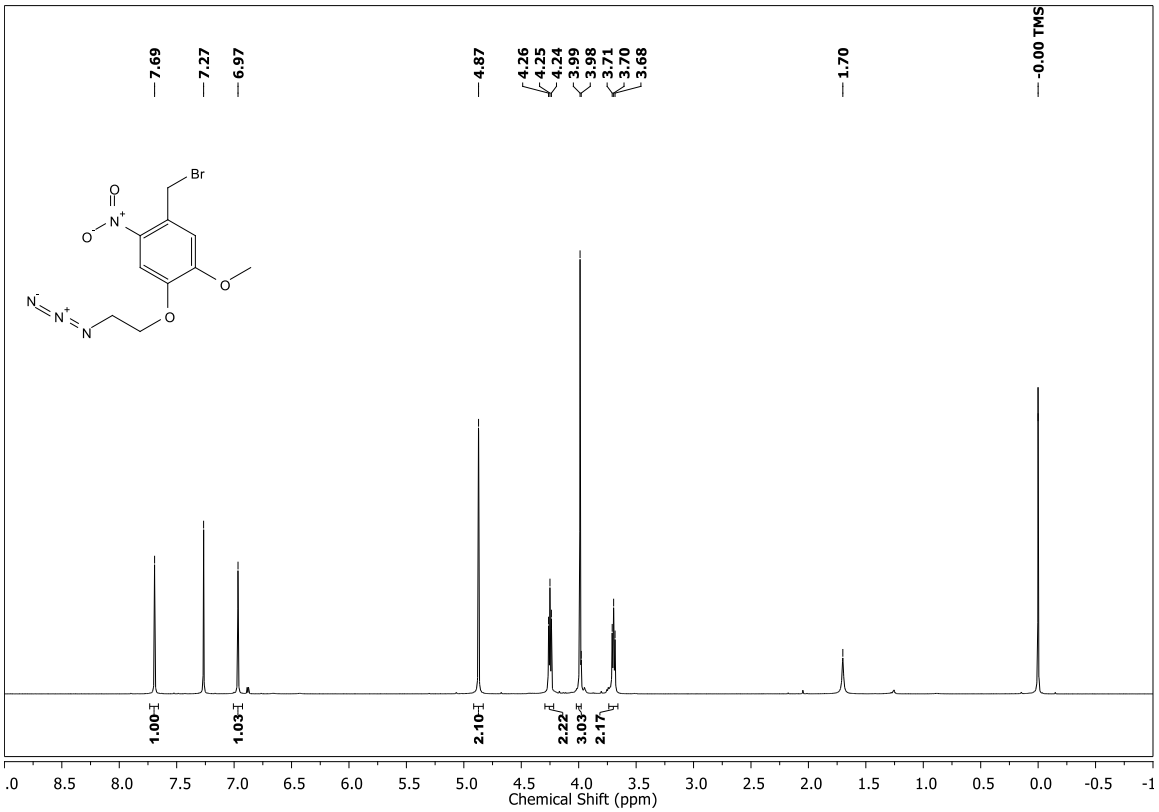

^{13}C NMR spectrum ($CDCl_3$, 100 MHz) of **13**

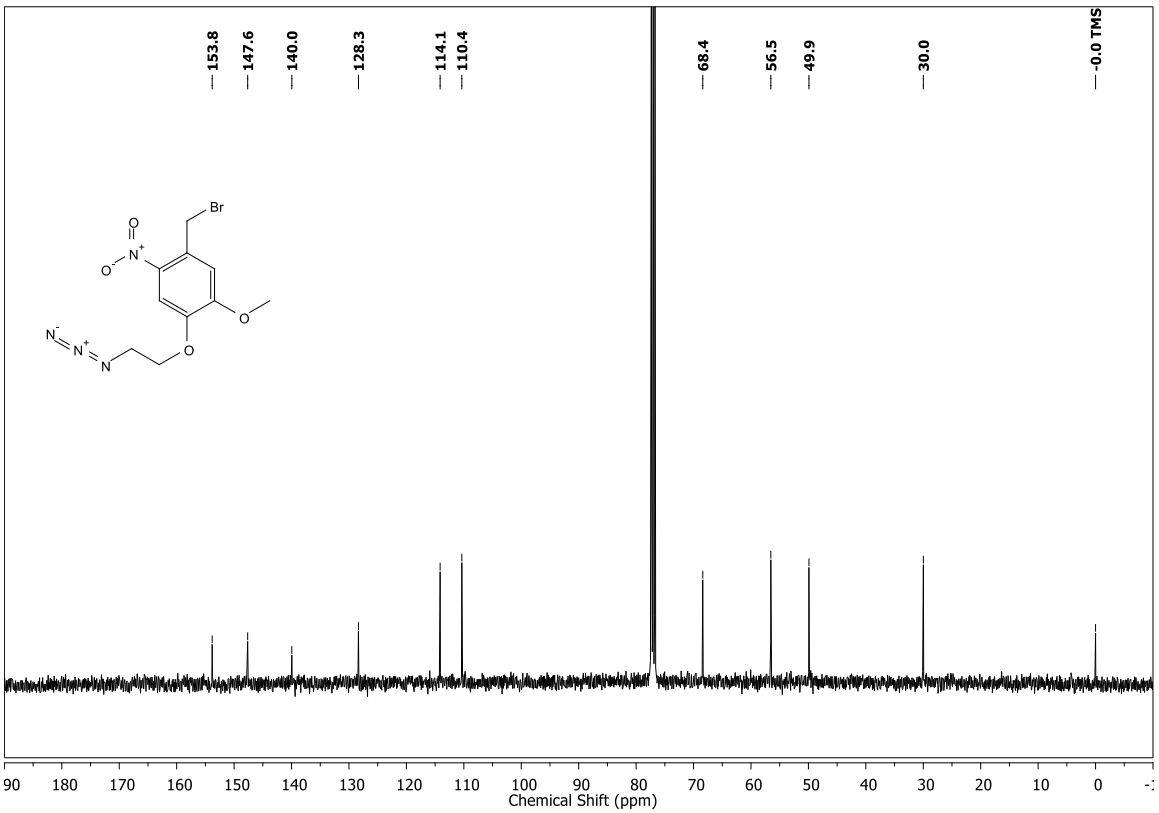

^{1}H NMR spectrum ($CDCl_3$, 400 MHz) of **4**

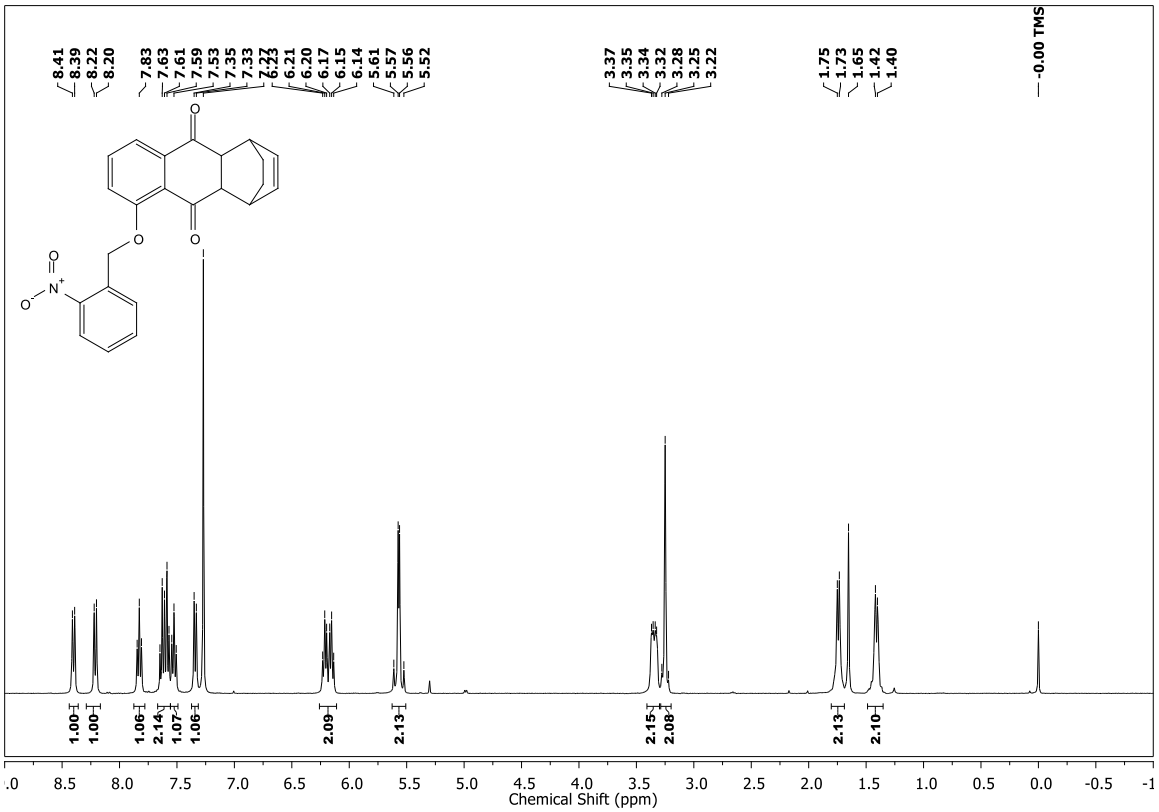

^{13}C NMR spectrum ($CDCl_3$, 100 MHz) of **4**

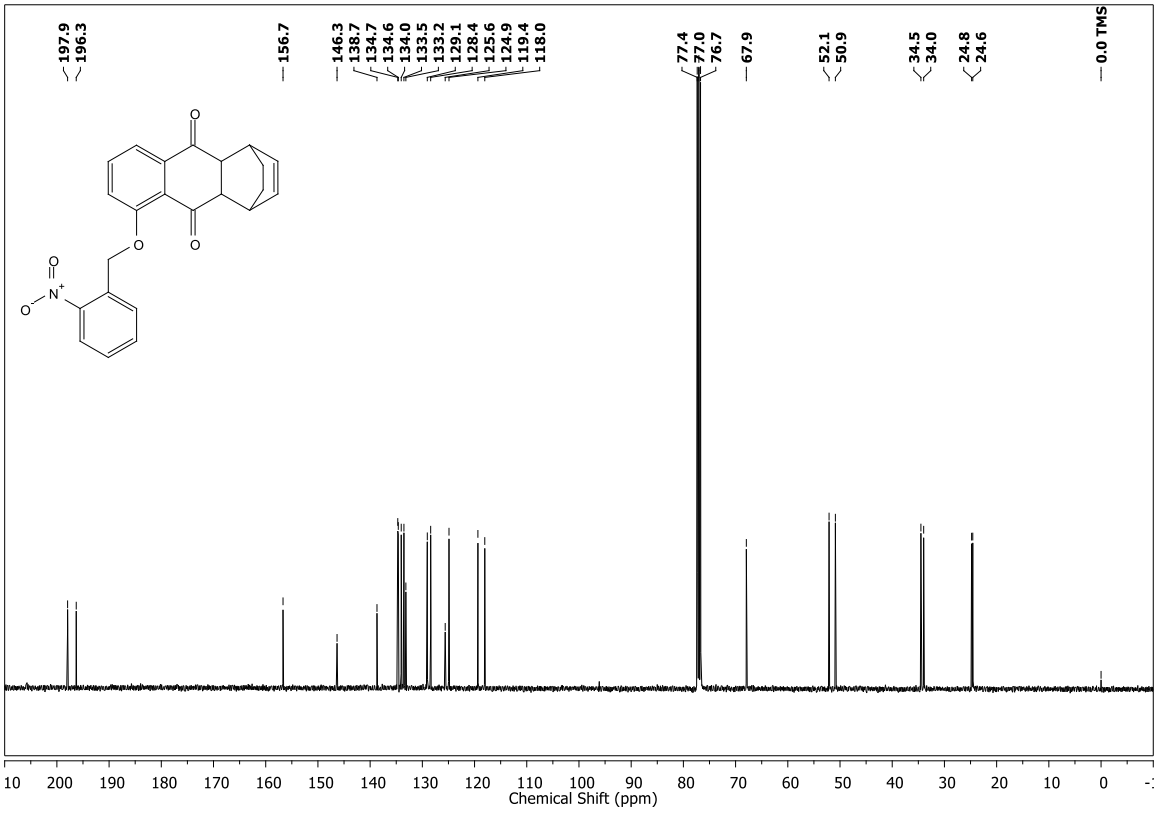

^{1}H NMR spectrum ($CDCl_3$, 400 MHz) of **5**

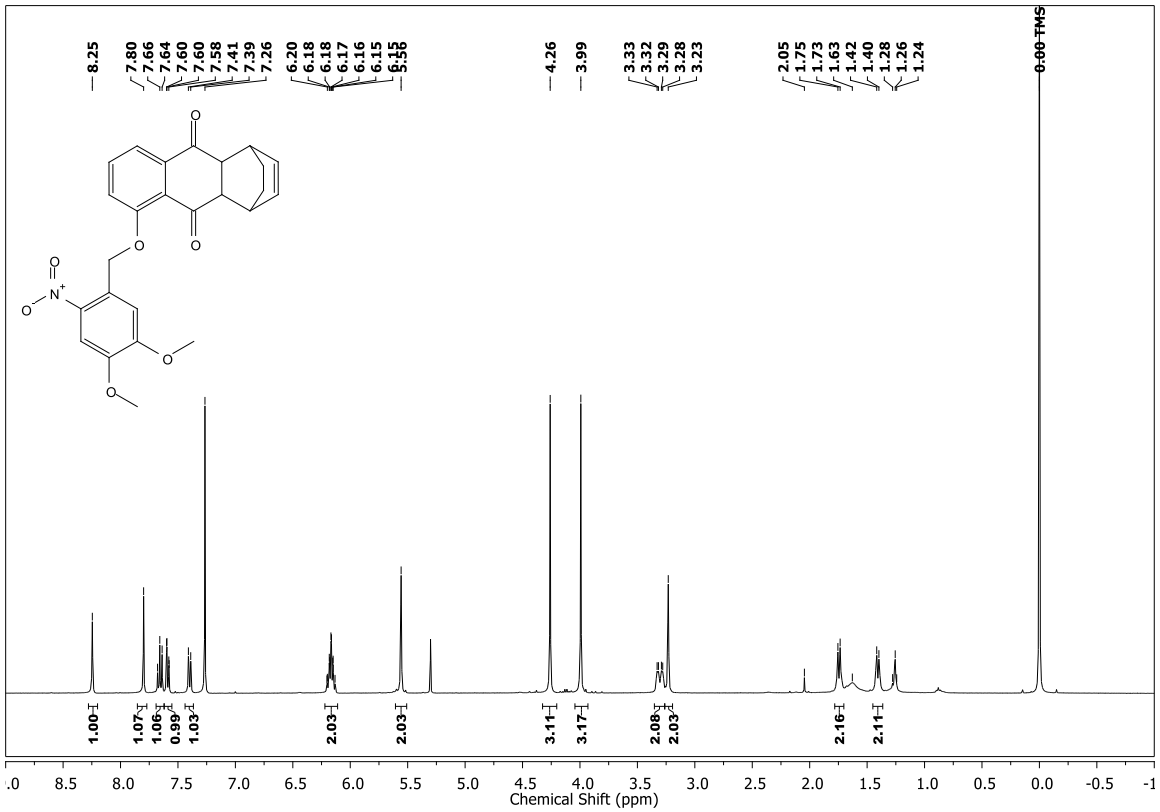

^{13}C NMR spectrum ($CDCl_3$, 100 MHz) of **5**

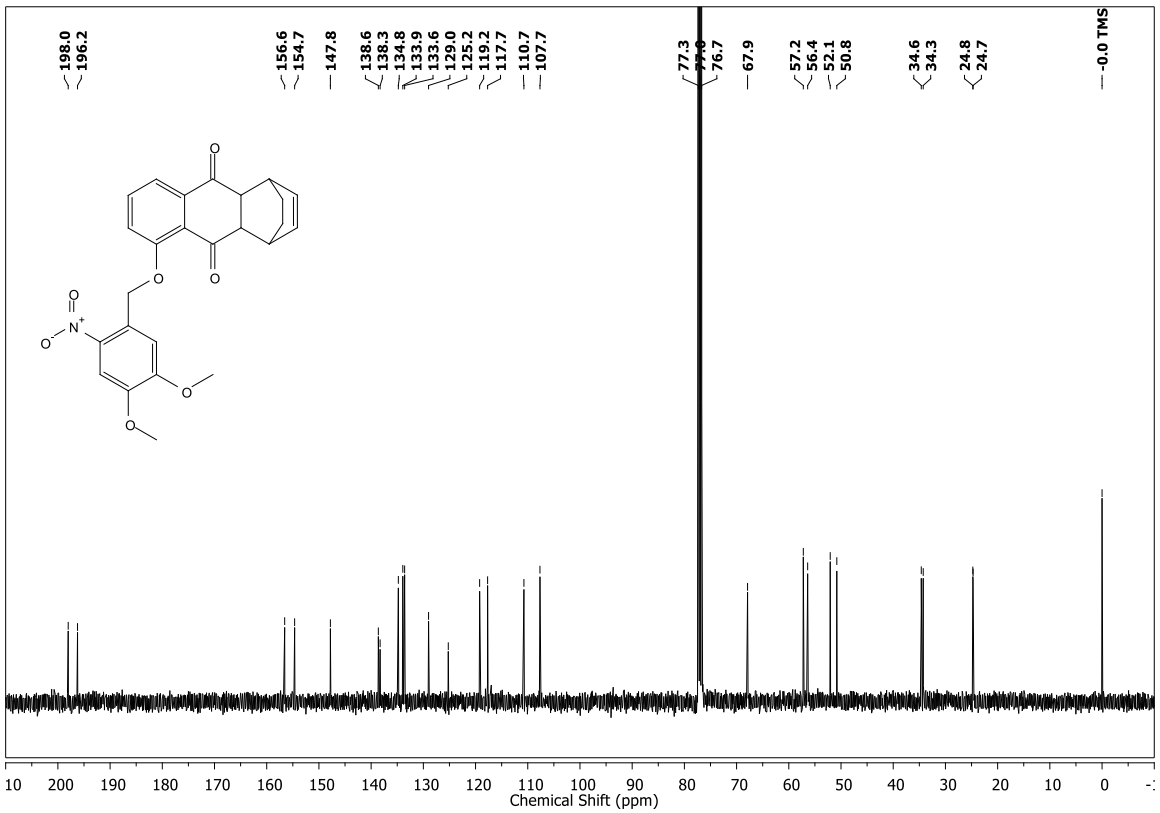

^{1}H NMR spectrum ($CDCl_3$, 400 MHz) of **7**

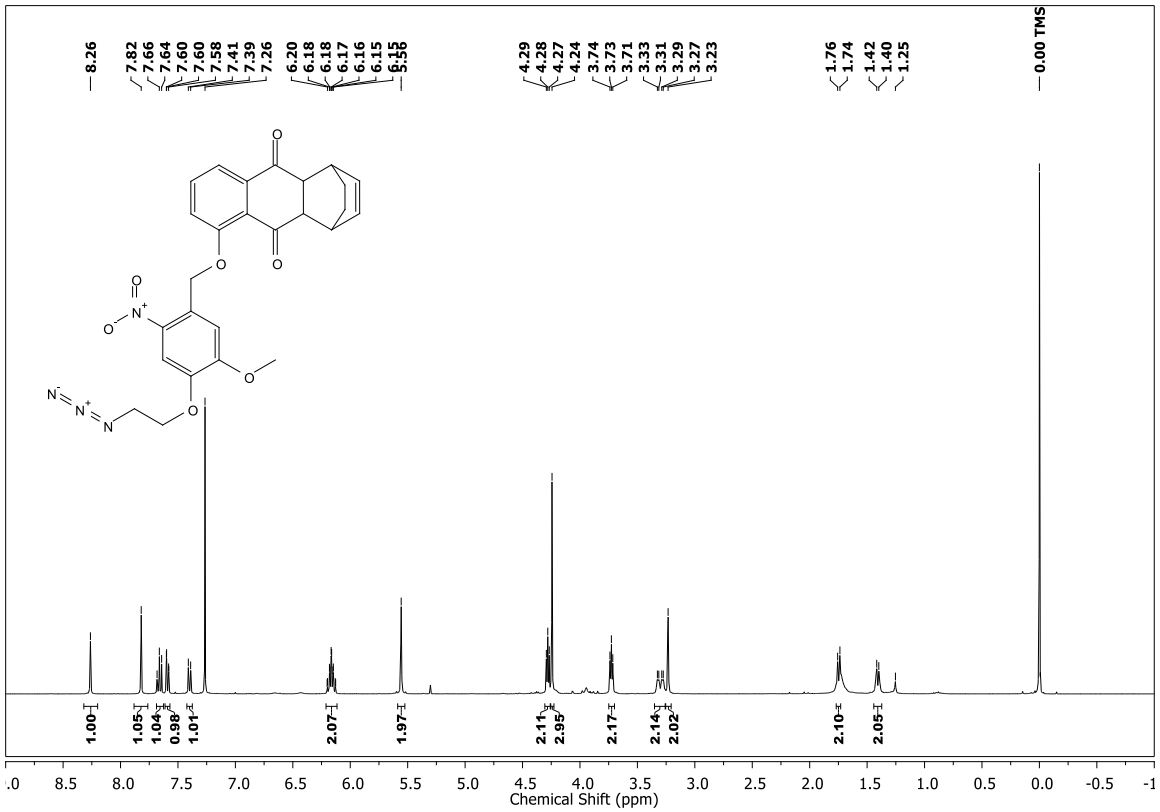

^{13}C NMR spectrum ($CDCl_3$, 100 MHz) of **7**

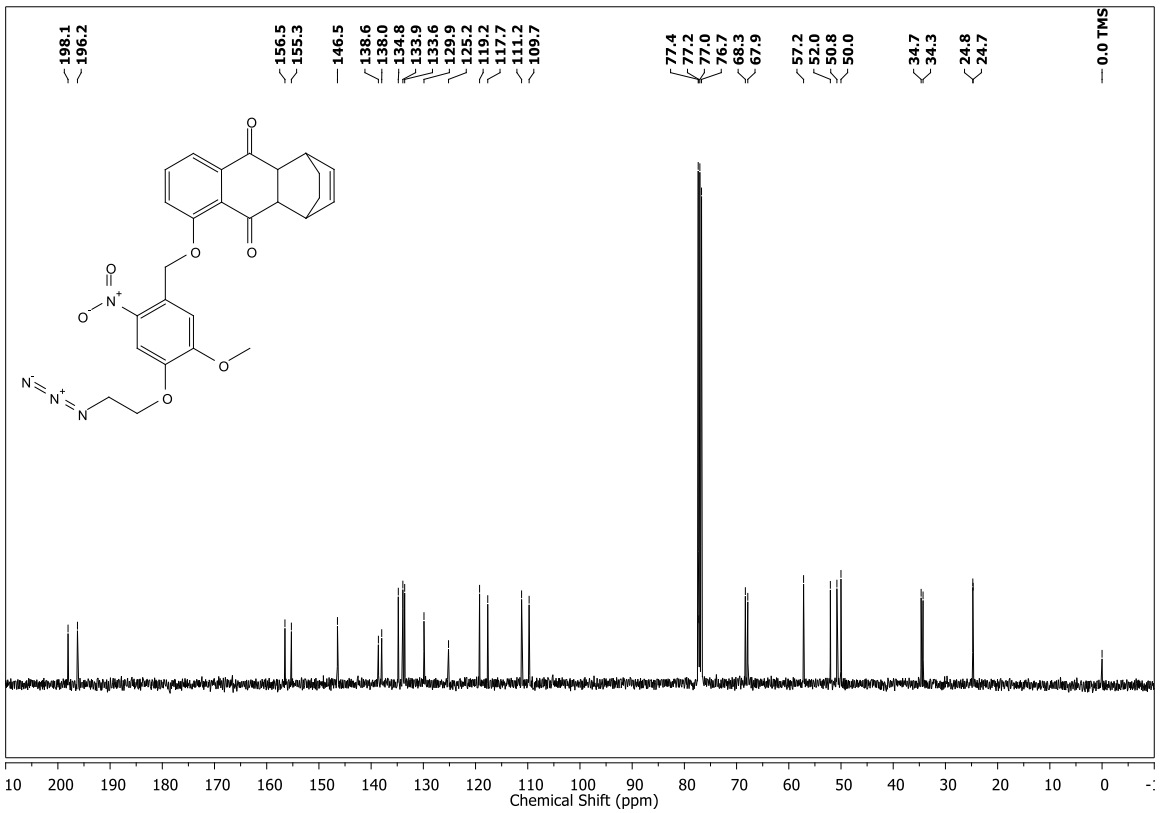

^{1}H NMR spectrum (DMSO-d_6, 400 MHz) of **8**

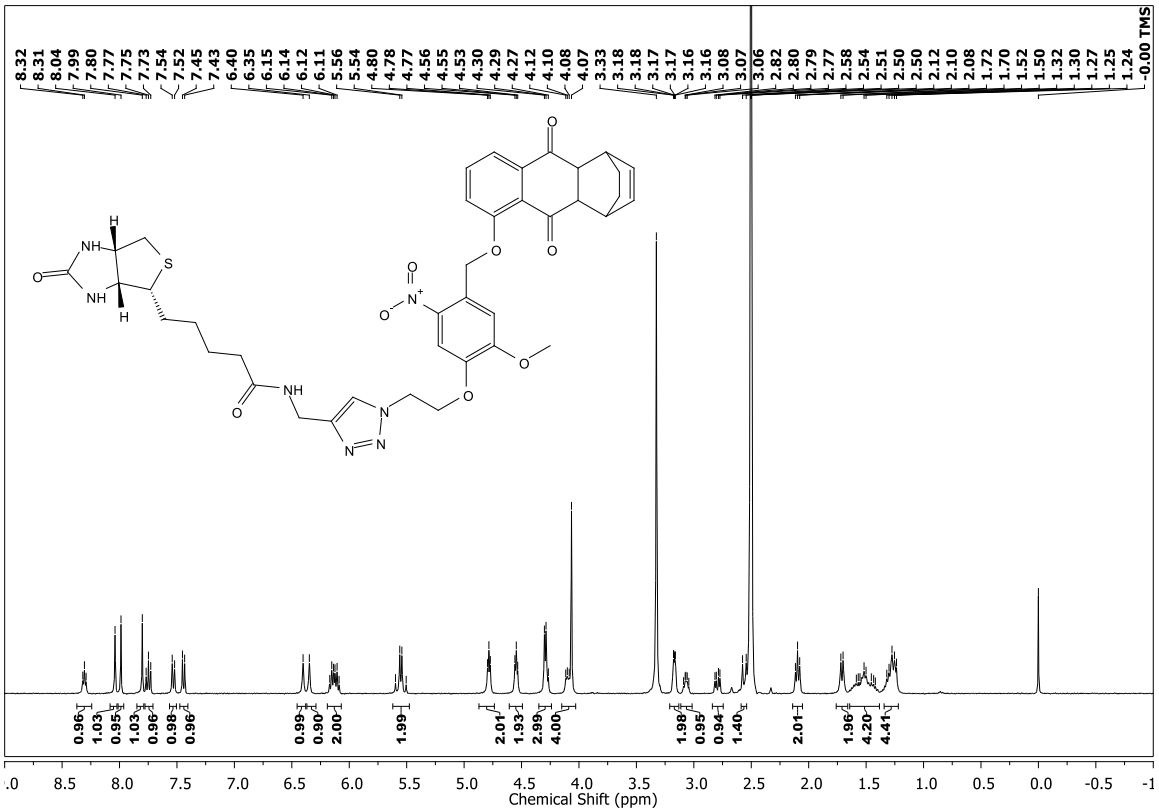

^{13}C NMR spectrum (DMSO-d_6, 100 MHz) of **8**

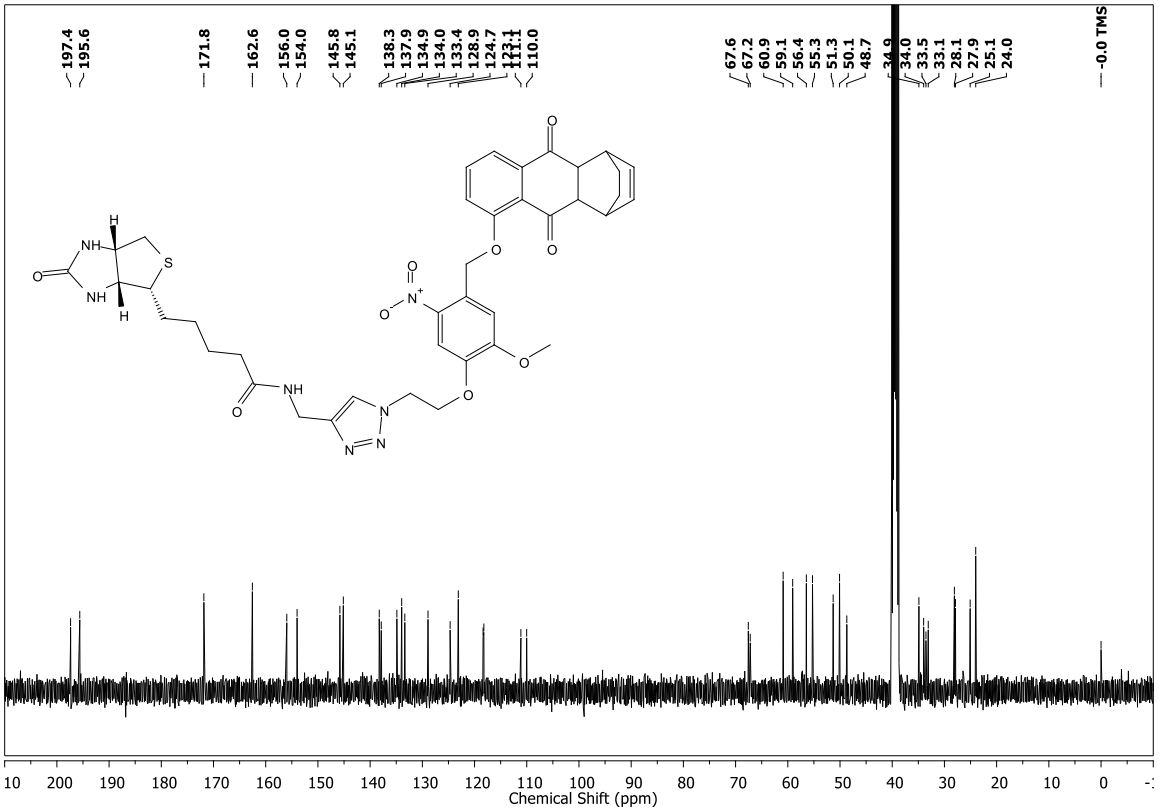

^{1}H NMR spectrum ($CDCl_3$, 400 MHz) of **9**

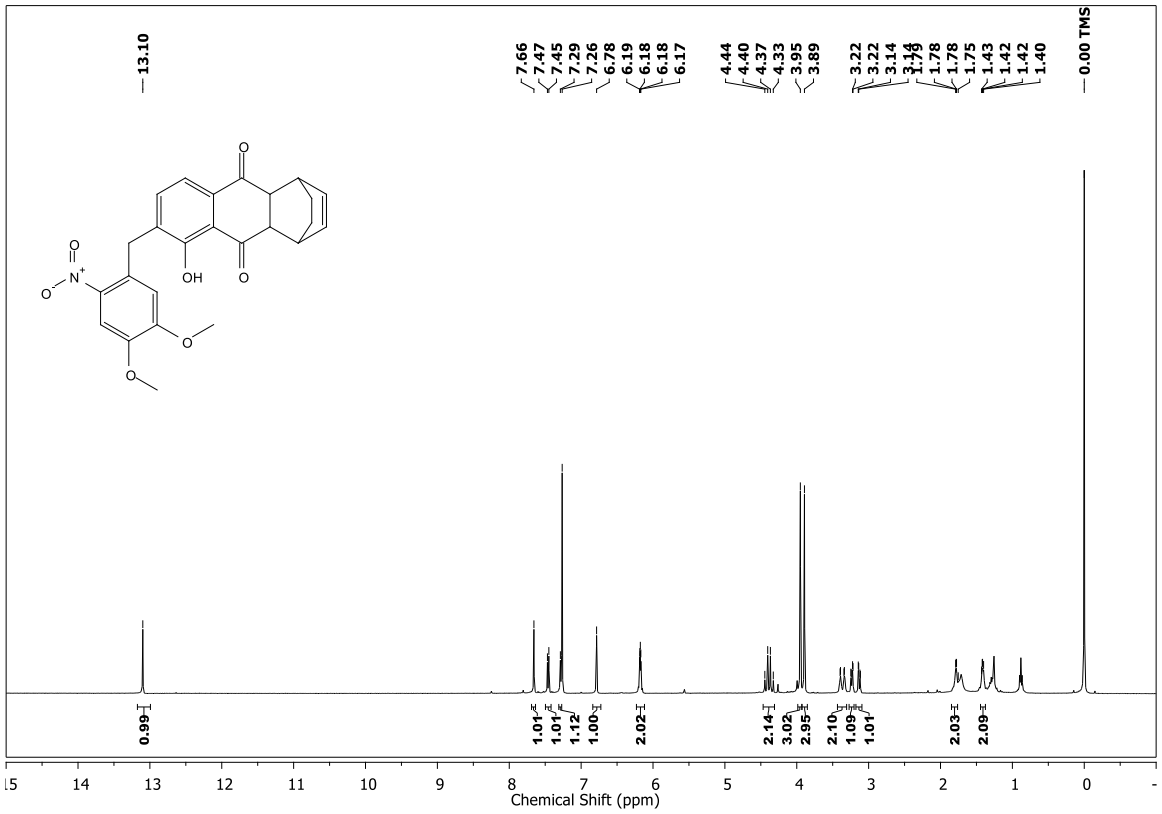

^{13}C NMR spectrum ($CDCl_3$, 100 MHz) of **9**

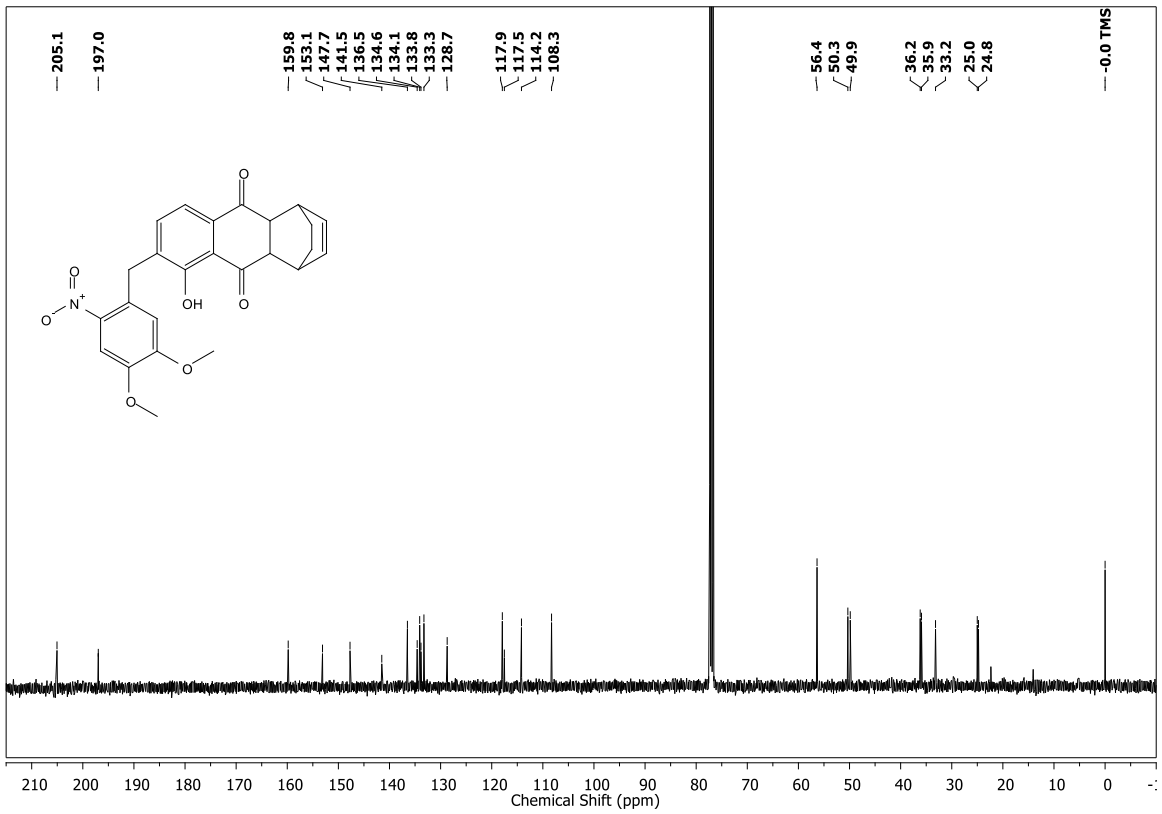

^{1}H-NMR spectrum (DMSO-d_6, 400 MHz) of **22**

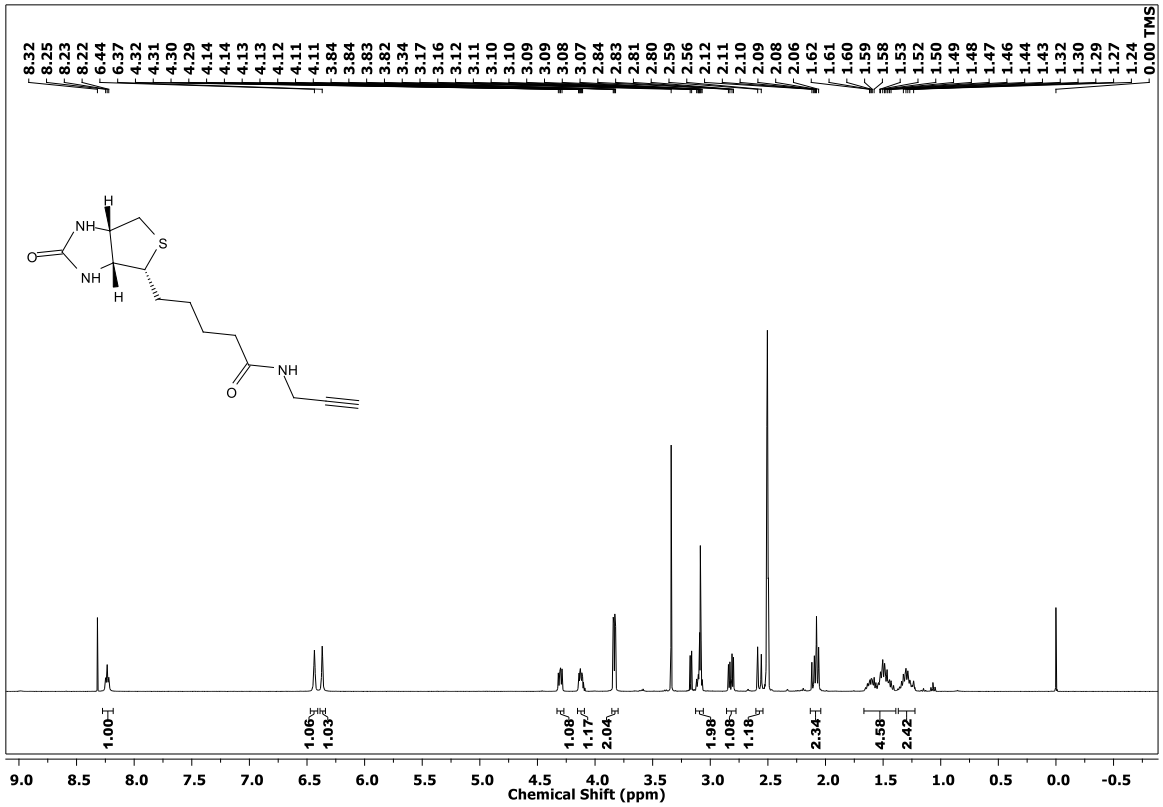

2.7 References

(1) Murphy, M. P. How Mitochondria Produce Reactive Oxygen Species. *Biochem. J.* **2009**, *417* (1), 1–13.

(2) Lambert, A. J.; Brand, M. D. Reactive Oxygen Species Production by Mitochondria. In *Methods in molecular biology.* **2009**, *554*, 165–181.

(3) Schieber, M.; Chandel, N. S. ROS Function in Redox Signaling and Oxidative Stress. *Curr. Biol.* **2014**, *24* (10), R453–R462.

(4) Finkel, T.; Holbrook, N. J. Oxidants, Oxidative Stress and the Biology of Ageing. *Nature* **2000**, *408* (6809), 239–247.

(5) Liu, J.; Wang, Z. Increased Oxidative Stress as a Selective Anticancer Therapy. *Oxid. Med. Cell. Longev.* **2015**, *2015*, 1–12.

(6) Banerjee, S.; Ghosh, J. Drug Metabolism and Oxidative Stress: Cellular Mechanism and New Therapeutic Insights. *Biochem. Anal. Biochem.* **2016**, 10.4172/2161-1009.1000255.

(7) Lenaz, G.; Bovina, C.; D'aurelio, M.; Fato, R.; Formiggini, G.; Genova, M. L.; Giuliano, G.; Pich, M. M.; Paolucci, U.; Castelli, G. P.; Et Al. Role Of Mitochondria in Oxidative Stress and Aging. *Ann. N. Y. Acad. Sci.* **2002**, *959* (1), 199–213.

(8) Hartwig, K.; Heidler, T.; Moch, J.; Daniel, H.; Wenzel, U. Feeding a ROS-Generator to Caenorhabditis Elegans Leads to Increased Expression of Small Heat Shock Protein HSP-16.2 and Hormesis. *Genes Nutr.* **2009**, *4* (1), 59–67.

(9) Criddle, D. N.; Gillies, S.; Baumgartner-Wilson, H. K.; Jaffar, M.; Chinje, E. C.; Passmore, S.; Chvanov, M.; Barrow, S.; Gerasimenko, O. V; Tepikin, A. V; et al. Menadione-Induced Reactive Oxygen Species Generation via Redox Cycling Promotes Apoptosis of Murine Pancreatic Acinar Cells. *J. Biol. Chem.* **2006**, *281* (52), 40485–40492.

(10) Halilovic, A.; Schmedt, T.; Benischke, A.-S.; Hamill, C.; Chen, Y.; Santos, J. H.; Jurkunas, U. V. Menadione-Induced DNA Damage Leads to Mitochondrial Dysfunction and Fragmentation During Rosette Formation in Fuchs Endothelial Corneal Dystrophy. *Antioxid. Redox Signal.* **2016**, *24* (18), 1072–1083.

(11) Beg, M. S.; Huang, X.; Silvers, M. A.; Gerber, D. E.; Bolluyt, J.; Sarode, V.; Fattah, F.; Deberardinis, R. J.; Merritt, M. E.; Xie, X.-J.; et al. Using a Novel NQO1 Bioactivatable Drug, Beta-Lapachone (ARQ761), to Enhance Chemotherapeutic Effects by Metabolic Modulation in Pancreatic Cancer. *J. Surg. Oncol.* **2017**, *116* (1), 83–88.

(12) Yang, Y.; Zhou, X.; Xu, M.; Piao, J.; Zhang, Y.; Lin, Z.; Chen, L. β-Lapachone

Suppresses Tumour Progression by Inhibiting Epithelial-to-Mesenchymal Transition in NQO1-Positive Breast Cancers. *Sci. Rep.* **2017**, *7* (1), 2681.

(13) Silvers, M. A.; Deja, S.; Singh, N.; Egnatchik, R. A.; Sudderth, J.; Luo, X.; Beg, M. S.; Burgess, S. C.; DeBerardinis, R. J.; Boothman, D. A.; et al. The NQO1 Bioactivatable Drug, β-Lapachone, Alters the Redox State of NQO1+ Pancreatic Cancer Cells, Causing Perturbation in Central Carbon Metabolism. *J. Biol. Chem.* **2017**, *292* (44), 18203–18216.

(14) Ough, M.; Lewis, A.; Bey, E. A.; Gao, J.; Ritchie, J. M.; Bornmann, W.; Boothman, D. A.; Oberley, L. W.; Cullen, J. J. Efficacy of Beta-Lapachone in Pancreatic Cancer Treatment: Exploiting the Novel, Therapeutic Target NQO1. *Cancer Biol. Ther.* **2005**, *4* (1), 102–109.

(15) Wang, X.; Luo, F.; Zhao, H. Paraquat-Induced Reactive Oxygen Species Inhibit Neutrophil Apoptosis via a P38 MAPK/NF-KB–IL-6/TNF-α Positive-Feedback Circuit. *PLoS One* **2014**, *9* (4), e93837.

(16) Kim, H.; Lee, S. W.; Baek, K. M.; Park, J. S.; Min, J. H. Continuous Hypoxia Attenuates Paraquat-Induced Cytotoxicity in the Human A549 Lung Carcinoma Cell Line. *Exp. Mol. Med.* **2011**, *43* (9), 494–500.

(17) Castello, P. R.; Drechsel, D. A.; Patel, M. Mitochondria Are a Major Source of Paraquat-Induced Reactive Oxygen Species Production in the Brain. *J. Biol. Chem.* **2007**, *282* (19), 14186–14193.

(18) Frank, D. M.; Arora, P. K.; Blumer, J. L.; Sayre, L. M. Model Study on the Bioreduction of Paraquat, MPP+, and Analogs. Evidence against a "Redox Cycling" Mechanism in MPTP Neurotoxicity. *Biochem. Biophys. Res. Commun.* **1987**, *147* (3), 1095–1104.

(19) DeGray, J. A.; Rao, D. N. R.; Mason, R. P. Reduction of Paraquat and Related Bipyridylium Compounds to Free Radical Metabolites by Rat Hepatocytes. *Arch. Biochem. Biophys.* **1991**, *289* (1), 145–152.

(20) Robb, E. L.; Gawel, J. M.; Aksentijević, D.; Cochemé, H. M.; Stewart, T. S.; Shchepinova, M. M.; Qiang, H.; Prime, T. A.; Bright, T. P.; James, A. M.; et al. Selective Superoxide Generation within Mitochondria by the Targeted Redox Cycler MitoParaquat. *Free Radic. Biol. Med.* **2015**, *89*, 883–894.

(21) Dharmaraja, A. T. Role of Reactive Oxygen Species (ROS) in Therapeutics and Drug Resistance in Cancer and Bacteria. *J. Med. Chem.* **2017**, *60* (8), 3221–3240.

(22) Adams, D. J.; Boskovic, Z. V.; Theriault, J. R.; Wang, A. J.; Stern, A. M.; Wagner, B. K.; Shamji, A. F.; Schreiber, S. L. Discovery of Small-Molecule Enhancers of Reactive

Oxygen Species That Are Nontoxic or Cause Genotype-Selective Cell Death. *ACS Chem. Biol.* **2013**, *8* (5), 923–929.

(23) Agostinis, P.; Berg, K.; Cengel, K. A.; Foster, T. H.; Girotti, A. W.; Gollnick, S. O.; Hahn, S. M.; Hamblin, M. R.; Juzeniene, A.; Kessel, D.; et al. Photodynamic Therapy of Cancer: An Update. *CA. Cancer J. Clin.* **2011**, *61* (4), 250–281.

(24) DeRosa, M. C.; Crutchley, R. J. Photosensitized Singlet Oxygen and Its Applications. *Coord Chem Rev* **2002**, *233–234*, 351–371.

(25) Onyango, A. N. Endogenous Generation of Singlet Oxygen and Ozone in Human and Animal Tissues: Mechanisms, Biological Significance, and Influence of Dietary Components. *Oxid. Med. Cell. Longev.* **2016**, *2016*, 2398573.

(26) Khodade, V. S.; Sharath Chandra, M.; Banerjee, A.; Lahiri, S.; Pulipeta, M.; Rangarajan, R.; Chakrapani, H. Bioreductively Activated Reactive Oxygen Species (ROS) Generators as MRSA Inhibitors. *ACS Med. Chem. Lett.* **2014**, *5* (7), 777–781.

(27) Dharmaraja, A. T.; Dash, T. K.; Konkimalla, V. B.; Chakrapani, H. Synthesis, Thiol-Mediated Reactive Oxygen Species Generation Profiles and Anti-Proliferative Activities of 2,3-Epoxy-1,4-Naphthoquinones. *Med. Chem. Commun.* **2012**, *3* (2), 219–224.

(28) Kelkar, D. S.; Ravikumar, G.; Mehendale, N.; Singh, S.; Joshi, A.; Sharma, A. K.; Mhetre, A.; Rajendran, A.; Chakrapani, H.; Kamat, S. S. A Chemical–Genetic Screen Identifies ABHD12 as an Oxidized-Phosphatidylserine Lipase. *Nat. Chem. Biol.* **2019**, *15* (2), 169–178.

(29) Carling, C.-J.; Viger, M. L.; Nguyen Huu, V. A.; Garcia, A. V; Almutairi, A. In Vivo Visible Light-Triggered Drug Release from an Implanted Depot. *Chem. Sci.* **2015**, *6* (1), 335–341.

(30) Venkatesh, Y.; Das, J.; Chaudhuri, A.; Karmakar, A.; Maiti, T. K.; Singh, N. D. P. Light Triggered Uncaging of Hydrogen Sulfide (H2S) with Real-Time Monitoring. *Chem. Commun.* **2018**, *54* (25), 3106–3109.

(31) Sharma, A. K.; Nair, M.; Chauhan, P.; Gupta, K.; Saini, D. K.; Chakrapani, H. Visible-Light-Triggered Uncaging of Carbonyl Sulfide for Hydrogen Sulfide (H2S) Release. *Org. Lett.* **2017**, *19* (18), 4822–4825.

(32) Wong, P. T.; Tang, S.; Cannon, J.; Mukherjee, J.; Isham, D.; Gam, K.; Payne, M.; Yanik, S. A.; Baker, J. R.; Choi, S. K. A Thioacetal Photocage Designed for Dual Release: Application in the Quantitation of Therapeutic Release by Synchronous Reporter Decaging. *ChemBioChem* **2017**, *18* (1), 126–135.

(33) Zhao, Y.; Bolton, S. G.; Pluth, M. D. Light-Activated COS/H2S Donation from Photocaged Thiocarbamates. *Org. Lett.* **2017**, *19* (9), 2278–2281.

(34) Linsley, C. S.; Wu, B. M. Recent Advances in Light-Responsive on-Demand Drug-Delivery Systems. *Ther. Deliv.* **2017**, *8* (2), 89–107.

(35) Patil, N. G.; Basutkar, N. B.; Ambade, A. V. Visible Light-Triggered Disruption of Micelles of an Amphiphilic Block Copolymer with BODIPY at the Junction. *Chem. Commun.* **2015**, *51* (100), 17708–17711.

(36) Miller, E. W.; Taulet, N.; Onak, C. S.; New, E. J.; Lanselle, J. K.; Smelick, G. S.; Chang, C. J. Light-Activated Regulation of Cofilin Dynamics Using a Photocaged Hydrogen Peroxide Generator. *J. Am. Chem. Soc.* **2010**, *132* (48), 17071–17073.

(37) Jackson, D. A.; Hassan, A. B.; Errington, R. J.; Cook, P. R. Oxidative Stress Is Involved in the UV Activation of P53. *J. Cell Sci.* **1996**, *107* (7), 1753–1760.

(38) Zhang, X.; Rosenstein, B. S.; Wang, Y.; Lebwohl, M.; Wei, H. Identification of Possible Reactive Oxygen Species Involved in Ultraviolet Radiation-Induced Oxidative DNA Damage. *Free Radic. Biol. Med.* **1997**, *23* (7), 980–985.

(39) Heck, D. E.; Vetrano, A. M.; Mariano, T. M.; Laskin, J. D. UVB Light Stimulates Production of Reactive Oxygen Species. *J. Biol. Chem.* **2003**, *278* (25), 22432–22436.

(40) Bossi, O.; Gartsbein, M.; Leitges, M.; Kuroki, T.; Grossman, S.; Tennenbaum, T. UV Irradiation Increases ROS Production via PKCδ Signaling in Primary Murine Fibroblasts. *J. Cell. Biochem.* **2008**, *105* (1), 194–207.

(41) de Jager, T. L.; Cockrell, A. E.; Du Plessis, S. S. Ultraviolet Light Induced Generation of Reactive Oxygen Species; Springer, Cham, 2017; pp 15–23.

(42) Wang, X.; Thomas, B.; Sachdeva, R.; Arterburn, L.; Frye, L.; Hatcher, P. G.; Cornwell, D. G.; Ma, J. Mechanism of Arylating Quinone Toxicity Involving Michael Adduct Formation and Induction of Endoplasmic Reticulum Stress. *Proc. Natl. Acad. Sci. U. S. A.* **2006**, *103* (10), 3604–3609.

(43) Chaudhuri, L.; Sarsour, E. H.; Goswami, P. C. 2-(4-Chlorophenyl)Benzo-1,4-Quinone Induced ROS-Signaling Inhibits Proliferation in Human Non-Malignant Prostate Epithelial Cells. *Environ. Int.* **2010**, *36* (8), 924–930.

(44) Cassagnes, L.-E.; Perio, P.; Ferry, G.; Moulharat, N.; Antoine, M.; Gayon, R.; Boutin, J. A.; Nepveu, F.; Reybier, K. In Cellulo Monitoring of Quinone Reductase Activity and Reactive Oxygen Species Production during the Redox Cycling of 1,2 and 1,4 Quinones. *Free Radic. Biol. Med.* **2015**, *89*, 126–134.

(45) Fato, R.; Bergamini, C.; Leoni, S.; Lenaz, G. Mitochondrial Production of Reactive

Oxygen Species: Role of Complex I and Quinone Analogues. *Biofactors* **2008**, *32* (1–4), 31–39.

(46) Bolton, J. L.; Dunlap, T. Formation and Biological Targets of Quinones: Cytotoxic versus Cytoprotective Effects. *Chem. Res. Toxicol.* **2017**, *30* (1), 13–37.

(47) Dharmaraja, A. T.; Alvala, M.; Sriram, D.; Yogeeswari, P.; Chakrapani, H. Design, Synthesis and Evaluation of Small Molecule Reactive Oxygen Species Generators as Selective Mycobacterium Tuberculosis Inhibitors. *Chem. Commun.* **2012**, *48* (83), 10325–10327.

(48) Dharmaraja, A. T.; Chakrapani, H. A Small Molecule for Controlled Generation of Reactive Oxygen Species (ROS). *Org. Lett.* **2014**, *16* (2), 398–401.

(49) Il'ichev, Y. V; Schwö, M. A.; Wirz, J. Photochemical Reaction Mechanisms of 2-Nitrobenzyl Compounds: Methyl Ethers and Caged ATP. *J. Am. Chem. Soc.* **2004**, *126* (14), 4581–4595.

(50) Fukushima, N.; Ieda, N.; Kawaguchi, M.; Sasakura, K.; Nagano, T.; Hanaoka, K.; Miyata, N.; Nakagawa, H. Development of Photo-Controllable Hydrogen Sulfide Donor Applicable in Live Cells. *Bioorg. Med. Chem. Lett.* **2015**, *25* (2), 175–178.

(51) Fukushima, N.; Ieda, N.; Sasakura, K.; Nagano, T.; Hanaoka, K.; Suzuki, T.; Miyata, N.; Nakagawa, H. Synthesis of a Photocontrollable Hydrogen Sulfide Donor Using Ketoprofenate Photocages. *Chem. Commun.* **2014**, *50* (5), 587–589.

(52) Hansen, M. J.; Velema, W. A.; Lerch, M. M.; Szymanski, W.; Feringa, B. L. Wavelength-Selective Cleavage of Photoprotecting Groups: Strategies and Applications in Dynamic Systems. *Chem. Soc. Rev* **2015**, *44*, 3358.

(53) Chen, S.; Zhao, X.; Chen, J.; Chen, J.; Kuznetsova, L.; Wong, S. S.; Ojima, I. Mechanism-Based Tumor-Targeting Drug Delivery System. Validation of Efficient Vitamin Receptor-Mediated Endocytosis and Drug Release. *Bioconjug. Chem.* **2010**, *21* (5), 979–987.

(54) Ren, W. X.; Han, J.; Uhm, S.; Jang, Y. J.; Kang, C.; Kim, J.-H.; Kim, J. S. Recent Development of Biotin Conjugation in Biological Imaging, Sensing, and Target Delivery. *Chem. Commun.* **2015**, *51* (52), 10403–10418.

(55) Kim, T.; Jeon, H. M.; Le, H. T.; Kim, T. W.; Kang, C.; Kim, J. S. A Biotin-Guided Fluorescent-Peptide Drug Delivery System for Cancer Treatment. *Chem. Commun.* **2014**, *50* (57), 7690.

(56) Luo, S.; Kansara, V. S.; Zhu, X.; Mandava, N. K.; Pal, D.; Mitra, A. K. Functional Characterization of Sodium-Dependent Multivitamin Transporter in MDCK-MDR1

Cells and Its Utilization as a Target for Drug Delivery. *Mol. Pharm.* **2006**, *3* (3), 329–339.

(57) Padilla, M. S.; Farley, C. A.; Chatkewitz, L. E.; Young, D. D. Synthesis and Incorporation of a Caged Tyrosine Amino Acid Possessing a Bioorthogonal Handle. *Tetrahedron Lett.* **2016**, *57* (42), 4709–4712.

(58) Fang, G.; Bi, X. Silver-Catalysed Reactions of Alkynes: Recent Advances. *Chem. Soc. Rev.* **2015**, *44* (22), 8124–8173.

(59) Zhao, H.; Joseph, J.; Fales, H. M.; Sokoloski, E. A.; Levine, R. L.; Vasquez-Vivar, J.; Kalyanaraman, B. Detection and Characterization of the Product of Hydroethidine and Intracellular Superoxide by HPLC and Limitations of Fluorescence. *Proc. Natl. Acad. Sci. U. S. A.* **2005**, *102* (16), 5727–5732.

(60) Zielonka, J.; Cheng, G.; Zielonka, M.; Ganesh, T.; Sun, A.; Joseph, J.; Michalski, R.; O'Brien, W. J.; Lambeth, J. D.; Kalyanaraman, B. High-Throughput Assays for Superoxide and Hydrogen Peroxide: Design of a Screening Workflow to Identify Inhibitors of NADPH Oxidases. *J. Biol. Chem.* **2014**, *289* (23), 16176–16189.

(61) Kalyanaraman, B.; Hardy, M.; Zielonka, J. A Critical Review of Methodologies to Detect Reactive Oxygen and Nitrogen Species Stimulated by NADPH Oxidase Enzymes: Implications in Pesticide Toxicity. *Curr. Pharmacol. Reports* **2016**, *2* (4), 193–201.

(62) Zielonka, J.; Vasquez-Vivar, J.; Kalyanaraman, B. Detection of 2-Hydroxyethidium in Cellular Systems: A Unique Marker Product of Superoxide and Hydroethidine. *Nat. Protoc.* **2008**, *3* (1), 8–21.

(63) Kalyanaraman, B.; Darley-Usmar, V.; Davies, K. J. A.; Dennery, P. A.; Forman, H. J.; Grisham, M. B.; Mann, G. E.; Moore, K.; Roberts, L. J.; Ischiropoulos, H. Measuring Reactive Oxygen and Nitrogen Species with Fluorescent Probes: Challenges and Limitations. *Free. Radic. Biol. Med.* **2012**, *52* (1), 1–6.

(64) Georgiou, C. D.; Papapostolou, I.; Grintzalis, K. Superoxide Radical Detection in Cells, Tissues, Organisms (Animals, Plants, Insects, Microorganisms) and Soils. *Nat. Protoc.* **2008**, *3* (11), 1679–1692.

(65) Miller, E. W.; Albers, A. E.; Pralle, A.; Isacoff, E. Y.; Chang, C. J. Boronate-Based Fluorescent Probes for Imaging Cellular Hydrogen Peroxide. *J. Am. Chem. Soc.* **2005**, *127* (47), 16652–16659.

(66) Khodade, V. S.; Kulkarni, A.; Gupta, A. Sen; Sengupta, K.; Chakrapani, H. A Small Molecule for Controlled Generation of Peroxynitrite. *Org. Lett.* **2016**, *18* (6), 1274–

1277.

(67) Zhou, M.; Diwu, Z.; Panchuk-Voloshina, N.; Haugland, R. P. A Stable Nonfluorescent Derivative of Resorufin for the Fluorometric Determination of Trace Hydrogen Peroxide: Applications in Detecting the Activity of Phagocyte NADPH Oxidase and Other Oxidases. *Anal. Biochem.* **1997**, *253* (2), 162–168.

(68) Mohanty, J. .; Jaffe, J. S.; Schulman, E. S.; Raible, D. G. A Highly Sensitive Fluorescent Micro-Assay of H2O2 Release from Activated Human Leukocytes Using a Dihydroxyphenoxazine Derivative. *J. Immunol. Methods* **1997**, *202* (2), 133–141.

(69) Mills, E. M.; Takeda, K.; Yu, Z. X.; Ferrans, V.; Katagiri, Y.; Jiang, H.; Lavigne, M. C.; Leto, T. L.; Guroff, G. Nerve Growth Factor Treatment Prevents the Increase in Superoxide Produced by Epidermal Growth Factor in PC12 Cells. *J. Biol. Chem.* **1998**, *273* (35), 22165–22168.

(70) Sundaresan, M.; Yu, Z. X.; Ferrans, V. J.; Irani, K.; Finkel, T. Requirement for Generation of H2O2 for Platelet-Derived Growth Factor Signal Transduction. *Science* **1995**, *270* (5234), 296–299.

(71) Hoshi, Y.; Xu, Y.; Ober, C. K. Photo-Cleavable Anti-Fouling Polymer Brushes: A Simple and Versatile Platform for Multicomponent Protein Patterning. *Polymer.* **2013**, *54* (7), 1762–1767.

(72) Nainar, S.; Kubota, M.; McNitt, C.; Tran, C.; Popik, V. V; Spitale, R. C. Temporal Labeling of Nascent RNA Using Photoclick Chemistry in Live Cells. *J. Am. Chem. Soc.* **2017**, *139* (24), 8090–8093.

Chapter 3.1. Synthesis and Evaluation of a Triggerable Hydroquinone Based ROS Releasing Molecule

3.1.1 Introduction

Chapter 2, described the development of UV light activatable ROS generators which cleave under 365 nm light to release molecule **1**, which then reacts with oxygen to generate ROS. To overcome the limitations associated with UV light based strategy,[1–5] a scaffold which would cleave upon irradiation with visible light to release ROS generating moiety is desired. In order to achieve the visible light triggered release of ROS, a well-known fluorescent molecule, boron-dipyrromethene (BODIPY)[6,7] was chosen as the photolabile moiety. The rationale behind choosing BODIPY over other photolabile scaffolds has been described in Chapter 1.

Scheme 3.1.1. Design of Visible light triggered ROS generating molecules

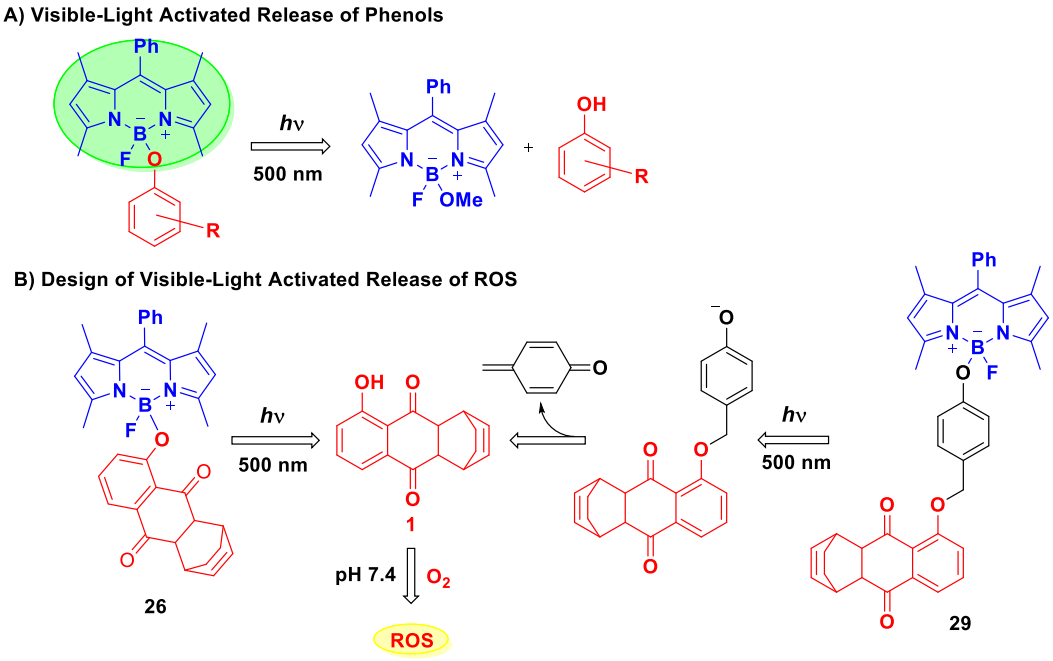

Release of several BODIPY-masked bioactive molecules under visible light has been demonstrated in literature.[8–17] However, we were particularly inspired by the work carried out by Urano and co-workers, wherein a phenolic group attached to the boron atom of BODIPY was shown to uncage under visible light (Scheme 3.1.1 A).[10] BODIPY moieties are typically fluorescent in nature, but the presence of an electron rich aryloxy substituent on the boron atom can result in the quenching of fluorescence, which is a result of photoinduced electron transfer (PET). These BODIPY derivatives form a charge-separation intermediate upon irradiation, which has a partial negative charge on the boron atom and a partial positive charge on the

oxygen atom of the aryloxy group. This intermediate further undergoes solvolysis to release the aryloxy group.

As described previously, compound **1** (which generates ROS) can be attached with the boron atom of BODIPY; the adduct, then, cleaves with visible light to release compound **1** (Scheme 3.1.1 B). Here, two possibilities of attaching compound **1** with BODIPY were described. First, where the phenolic group can be directly attached to the boron of BODIPY and another, where a 4-hydroxybenzyl group can be used as a self-immolative linker between compound **1** and the boron atom of BODIPY. This linker might decrease the steric hindrance between the BODIPY core and compound **1** that may provide further stability to the scaffold. These designed compounds should photocleave under visible light to release compound **1**, which is known to generate superoxide ($O_2^{\bullet-}$) under ambient aerobic conditions.

3.1.2 Results and Discussion

3.1.2.1 Synthesis

To synthesize the designed molecules, first, synthesis of compound **26** was attempted, where **1** would be directly attached with BODIPY. To synthesize compound **26**, BODIPY **25** was reacted with compound **1** in the presence of $AlCl_3$, but under the given conditions, the desired compound **26** was not obtained (Scheme 3.1.2). A possible reason for failure in the synthesis of **26** could be the poor stability of compound **1** in the presence of the Lewis acidic ($AlCl_3$), resulting in non-specific decomposition.

Scheme 3.1.2. Attempted synthesis of a visible light ROS generator

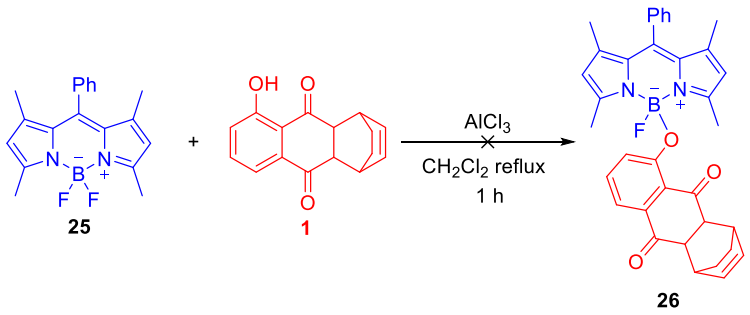

After unsuccessful attempts to synthesize compound **26**, compound **29**, where a self-immolative linker would be incorporated between compound **1** and BODIPY, was designed. To synthesize **29**, first, BODIPY **25** was reacted with 4-hydroxybenzaldehyde in the presence of $AlCl_3$ to give compound **26**, which was then reduced in the presence of $NaBH_4$ to afford compound **27**[10] (Scheme 3.1.3). Further attempts to synthesize **28** by brominative

dehydroxylation of the alcohol **27** in the presence of PBr_3 failed. Hence, the desired product **29** was not obtained. The problem in the brominative dehydroxylation reaction is likely the poor stability of the B-O bond in acidic conditions. As it is known that nature of PBr_3 is acidic, which may contribute to the falling off of 4-hydroxybenzyl alcohol.

Scheme 3.1.3. Attempted synthesis of a visible light ROS generator

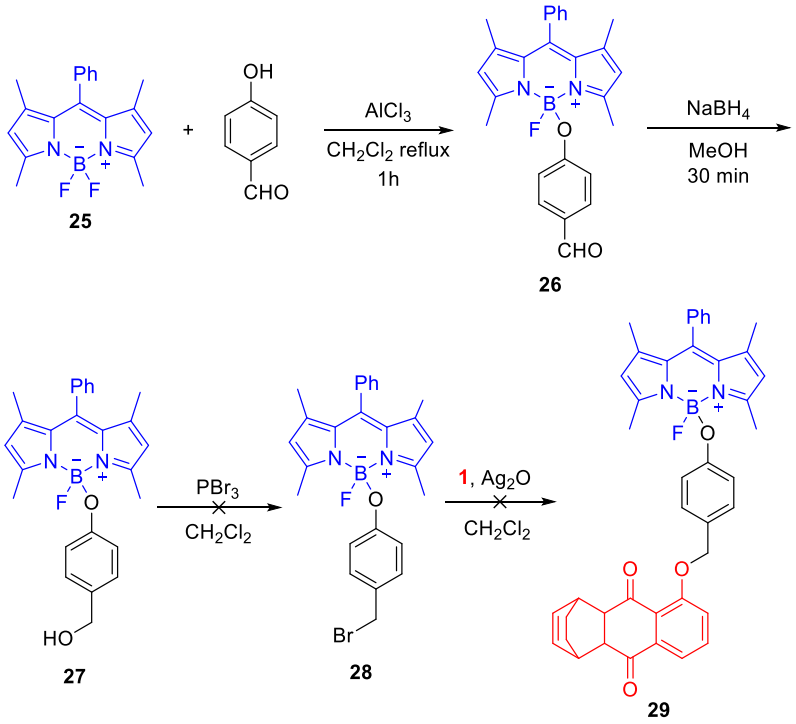

3.1.2.2 Limitations of Compound 1

As described that compound **1** is an excellent ROS generator; however, there are few limitations associated with it.

1. The reduced stability of compound **1** even in mild basic and acidic conditions precludes exploration of different methodologies for derivatization.

2. Any structural modification in compound **1** diminishes its ROS generation capability; hence, any modification to functionalize for the site-specific delivery of ROS is complicated.

3. Compound **1** reacts with halogenated electrophiles. However, it does not offer wide range of reactivity with other electrophiles; this could be due to the lesser nucleophilicity of its hydroxy group as compared to other phenols.

To surmount these limitations, a scaffold for ROS generation need to be developed, which would have a site to functionalize, for making it selective towards a particular organelle in a

cell or towards one cell type, without compromising the ability to generate ROS. Further, the scaffold should also be stable in mild acidic and basic conditions and also should be compatible with a range of electrophiles of different triggers.

3.1.3 Design of Revised ROS Generator

Previous studies from our laboratory have shown that for derivatives of 1,4-hydroquinone (1,4-HQ), an enol and a keto form are found to be in equilibrium (Scheme 3.1.4).[18] This equilibrium can be shifted towards the enol form by substituting the 1,4-quinone/1,4-hydroquinone ring with an electron withdrawing group (EWG). The EWG stabilizes the enol form, resulting in rapid generation of ROS, whereas an electron donating group (EDG) stabilizes the keto form, which produces ROS in a slow manner.[18] This concept may be utilized to manipulate the rate of ROS production.

Scheme 3.1.4. Equilibrium of keto-enol forms of 6-aryl-2,3-dihydro-1,4-benzoquinones to produce ROS

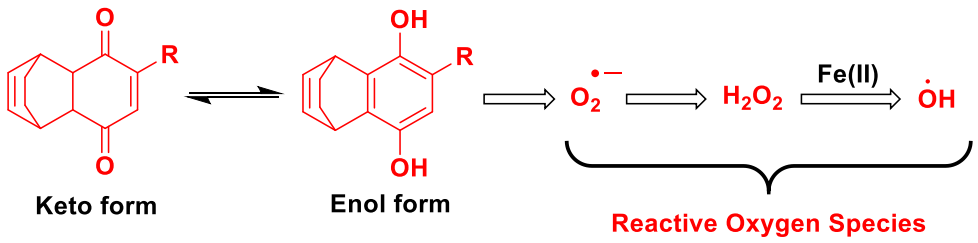

Directed delivery of ROS to a particular organelle can be achieved by functionalizing benzylhydroxy or benzylamino group on the phenyl ring attached with 1,4-quinone/1,4-HQ ring. The O or N can be functionalized using an organelle specific group (Figure 3.1.1) such as triphenylphosphonium to target mitochondria,[19] morpholine for lysosomal delivery[20] and folate or biotin for targeting cancer cells.[21]

Figure 3.1.1. General design of 1,4-hydroquinone-based ROS generator

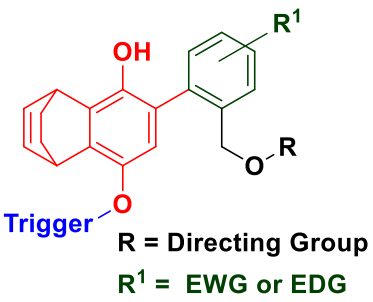

As a proof-of-concept, compound **36**, where one hydroxyl group is masked with an ether linkage and further linked with an ester group, was designed. This compound was envisaged to react with an esterase to release formaldehyde and 1,4-HQ, which would further react with molecular oxygen to produce ROS (Scheme 3.1.5).

Scheme 3.1.5. Design of an esterase activated ROS generator

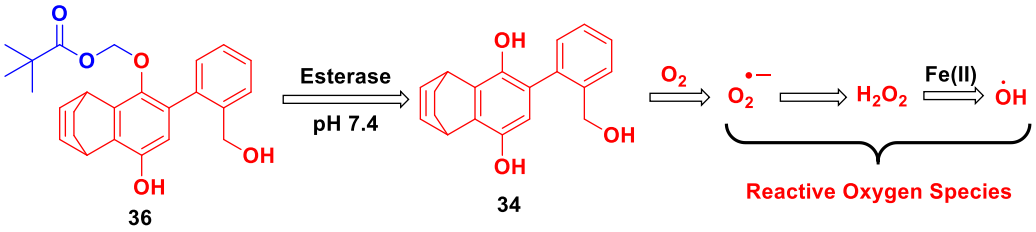

3.1.4 Result and Discussion for the Revised ROS Generator

3.1.4.1 Synthesis of Revised ROS Generator

To synthesize the designed molecules, benzoquinone and methyl anthranilate were reacted in the presence of *tert*-butyl nitrite to form compound **30**, which was subjected to Diels-Alder reaction with 1,3 cyclohexadiene to form a cyclohexadiene adduct. This adduct unexpectedly lactonized during purification to give **31** in less than 10% yield. To improve the yield of **31**, the crude product of Diels-Alder reaction was treated with conc. HCl, which promoted the enolization, followed by lactonization, providing a good yield (50%) of **31.**

Scheme 3.1.6. Synthesis of ROS generator **34**

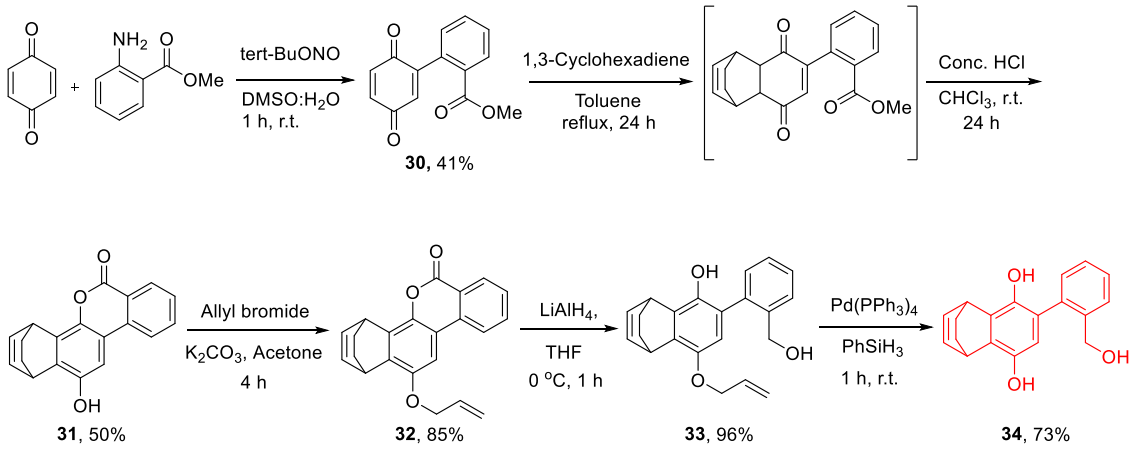

Compound **31** has a hydroxyl group that might interfere in the next step; thus, to protect this, allylation was carried out in the presence of allyl bromide and K_2CO_3 to provide **32** as a white solid. Next, the cyclic ester needed breaking to free up the phenolic group, which was

accomplished by reduction using lithium aluminum hydride ($LiAlH_4$) to give compound **33**. Finally, the compound **34** was obtained by deallylation of compound **33** using $Pd(PPh_3)_4$ as a catalyst and phenylsilane as a hydride source (Scheme 3.1.6).

To synthesize the esterase activated compound **36**, compound **33** was reacted with iodomethyl pivalate in the presence of K_2CO_3 to provide compound **35** which was further subjected to deallylation in the presence of $Pd(PPh_3)_4$ as a catalyst and phenylsilane as a hydride source to afford compound **36** (Scheme 3.1.7). These compounds were characterized by NMR and IR spectroscopies and HRMS.

Scheme 3.1.7. Synthesis of esterase activated ROS generator

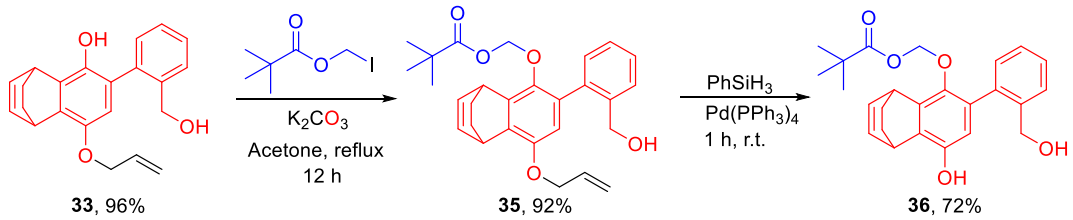

3.1.4.2 Esterase Triggered Cleavage of 36

After successfully synthesizing compound **36**, it was studied for possible ester hydrolysis in the presence of esterase; the enzyme has a serine at its active site, which attacks the ester carbonyl to release an alcohol. This alcohol further rearranges to produce compound **34**, with formaldehyde as a byproduct (Scheme 3.1.8). The compound **34** may possibly react with molecular oxygen to form $O_2^{\bullet-}$.

When compound **36** was treated with 0.5 U/mL of esterase, the complete disappearance of a peak corresponding to **36** was observed within 30 min incubation and a new peak was appeared at 5.4 min in the HPLC trace, which was attributable to compound **34** (Figure 3.1.2). As the compound **34** has both its hydroxyl groups free, it should react with oxygen to form a quinone derivative **37** (Scheme 3.1.9). When the esterase treated mixture was further incubated at 37 ºC, the intensity of the peak at 5.4 min was reducing over a period of time (Figure 3.1.2) and the intensity of a peak at 8.00 min was increasing with time, which was attributed to the quinone derivative **37**; the assignment was confirmed by MALDI-TOF analysis (here, $[M+K^+]$ calcd: 331.07; found 331.04) (Scheme 3.1.9). The presence of these intermediates suggested that the hydroquinone derivative (**34**) reacts with oxygen to form the quinone derivative (**37**), which indirectly indicated the formation of $O_2^{\bullet-}$.

Figure 3.1.2. HPLC traces of ester hydrolysis of **36** in the presence and absence of esterase (ES: Esterase)

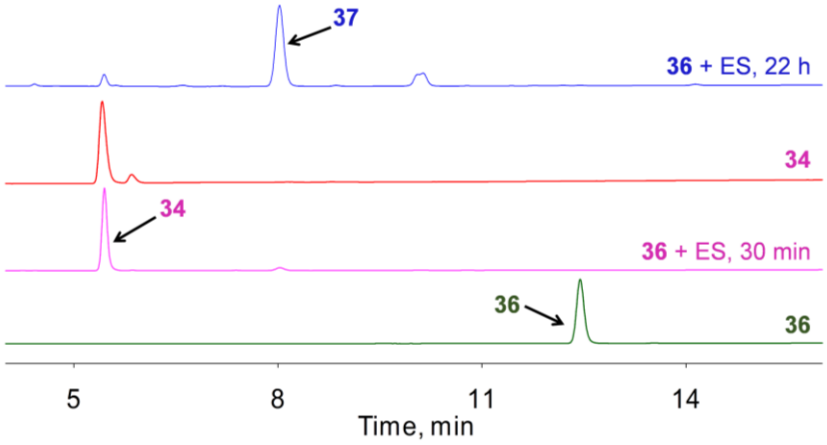

Scheme 3.1.8. Plausible reaction mechanism for reaction of **36** with esterase and subsequent ROS generation

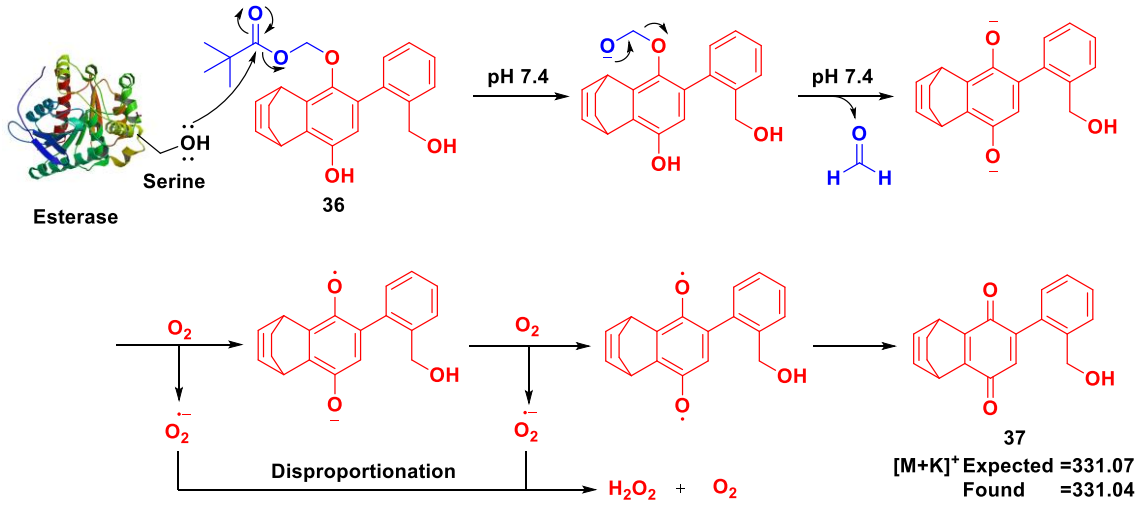

3.1.4.3 ROS Detection

HPLC studies suggested that esterase hydrolyzes compound **36** to form the intermediate **34**, which then converts into compound **37** over a period of time. This conversion from **34** to **37** is possible only when **34** reacts with molecular oxygen. This reaction with molecular oxygen would result in the formation of $O_2^{\bullet-}$, which in turn can disproportionate to H_2O_2 and O_2 (Scheme 3.1.8). These reactive species can be detected by the following assays.

3.1.4.3.1 Superoxide Detection by DHE Assay

As described in Chapter 2, dihydroethidium (DHE) is a dye which reacts with $O_2^{\bullet-}$ and other ROS to form 2-hydroxyethidium (2-OH-E^+) and ethidium (E^+) respectively.[22–24] The species

2-OH-E^+ and E^+ are fluorescent in nature and give two distinct peaks that can be separated *via* HPLC. The present assay has been performed with compound **36**; an intense peak for 2-OH-E^+ was observed only in the presence of esterase and this signal was seen to diminish when the reaction mixture was treated with superoxide dismutase (SOD), a known quencher of $O_2^{\bullet-}$, suggesting that the signal observed in HPLC corresponds to the formation of $O_2^{\bullet-}$ (Figure 3.1.3). A similar experiment was also performed with compound **34** and as expected, the highly intense peak for 2-OH-E^+ was again observed in the presence and absence of esterase and the signal was seen to diminish when the reaction mixture was treated with SOD. In compound **34**, both the hydroxyl groups are unmasked and expected to generate $O_2^{\bullet-}$ even without esterase (Figure 3.1.4). This experiment confirms the generation of $O_2^{\bullet-}$ by compounds **36** and **34**.

Figure 3.1.3. Superoxide detection using DHE assay for compound **36** (ES: Esterase)

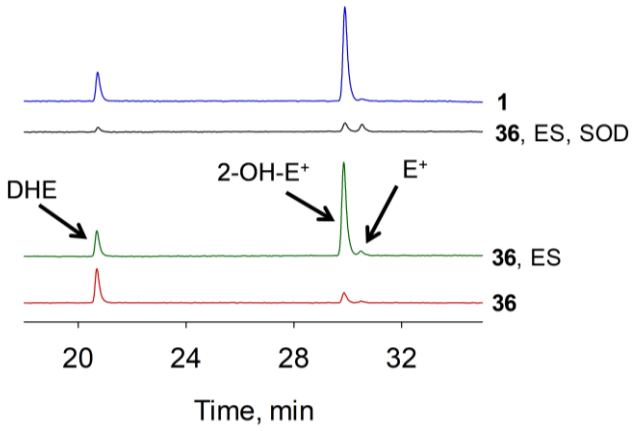

Figure 3.1.4. Superoxide detection using DHE assay for compound **34** (ES: Esterase)

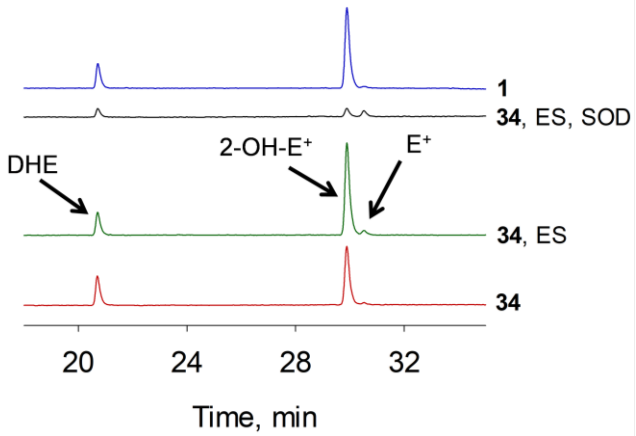

3.1.4.3.2 Hydrogen Peroxide Detection Using Boro-Umb Dye 23

The boronate ester of the umbelliferone derivative **23** was used as an H_2O_2 probe, which is weakly-fluorescent but upon oxidation of its boronate-ester with H_2O_2, a highly fluorescent umbelliferone derivative **24** is formed. The enhanced fluorescence signal can be measured by a fluorimeter. H_2O_2 detection was performed using compound **36** in the presence and absence of esterase and it was found that an enhanced fluorescence signal was observed in the enzyme-treated samples. As expected, enhanced fluorescence signal was not observed in the absence of enzyme (Figure 3.1.4). This study suggests that compound **36** produces H_2O_2 only in the presence of esterase. By contrast, in compound **34**, both the hydroxyl groups of its 1,4-HQ are free, so that it should spontaneously produce H_2O_2 in buffer. To test this hypothesis, compound **34** was assessed for H_2O_2 generation in the absence of esterase and as expected, compound **34** indeed produces H_2O_2 without enzymatic activation; however, the signal was diminished in the esterase treated samples. This study suggests that the esterase used for the study may, in some way, be quenching H_2O_2 and hence, a less intense signal was observed in the enzyme treated samples (Figure 3.1.5).

Figure 3.1.5. H_2O_2 detection by boronate dye **23**; data represent (mean ± s.d.) for three independent experiments per group (ES: Esterase)

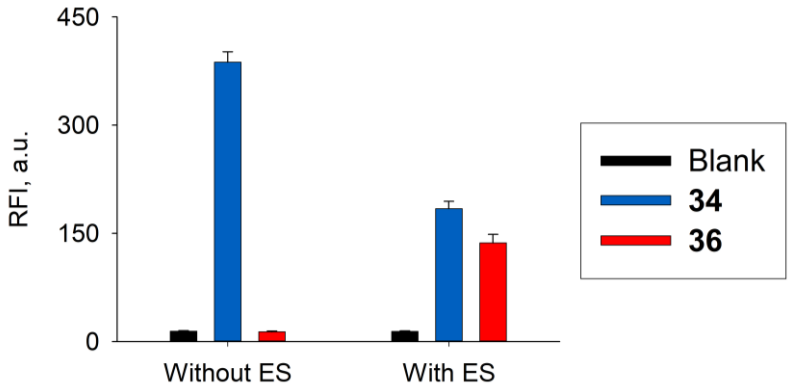

3.1.4.4 Effect on Cellular Growth

As described by *in vitro* experiments, both the compounds **34** and **36** produce ROS in the presence of esterase. Increasing the level of ROS endogenously may damage essential bio-molecules, which might, then, result in cell death. Here, the growth inhibitory activity of these compounds was assayed. For this experiment, lung cancer cells, A549 were chosen and the cell growth inhibition assay was performed using the standard MTT dye. The cellular growth inhibition assay was performed by means of varying the concentrations of compounds **36** and **34** and growth inhibition was observed in a dose dependent manner (Figure 3.1.6). The IC_{50}

values of **34** and **36** were found to be 5.2 µM and 17.9 µM respectively (Figure 3.1.7). Due to the wide prevalence of esterase, compound **36** would likely cleave in cells and release compound **34** to produce ROS; this would damage the essential bio-macromolecules of cells, resulting in inhibition of growth.

Figure 3.1.6. Cellular growth inhibition assay using MTT dye with A) esterase activated compound **36** B) compound **34**; data represent the (mean ± s.e.m.) for three independent experiments per group

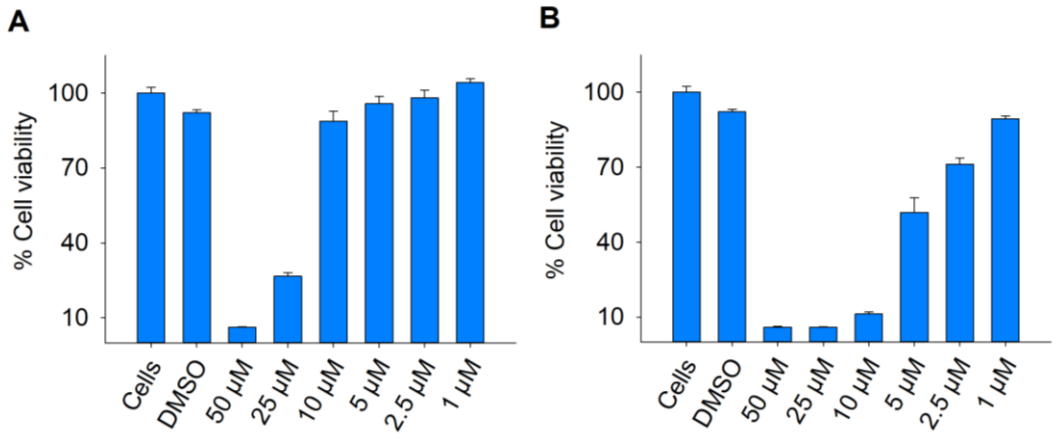

Figure 3.1.7. Cellular Growth inhibition curve with compounds **36** (IC_{50}: 17.9 µM) and **34** (IC_{50}: 5.2 µM); data represent the (mean ± s.e.m.) for three independent experiments per group

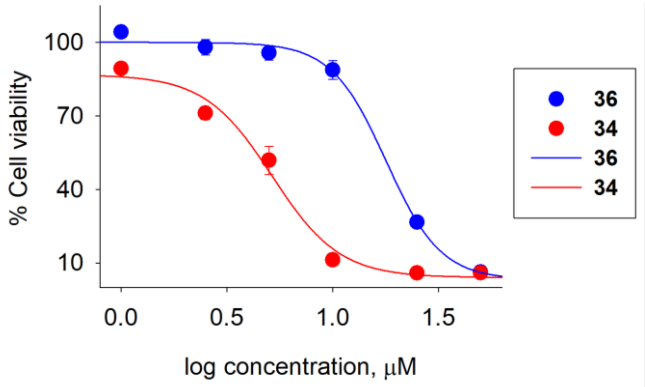

3.1.5 Conclusion

To arrive at a proof-of-concept regarding the design of ROS generating moieties, an esterase activated ROS donor was designed and synthesized. In the presence of esterase. an intermediate **34** is produced, which, in turn, underwent oxidation to form a quinone derivative. The capability of generation of $O_2^{\bullet-}$ was assessed using the DHE assay where $O_2^{\bullet-}$ was produced by compounds **36** and **34**. In addition, the generated H_2O_2 from these compounds was also

detected; however, the presence of the esterase appears to interfere with the detection of H_2O_2. Compound **36** has a free hydroxyl group in the scaffold. Further modification to append an organelle-specific tag (that may direct it towards a specific location within the cell) to generate ROS is possible. The ROS generating scaffold **36** does not offer selectivity to particular types of cells over others, owing to the ubiquity of the trigger: esterase. Apart from selectivity, the esterase possibly quenches the generated H_2O_2 and hence, interferes with the *in vitro* detection of H_2O_2. Taken together, a new triggerable ROS-generating scaffold has been developed. The next section describes our efforts to derivatize this with a photocleavable group.

3.1.6 Synthesis Protocols and Characterization data

3.1.6.1 Synthesis Protocols

Compound **1**,[25] **23**,[26] **25**,[10] **27**[10] and **30**[27] were synthesized according to reported procedure and data were consistent with reported data. ^{1}H NMR spectrum of **30** is attached.

Synthesis of 12-hydroxy-1,4-dihydro-6H-1,4-ethanodibenzo[c,h]chromen-6-one (31): To

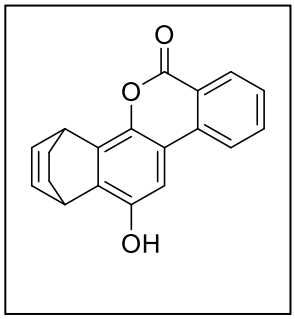

a solution of **30** (1.84, 7.6 mmol) in anhydrous toluene (40 mL) was added 1,3 cyclohexadiene (1.5 mL, 15.74 mmol) and refluxed for 24 h in inert atmosphere. After complete consumption of starting material which was confirmed by TLC analysis and 2-4 dinitrophenylhydrazine staining, toluene was evaporated to obtain solid residue which was further dissolved in chloroform, conc. HCl (5 mL) was added and allowed to stir for 24 h at r.t. to form a precipitate which indicated the formation of hydroxyl-compound. At this point, chloroform was evaporated, diluted the mixture with water and extracted with ethyl acetate. The organic layers were combined, dried over anhydrous Na_2SO_4 and concentrated under reduced pressure to get solid residue which was purified by silica gel chromatography using hexane: ethyl acetate (85:15) as a eluent to afford compound **31** as a white solid (1.1 g, 50%); FT-IR (ν_{max}, cm^{-1}): 3743, 2366, 2319, 1690, 1677, 1514; ^{1}H NMR (400 MHz, DMSO-d_6): δ 9.58 (s, 1H), 8.24 (dd, J = 8.0, 1.4 Hz, 1H), 8.15 – 8.09 (m, 1H), 7.96 – 7.86 (m, 1H), 7.64 - 7.60 (m, 1H), 7.38 (s, 1H), 6.60 – 6.54 (m, 2H), 4.57-4.54 (m, 1H), 4.46-4.43 (m, 1H), 1.59 – 1.44 (m, 2H), 1.41 – 1.29 (m, 1H); ^{13}C NMR (100 MHz, DMSO-d_6): δ 160.5, 147.7, 138.6, 135.2, 135.0, 134.6, 134.5, 133.1, 129.8, 128.4, 122.1, 120.1, 114.6, 105.0, 79.1, 32.9, 32.7, 24.7, 24.5; HRMS (ESI-TOF) for $[C_{19}H_{14}O_3 + H]^+$ calcd: 291.1021; found: 291.1027.

Synthesis of 12-(allyloxy)-1,4-dihydro-6H-1,4-ethanodibenzo[c,h]chromen-6-one (32) : To

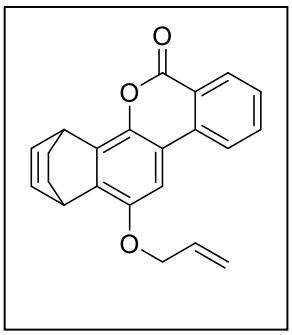

a solution of **31** (1.27 g, 4.37 mmol) in anhydrous acetone (30 mL) were added K_2CO_3(1.85 g, 13.39 mmol) and allyl bromide (800 µL, 9.26 mmol). The mixture was refluxed for 4 h in inert atmosphere. After completion of reaction acetone was evaporated, diluted with water and extracted with dichloromethane. Organic layer was combined, dried over anhydrous Na_2SO_4 and concentrated under reduced pressure to obtained solid residue which was purified by silica gel column chromatography using Hexane: ethyl acetate (100:0 - 94:6) as a mobile phase

to afford compound **32** as a white solid (1.23 g, 85%); FT-IR (ν_{max}, cm^{-1}): 2945, 2869, 1723, 1607, 1486, 1101, 1314; ^{1}H NMR (400 MHz, $CDCl_3$): δ 8.40 (dd, *J* = 8, 1 Hz, 1H), 8.01 (d, *J* = 8.1 Hz, 1H), 7.84 – 7.73 (m, 1H), 7.58 – 7.48 (m, 1H), 7.27 (s, 1H), 6.60 – 6.52 (m, 2H), 6.15 (ddt, *J* = 17.2, 10.5, 5.2 Hz, 1H), 5.50 (dd, *J* = 17.3, 1.5 Hz, 1H), 5.35 (dd, *J* = 10.5, 1.4 Hz, 1H), 4.86 – 4.73 (m, 1H), 4.73 – 4.60 (m, 2H), 4.60 – 4.51 (m, 1H), 1.60 (d, *J* = 7.2 Hz, 2H), 1.50 – 1.39 (m, 2H); ^{13}C NMR (100 MHz, $CDCl_3$): δ 161.8, 149.5, 140.6, 137.4, 135.8. 135.2, 135.1, 134.7, 134.6, 134.4, 133.5, 130.8, 128.2, 121.7, 121.0, 117.8, 115.1, 102.4, 70.1, 33.6, 33.4, 25.1, 25.0; HRMS (ESI-TOF) for $[C_{22}H_{18}O_3 + H]^+$ calcd: 331.1334; found: 331.1340.

Synthesis of 8-(allyloxy)-6-(2-(hydroxymethyl)phenyl)-1,4-dihydro-1,4-ethanonaphthalen-5-ol (33): A round bottomed flask was added anhydrous THF (40 mL) and

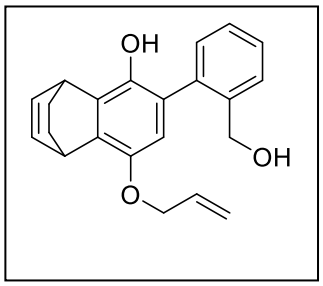

kept at ice bath for 5 min. $LiAlH_4$ (480 mg, 12.65 mmol) was added portion wise at continuous stirring. Compound **32** (500 mg, 1.51 mmol) was added portion-wise which was further stirred for 1 h at ice-cold condition. After completion of reaction (confirmed by TLC analysis), ice-cold 1 N HCl was added drop-wise and extracted with ethyl acetate. Organic layers were combined, dried over anhydrous sodium sulphate and concentrated under reduced pressure to obtained semisolid crude which was purified by column chromatography to afford compound **33** as a semisolid (488 mg, 96%); FT-IR (ν_{max}, cm^{-1}): 3416, 2938, 1467, 1421; ^{1}H NMR (400 MHz, $CDCl_3$): δ 7.56 – 7.50 (m, 1H), 7.45 – 7.35 (m, 2H), 7.32 – 7.21 (m, 1H), 6.57 – 6.51 (m, 2H), 6.42 (s, 1H), 6.13 – 6.00 (m, 1H), 5.39 (dq, *J* = 17.3, 1.6 Hz, 1H), 5.25 (dq, *J* = 10.5, 1.4 Hz, 1H), 4.57 – 4.50 (m, 1H), 4.49 – 4.43 (m, 4H), 4.43 – 4.38 (s, 1H), 2.00 (s, 1H), 1.61 – 1.51 (m, 2H), 1.47 (t, *J* = 7.9 Hz, 4H); ^{13}C NMR (100 MHz, $CDCl_3$): δ 146.5, 141.3, 141.2, 139.3, 139.1, 137.3, 137.2, 135.5, 135.4, 135.3, 134.5, 134.3, 134.0, 133.3, 131.3, 131.2, 129.4, 129.3, 128.5, 124.7, 117.2, 111.8, 70.3, 63.9, 63.8, 60.6, 33.7, 33.3, 21.2; HRMS (ESI-TOF) for $[C_{22}H_{22}O_3 + Na]^+$ calcd: 357.1467; found: 357.1467.

Synthesis of 6-(2-(hydroxymethyl)phenyl)-1,4-dihydro-1,4-ethanonaphthalene-5,8-diol

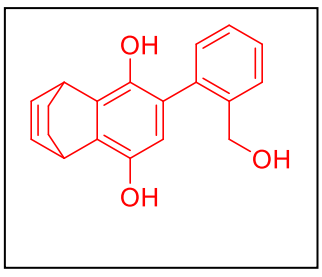

(34): To a solution of **33** (500 mg, 1.5 mmol) and Tetrakis(triphenylphosphine)palladium(0) (173 mg, 150 µmol) in anhydrous dichloromethane (20 mL) was added $PhSiH_3$ (560 µL, 4.54 mmol) and stirred for 1 h at r.t. After complete consumption of starting material, solvent was evaporated, diluted with water

and extracted with ethyl acetate. The organic layers were combined, dried over anhydrous sodium sulfate and concentrated under reduced pressure to get solid residue which was purified by column chromatography using silica gel as stationary phase and hexane: ethyl acetate (100:0 to 75:25) as mobile phase to afford compound **34** as a white solid compound (320 mg, 73%). FT-IR (ν_{max}, cm^{-1}): 3742, 3616, 2929; ^1H NMR (400 MHz, DMSO-d_6): δ 8.61 (s, 1H), 7.71 (s, 1H), 7.50 (d, J = 7.4 Hz, 1H), 7.35 – 7.17 (m, 2H), 7.15 – 6.97 (m, 1H), 6.60 – 6.39 (m, 2H), 6.22 (s, 1H), 5.06 – 4.96 (m, 1H), 4.48 – 4.32 (m, 2H), 4.32 – 4.16 (m, 2H), 1.49 –1.38 (m, 2H), 1.37 – 1.27 (m, 2H); HRMS (ESI-TOF) for $[C_{19}H_{18}O_3 + Na]^+$ calcd: 317.1154; found: 317.1133.

Synthesis of ((8-(allyloxy)-6-(2-(hydroxymethyl)phenyl)-1,4-dihydro-1,4-ethanonaphthalen-5-yl)oxy)methyl pivalate (35): To a solution of **33** (363 mg, 1.09 mmol),

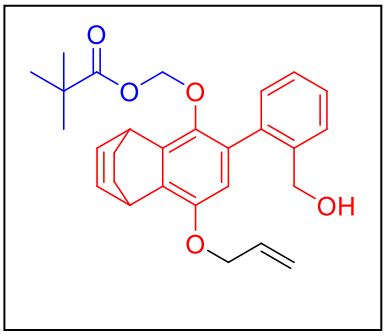

K_2CO_3 (450 mg, 326 mmol) and iodomethyl pivalate (396 mg, 1.64 mmol) in acetone (35 mL) was refluxed for 12 h. After completion of reaction, acetone was evaporated and diluted with water and extracted with dichloromethane. Organic layers were combined, dried over anhydrous sodium sulphate and concentrated under reduced pressure to get semisolid crude which was purified by column chromatography using silica gel as stationary phase and hexane: ethyl acetate (100:0 to 80:20) as mobile phase to obtain **35** as a semisolid compound (450 mg, 92%); FT-IR (ν_{max}, cm^{-1}): 3515, 2976, 1736; ^1H NMR (400 MHz, $CDCl_3$): δ 7.58 (dd, J = 7.5, 1.2 Hz, 1H), 7.39 (td, J = 7.4, 1.6 Hz, 1H), 7.37 – 7.31 (m, 1H), 7.31 – 7.22 (m, 1H), 6.60 – 6.50 (m, 2H), 6.50 (s, 1H), 6.06 (ddt, J = 17.2, 10.4, 5.2 Hz, 1H), 5.41 (dq, J = 17.3, 1.6 Hz, 1H), 5.27 (dq, J = 10.5, 1.4 Hz, 1H), 5.09 – 5.05 (m, 2H), 4.55 – 4.31 (m, 6H), 1.59 – 1.51 (m, 2H), 1.50 – 1.40 (m, 2H), 1.13 – 1.07 (m, 9H); ^{13}C NMR (100 MHz, $CDCl_3$): δ 177.8, 149.3, 143.2, 142.9, 139.6, 138.5, 138.3, 137.5, 135.8, 135.5, 135.1, 134.8, 133.8, 133.7, 130.5, 130.3, 129.5, 128.2, 127.8, 117.4, 112.1, 90.6, 69.7, 63.6, 63.5, 53.8, 38.8, 34.5, 34.4, 33.1, 27.1, 25.5, 25.4, 25.1; HRMS (ESI-TOF) for $[C_{28}H_{32}O5 + Na]^+$ calcd: 471.2147; found: 471.2156.

Synthesis of ((8-hydroxy-6-(2-(hydroxymethyl)phenyl)-1,4-dihydro-1,4-ethanonaphthalen-5-yl)oxy)methyl pivalate (36): To a solution of **35** (160 mg, 357 µmol) and Tetrakis(triphenylphosphine)palladium(0) (42 mg, 36.4 µmol) in anhydrous dichloromethane (5 mL) was added $PhSiH_3$ (132 µL, 1.07 mmol) and stirred it for 1 h at r.t. After complete consumption of starting material, mixture was diluted with water, extracted

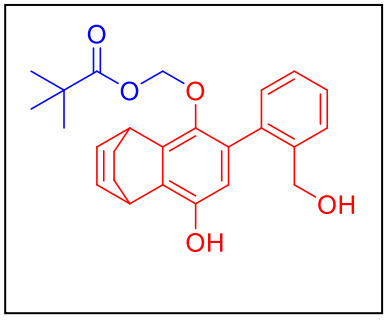

with dichloromethane. Organic layers were combined, dried over anhydrous sodium sulfate and concentrated under reduced pressure to obtain a solid residue which was purified by column chromatography using silica gel as stationary phase and hexane: ethyl acetate (100:0 to 75:25) as mobile phase to afford **36** as a white solid compound (105 mg, 72%). FT-IR (ν_{max}, cm^{-1}): 3356, 3056, 2668, 2870, 1732, 1472, 1732, 1429, 1282, 1207, 1156, 1076, 1028. ^{1}H NMR (400 MHz, $CDCl_3$): δ 7.55 (dd, *J* = 7.6, 1.5 Hz, 1H), 7.37 (td, *J* = 7.4, 1.6 Hz, 1H), 7.31 (t, *J* = 7.3 Hz, 1H), 7.23 (t, *J* = 8.0 Hz, 1H), 6.60 - 6.47 (m, 2H), 6.42 (s, 1H), 5.23 (s, 1H), 5.04 (s, 2H), 4.55 - 4.36 (m, 2H), 4.36-4.30 (m, 2H), 2.80 (bs, 1H), 1.60 – 1.41 (m, 4H), 1.10 (s, 9H); ^{13}C NMR (100 MHz, $CDCl_3$): δ 177.7, 146.1, 139.1, 137.0, 135.4, 135.1, 135.1, 135.0, 135.0 134.7, 130.4, 129.5, 128.1, 127.7, 114.8, 90.5, 63.5, 38.7, 34.4, 34.3, 33.2, 26.9, 25.0; HRMS (ESI-TOF) for $[C_{25}H_{28}O_5 + H]^+$ calcd: 431.1834; found: 431.1805.

3.1.6.2 General Preparation

10 mM stocks of the compounds **34** and **36** were prepared and stored at -4 °C. 10 mM stocks of Boro-Umb probe **23** and dihydroethidium (DHE) were prepared in DMSO and stored at -20 °C. 100 U/mL stocks of Superoxide dismutase (SOD), 100 U/mL stocks of Esterase enzyme were prepared in phosphate buffer (50 mM) of pH 7.4 and stored at -4 °C. At the time of assay 100 U/mL stock of esterase enzyme was further diluted to 1 U/mL and stored at 0 °C.

3.1.6.3 Esterase Triggered Cleavage Study of 36 Using HPLC

To a solution of Compound **36** (5 µL of 10 mM) and esterase enzyme (500 µL of 1 U/mL) was added in phosphate buffer pH 7.4 (490 µL) and incubated at 37 ºC for 30 min. Aliquots from the reaction mixture was taken out at a particular time point, filtered (0.22 µm) and injected (25 µL) in an Agilent high performance liquid chromatography (HPLC). This HPLC system was attached with a diode-array detector (detection wavelength was 250 nm) and a Phenomenex C-18 reversed phase column (250 mm × 4.6 mm, 5µm). A mobile phase of water:acetonitrile was used with a run time of 20 min. Multistep gradient starting with 0 min 50:50 → 0 min, 35:65 → 0 – 5 min, 25:75 →5 – 10 min, 15: 85 → 10 – 15 min, 25:75 → 15 – 18 min, 50:50 → 18 – 20 min was used with the flow rate of 1 mL/min.

3.1.6.4 Superoxide Detection Using DHE Assay

A microcentrifuge tube containing compounds **34** and **36** (1.25 µL of 10 mM) in phosphate buffer of pH 8.0 (490 µL) was incubated independently with DHE (2.5 µL of 10 mM) in the absence and presence of esterase enzyme (5 µL of 100 U/mL) for 2 h at 37 °C. The reaction mixture was filtered (0.45 µm) and injected (50 µL) in an Agilent high performance liquid chromatograph (HPLC) attached with a fluorescence detector (excitation at 480 nm; emission at 580 nm). The column used was Agilent1260-infinity with Phenomenex®C-18 reverse phase column (250 mm × 4.6 mm, 5 µm), the mobile phase was water: acetonitrile containing 0.1% trifluoroacetic acid and a gradient starting with 90: 10 % → 0 min, 10: 90 to 44: 56 → 0 – 35 min, 0: 100 → 35 – 37 min, 0: 100 → 37 – 40 min, 10: 90 → 40 – 42 min, 10: 90 → 42 – 45 min. Compound **1**, a known $O_2^{\bullet-}$ generator (1.25 µL of 10 mM) were mixed in phosphate buffer (pH 8.0, 50 mM) along with DHE (2.5 µL of 10 mM) for 1 h and served as a positive control. Known scavenger of $O_2^{\bullet-}$, SOD (5 µL of 100 U/mL) was also used as a control with the irradiated sample. Signal for $O_2^{\bullet-}$ was not observed in SOD treated samples.

3.1.6.5 H_2O_2 Detection Using Probe 23

For Detection of H_2O_2, 2 mM solutions of Dye **23**, Compounds **34** and **36** were prepared in ACN and stored at 0 ºC. Compound **34** and **36** (10 µL of 2 mM) were independently incubated with dye **23** (20 µL of 2 mM) in phosphate buffer of pH 7.4 (170 µL) in 96 well plate in triplicates without esterase enzyme. Same concentration of compounds and dye were also independently incubated with esterase enzyme (100 µL of 1 U/mL) in phosphate buffer of pH 7.4 (70 µL) in 96 well plate in triplicates. These reaction mixtures were incubated at 37 ºC for 4 h. The fluorescence was measured using Thermo Scientific Varioskan microtiter plate reader (λ_{ex} = 320 nm and λ_{em} = 460 nm).

3.1.6.6 Cell Viability Assay Using MTT Dye

Human adenocarcinomic alveolar basal epithelial cells, A549 were seeded at a concentration of 1×10^3 cells/well overnight in a 96-well plate in complete RPMI media. Cells were exposed to varying concentrations of the compound **34** and **36** prepared as a 10 mM DMSO stock solution so that the final concentration of DMSO was 0.5% and incubated for 72 h at 37 ºC. A solution of 3-(4, 5-dimethylthiazol-2-yl)-2, 5-diphenyl tetrazolium bromide (MTT) was prepared by dissolving MTT reagent (3.5 mg) in 7 mL RPMI media. 100 µL of this solution was added to each well. After 4 h incubation, the media was removed carefully and 100 µL of DMSO was added. Spectrophotometric analysis of each well was carried out at 570 nm using a Thermo Scientific Varioskan microplate reader to estimate cell viability.

3.1.7 Spectral Chart

^{1}H NMR spectrum (400 MHz, $CDCl_3$) of **30**

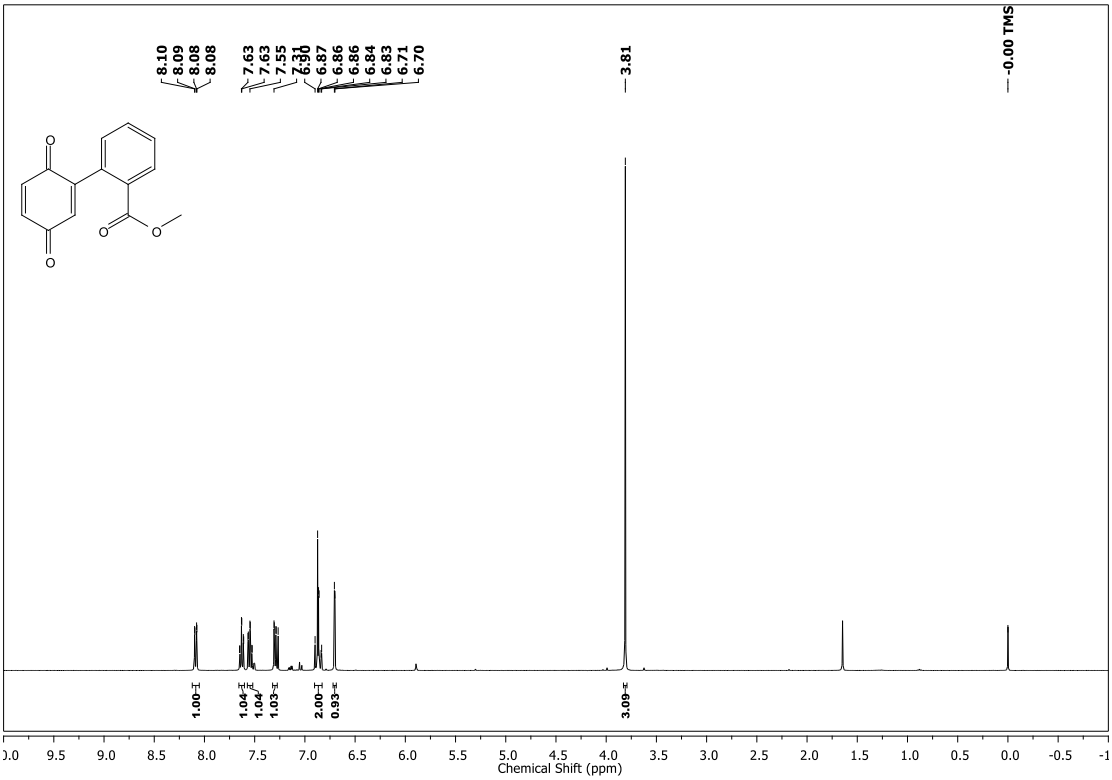

^{1}H NMR spectrum (400 MHz, DMSO-d_6) of **31**

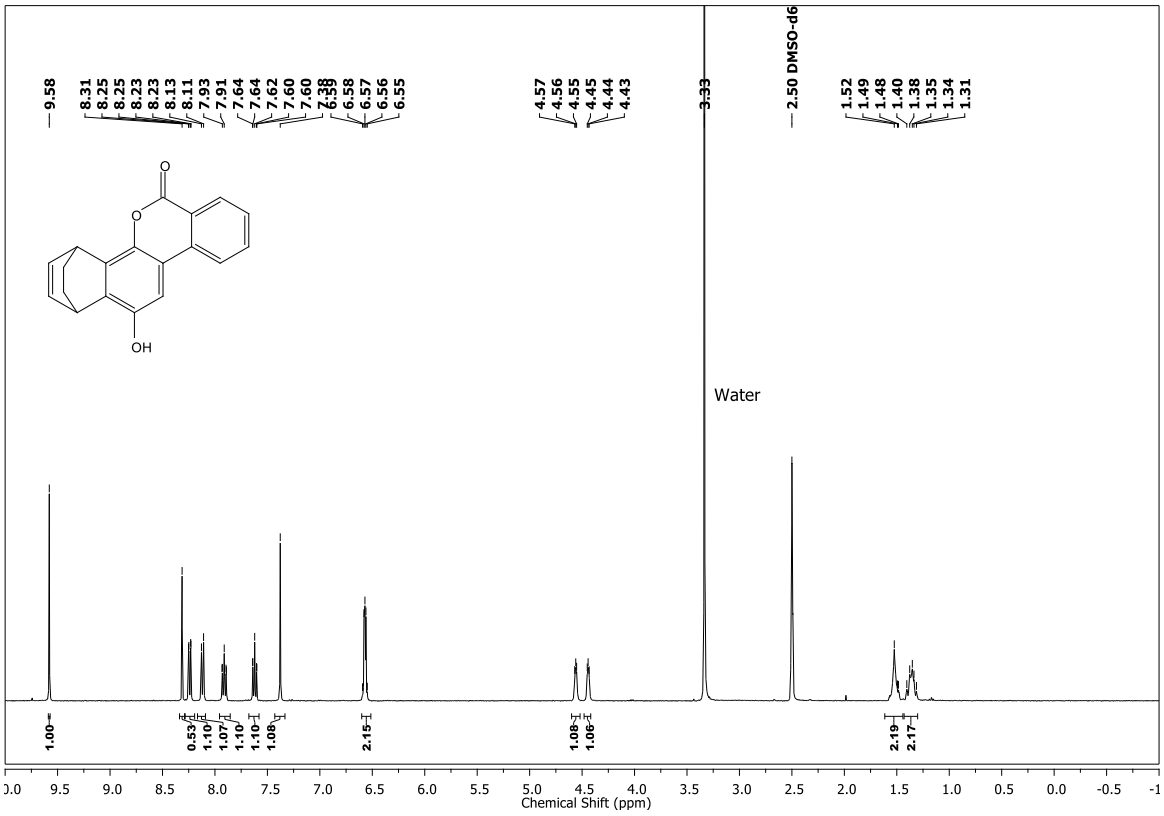

^{13}C NMR spectrum (100 MHz, DMSO-d_6) of **31**

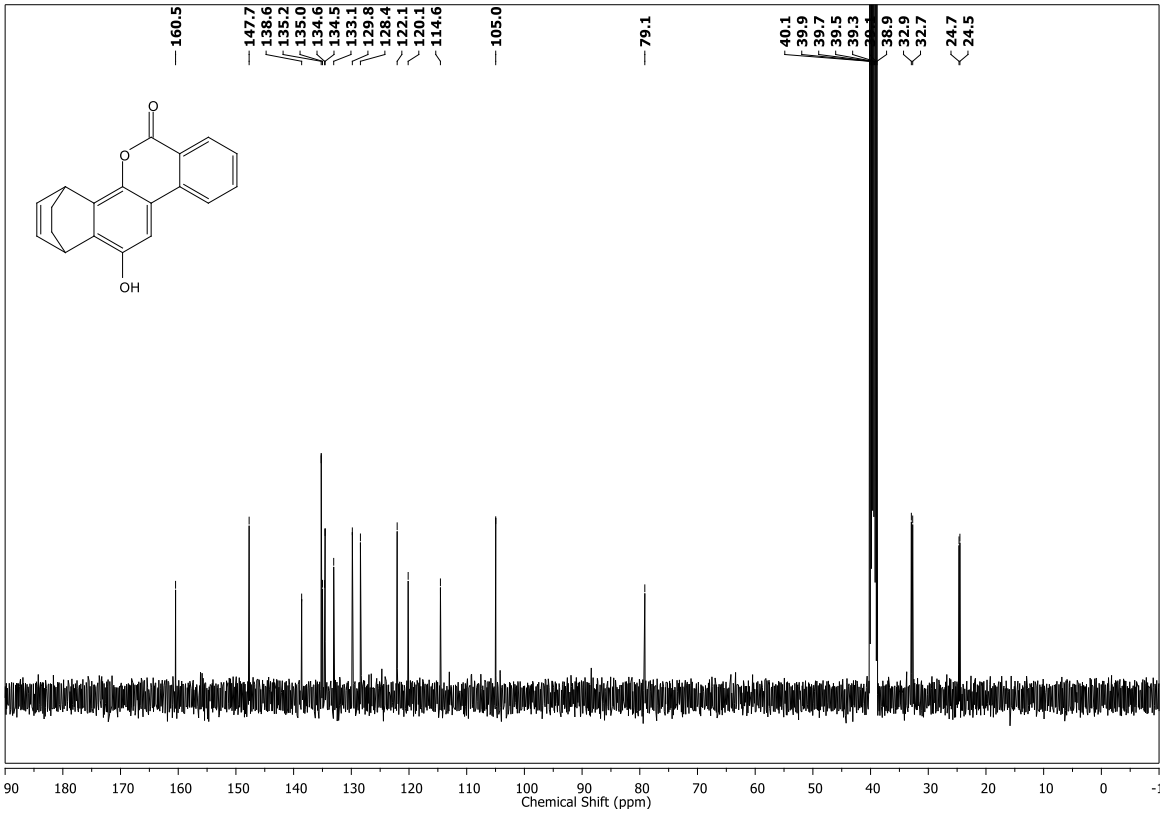

^{1}H NMR spectrum (400 MHz, $CDCl_3$) of **32**

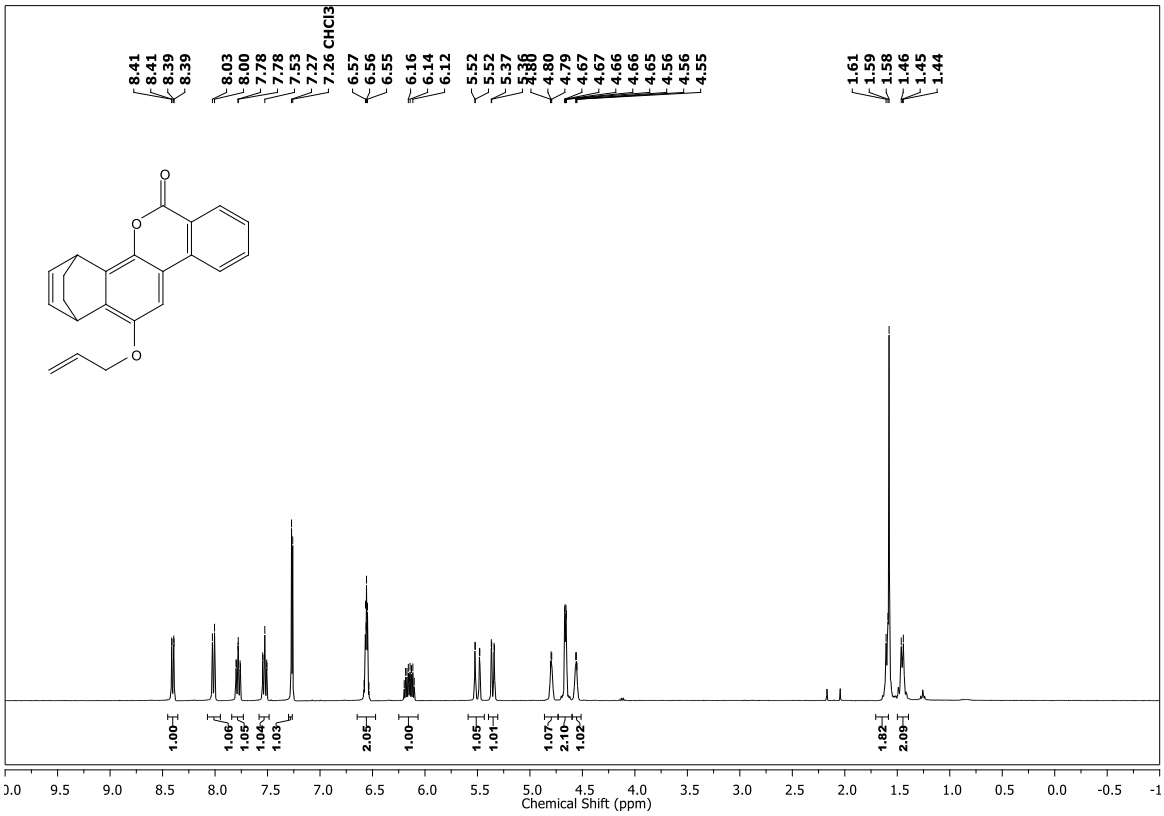

^{13}C NMR spectrum (100 MHz, $CDCl_3$) of **32**

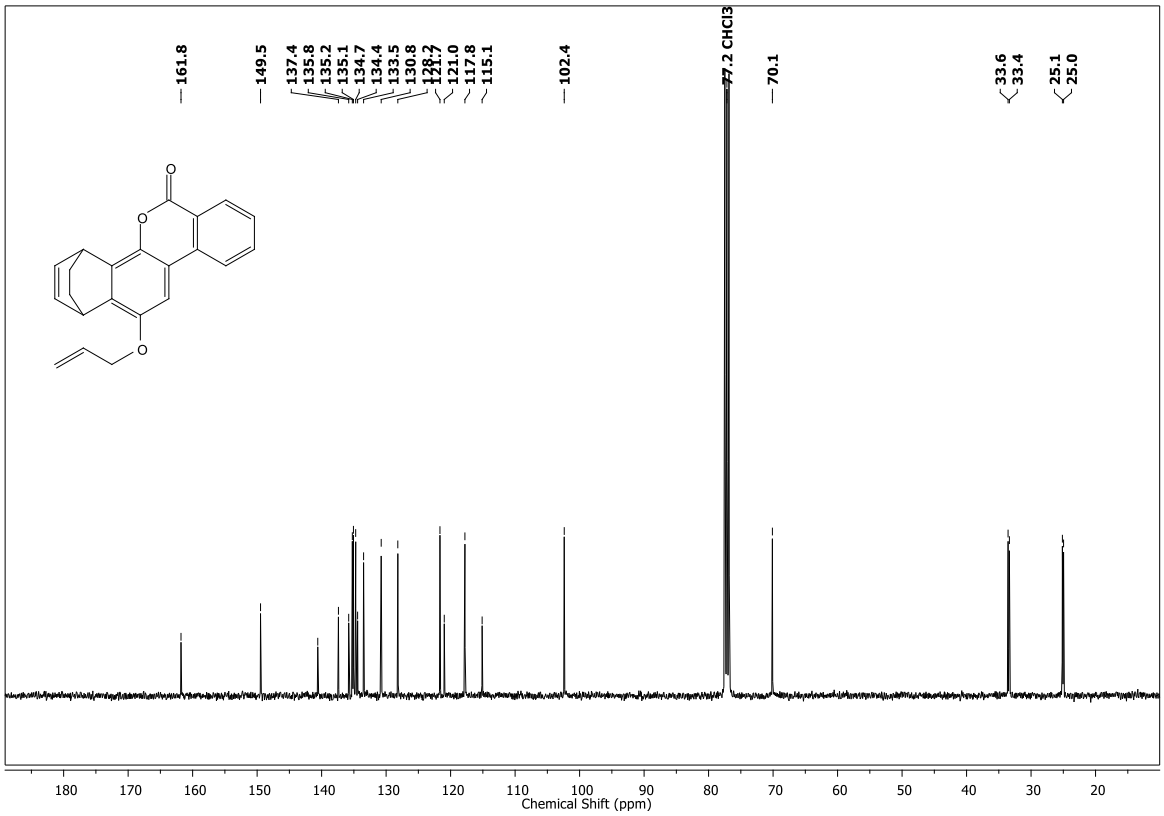

^{1}H NMR spectrum (400 MHz, $CDCl_3$) of **33**

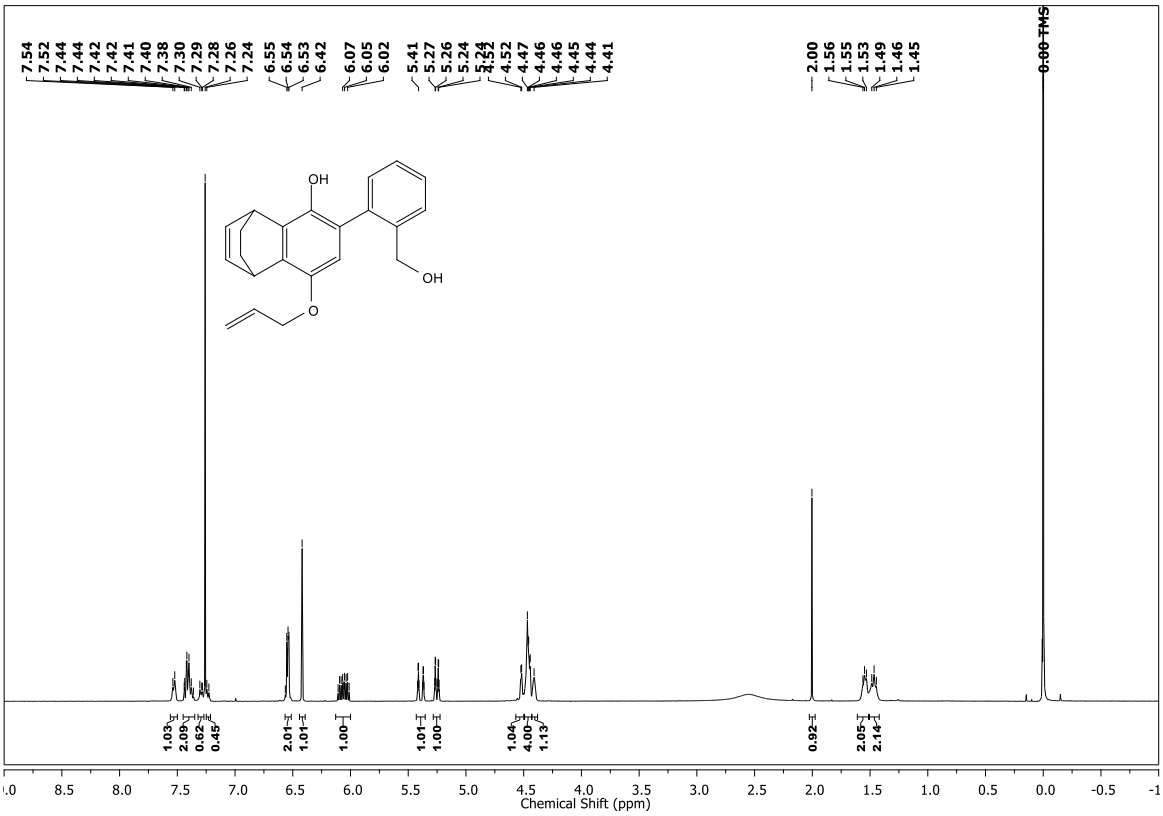

^{13}C NMR spectrum (100 MHz, $CDCl_3$) of **33**

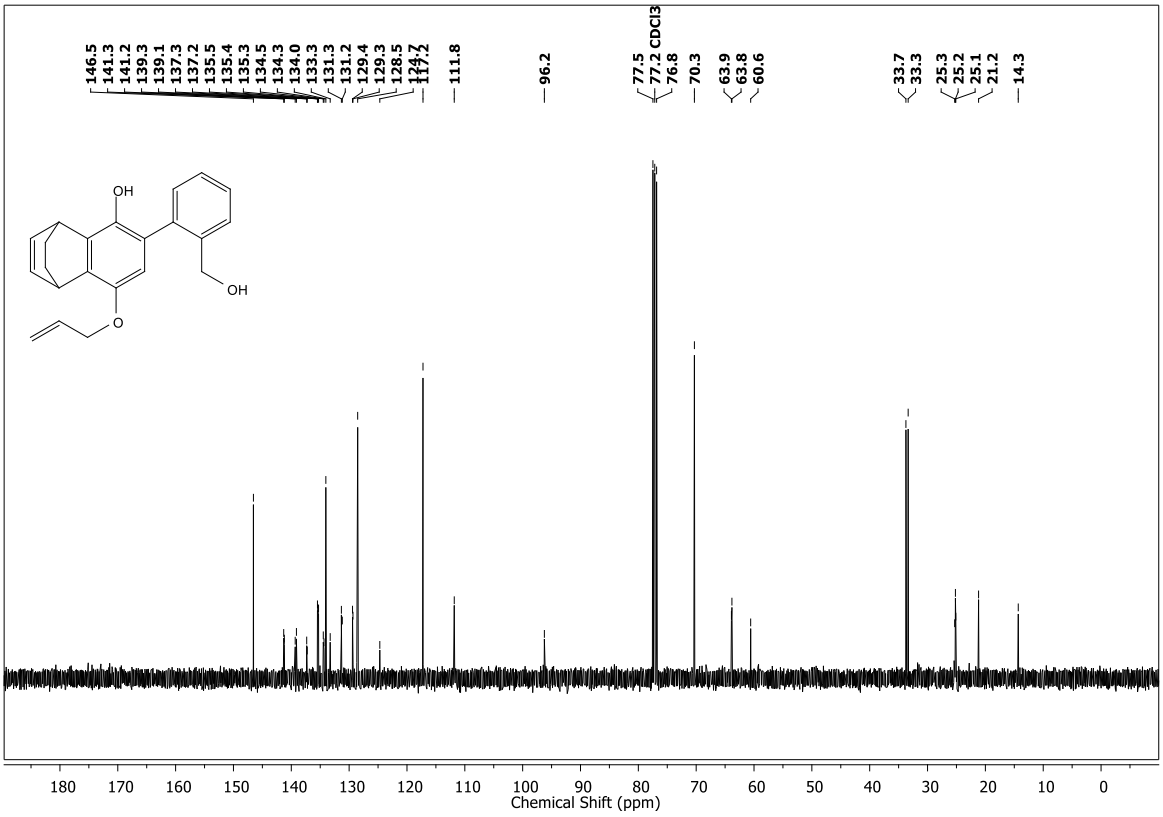

^{1}H NMR spectrum (400 MHz, DMSO-d_6) of **34**

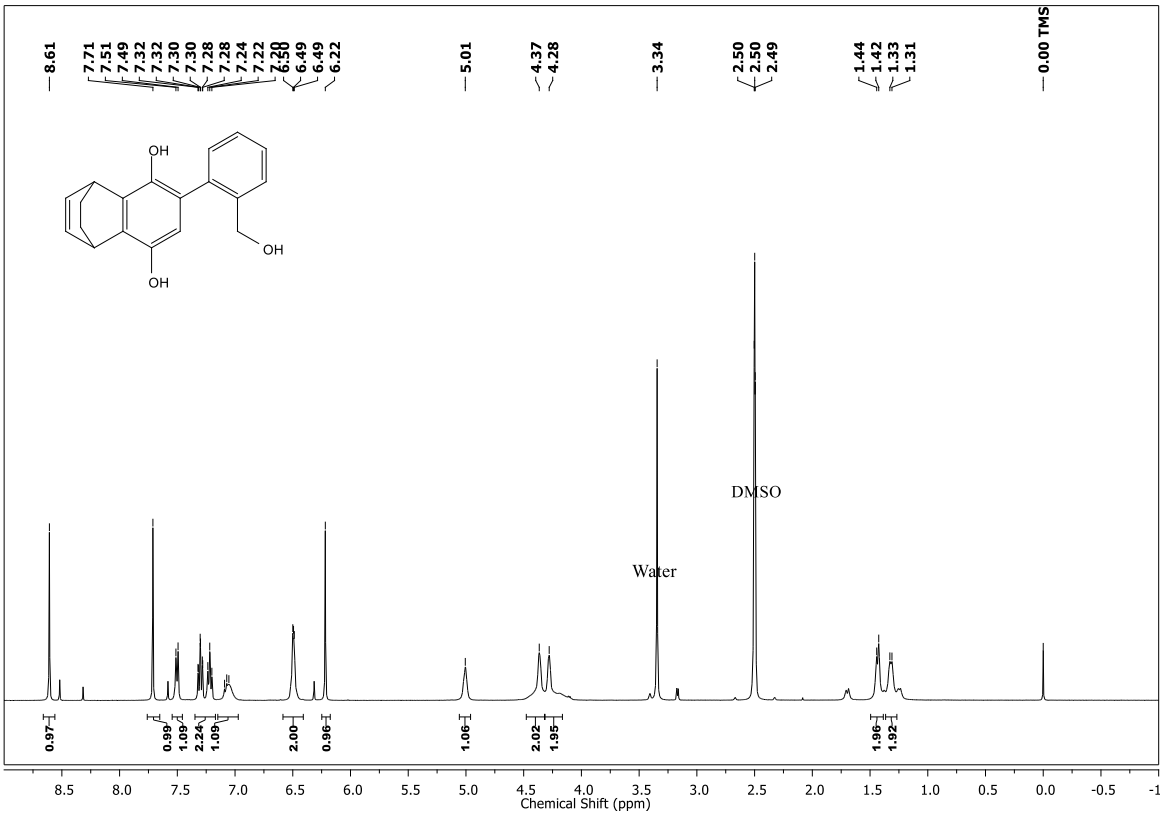

^{1}H NMR spectrum (400 MHz, $CDCl_3$) of **35**

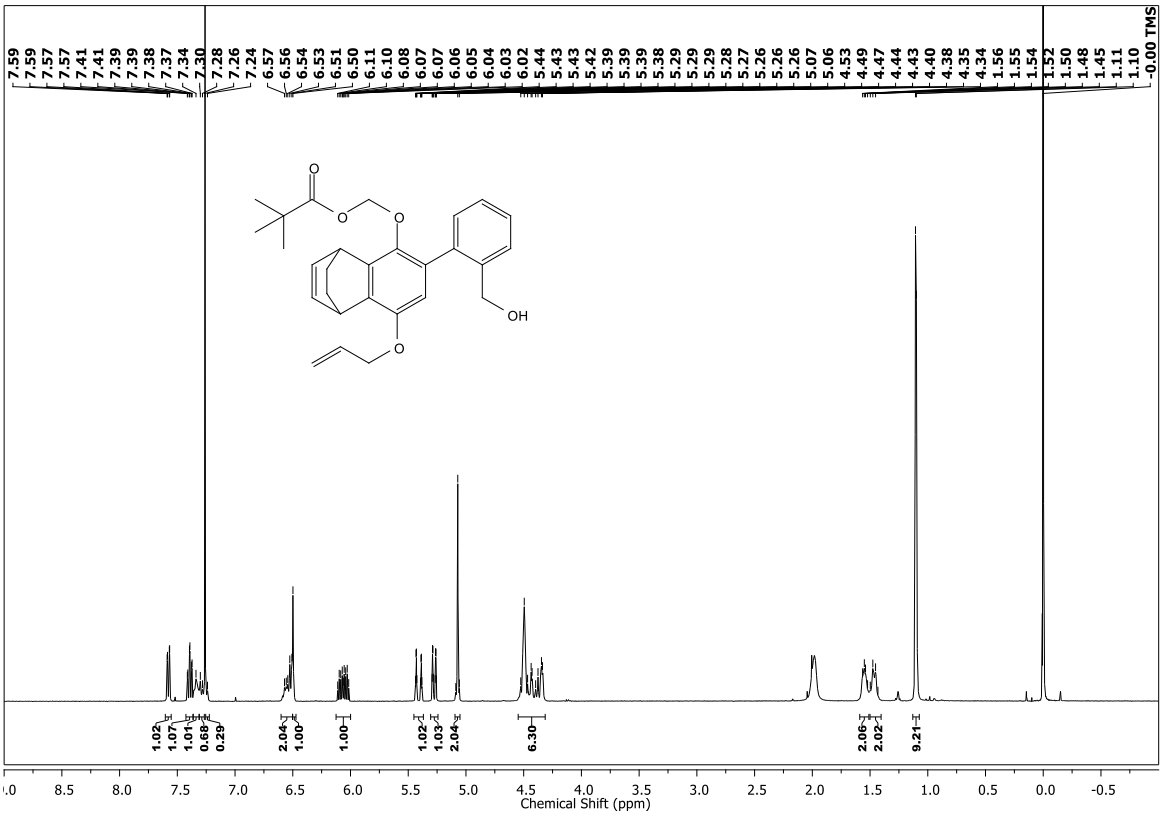

^{13}C NMR spectrum (100 MHz, $CDCl_3$) of **35**

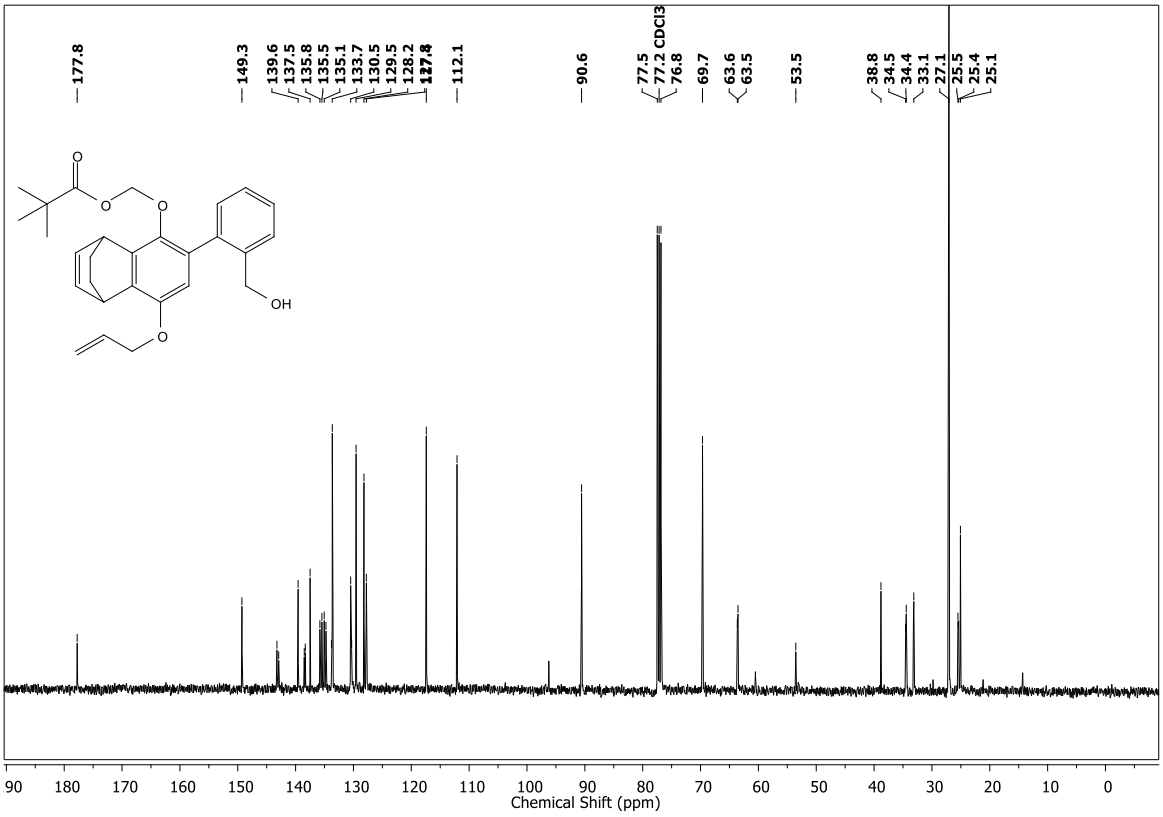

^{1}H NMR spectrum (400 MHz, $CDCl_3$) of **36**

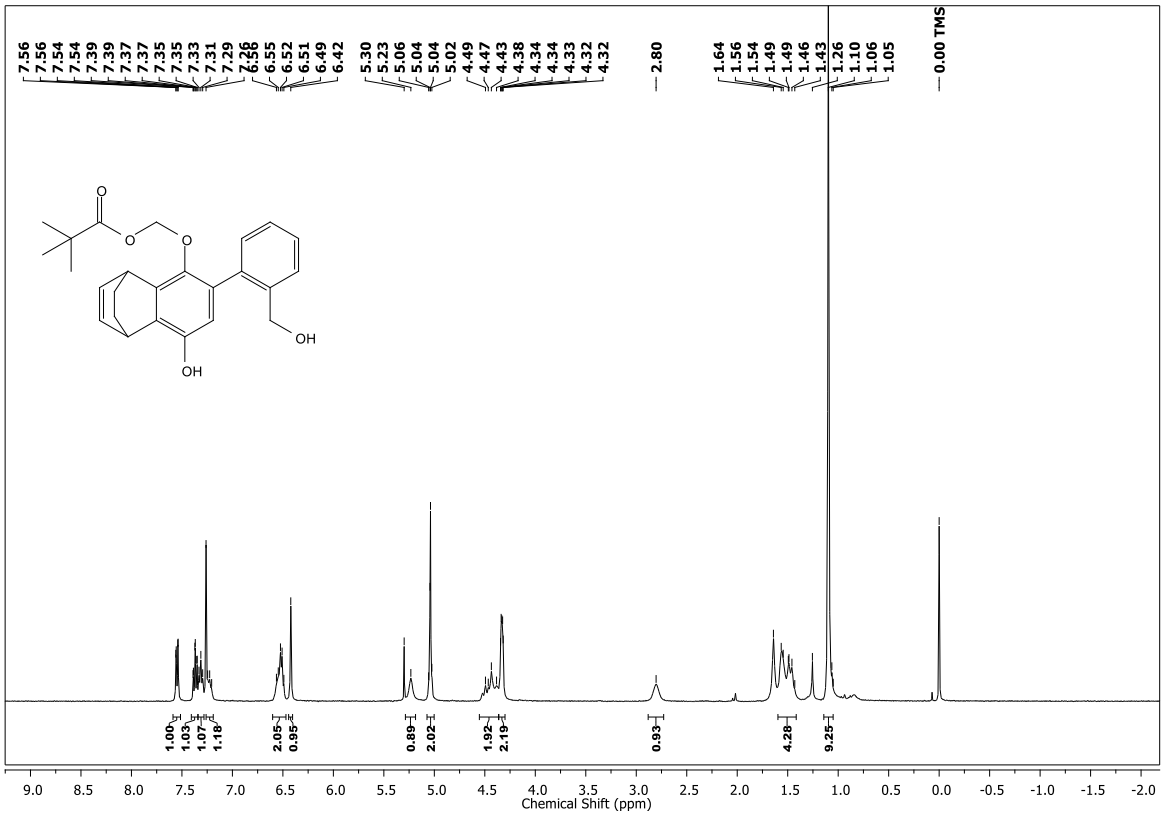

^{13}C NMR spectrum (100 MHz, $CDCl_3$) of **36**

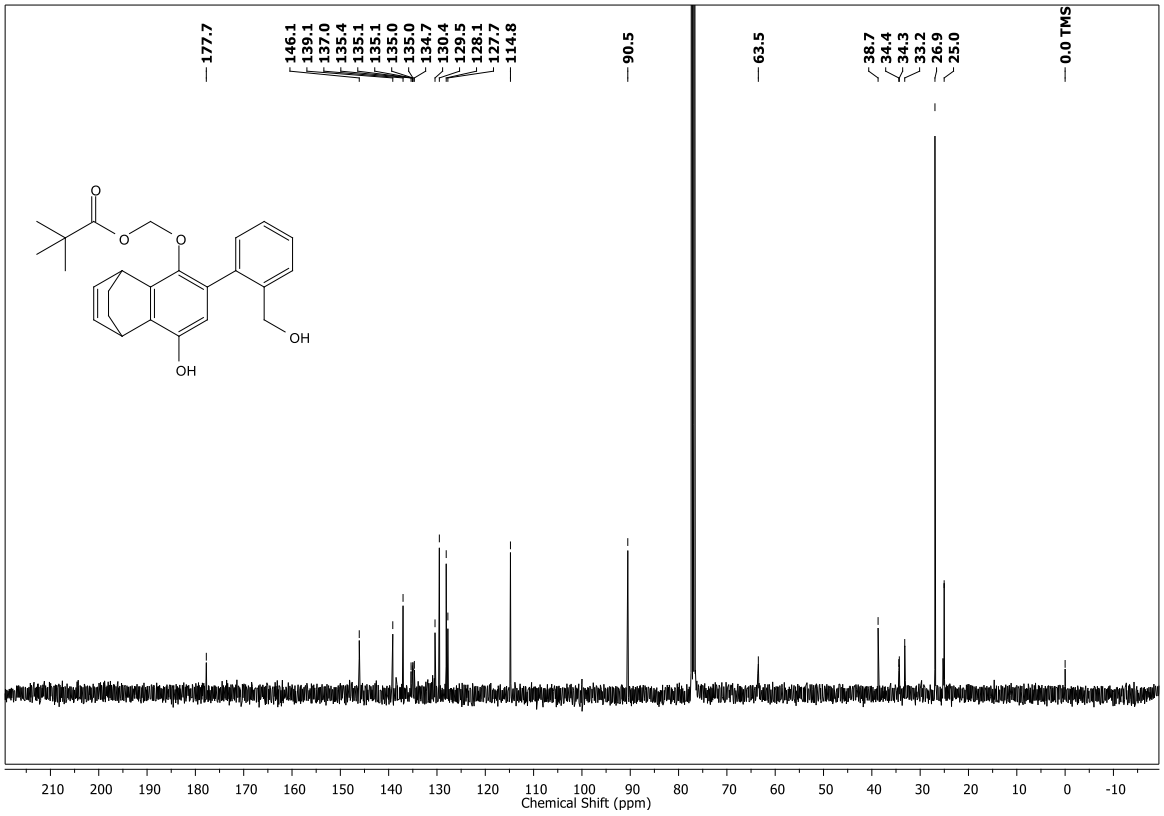

3.1.8 References

(1) Jackson, D. A.; Hassan, A. B.; Errington, R. J.; Cook, P. R. Oxidative Stress Is Involved in the UV Activation of P53. *J. Cell Sci.* **1996**, *107* (7), 1753–1760.

(2) Zhang, X.; Rosenstein, B. S.; Wang, Y.; Lebwohl, M.; Wei, H. Identification of Possible Reactive Oxygen Species Involved in Ultraviolet Radiation-Induced Oxidative DNA Damage. *Free Radic. Biol. Med.* **1997**, *23* (7), 980–985.

(3) Heck, D. E.; Vetrano, A. M.; Mariano, T. M.; Laskin, J. D. UVB Light Stimulates Production of Reactive Oxygen Species. *J. Biol. Chem.* **2003**, *278* (25), 22432–22436.

(4) Bossi, O.; Gartsbein, M.; Leitges, M.; Kuroki, T.; Grossman, S.; Tennenbaum, T. UV Irradiation Increases ROS Production via PKCδ Signaling in Primary Murine Fibroblasts. *J. Cell. Biochem.* **2008**, *105* (1), 194–207.

(5) de Jager, T. L.; Cockrell, A. E.; Du Plessis, S. S. Ultraviolet Light Induced Generation of Reactive Oxygen Species; Springer, Cham, 2017; pp 15–23.

(6) Ulrich, G.; Ziessel, R.; Harriman, A. The Chemistry of Fluorescent Bodipy Dyes: Versatility Unsurpassed. *Angew. Chemie Int. Ed.* **2008**, *47* (7), 1184–1201.

(7) and, A. L.; Burgess*, K. BODIPY Dyes and Their Derivatives: Syntheses and Spectroscopic Properties. *Chem. Rev.* **2007**, *107* (11), 4891–4932.

(8) Palao, E.; Slanina, T.; Muchová, L.; Šolomek, T.; Vítek, L.; Klán, P. Transition-Metal-Free CO-Releasing BODIPY Derivatives Activatable by Visible to NIR Light as Promising Bioactive Molecules. *J. Am. Chem. Soc.* **2016**, *138* (1), 126–133.

(9) Sharma, A. K.; Nair, M.; Chauhan, P.; Gupta, K.; Saini, D. K.; Chakrapani, H. Visible-Light-Triggered Uncaging of Carbonyl Sulfide for Hydrogen Sulfide (H2S) Release. *Org. Lett.* **2017**, *19* (18), 4822–4825.

(10) Umeda, N.; Takahashi, H.; Kamiya, M.; Ueno, T.; Komatsu, T.; Terai, T.; Hanaoka, K.; Nagano, T.; Urano, Y. Boron Dipyrromethene As a Fluorescent Caging Group for Single-Photon Uncaging with Long-Wavelength Visible Light. *ACS Chem. Biol.* **2014**, *9* (10), 2242–2246.

(11) Kumari, P.; Kulkarni, A.; Sharma, A. K.; Chakrapani, H. Visible-Light Controlled Release of a Fluoroquinolone Antibiotic for Antimicrobial Photopharmacology. *ACS*

omega **2018**, *3* (2), 2155–2160.

(12) Goswami, P. P.; Syed, A.; Beck, C. L.; Albright, T. R.; Mahoney, K. M.; Unash, R.; Smith, E. A.; Winter, A. H. BODIPY-Derived Photoremovable Protecting Groups Unmasked with Green Light. *J. Am. Chem. Soc.* **2015**, *137* (11), 3783–3786.

(13) Rubinstein, N.; Liu, P.; Miller, E. W.; Weinstain, R. Meso-Methylhydroxy BODIPY: A Scaffold for Photo-Labile Protecting Groups. *Chem. Commun.* **2015**, *51* (29), 6369–6372.

(14) Patil, N. G.; Basutkar, N. B.; Ambade, A. V. Visible Light-Triggered Disruption of Micelles of an Amphiphilic Block Copolymer with BODIPY at the Junction. *Chem. Commun.* **2015**, *51* (100), 17708–17711.

(15) Sitkowska, K.; Feringa, B. L.; Szymański, W. Green-Light-Sensitive BODIPY Photoprotecting Groups for Amines. *J. Org. Chem.* **2018**, *83* (4), 1819–1827.

(16) Štacko, P.; Muchová, L.; Vítek, L.; Klán, P. Visible to NIR Light Photoactivation of Hydrogen Sulfide for Biological Targeting. *Org. Lett.* **2018**, *20* (16), 4907–4911.

(17) Blangetti, M.; Fraix, A.; Lazzarato, L.; Marini, E.; Rolando, B.; Sodano, F.; Fruttero, R.; Gasco, A.; Sortino, S. A Nonmetal-Containing Nitric Oxide Donor Activated with Single-Photon Green Light. *Chem. - A Eur. J.* **2017**, *23* (38), 9026–9029.

(18) Dharmaraja, A. T.; Jain, C.; Chakrapani, H. Substituent Effects on Reactive Oxygen Species (ROS) Generation by Hydroquinones. *J. Org. Chem.* **2014**, *79* (19), 9413–9417.

(19) Smith, R. A. J.; Hartley, R. C.; Murphy, M. P. Mitochondria-Targeted Small Molecule Therapeutics and Probes. *Antioxid. Redox Signal.* **2011**, *15* (12), 3021–3038.

(20) Yu, H.; Xiao, Y.; Jin, L. A Lysosome-Targetable and Two-Photon Fluorescent Probe for Monitoring Endogenous and Exogenous Nitric Oxide in Living Cells. *J. Am. Chem. Soc.* **2012**, *134* (42), 17486–17489.

(21) Chen, S.; Zhao, X.; Chen, J.; Chen, J.; Kuznetsova, L.; Wong, S. S.; Ojima, I. Mechanism-Based Tumor-Targeting Drug Delivery System. Validation of Efficient Vitamin Receptor-Mediated Endocytosis and Drug Release. *Bioconjug. Chem.* **2010**, *21* (5), 979–987.

(22) Zhao, H.; Joseph, J.; Fales, H. M.; Sokoloski, E. A.; Levine, R. L.; Vasquez-Vivar, J.; Kalyanaraman, B. Detection and Characterization of the Product of Hydroethidine and Intracellular Superoxide by HPLC and Limitations of Fluorescence. *Proc. Natl. Acad. Sci. U. S. A.* **2005**, *102* (16), 5727–5732.

(23) Georgiou, C. D.; Papapostolou, I.; Grintzalis, K. Superoxide Radical Detection in Cells, Tissues, Organisms (Animals, Plants, Insects, Microorganisms) and Soils. *Nat. Protoc.* **2008**, *3* (11), 1679–1692.

(24) Zielonka, J.; Vasquez-Vivar, J.; Kalyanaraman, B. Detection of 2-Hydroxyethidium in Cellular Systems: A Unique Marker Product of Superoxide and Hydroethidine. *Nat. Protoc.* **2008**, *3* (1), 8–21.

(25) Dharmaraja, A. T.; Alvala, M.; Sriram, D.; Yogeeswari, P.; Chakrapani, H. Design, Synthesis and Evaluation of Small Molecule Reactive Oxygen Species Generators as Selective Mycobacterium Tuberculosis Inhibitors. *Chem. Commun.* **2012**, *48* (83), 10325–10327.

(26) Khodade, V. S.; Kulkarni, A.; Gupta, A. Sen; Sengupta, K.; Chakrapani, H. A Small Molecule for Controlled Generation of Peroxynitrite. *Org. Lett.* **2016**, *18* (6), 1274–1277.

(27) Lamblin, M.; Naturale, G.; Dessolin, J.; Felpin, F.-X. Direct C-H Arylation of Quinones with Anilines. *Synlett* **2012**, *23* (11), 1621–1624.

Chapter 3.2. Synthesis and Evaluation of Visible Light Triggerable ROS Generator

3.2.1 Introduction

To solve the problems encountered in the chapter 3.1, a different class of ROS releasing scaffolds were developed which was based on the 1,4-hydroquinone (1,4-HQ)[1] moiety masked with an ester moiety. It was established that ester-protected 1,4-HQ molecule hydrolyzes in the presence of esterase to release 1,4-HQ, which produces ROS. Here, a molecule was designed where one of the hydroxyl groups of 1,4-HQ derivative was masked with BODIPY,[2] a visible light responsive moiety and the other hydroxyl group, with an esterase cleavable moiety (Scheme 3.2.1) which, upon visible light irradiation and esterase treatment, should free up both the hydroxyl groups of 1,4-HQ and the released molecule may react with molecular oxygen to produce ROS.

Scheme 3.2.1. Revised design of Visible light activated ROS generation

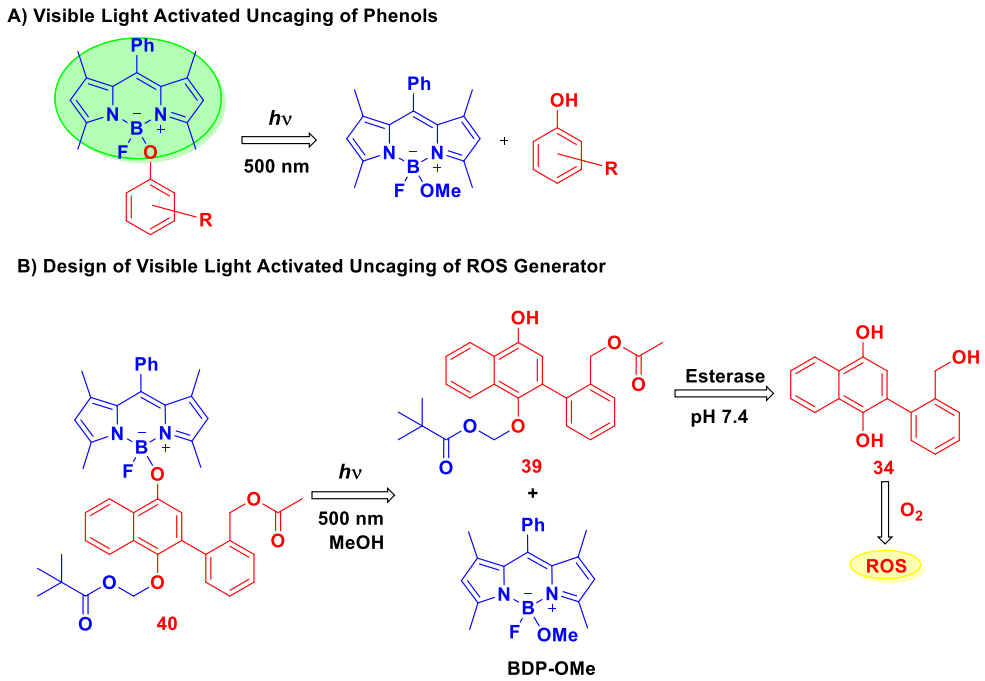

3.2.2 Results and Discussion

3.2.2.1 Synthesis

The synthesis of the designed compound **40** was done in multiple steps (Scheme 3.2.2); the benzylic -OH of compound **35** was acylated using acetic anhydride in the presence of pyridine to obtain **32** as a semi-solid, which was then deallylated using [$Pd(PPh_3)_4$] as a catalyst and phenylsilane as a hydride source, to afford **39**. Next, compound **39** was reacted with BODIPY **25** in the presence of $AlCl_3$, a Lewis acid which abstracts one of the fluorides from the BODIPY moiety, leaving a vacancy for the phenolic nucleophile to attack. The free phenolic group of compound **39** attacks the vacant site of boron in BODIPY, resulting in the formation of compound **40** as an orange colored solid.

Scheme 3.2.2. Synthesis of a BODIPY-coupled ROS donor

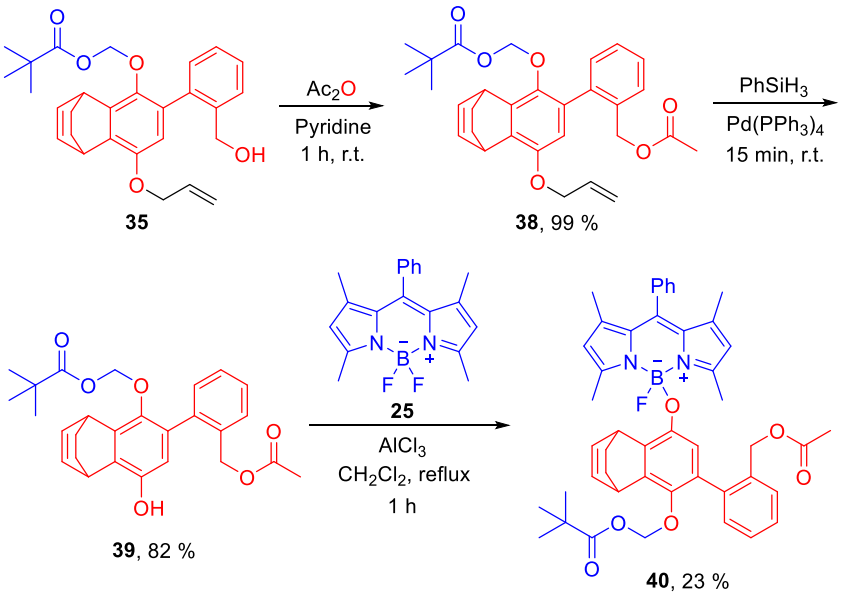

3.2.2.2 Visible Light Triggered Cleavage of 40

In order to test the photocleavage property, compound **40** was irradiated using 500 nm light for 30 min. HPLC analysis revealed two new peaks that could correspond to BDP-OMe (Figure 3.2.2) and **39** (Figure 3.2.1). Intermediate **39** might hydrolyze in the presence of esterase to produce **34**, an active ROS generator. However, no cleavage was found to occur in the dark. This study suggests that compound **40** was stable in the dark and cleaves upon irradiation with visible light.

Figure 3.2.1. Photocleavage study of compound **40** in visible light; HPLC was operated using 500 nm detector

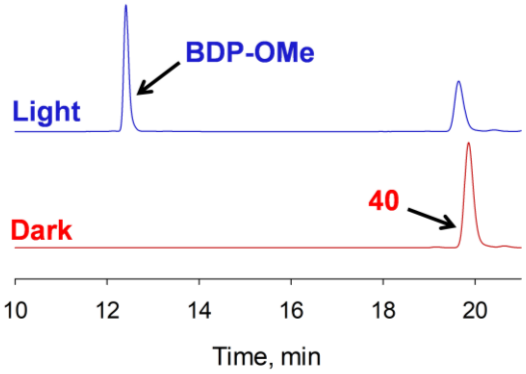

Figure 3.2.2. Photocleavage study of compound **40** in visible light; HPLC was operated using 250 nm detector

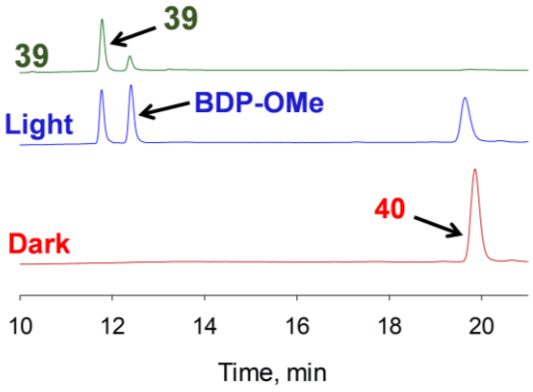

3.2.2.3 ROS Detection

The above photolysis study suggests the formation of **39** which should hydrolyze in the presence of esterase to produce ROS. To investigate the production of ROS, DHE assay was conducted for $O_2^{\bullet-}$ detection.

3.2.2.3.1 Superoxide Detection Using the DHE Assay

As discussed in Chapter 3.1, the DHE assay can be used for $O_2^{\bullet-}$ detection.[3–6] Here, the detection of $O_2^{\bullet-}$ with compound **40** was carried out, where a highly intense peak at 29.5 min in the HPLC trace was observed only in the presence of light and esterase and this signal was diminished when the reaction mixture was treated with superoxide dismutase (SOD), a known quencher of $O_2^{\bullet-}$. This suggests that the observed intense signal in HPLC, is attributable to $O_2^{\bullet-}$ (Figure 3.2.3). However, signal for $O_2^{\bullet-}$ was very weak in the dark, only-esterase-treated and only-irradiated samples.

Figure 3.2.3. Superoxide detection using the DHE assay

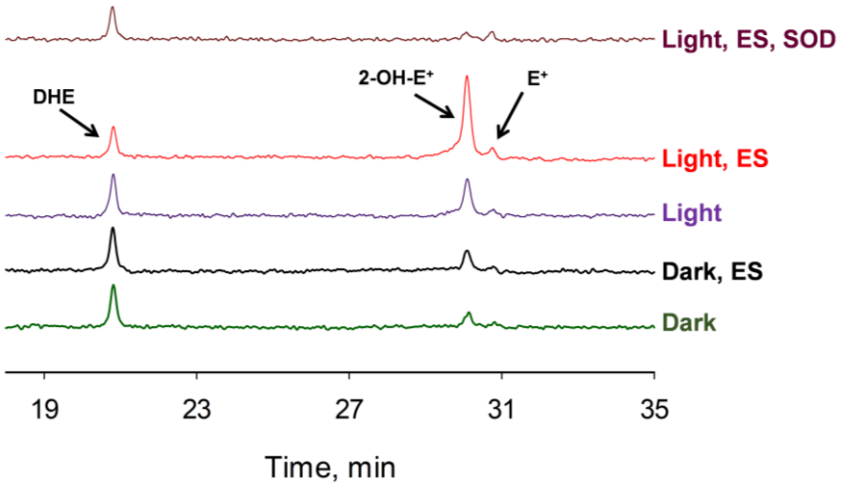

The DHE assay suggests that the generation of $O_2^{\bullet-}$ takes place only when both the stimuli – light and esterase – are given to compound **40**. As a consequence of the double deprotection (that of both the hydroxyl groups), the formed HQ reacts with molecular oxygen to generate $O_2^{\bullet-}$. Taken together, this assay confirms the possibility of $O_2^{\bullet-}$ generation by compound **40** in the presence of both stimuli, visible light and esterase.

3.2.3 Conclusion

In Chapter 3.2, a triggerable ROS donor was developed, using BODIPY as a photolabile linker and a 1,4-hydroquinone derivative as an ROS generating moiety. One of the phenolates of the 1,4-hydroquinone moiety was covalently connected to boron atom of BODIPY moiety. In the presence of visible light, the B-O bond cleaves and releases the 1,4-hydroquinone moiety. In addition, the other phenolate of 1,4-hydroquinone was protected with an ester moiety which was hydrolyzed in the presence of esterase. When both the hydroxyl groups of 1,4-hydroquinone are free, then, it can react with molecular oxygen to produce ROS. The photocleavage studies were performed under visible condition the release of the ROS donor was detected through HPLC. Subsequently, ROS detection was performed using the DHE assay and as expected, the compound photocleaved and hydrolyzed with esterase to produce $O_2^{\bullet-}$. This compound may find a potential application in studying ROS mediated signaling in a spatio-temporally controlled manner, using a visible light-and-esterase activation method.

3.2.4 Synthesis Protocols and Characterization Data

3.2.4.1 Synthesis Protocols

Compound **25**[2] and **30**[7] were synthesized according to reported procedure and data were consistent with reported data. Synthesis of compound **35** was described in the chapter 3.1.

Synthesis of ((6-(2-(acetoxymethyl)phenyl)-8-(allyloxy)-1,4-dihydro-1,4-ethanonaphthalen-5-yl)oxy)methyl pivalate (38): To a solution of **35** (497 mg, 1.11 mmol)

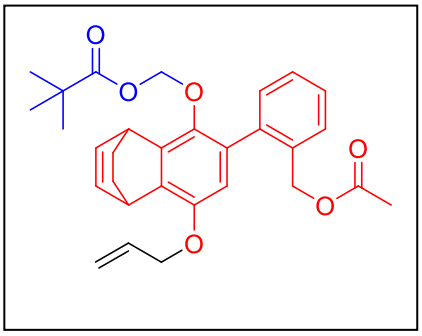

and pyridine (270 µL, 3.35 mmol) in acetic anhydride (5 mL) was stirred for 1 h at r.t. in inert atmosphere. After complete consumption of starting material, mixture was diluted with water and extracted with ethyl acetate. Organic layers were combined, dried over anhydrous sodium sulfate and concentrated under reduced pressure to obtain a solid residue which was purified by column chromatography using silica gel as stationary phase and hexane: ethyl acetate as mobile phase to afford **38** as a semisolid compound (540 mg, 99%). FT-IR (ν_{max}, cm^{-1}): 2927, 1740, 1470; ^{1}H NMR (400 MHz, $CDCl_3$): δ 7.48 – 7.42 (m, 1H), 7.39 – 7.28 (m, 3H), 6.58 – 6.48 (m, 3H), 6.07 (ddd, *J* = 16.2, 10.4, 5.2 Hz, 1H), 5.45 – 5.37 (m, 1H), 5.30 – 5.24 (m, 1H), 5.14 (d, *J* = 12.9 Hz, 1H), 5.08 – 4.86 (m, 3H), 4.55 – 4.44 (m, 3H), 4.39 – 4.33 (m, 1H), 1.98 (d, *J* = 9.0 Hz, 3H), 1.59 – 1.50 (m, 2H), 1.50 – 1.42 (m, 2H), 1.13 (s, 9H); ^{13}C NMR (100 MHz, $CDCl_3$): δ 176.5, 170.7, 148.9, 138.1, 135.5, 135. 3, 134.9, 134.4, 133.6, 130.9, 129.5, 128.7, 128.6, 128.1, 128.0, 127.7, 117.3, 111.9, 90.7, 69.6, 64.7, 38.7, 34.3, 33.1, 27.0, 25.0, 20.9, 20.6; HRMS (ESI-TOF) for $[C_{30}H_{34}O_6 + Na]^+$: calcd., 513.2252, found, 513.2252.

Synthesis of ((6-(2-(acetoxymethyl)phenyl)-8-hydroxy-1,4-dihydro-1,4-ethanonaphthalen-5-yl)oxy)methyl pivalate (39): To a solution of **38** (520 mg, 1.06 mmol)

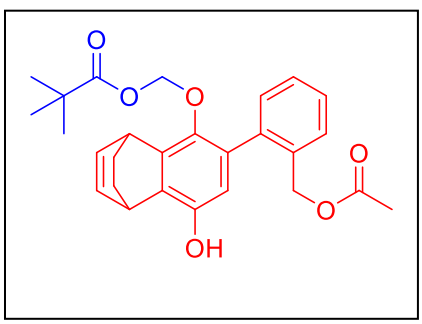

and Tetrakis(triphenylphosphine)palladium(0) (120 mg, 104 µmol) in anhydrous dichloromethane (30 mL) was added $PhSiH_3$ (270 µL, 2.19 mmol) and stirred for 15 min at r.t. in inert atmosphere. After complete consumption of starting material, mixture was diluted with water and extracted with dichloromethane. Organic layers were combined, dried over anhydrous sodium sulfate and

concentrated under reduced pressure to obtain a solid residue which was purified by column chromatography using silica gel as stationary phase and hexane: ethyl acetate as mobile phase to afford **39** as a semisolid compound (390 mg, 82%). FT-IR (ν_{max}, cm^{-1}): 3430, 2930, 1738; ^{1}H NMR (400 MHz, $CDCl_3$): δ 7.46 – 7.40 (m, 1H), 7.38 – 7.29 (m, 3H), 6.57 – 6.47 (m, 2H), 6.45 (s, 1H), 5.15 – 5.09 (m, 1H), 5.06 – 4.97 (m, 3H), 4.38 – 4.29 (m, 2H), 1.98 (d, *J* = 10.9 Hz, 3H), 1.59 – 1.51 (m, 2H),1.51 – 1.44 (m, 2H), 1.13 (s, 9H); ^{13}C NMR (100 MHz, $CDCl_3$): δ 177.6, 170.9, 145.7, 137.5, 135.1, 135.0, 134.4, 131.0, 130.8, 130.2, 129.9, 128.5, 128.0, 127.7, 114.6, 90.7, 64.7, 38.7, 34.3, 33.2, 27.0, 25.1, 20.9, 20.4; HRMS (ESI-TOF) for $[C_{27}H_{30}O_6 + Na]^+$: calcd., 473.1939, found, 473.1937.

Synthesis of ((6-(2-(acetoxymethyl)phenyl)-8-((5-fluoro-1,3,7,9-tetramethyl-10-phenyl-5H-4λ^4,5λ^4-dipyrrolo[1,2-c:2',1'-f][1,3,2]diazaborinin-5-yl)oxy)-1,4-dihydro-1,4-ethanonaphthalen-5-yl)oxy)methyl pivalate (40): To a solution of $AlCl_3$ (36 mg, 270 µmol) and **25** (175 mg, 540 µmol) in anhydrous dichloromethane (20 mL) was added and refluxed for 10 min under inert atmosphere. Compound **39** (240 mg, 533 µmol) in dichloromethane solution (10 mL) was added dropwise and the mixture was further refluxed for 1 h. The reaction was monitored by TLC and cooled to room temperature which was purified by column chromatography using neutral alumina as the stationary phase and hexane: ethyl acetate as the mobile phase which was further purified by preparative HPLC using Kromasil®C-18 column and water: acetonitrile as mobile phase to afford compound 40 as an orange solid (95 mg, 23%). FT-IR (ν_{max}, cm^{-1}): 2924, 1739, 1470, 1405; ^{1}H NMR (400 MHz, $CDCl_3$): δ 7.50 – 7.27 (m, 5H), 7.24 – 7.10 (m, 3H), 7.07 – 6.93 (m, 1H), 6.58 – 6.43 (m, 2H), 6.12 – 6.02 (m, 1H), 5.93 (d, *J* = 7.4 Hz, 1H), 5.88 (d, *J* = 4.2 Hz, 1H), 5.83 (d, *J* = 6.1 Hz, 1H), 5.10 – 4.97 (m, 2H), 4.95 (m, 1H), 4.84 – 4.59 (m, 2H), 4.38 – 4.26 (bs, 1H), 2.53 (d, *J* = 5.5 Hz, 3H), 2.48 (d, *J* = 4.2 Hz, 3H), 1.88 (d, *J* = 1.9 Hz, 3H), 1.59 – 1.50 (m, 2H), 1.48 – 1.40 (m, 2H), 1.32 – 1.26 (m, 3H), 1.26 – 1.21 (m, 3H), 1.11 (d, *J* = 5.6 Hz, 9H); ^{13}C NMR (100 MHz, $CDCl_3$): δ 177.6, 170.5, 156.2, 146.5, 143.0, 142.9, 142.2, 141.9, 141.6, 138.5, 138.4, 137.8, 137.6, 135.9, 135.6, 135.0, 134.8, 134.7, 134.6, 131.8, 130.9, 130.8, 129.1, 128.8, 128.6, 127.8, 127. 7, 127.6, 127.5, 127.4, 127.1, 121.7, 121.5, 115.1, 91.1, 91.0,

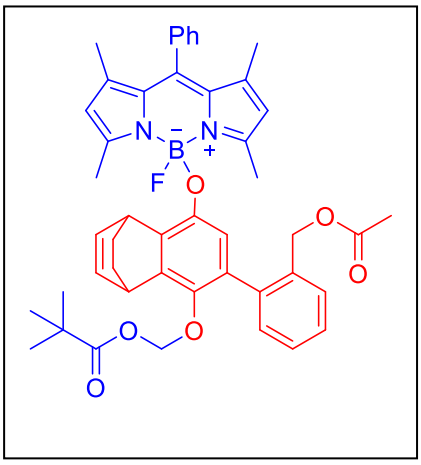

64.5, 64.3, 38.7, 34.4, 34.3, 33.3, 27.0, 25.5, 25.3, 20.7, 14.8, 14.2; HRMS (ESI-TOF) for $[C_{46}H_{48}BFN_2O_6 + Na]^+$: calcd., 777.3487, found, 777.3667.

3.2.4.2 General Preparation

10 mM stocks of compounds **39** and **40** were prepared in DMSO and stored in the dark at -4 °C. 10 mM stock dihydroethidium (DHE) was prepared in DMSO and stored at -20 °C. 100 U/mL stocks of Superoxide dismutase (SOD) and Esterase enzyme were prepared in phosphate buffer (50 mM) of pH 7.4 and stored at -4 °C.

3.2.4.3 Procedure for Irradiation

A quartz cuvette containing compound **40** in MeOH or phosphate buffer was irradiated using 500 nm (50 mW/cm^2) LED at room temperature in a closed chamber. This solution was used for further analysis as described below.

3.2.4.4 Photo-Cleavage Study by HPLC

A quartz cuvette containing compound **40** (2.5 µL of 10 mM) in MeOH (497 µL) was irradiated for 30 min in 500 nm Light using Cyan LED. Similarly, compound **40** (2.5 µL of 10 mM) in MeOH (497 µL) was kept in dark for 30 min. 25 µL of aliquot from each irradiated and non-irradiated sample were injected in HPLC and analysis was conducted using a diode array detector (DAD) operating at 250 nm and 500 nm. The column used was Phenomenex® C-18 reverse phase column (250 mm × 4.6 mm, 5 µm), the mobile phase was water: acetonitrile for 25 min and a gradient starting with 40: 60 % → 0 – 2 min, 40: 60 to 2: 98 → 2 – 10 min, 2: 98 → 10 – 21 min, 2: 98 to 40:60 → 21 – 22 min, 40: 60 → 22 – 25 min was used with a flow rate of 1 mL/min.

3.2.4.5 Superoxide Detection Using DHE Assay[3–6,8–10]

A quartz cuvette containing compound **40** (1.25 µL of 10 mM) in phosphate buffer of pH 8.0 (496 µL) was irradiated. Similarly, compound **40** (1.25 µL of 10 mM) in phosphate buffer of pH 8.0 (496 µL) was kept in dark for 30 min. In the non-irradiated and irradiated samples, DHE (2.5 µL of 10 mM) was added and incubated for 2 h at 37 °C. The same experiment was also

performed in the presence of 1 U/mL esterase enzyme where one of the irradiated samples was treated with esterase enzyme (5 µL of 100 U/mL) and DHE (2.5 µL of 10 mM) followed by incubation for 2 h at 37 °C. The reaction mixture was filtered (0.45 µm) and injected (50 µL) in an Agilent high performance liquid chromatograph (HPLC) attached with a fluorescence detector (excitation at 480 nm; emission at 580 nm). The column used was Agilent1260-infinity with Phenomenex® C-18 reverse phase column (250 mm × 4.6 mm, 5 µm), the mobile phase was water: acetonitrile containing 0.1% trifluoroacetic acid and a gradient starting with 90: 10 % → 0 min, 10: 90 to 44: 56 → 0 – 35 min, 0: 100 → 35 – 40 min, 0: 100 → 37 – 40 min, 10: 90 → 40 – 42 min, 10: 90 → 42 – 45 min was used with a flow rate of 0.5 mL/min. A known scavenger of superoxide, Superoxide dismutase enzyme (5 µL of 100 U/mL) was also used as a control with the irradiated sample in the presence of esterase enzyme. Signal for $O_2^{\bullet -}$ was not observed in SOD treated samples.

3.2.5 Spectral Chart

^{1}H NMR spectrum (400 MHz, $CDCl_3$) of **38**

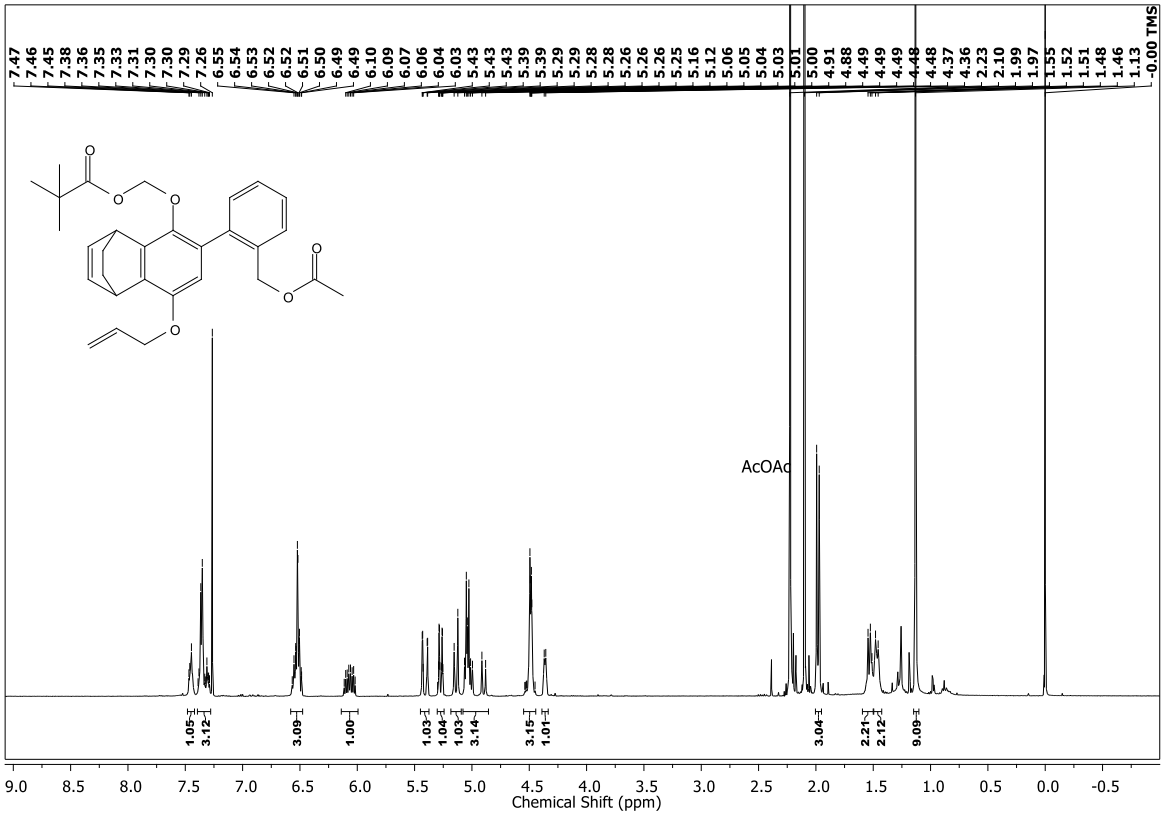

^{13}C NMR spectrum (100 MHz, $CDCl_3$) of **38**

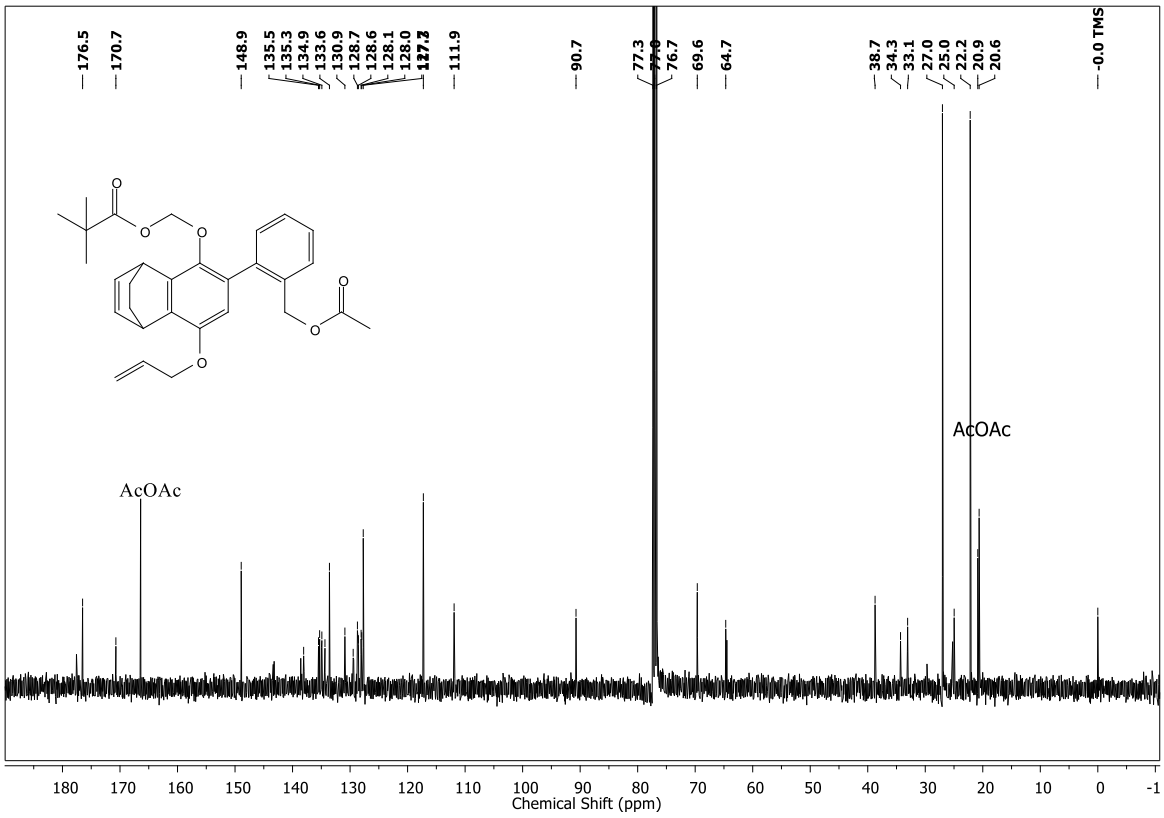

^{1}H NMR spectrum (400 MHz, $CDCl_3$) of **39**

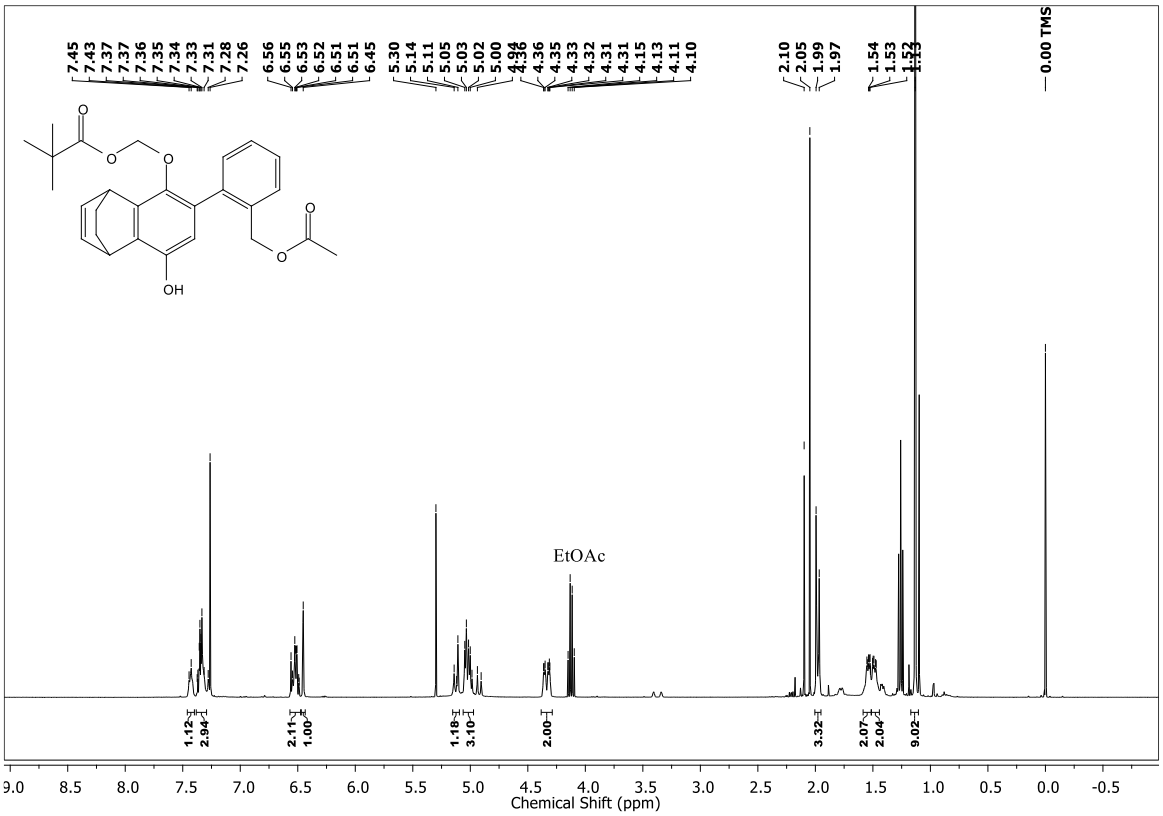

^{13}C NMR spectrum (100 MHz, $CDCl_3$) of **39**

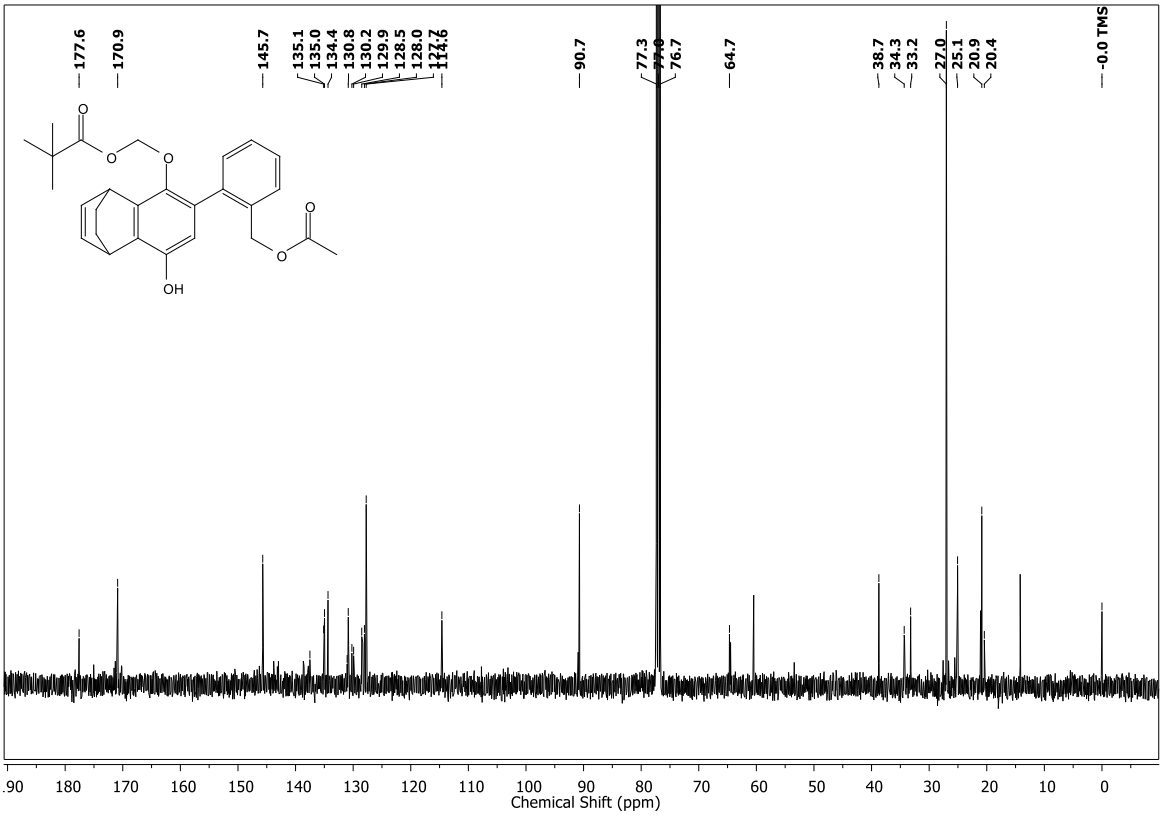

^{1}H NMR spectrum (400 MHz, $CDCl_3$) of **40**

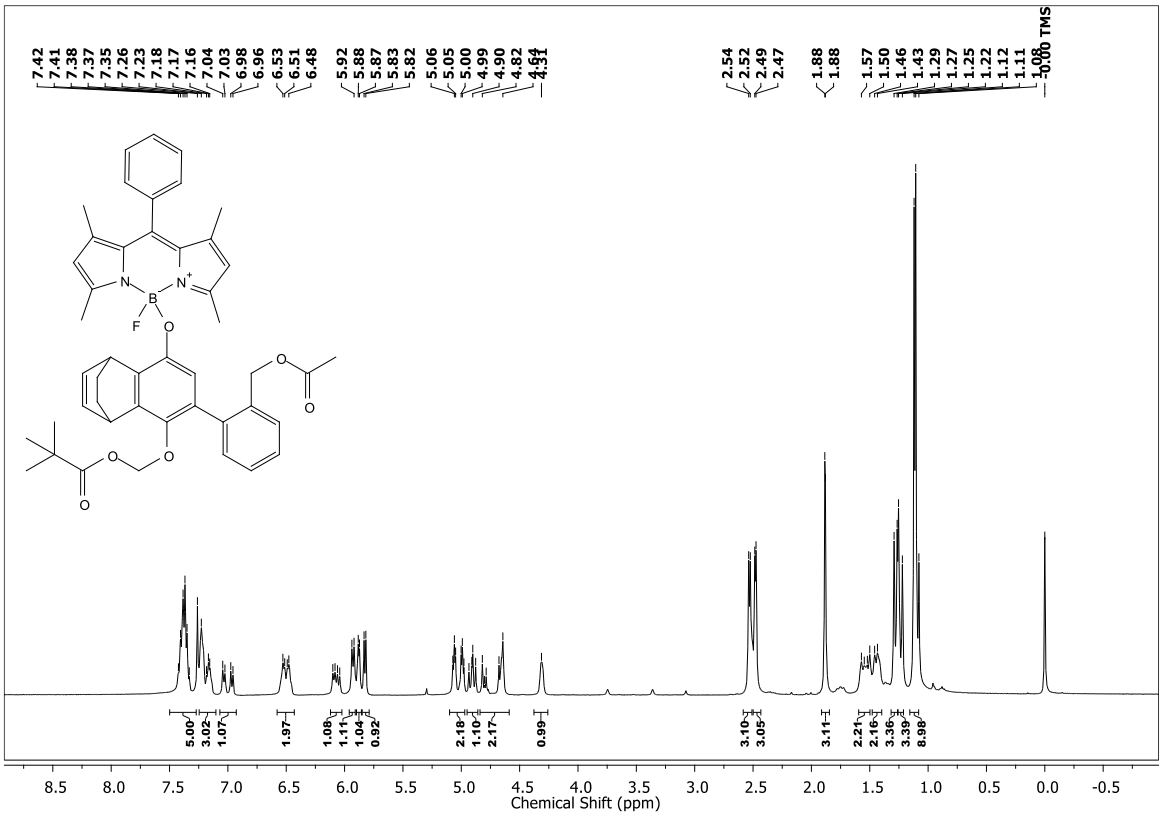

^{13}C NMR spectrum (100 MHz, $CDCl_3$) of **40**

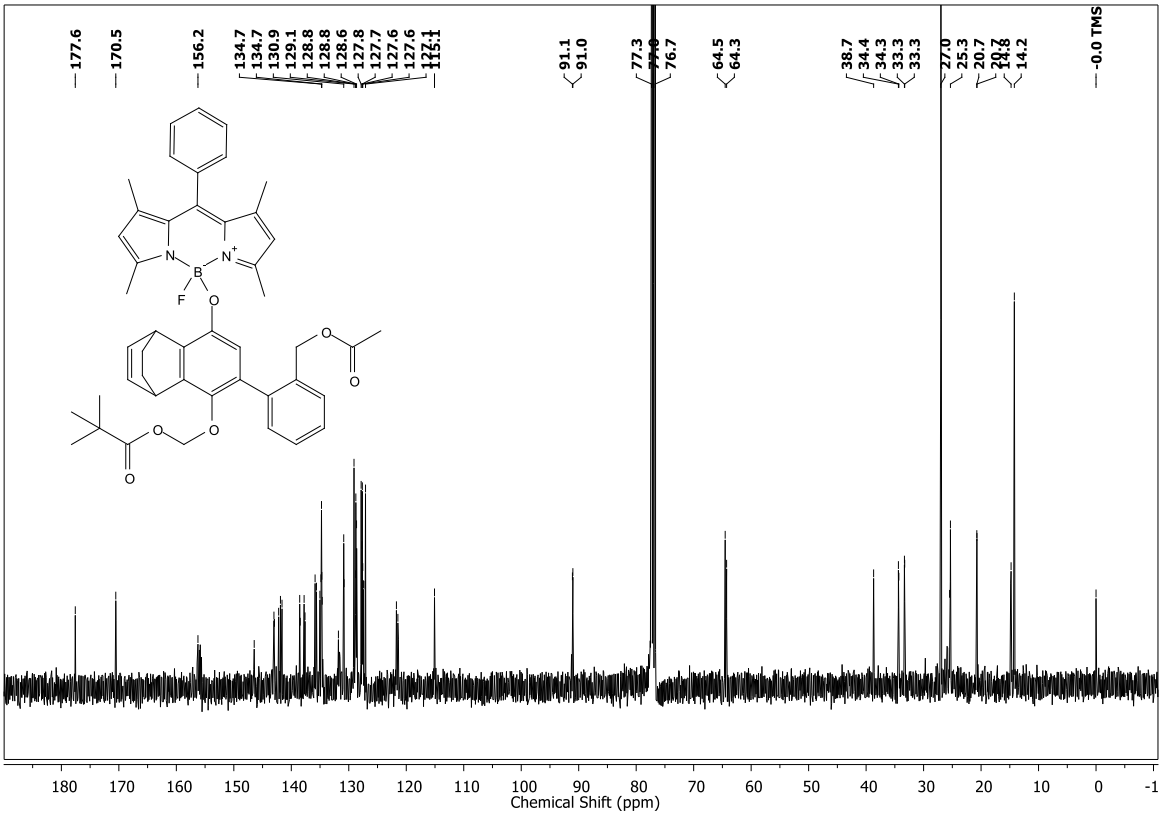

3.2.6 References

(1) Dharmaraja, A. T.; Jain, C.; Chakrapani, H. Substituent Effects on Reactive Oxygen Species (ROS) Generation by Hydroquinones. *J. Org. Chem.* **2014**, *79* (19), 9413–9417.

(2) Umeda, N.; Takahashi, H.; Kamiya, M.; Ueno, T.; Komatsu, T.; Terai, T.; Hanaoka, K.; Nagano, T.; Urano, Y. Boron Dipyrromethene As a Fluorescent Caging Group for Single-Photon Uncaging with Long-Wavelength Visible Light. *ACS Chem. Biol.* **2014**, *9* (10), 2242–2246.

(3) Zhao, H.; Joseph, J.; Fales, H. M.; Sokoloski, E. A.; Levine, R. L.; Vasquez-Vivar, J.; Kalyanaraman, B. Detection and Characterization of the Product of Hydroethidine and Intracellular Superoxide by HPLC and Limitations of Fluorescence. *Proc. Natl. Acad. Sci. U. S. A.* **2005**, *102* (16), 5727–5732.

(4) Zielonka, J.; Vasquez-Vivar, J.; Kalyanaraman, B. Detection of 2-Hydroxyethidium in Cellular Systems: A Unique Marker Product of Superoxide and Hydroethidine. *Nat. Protoc.* **2008**, *3* (1), 8–21.

(5) Zielonka, J.; Cheng, G.; Zielonka, M.; Ganesh, T.; Sun, A.; Joseph, J.; Michalski, R.; O'Brien, W. J.; Lambeth, J. D.; Kalyanaraman, B. High-Throughput Assays for Superoxide and Hydrogen Peroxide: Design of a Screening Workflow to Identify Inhibitors of NADPH Oxidases. *J. Biol. Chem.* **2014**, *289* (23), 16176–16189.

(6) Kalyanaraman, B.; Hardy, M.; Zielonka, J. A Critical Review of Methodologies to Detect Reactive Oxygen and Nitrogen Species Stimulated by NADPH Oxidase Enzymes: Implications in Pesticide Toxicity. *Curr. Pharmacol. Reports* **2016**, *2* (4), 193–201.

(7) Lamblin, M.; Naturale, G.; Dessolin, J.; Felpin, F.-X. Direct C-H Arylation of Quinones with Anilines. *Synlett* **2012**, *23* (11), 1621–1624.

(8) Kalyanaraman, B.; Darley-Usmar, V.; Davies, K. J. A.; Dennery, P. A.; Forman, H. J.; Grisham, M. B.; Mann, G. E.; Moore, K.; Roberts, L. J.; Ischiropoulos, H. Measuring Reactive Oxygen and Nitrogen Species with Fluorescent Probes: Challenges and Limitations. *Free. Radic. Biol. Med.* **2012**, *52* (1), 1–6.

(9) Dharmaraja, A. T.; Alvala, M.; Sriram, D.; Yogeeswari, P.; Chakrapani, H. Design, Synthesis and Evaluation of Small Molecule Reactive Oxygen Species Generators as

Selective Mycobacterium Tuberculosis Inhibitors. *Chem. Commun.* **2012**, *48* (83), 10325–10327.

(10) Dharmaraja, A. T.; Chakrapani, H. A Small Molecule for Controlled Generation of Reactive Oxygen Species (ROS). *Org. Lett.* **2014**, *16* (2), 398–401.

Chapter 4. Visible Light Triggered Uncaging of COS/H_2S

4.1 Introduction

Cellular antioxidant mechanisms exploit the thiol moiety as a reactive center because of its propensity to undergo oxidation as well as reduction reactions. This makes it a suitable redox active center in cellular pathways.[1–3] In one particular antioxidant mechanism, glutathione and its dimeric form, GSSG (*i.e.*, the GSH/GSSG system) regulate the level of ROS in the presence of GSH reductase[4] and thioredoxin (TrX)[5–8]; this serves to maintain the redox homeostasis of the cell. As it was described, ROS is essential for several signaling pathways. Apart from ROS, there are other redox active species, *i.e.*, carbon monoxide (CO),[9–15] nitric oxide (NO)[13,17,18–23] and hydrogen sulfide (H_2S)[23–32] in cells, which play a crucial role in regulating the various signaling pathways. These species are gaseous and are synthesized endogenously and regulated by several pathways. CO and NO are known to essay a vital role in neuronal signal transduction and are hence called neurotransmitters. These species can also act as antioxidants which help reduce cellular oxidative stress.

As discussed in Chapter 1, H_2S is a sulfur containing gaseous molecule which is endogenously synthesized and plays a crucial role in signaling mechanisms.[27–29] However, the exact effects of H_2S are concentration- and location-dependent, so that studying these effects is challenging due to its highly diffusible nature and reactivity towards multiple sites in a cellular system.[33] Thus, a tool is needed to deliver this gaseous species in cells to study its physiological effects. In the process of searching for the tools for H_2S-delivery, there are several methods reported in literature which have already been illustrated in Chapter 1.

Chapter 3 deals with the synthesis and evaluation of a potential BODIPY-based 1,4-hydroquinone derivative, which produces ROS after visible light activation. Here, releasing another redox active species, H_2S, using a BODIPY-based visible light uncaging group is attempted. Our group has previously reported a scaffold which is activated by esterase to release a phenolate intermediate.[34] This phenolate intermediate subsequently self-immolates to release carbonyl sulfide (COS), a gaseous molecule which produces H_2S upon hydrolysis with carbonic anhydrase (CA), a widely prevalent enzyme. To generate H_2S in a spatio-temporally controlled manner under ambient conditions, a phenolate (linked with a carbamothioate moiety) can be masked with BODIPY, such that the phenolate can be released upon irradiation with visible light.[35] This phenolate should self-immolate to release a carbamothioate

intermediate which, then, should release COS to produce H_2S upon hydrolysis with CA (Figure 4.1).[34,36–40] This method may generate H_2S in a spatio-temporally controlled manner under ambient conditions.

Figure 4.1. Rational design for the visible light triggered uncaging of H_2S

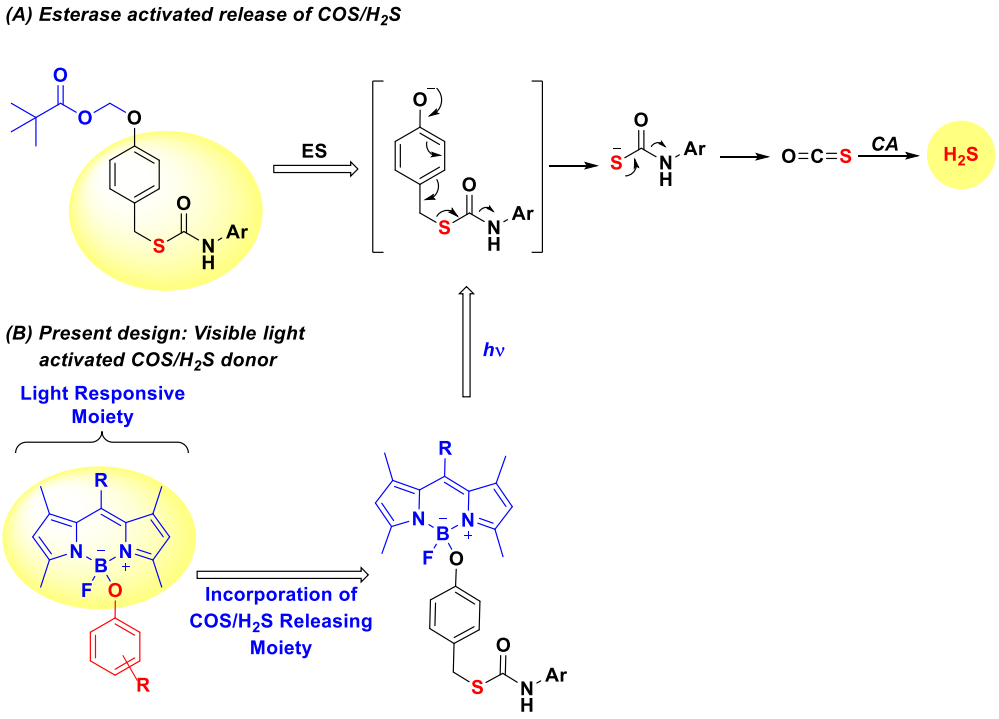

4.2 Results and Discussion

4.2.1 Synthesis

Compound **47** was synthesized in several steps (Scheme 4.1).[41] Intermediates such as the BODIPY derivative (**41**),[42] 4-hydroxybenzyl thioacetate (**42**),[43] 4-nitrophenyl (4-methoxyphenyl)carbamate (**44**)[44] and azido-tetraethylene glycol (**46**)[45] were synthesized using previously reported methods. In order to synthesize compound **47**, compound **41** was reacted with 4-hydroxybenzyl thioacetate (**42**) in the presence of $AlCl_3$, a Lewis acid, to form compound **43** as a thioacetate derivative. This thioacetate derivative was deprotected using potassium carbonate in methanol to obtain the free thiol. The thiol was not isolated due to its inherent propensity for dimerization and was subsequently reacted with compound **44** in the presence of triethylamine to afford a red coloured compound **45**.

Compound **45** is less soluble in aqueous media due to the presence of several hydrophobic groups. To increase the aqueous solubility of **45,** an alkyne tag which is present in **45,** can be used to incorporate a hydrophilic substituent. To do this, azide **46,** having a short oligo-ethylene glycol chain was reacted with compound **45** using copper catalyzed alkyne-azide click (CuAAC) reaction to obtain **47** as an orange colored solid (Scheme 4.1).

Scheme 4.1. Synthesis of compound **47**

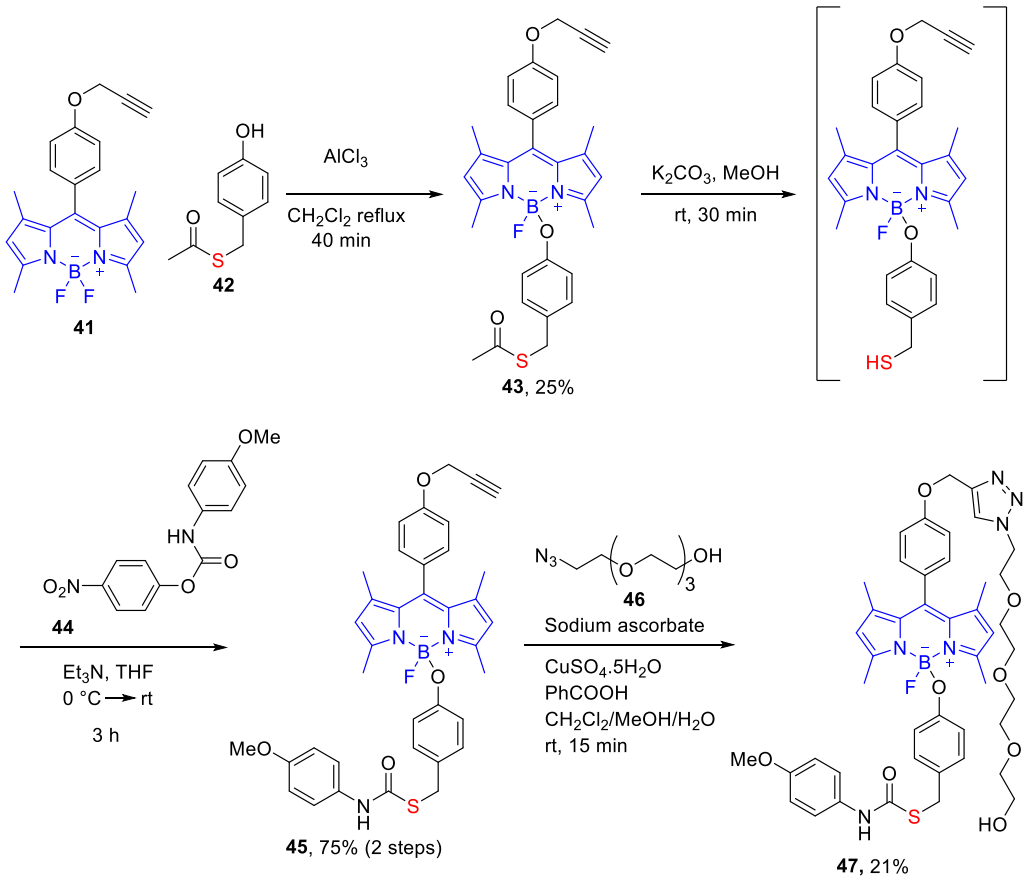

Next, to synthesize compound **50**, compound **41** was reacted with 4-hydroxybenzaldehyde in the presence of $AlCl_3$ to form compound **48**, which was reduced by $NaBH_4$ to obtain **49**. The compound **49** was, then, further reacted with **46** using copper mediated click reaction to afford **50** (Scheme 4.2). This molecule may undergo cleavage in visible light but may not produce H_2S, which may serve as a negative control for H_2S release.

Scheme 4.2. Synthesis of negative control **50**

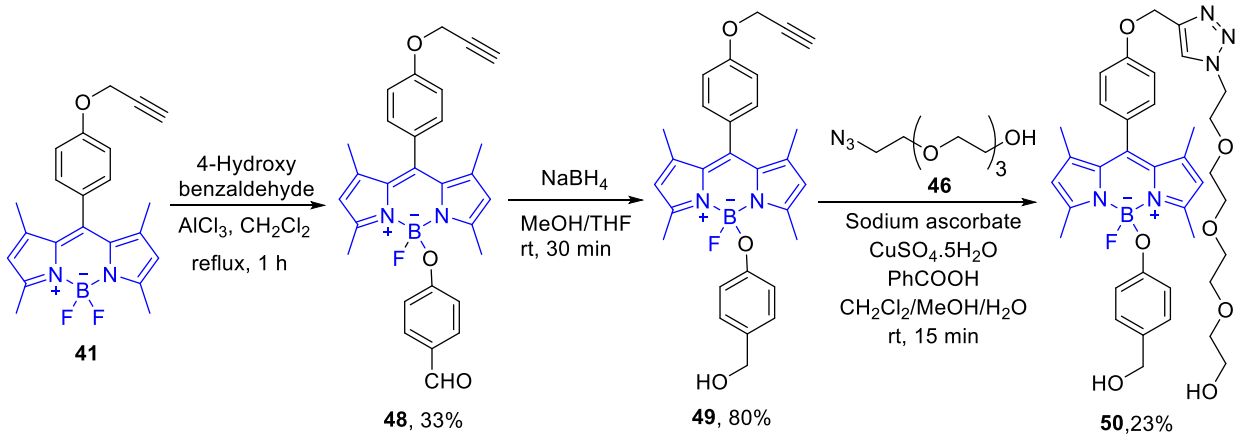

4.2.2 Photo-Cleavage Studies by Means of HPLC

In order to look for possible photo-cleavage, previously reported conditions for the same were used. A methanolic solution of **47** was irradiated using visible light (470 nm, 30 mW/cm^2) for predetermined time points and was analyzed by HPLC, connected with a diode array detector (DAD) operated at 250 nm, 500 nm and Fluorescence detector (Excitation wavelength 470 nm, Emission at 540 nm) using a reverse phase C-18 column. It was found that the peak at 20.4 min corresponds to compound **47** had disappeared after 20 min of irradiation (Figure 4.2). The kinetics of disappearance of **47** was also performed and a curve fitting first order kinetics gave us 0.16 min^{-1} as a rate constant (Figure 4.4). This cleavage resulted in the formation of two additional peaks (Figure 4.3). One of the peaks with retention time of 13.2 min was highly intense in the HPLC trace recorded by operating a DAD at 500 nm (Figure 4.2). This peak was also highly fluorescent and was found to be methoxy-BODIPY (**51**) by mass spectrometric analysis (Figure 4.5). The time course for the formation of the compound **51** was assessed and a curve fitting for first order kinetics gave 0.2 min^{-1} as a rate constant (Figure 4.4).

Scheme 4.3. Photo-cleavage reaction of compound **47** to form the shown putative intermediates

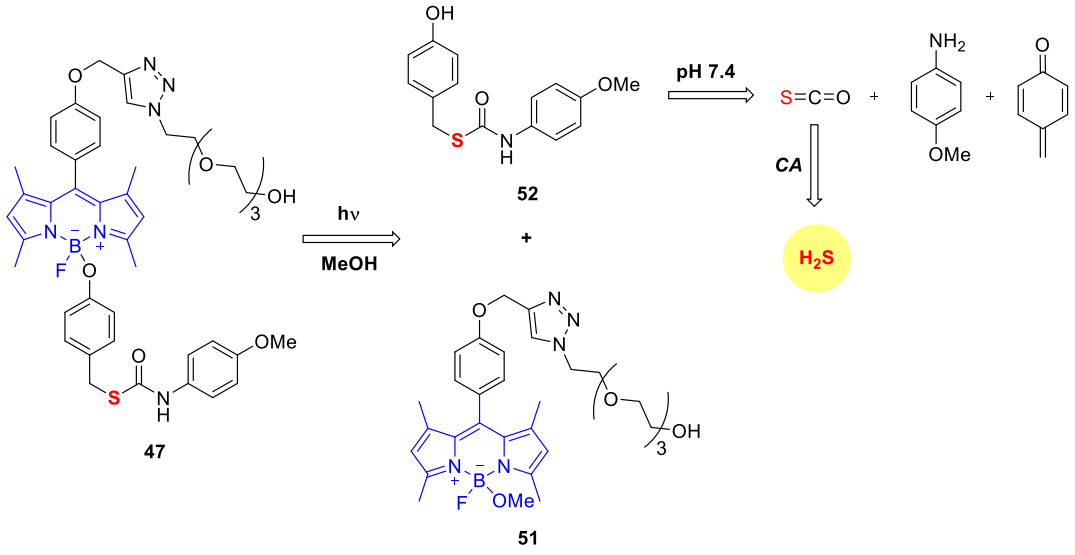

Figure 4.2. HPLC traces before and after irradiation with 470 nm light (30 mW/cm2) for 20 min in MeOH (detector was operated at 500 nm). Adapted with permission from *Org. Lett.* **2017**, *19* (18), 4822-4825. Copyright (2017) American Chemical Society.

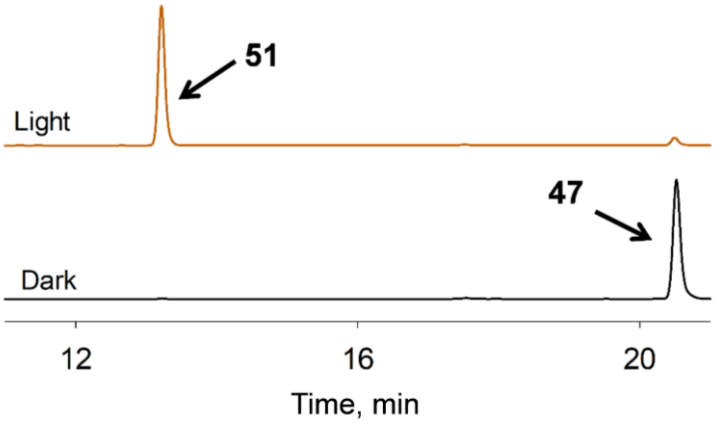

Figure 4.3. HPLC traces for **47** before and after irradiation with 470 nm light (30 mW/cm^2) for 20 min in MeOH (detector was operated at 250 nm). Adapted with permission from *Org. Lett*. **2017**, *19* (18), 4822-4825. Copyright (2017) American Chemical Society.

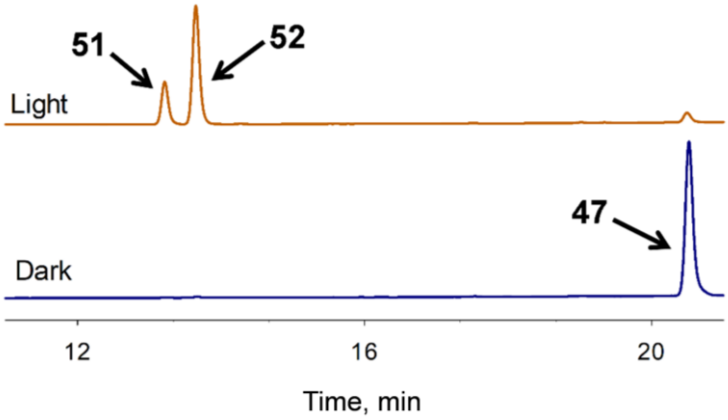

Figure 4.4. Time courses for disappearance of **47** and formation of BDP-OMe (**51)** after irradiation. Adapted with permission from *Org. Lett*. **2017**, *19* (18), 4822-4825. Copyright (2017) American Chemical Society.

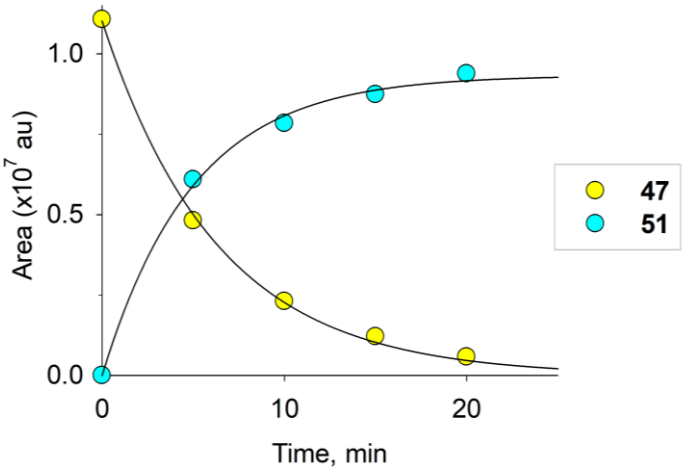

In addition to the highly fluorescent peak, another peak was observed in the trace at 13.6 min, recorded using 250 nm Diode Array Detector (DAD) (Figure 4.3). This peak may correspond to the phenolate intermediate **52** which would self-immolate in a pH 7.4 buffer to release COS. In order to investigate this self-immolation of the putative intermediate **52**, the time course decomposition was studied using HPLC where complete disappearance of **52** was observed within 2 h of incubation in buffer (Figure 4.6 A) and a curve fitting first order kinetics

gave us 0.02 min^{-1} as a rate constant (Figure 4.6 B). Taken together, these studies suggest that the compound **47** undergoes photo-cleavage resulting in a putative intermediate **52** that self-immolates in buffer. This self-immolation might lead to the formation of COS, which, upon hydrolysis produces H_2S.

Figure 4.5. Detection of **51** by mass spectrometry. Adapted with permission from *Org. Lett.* **2017**, *19* (18), 4822-4825. Copyright (2017) American Chemical Society.

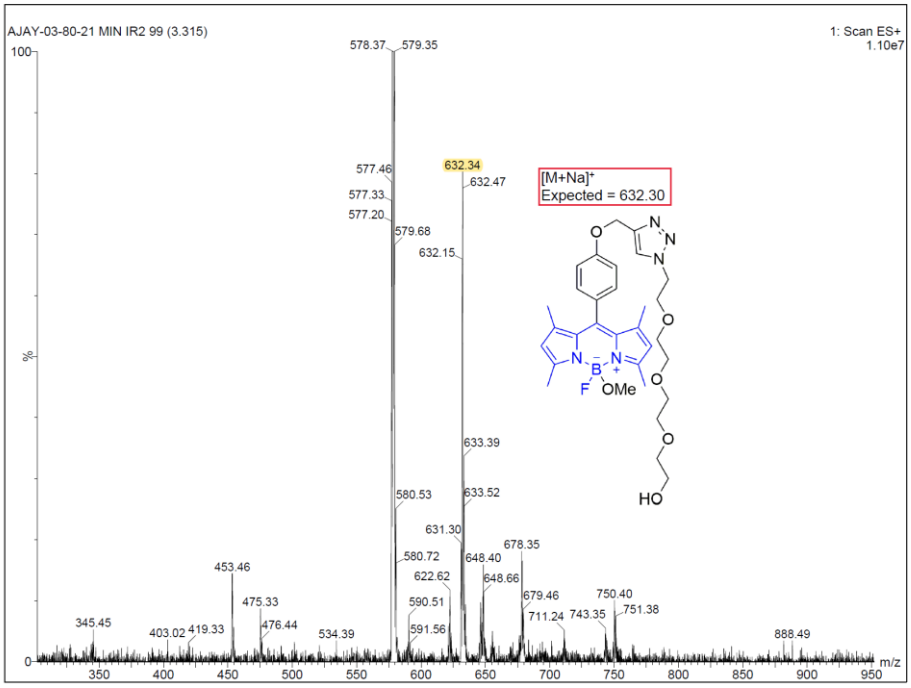

Figure 4.6. Self-immolation of the putative intermediate **52** in buffer (A) HPLC traces of time course analysis; (B) curve fitting of disappearance of **52**. Adapted with permission from *Org. Lett*. **2017**, *19* (18), 4822-4825. Copyright (2017) American Chemical Society.

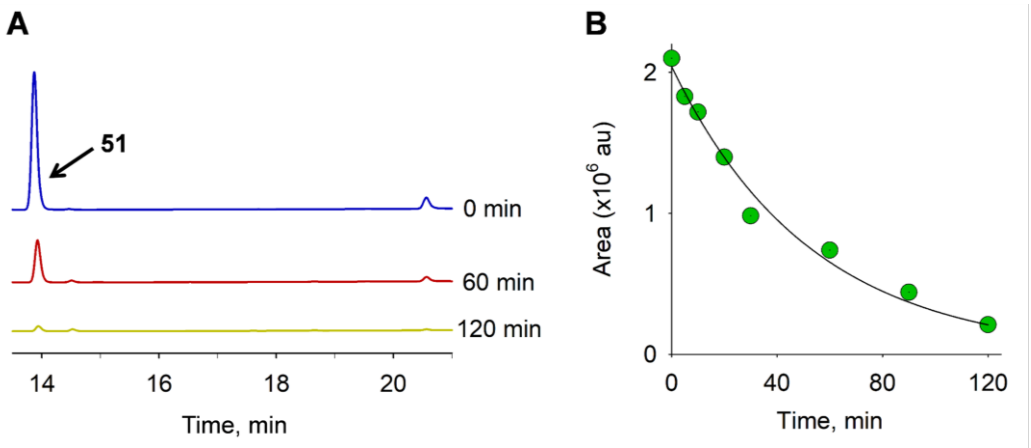

4.2.3 *In Vitro* Fluorescence Enhancement Assay

BODIPY containing electron rich aryloxy substituents on the boron atom can quench the typically observed fluorescence of this moiety, through a photoinduced electron transfer (PET) mechanism.[35] This PET mechanism may result in a weakly fluorescent molecule as compared to the native BODIPY. After photolysis, the aryloxy group would be released and concomitantly result in the formation of a highly fluorescent BODIPY derivative.

Here, in the molecule **47**, an aryloxy/phenolic substituent attached to the boron atom of BODIPY which quenches fluorescence, making **47** a weakly fluorescent molecule. If compound **47** is irradiated with visible light, it should release an aryloxy substituent and a highly fluorescent BODIPY photo-product. To test this hypothesis, the fluorescence intensity of **47** before and after irradiation was compared using a 96-well plate reader and a 20-fold enhancement was found in the fluorescence signal after irradiation (Figure 4.8). Similar results were also observed in HPLC traces where the peak corresponding to compound **47** is weakly intense; however, that corresponding to the BODIPY product **52** is a highly intense one, when HPLC was operated using a fluorescence detector (Figure 4.7). This study suggested that the compound **47** forms a highly fluorescent molecule after photo-cleavage. Hence, real time monitoring of the release of an aryloxy substituent is possible.

Figure 4.7. HPLC traces recorded before and after irradiation in methanol. Here, a fluorescence detector was used with excitation wavelength 470 nm and emission wavelength 540 nm. Adapted with permission from *Org. Lett.* **2017**, *19* (18), 4822-4825. Copyright (2017) American Chemical Society.

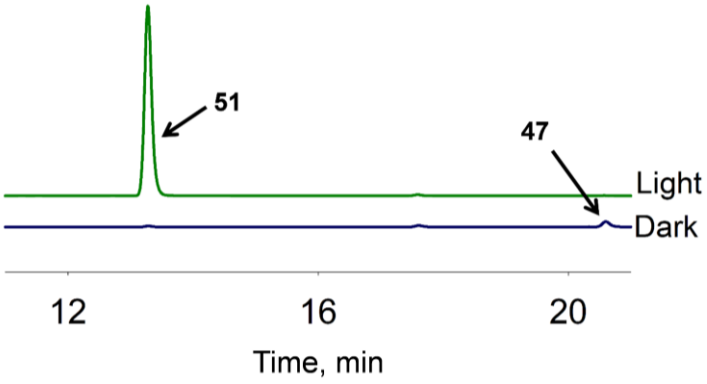

Figure 4.8. Fluorescence was recorded before and after irradiation of **47** in methanol (excitation wavelength 470 nm and emission wavelength 540 nm). Adapted with permission from *Org*. *Lett*. **2017**, *19* (18), 4822-4825. Copyright (2017) American Chemical Society.

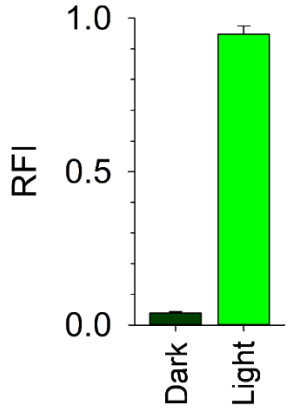

4.2.4 H_2S Detection

As it was established, compound **47** cleaves under visible light and releases a phenolate intermediate which, then, self-immolates in buffer. This self-immolation should result in the generation of COS, which is known to hydrolyze in the presence of carbonic anhydrase to produce H_2S. To test the formation of H_2S from **47** in the presence of light and carbonic anhydrase, two independent assays were conducted.

4.2.4.1 Methylene Blue Assay

Methylene blue (MB) is a well-known dye; it is also used as a bacteriologic stain. The synthesis of MB is accomplished using Na_2S, *N*,*N*-dimethyl-*p*-phenylenediamine and $FeCl_3$ in an acidic medium, which can be exploited to detect H_2S, where *N*,*N*-dimethyl-*p*-phenylenediamine can be treated with an H_2S releasing moiety in the presence of $FeCl_3$ in acidic conditions to form the MB dye (Scheme 4.3).[46] This MB has an absorption maximum at 676 nm which can be measured using a spectrophotometer.

In order to infer the production of H_2S, a methanolic solution of compound **47** was irradiated for 25 min using blue light (470 nm) and subsequently, diluted in a buffer containing CA and zinc acetate and incubated at 37 ºC for predetermined time points. These samples were independently reacted with the methylene blue cocktail (*N*,*N*-dimethyl-*p*-phenylenediamine solution in 7.2 M HCl and $FeCl_3$ solution in 1.2 M HCl) and further incubated for 30 min at 37 ºC. These solutions were transferred to a 96 well plate and the absorbance spectra were

recorded. It was observed that, in the irradiated samples, the absorbance peak at 676 nm increased gradually with incubation time and a curve fitting first order kinetics gave 0.03 min^{-1} as a rate constant (Figure 4.9) while in the non-irradiated samples, the peak at 676 nm was not observed. In addition to this, this assay was also conducted in the absence of CA (Figure 4.10) and no signal was observed for the MB formation; this suggests that CA is essential for hydrolyzing the generated COS to H_2S.

Scheme 4.4. Formation of Methylene blue *via* H_2S

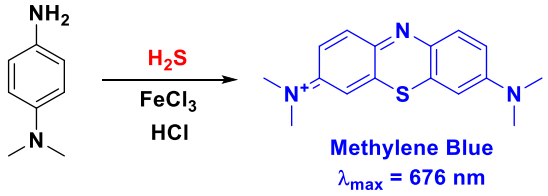

To test any possible interference due to the BODIPY photo-product, the MB assay was also carried out with compound **50**, a compound which does not contain a COS/H_2S releasing moiety. After irradiation, the compound **50** can produce the same BODIPY photo-product as compound **47**. When this assay was performed compound **50**, no signal was observed for MB in the irradiated as well as non-irradiated samples (Figure 4.11), suggesting that the BODIPY photoproduct is not responsible for any signal at 676 nm.

Figure 4.9. H_2S detection by the Methylene blue assay (A) Compound **47** was irradiated with 470 nm light for 25 min followed by incubation with carbonic anhydrase in pH 7.4 buffer for predetermined time points (B) Curve fitting for first order kinetics gives rate constant = 0.03 min^{-1} (R^2 = 0.995). Adapted with permission from *Org. Lett.* **2017**, *19* (18), 4822-4825. Copyright (2017) American Chemical Society.

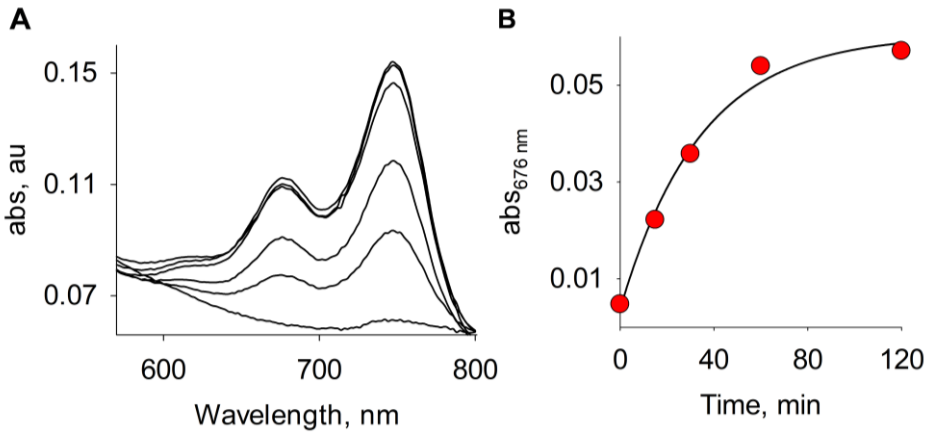

Figure 4.10. Methylene Blue assay for H_2S detection with compound **47** in the presence and absence of the enzyme carbonic anhydrase. Adapted with permission from *Org. Lett.* **2017**, *19* (18), 4822-4825. Copyright (2017) American Chemical Society.

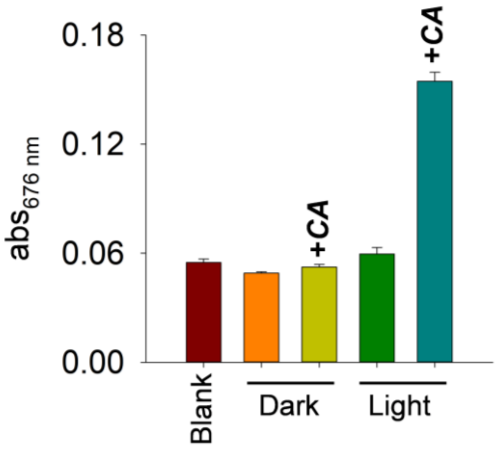

Figure 4.11. Methylene Blue assay for H_2S detection with Na_2S (50 μM) and after irradiation of compound **50** (50 μM). Adapted with permission from *Org. Lett.* **2017**, *19* (18), 4822-4825. Copyright (2017) American Chemical Society.

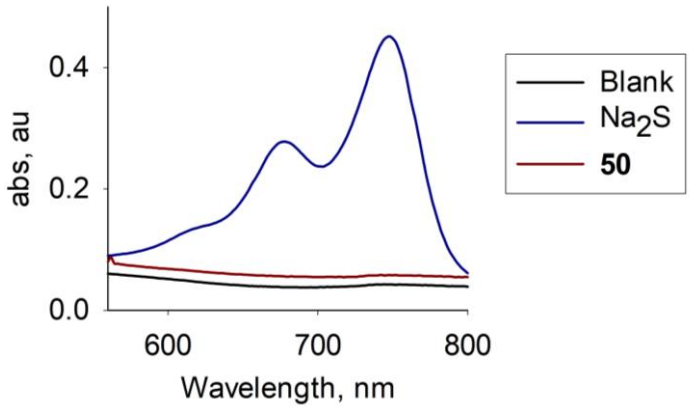

4.2.4.2 Electrochemical H_2S Detection

Here, the detection of H_2S has been carried out using a highly sensitive and specific amperometric H_2S sensor as an independent technique. This electrode contains ferricyanide/ferrocyanide based redox mediator which reacts with H_2S to change the ratio of ferricyanide/ferrocyanide as well as the pH.[47] Using electrochemical methods, these changes can be detected and converted into a digital signal, which corresponds to H_2S. In order to infer the production of H_2S, the compound **47** was irradiated and incubated in a buffer containing CA and measured the H_2S release by the said electrode and a gradual enhancement in the signal was observed over a period of time. However, no significant enhancement was appeared when

the analysis was conducted with the non-irradiated sample (Figure 4.12). This experiment suggested that compound **47** produces H_2S only after activation with light.

Figure 4.12. H_2S generation was assessed by a H_2S-sensitive electrode for the irradiated and non-irradiated samples of compound **47**. Adapted with permission from *Org. Lett.* **2017**, *19* (18), 4822-4825. Copyright (2017) American Chemical Society.

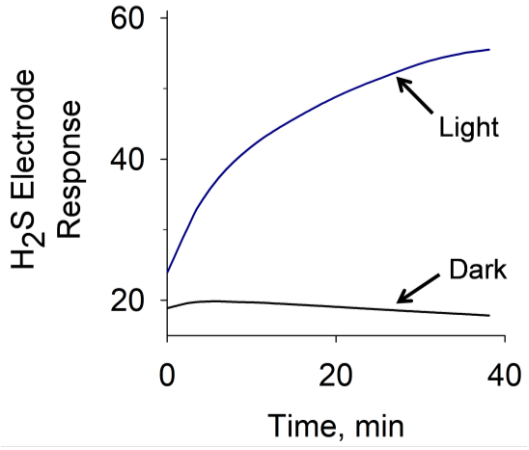

4.2.5 Mechanism of H_2S Generation

I was illustrated that when compound **47** is treated with radiation of wavelength 470 nm, it produces a BODIPY photoproduct **51** and a phenolate intermediate **52**. The kinetics of the said photocleavage was also performed and the first order rate constant was found to be 0.16 min^{-1} (Scheme 4.5). The phenolate intermediate **52** rearranges to produce a quinone methide and anisidine, along with COS. The first order rate constant for the decomposition of the putative intermediate **52** was found to be 0.02 min^{-1}. The produced COS was hydrolyzed to form H_2S and the rate constant of this reaction is reported to be 1.82 s^{-1}.[48] The kinetics study of H_2S generation *via* an MB assay was also performed and the first order rate constant was found to be 0.03 min^{-1}. Taken together, all these results suggest that the rate determining step of H_2S generation was the self-immolation step, which was comparable with the determined overall rate of release of H_2S.

Scheme 4.5. Proposed mechanism of formation of H_2S after photoirradiation of **47**. Adapted with permission from *Org. Lett.* **2017**, *19* (18), 4822-4825. Copyright (2017) American Chemical Society.

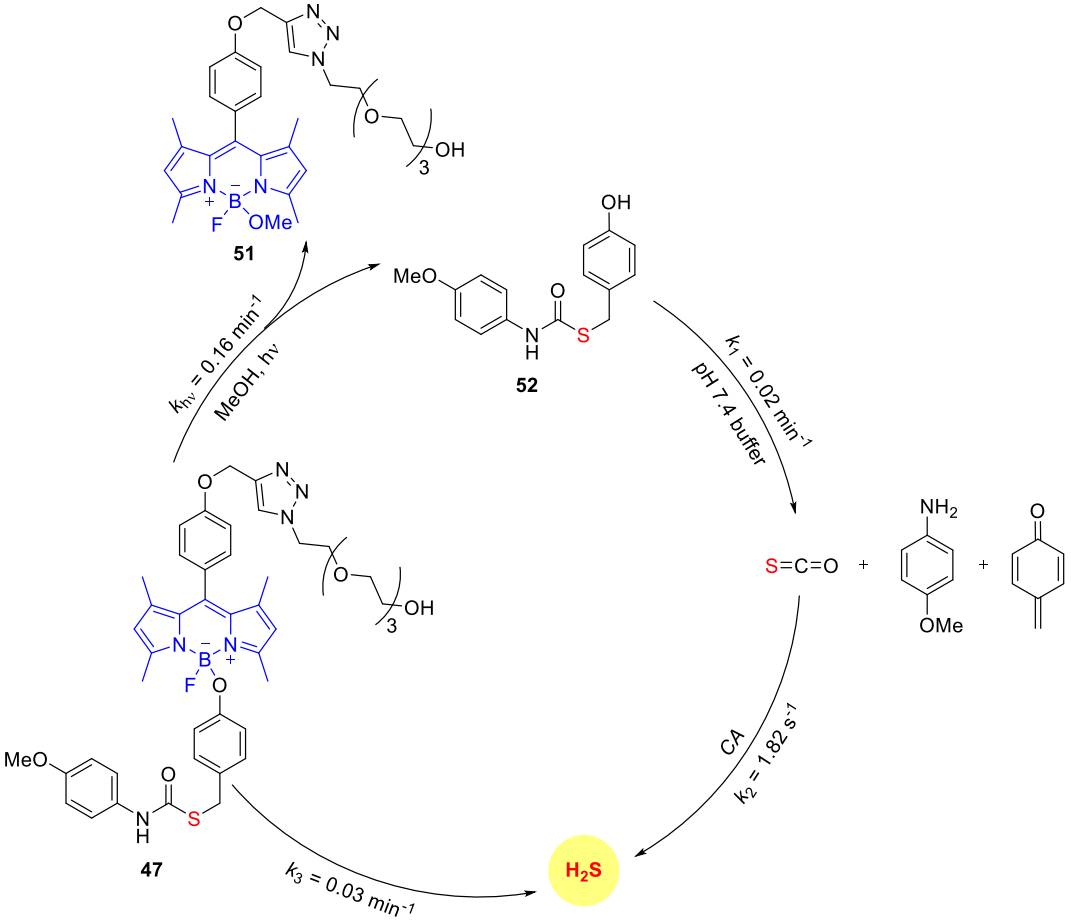

4.2.6 Cellular Assays

4.2.6.1 Fluorescence Enhancement in Cells

As described in section 4.2.3, BODIPY having an electron rich aryloxy substituent on the boron can result in quenching the fluorescence of BODIPY molecule through PET mechanism. This PET mechanism may result in a weakly fluorescent molecule as compared to native BODIPY. After photolysis, the BODIPY moiety releases the aryloxy group which results in restoring the fluorescence properties of BODIPY derivative.

Further, to test fluorescence enhancement in cells, HeLa cells were treated with compound **47**, and subsequently irradiated using visible light where a significant enhancement in fluorescence was observed for irradiated cells (Figure 4.13). This study suggests that

compound **47** photocleaves to releases a highly fluorescent BODIPY derivative in cells, which can be used for the real time monitoring of the release of its aryloxy substituent.

Figure 4.13. (A) HeLa cells pre-treated with compound **47** (10 µM) were irradiated for 2 min with 470 nm light; imaging showed an increased fluorescence signal (YFP channel); Scale bar = 50 mm (B) Fluorescence enhancement data for the cellular experiment. Data provided by Kavya Gupta & Dr. Deepak Saini, IISc Bangalore. Adapted with permission from *Org. Lett.* **2017**, *19* (18), 4822-4825. Copyright (2017) American Chemical Society.

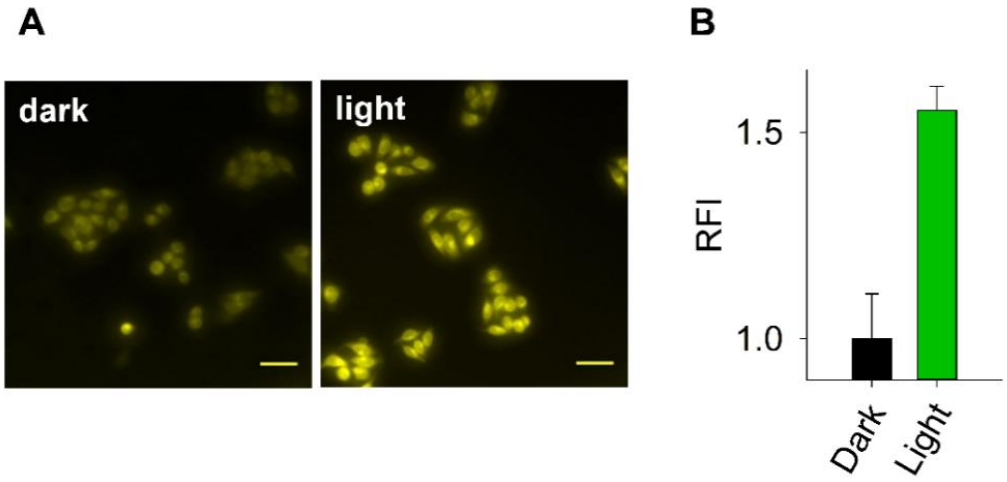

4.2.6.2 Effects on Cellular Proliferation

To test the effect of compound **47** on cellular growth, two independent assays was conducted on different cancer cell lines.

4.2.6.2.1 MTT Assay

Human cervical carcinoma (HeLa) cells, were treated with varying concentrations of compound **47** and were irradiated with 470 nm light for 5 min, followed by incubation for 24 h at 37 ºC. MTT was added, and incubation for an additional 4 h was done, followed by recording the absorbance at 570 nm. No toxicity was observed for compound **47** up to 50 µM (Figure 4.14), in mammalian cells.

Figure 4.14. Effect of **47** on cell proliferation was determined by MTT assay. HeLa cells with increasing doses of **47** followed by irradiation with 470 nm light for 5 min (24 h incubation). Data provided by Preeti Chauhan, IISER Pune. Adapted with permission from *Org. Lett.* **2017**, *19* (18), 4822-4825. Copyright (2017) American Chemical Society.

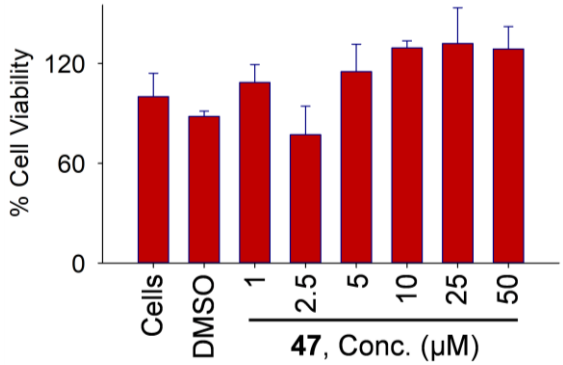

4.2.6.2.2 Crystal Violet Assay

Crystal violet is a dye which only stains viable cells. Human adenocarcinomic alveolar basal epithelial (A549) cells were treated with varying concentrations of compound **47** and were irradiated with 470 nm light for 5 min and incubated for 24 h. Again, no toxicity was nobserved for compound **47** up to 50 μM (Figure 4.15), suggesting that compound **47** is well tolerated by mammalian cells up to 50 μM concentration.

Figure 4.15. Effect of **47** on cell proliferation was determined by the Crystal violet assay. A549 cells were treated with compound **47**, followed by irradiation with 470 nm light for 5 min (24 h incubation). Data provided by Preeti Chauhan, IISER Pune. Adapted with permission from *Org. Lett.* **2017**, *19* (18), 4822-4825. Copyright (2017) American Chemical Society.

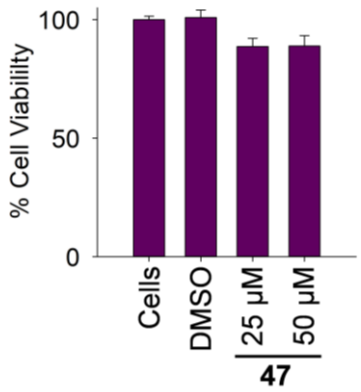

4.2.6.2.3 Cytoprotection from ROS Induced Damage

Hydrogen sulfide is a known antioxidant and has the ability to attenuate the cellular toxicity caused by ROS; this implies it has a role in cytoprotection against ROS induced damage. As it was confirmed through different assays that compound **47** generates H_2S upon irradiation. Here, to test the cytoprotective ability of compound **47** against H_2O_2-induced toxicity, lung carcinoma (A549) cells were pretreated with H_2O_2, and afterwards, with compound **47**; they were subsequently irradiated with 470 nm light for 5 min. These cells were incubated for 24 h at 37 ºC and cell viability was determined by the standard MTT assay. It was found that viability of cells treated with only H_2O_2 was 35%. When H_2O_2-treated cells were incubated with compound **47** and irradiated with light, the viability was found to be 75%. However, no attenuation of cell viability was observed with the negative control compound **50** (Figure 4.16). This study suggested that the released H_2S might play the role of a cytoprotecting agent against H_2O_2-induced damage.

Figure 4.16. Cytoprotective effect of **47** against H_2O_2-induced damage: A549 cells treated with increasing doses of **47**, followed by irradiation with 470 nm light for 5 min (24 h incubation, MTT assay). Data provided by Preeti Chauhan, IISER Pune.

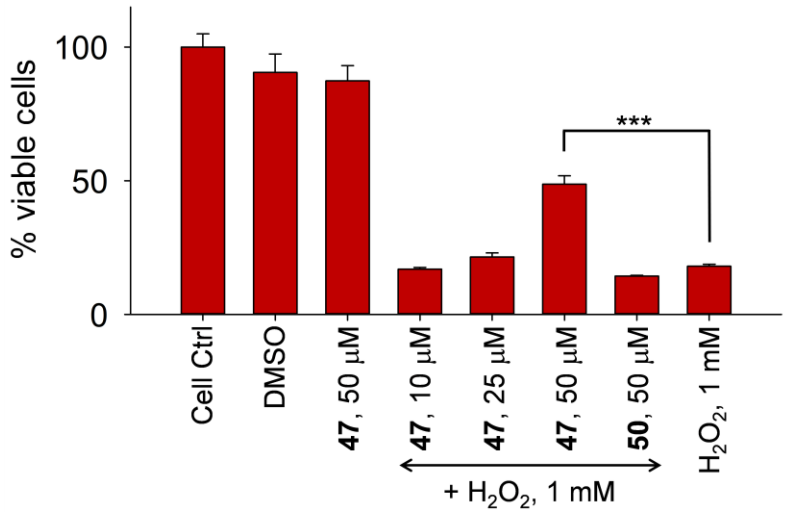

4.3 Conclusion

In Chapter 4, the synthesis of a BODIPY-based visible light activated H_2S donor was discussed, where, **47** was found to be stable in the dark. The molecule cleaves upon irradiation with 470 nm light, as confirmed by way of an HPLC study. This cleavage results in the formation of a

highly fluorescent BODIPY photoproduct **51** and a putative phenolate intermediate **52**. This phenolate intermediate **52** undergoes self-immolation to release COS, which, upon hydrolysis (in the presence of CA), releases H_2S. The released H_2S was detected through a standard MB assay and further, using an amperometric electrode. The compound **47** was also seen to be well tolerated by mammalian cells. This compound was finally evaluated as an antioxidant which protects cells from H_2O_2-induced stress.

For activating compound **47,** 470 nm light is used; it shows a marginal increase in cellular ROS levels and also displays phototoxicity[49] to cells. Here, to address the problem associated with phototoxicity of 470 nm light, a Pyridine-BODIPY-based compound **53** was designed and synthesized (Scheme 4.6). Photolysis of compound **53** was performed using 530 nm light, which may not cause an increase in cellular ROS levels. The cleavage of compound **53** releases a putative phenolate intermediate **52** (Figure 4.17), which further rearranges to produce COS. This COS hydrolyzes due to CA-activity to release H_2S, which was detected in an MB assay (Figure 4.18). A cell viability assay was also carried out and it was found that compound **53** is not toxic in the presence and absence of 530 nm light (Figure 4.19). Compound **53** activates under green light; this radiation does not cause an increasing of ROS levels in the cell, and thus, this strategy may provide us an opportunity to understand H_2S-mediated signaling pathways of cells in a spatio-temporally controlled manner.

Scheme 4.6. Design of Green light activated H_2S donor

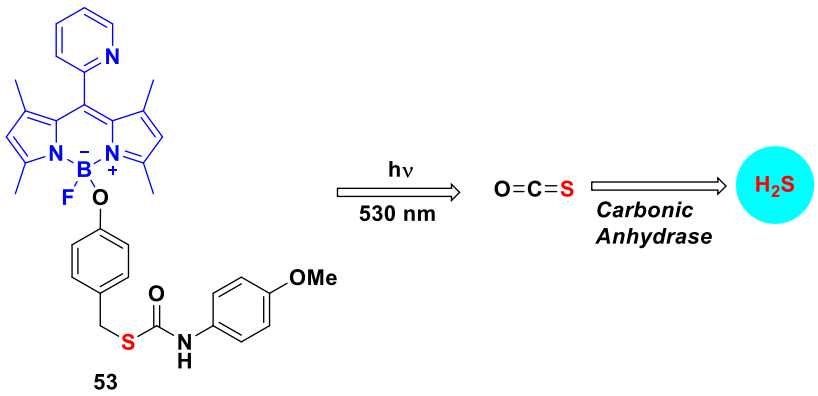

Figure 4.17. HPLC traces of photocleavage study with 50 µM of compound **53.** Data provided by Aswin PK, IISER Pune.

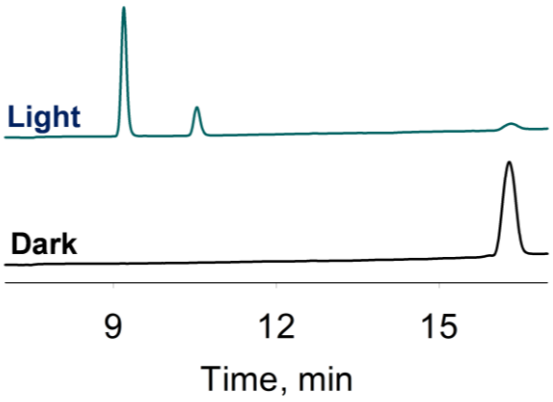

Figure 4.18. H_2S detection for compound **53** *via* the standard methylene blue assay. Data provided by Aswin PK, IISER Pune.

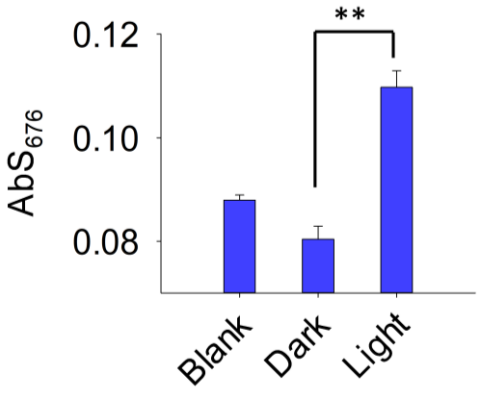

Figure 4.19. Cell viability assay for compound **53** in the absence and presence of green light

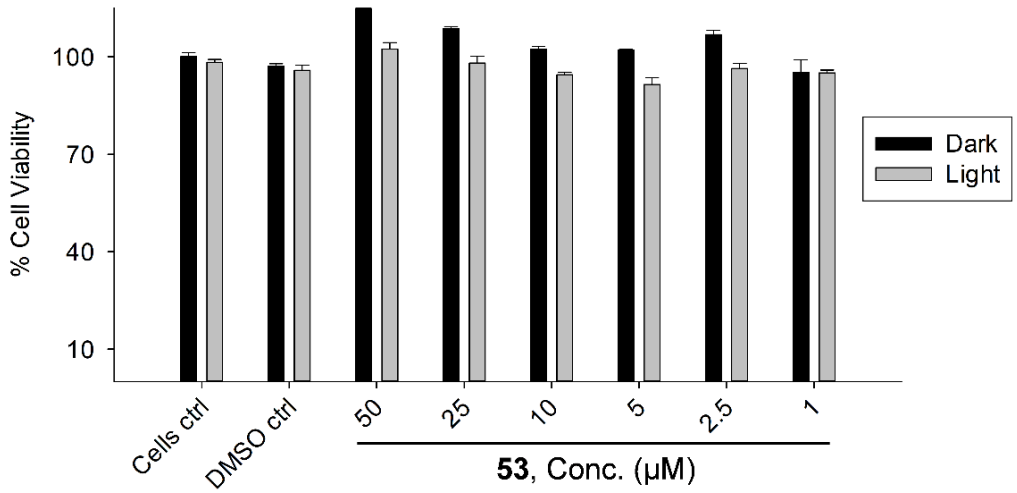

4.4 Experimental Protocols and Characterization Data

4.4.1 Synthesis Protocols

Compounds **41**,[42] **42**,[43] **44**,[44] **46**,[45] **48**[42] and **49**[42] were synthesized using previously reported procedures and analytical data were consistent with reported values.^{1}H NMR spectra of **41** and **49** are attached.

Synthesis of S-(4-((5-fluoro-1,3,7,9-tetramethyl-10-(4-(prop-2-yn-1-yloxy)phenyl)-5H-4λ^4,5λ^4-dipyrrolo[1,2-c:2',1'-f][1,3,2]diazaborinin-5-yl)oxy)benzyl) ethanethioate (43): To

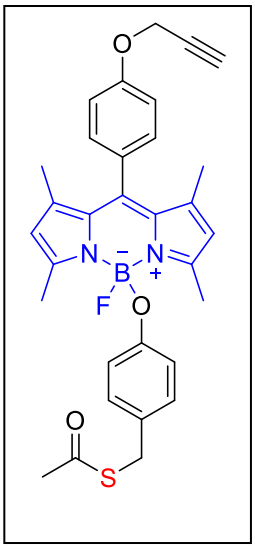

a solution of **41** (986 mg, 2.61 mmol) in anhydrous dichloromethane was added $AlCl_3$ (180 mg, 1.35 mmol) and refluxed for 10 min under N_2 atmosphere. A dichloromethane solution of **42** (528 mg, 2.90 mmol) was added dropwise which was further refluxed for 30 min. The reaction was monitored by TLC and cooled to room temperature which was purified by column chromatography using neutral alumina as the stationary phase and hexane:EtOAc (9:1) as the mobile phase to obtain a crude product. This crude was further purified by preparative HPLC using Kromasil®C-18 column and water: acetonitrile as mobile phase to afford the desired product **43** (350 mg, 25%) as a red-orange solid. FT-IR (ν_{max}, cm^{-1}): 1688, 1468, 1409, 1369; ^{1}H NMR (400 MHz, $CDCl_3$): δ 7.26 – 7.14 (m, 2H), 7.14 – 7.08 (m, 2H), 6.99 (d, *J* = 8.5 Hz, 2H), 6.47 (d, *J* = 8.6 Hz, 2H), 5.92 (s, 2H), 4.78 (d, *J* = 2.3 Hz, 2H), 4.00 (s, 2H), 2.57 (t, *J* = 2.3 Hz, 1H), 2.49 (s, 6H), 2.32 (s, 3H), 1.43 (s, 6H); HRMS (ESI-TOF) for $[C_{31}H_{30}BFN_2O_3S + Na]^+$: calcd., 563.1951, found, 563.1943.

Synthesis of *S*-(4-((5-fluoro-1,3,7,9-tetramethyl-10-(4-(prop-2-yn-1-yloxy)phenyl)-5H-4λ^4,5λ^4-dipyrrolo[1,2-c:2',1'-f][1,3,2]diazaborinin-5-yl)oxy)benzyl) (4-methoxyphenyl)carbamothioate(45)

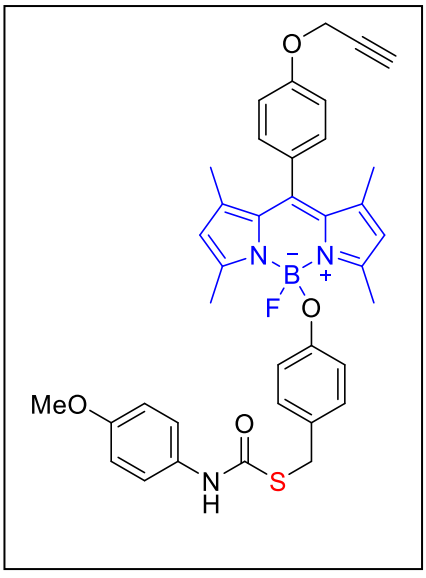

To a solution of compound **43** (73 mg, 0.14 mmol) in anhydrous methanol (10 mL) was added K_2CO_3 (62 mg, 0.45 mmol) and stirred under inert atmosphere for 30 min at room temperature. After completion of the reaction as monitored by TLC, the reaction was quenched by adding water and extracted with EtOAc. Organic layers were combined, dried over anhydrous sodium sulphate which was concentrated under reduced pressure to obtain a thiol intermediate as a red colored residue. To a solution of the

thiol intermediate in anhydrous THF (5 mL), Et_3N (0.06 mL, 0.43 mmol) was added the THF solution of **44** (55 mg, 0.19 mmol) dropwise at 0 ºC. The reaction mixture was stirred under inert atmosphere for 3 h at room temperature. After completion of the reaction as monitored by TLC, the reaction was quenched by adding water and extracted with ethyl acetate. Organic fractions were combined, dried over anhydrous Na_2SO_4 and concentrated under reduced pressure to obtained a red colored crude which was purified by column chromatography using neutral alumina as the stationary phase and hexane:EtOAc (3:1) as the mobile phase followed by purification with preparative HPLC using Kromasil®C-18 column and water: acetonitrile as mobile phase to afford **45** (66 mg, 75% of 2 steps) as a red-orange solid. FT-IR (ν_{max}, cm^{-1}): 3286, 1674, 1468, 1408, 1371; ^1H NMR (400 MHz, $CDCl_3$): δ 7.32 – 7.26 (m, 2H), 7.25 – 7.14 (m, 2H), 7.13 – 7.08 (m, 2H), 7.06 (d, *J* = 8.5 Hz, 2H), 6.92 (s, 1H), 6.87 – 6.80 (m, 2H), 6.55 – 6.41 (m, 2H), 5.91 (s, 2H), 4.77 (d, *J* = 2.4 Hz, 2H), 4.09 (s, 2H), 3.78 (s, 3H), 2.57 (t, *J* = 2.3 Hz, 1H), 2.49 (s, 6H), 1.42 (s, 6H); ^{13}C NMR (125 MHz, $CDCl_3$): δ 158.3, 156.9, 156.0, 143.3, 141.7, 132.2, 130.4, 129.9, 129.5, 129.4, 128.6, 128.2, 121.8, 118.2, 115.9, 115.8, 114.5, 78.2, 76.0, 56.2, 55.6, 34.4, 15.0, 14.8; HRMS (ESI-TOF) for $[C_{37}H_{35}BFN_3O_4S + Na]^+$: calcd., 670.2322, found, 670.2321. (Note: ^{13}C NMR was recorded on a 500 MHz instrument)

Synthesis of *S*-(4-((5-fluoro-10-(4-((1-(2-(2-(2-(2-hydroxyethoxy)ethoxy)ethoxy)ethyl)-1H-1,2,3-triazol-4-yl)methoxy)phenyl)-1,3,7,9-tetramethyl-5H-4λ⁴,5λ⁴-dipyrrolo[1,2-c:2',1'-f][1,3,2]diazaborinin-5-yl)oxy)benzyl) (4-methoxyphenyl)carbamothioate(47): A solution of **45** (51 mg, 0.08 mmol), **46** (26 mg, 0.12 mmol), sodium ascorbate (17 mg, 0.09 mmol), copper sulphate pentahydrate (21 mg, 0.08 mmol) and benzoic acid (17 mg, 0.14 mmol) in dichloromethane (2 mL), methanol (2 mL) and water (1 mL) was stirred for 15 min at room temperature. After completion of the reaction as monitored by TLC, the reaction mixture was purified by neutral alumina column chromatography using pet ether: EtOAc (0:100) and EtOAc: methanol (96:4) as the mobile phase which was further purified by preparative HPLC using Kromasil®C-18 column and water: acetonitrile as mobile phase to afford **1** (14 mg, 21%) as a red solid. FT-IR (ν_{max}, cm^{-1}): 3397, 3358, 3315, 1678, 1464, 1406, 1374; ^1H NMR (400 MHz, $CDCl_3$): δ 7.92 (s, 1H), 7.30 (d, *J* = 8.7 Hz, 2H), 7.24-7.17 (m, 2H), 7.18 – 7.10 (m, 2H), 7.10 – 7.07 (m, 1H), 7.05 (d, *J* = 8.5 Hz,

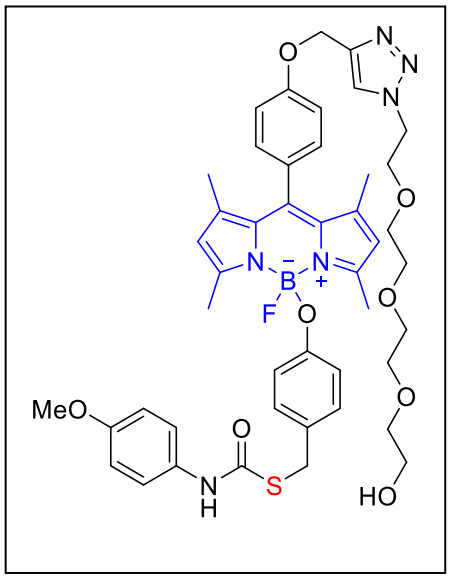

2H), 6.83 (d, *J* = 8.9 Hz, 2H), 6.44 (d, *J* = 8.5 Hz, 2H), 5.91 (s, 2H), 5.25 (s, 2H), 4.59 (t, *J* = 4.9 Hz, 2H), 4.09 (s, 2H), 3.90 (t, *J* = 4.9 Hz, 2H), 3.77 (s, 3H), 3.75 – 3.70 (m, 2H), 3.69-3.65 (m, 2H), 3.65 – 3.56 (m, 8H), 2.73-2.57 (br, 1H), 2.51 (s, 6H), 1.40 (s, 6H); ^{13}C NMR (150 MHz, $CDCl_3$): δ 159.1, 155.9, 155.8, 143.6, 143.3, 141.8, 132.3, 130.0, 129.6, 129.4, 128.7, 127.8, 124.6, 121.7, 118.5, 115.6, 114.4, 72.6, 70.8, 70.7, 70.6, 70.4, 69.6, 62.2, 61.8, 55.7, 50.6, 34.4, 15.1, 14.8; HRMS (ESI-TOF) for $[C_{45}H_{52}BFN_6O_8S + H]^+$: calcd., 867.3722, found, 867.3732. (Note: ^{13}C NMR was recorded on a 600 MHz instrument)

Synthesis of 2-(2-(2-(2-(4-((4-(5-fluoro-5-(4-(hydroxymethyl)phenoxy)-1,3,7,9-tetramethyl-5H-4λ^4,5λ^4-dipyrrolo[1,2-c:2',1'-f][1,3,2]diazaborinin-10-yl)phenoxy)methyl)-1H-1,2,3-triazol-1-yl)ethoxy)ethoxy)ethoxy)ethan-1-ol (50): A

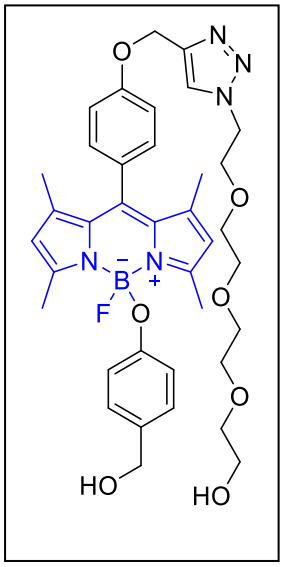

solution of **49** (50 mg, 0.10 mmol), **6** (34 mg, 0.16 mmol), sodium ascorbate (23 mg, 0.12 mmol), copper sulphate pentahydrate (29 mg, 0.12 mmol) and benzoic acid (26 mg, 0.21 mmol) in dichloromethane (2 mL), methanol (2 mL) and water (1 mL) was stirred for 15 min at room temperature. After completion of the reaction as monitored by TLC, the mixture was purified by neutral alumina column using pet ether: EtOAc (0:100) and EtOAc: methanol (92:8) as the mobile phase followed by preparative HPLC using Kromasil®C-18 column and water: acetonitrile as mobile phase to afford **50** (17 mg, 23%) as a red solid. FT-IR (ν_{max}, cm^{-1}): 3437, 1467, 1407, 1367; ^{1}H NMR (400 MHz, $CDCl_3$): δ 7.92 (s, 1H), 7.25 – 7.20 (m, 1H), 7.16 – 7.10 (m, 3H), 7.08 (d, *J* = 8.5 Hz, 2H), 6.58 – 6.50 (m, 2H), 5.91 (s, 2H), 5.25 (s, 2H), 4.58 (t, *J* = 5.0 Hz, 2H), 4.51 (s, 2H), 3.95 – 3.85 (m, 2H), 3.73 – 3.68 (m, 2H), 3.68 – 3.64 (m, 2H), 3.63 – 3.57 (m, 8H), 2.50 (s, 6H), 1.42 (s, 6H); ^{13}C NMR (100 MHz, $CDCl_3$): δ 159.1, 156.3, 156.2, 155.9, 143.4, 143.3, 141.7, 132.2, 132.0, 129.5, 129.4, 128.7, 127.7, 124.5, 121.7, 118.1, 115.7, 115.5, 77.4, 72.6, 70.7, 70.5, 70.4, 69.6, 65.4, 62.2, 61.8, 50.5, 15.0, 14.8; HRMS (ESI-TOF) for $[C_{37}H_{45}BFN_5O_7 + Na]^+$: calcd., 724.3293; found: 724.3287.

4.4.2 Procedure for Irradiation

A quartz cuvette containing **47** in methanol was irradiated at 470 nm (30 mW/cm^2) by blue LED at room temperature in a closed chamber. This solution was used for further analysis as described below.

4.4.3 Photo-Cleavage Study by HPLC

Compound **47** (50 μM, 500 μL) in MeOH was irradiated for 5, 10, 15 and 20 min and HPLC analysis of the aliquot was conducted. A diode array detector (DAD) operating at 250 nm and 500 nm and a fluorescence detector (FLD; λ_{ex} = 470 nm and λ_{em} = 540 nm) were used. A mobile phase of water: acetonitrile was used with a run time of 25 min. A multistep gradient was used with a flow rate of 1 mL/min starting with 70: 30 →0 min, 70:30 to 20: 80 → 0 - 20 min, 20:80 to 50: 50 → 20 - 22 min, 50:50 to 70: 30 →22 – 24 min. Retention time for **47** is 20.5 min, for **51** is 13.2 min and for intermediate (I) is 13.6 min (Figure S1)

4.4.4 Detection of 51 by Mass Spectrometry

Compound **47** (50 μM, 500 μL) was irradiated for 20 min and aliquot of the irradiated sample was analyzed by a UPLC (Waters Co.) equipped with a Phenomenex®C-18 reversed phase column (250 mm × 4.6 mm, 5 μm), which is coupled with an ESI-MS.

4.4.5 *In Vitro* Fluorescence Enhancement Assay

Solution of compound **47** (200 μM, 500 μL) in methanol was irradiated using LED for 25 min. Non – irradiated sample of same concentration was used as a control and was incubated in dark for 25 min. After incubation, the samples (250 μL) were transferred to a 1.5 mL vial containing 750 μL phosphate buffer (pH 7.4). Further aliquots (200 μL) of these solutions were transferred to the 96 well-plate in triplicates and the fluorescence was measured using microtiter plate reader (λ_{ex} = 470 nm and λ_{em} = 540 nm).

4.4.6 H_2S Detection by Methylene Blue Assay

100 μL of irradiated samples of were added to 1.5 mL vials containing 292 μL of phosphate buffer (pH 7.4), 4μL of carbonic anhydrase (1% stock in HEPES buffer) and 4 μL of $Zn(OAc)_2$ (40 mM stock in H_2O). The reaction mixtures were incubated at 37 ^oC for predetermined time points. To this, 400 μL of $FeCl_3$ (30 mM stock in 1.2 M HCl) and 400 μL of N,N–dimethyl-*p*-pheneylenediamine sulfate (20 mM stock in 7.2 M HCl) was added. The reaction mixtures were incubated at 37 ^oC for 30 min to allow the formation of methylene blue complex. After completion of the reaction, aliquots were transferred to a 96 well plate (250 μL/well) and the absorbance spectra were collected from 550 to 800 nm using microplate reader (Thermo Scientific Varioskan) and the absorbance values were measured at 676 nm.

4.4.7 H_2S Detection Using Electrode

The manufacturer's protocol was followed to make antioxidant buffer. The calibration of the electrode (Lazar Research Laboratories, Inc.) was done using a freshly prepared $Na_2S.9H_2O$

solution in antioxidant buffer. Compound **47** (200 μM, 600 μL) was irradiated and in another vial similar solution was prepared and kept in the dark for 25 min. The irradiated and non-irradiated samples (250 μL) were transferred to 1.5 mL vial containing 725 μL phosphate buffer (pH 7.4) along with carbonic anhydrase (25 μL) and a small magnetic bead. The electrode was then inserted into the vial and the solution was incubated at 37 ºC to measure the H_2S.

4.4.8 Cell Culture Protocol

HeLa cells were grown overnight at 37°C with 5% CO_2 in the modified Dulbecco's medium DMEM & 10% fetal bovine serum from Sigma Aldrich (St. Louis, USA). For trypsinization 0.05% trypsin-EDTA from ThermoFisher Scientific was used.

4.4.9 Fluorescence Enhancement Assay in Cellular System

HeLa cells ($0.1x10^6$) were seeded in 6 well plate (NEST, China) and incubated overnight at 37 ºC with 5% CO_2. Cells were washed with 1X PBS and incubated with only DMEM. Compound **47 (**10 μM in DMSO) was then added followed by incubation for 30 minutes at 37 ºC with 5% CO_2 in dark. Cells were washed with 1X PBS three times and irradiated with 470 nm light for 2 minutes. Images were acquired using an inverted epifluorescence microscope (Olympus IX83, Japan) with 20× objective in YFP channel (excitation, 514 nm and emission, 527nm). All devices were controlled using Slidebook 6 software (3i Inc., USA). Total image & background intensity was calculated using ImageJ (NIH, US). Background intensity was subtracted from total image intensity and resulting total fluorescence intensity was plotted as fold change.

4.4.10 Cell Viability Assay Using MTT Dye

Human cervical cancer, HeLa cells, were seeded at a concentration of 1×10^4 cells/well overnight in a 96-well plate in complete DMEM media. Cells were exposed to varying concentrations of the compound **47** prepared as a DMSO stock solution so that the final concentration of DMSO was 0.5%. Cells were first exposed to light for 5 min and then incubated for 24 h at 37 ºC. A solution of 3-(4, 5-dimethylthiazol-2-yl)-2, 5-diphenyl tetrazolium bromide (MTT) was prepared by dissolving MTT reagent (3.5 mg) in 7 mL DMEM media. 100 μL of this solution was added to each well. After 4 h incubation, the media was removed carefully and 100 μL of DMSO was added. Spectrophotometric analysis of each well was carried out at 570 nm using a microplate reader (Thermo Scientific Varioskan) to estimate cell viability.

4.4.11 Cell Viability Assay Using Crystal Violet Dye

Human adenocarcinomic alveolar basal epithelial cells, A549 cells, were plated in a poly-D-lysine coated 12 well plate in complete DMEM media. Confluent cells were treated with varying concentrations of **47** and incubated at 37 ºC for 30 min. Cells were then exposed to light for 5 min and further incubated for 24 h at 37 ºC. Cells were washed thoroughly with 1xPBS (3 times). 500 µL of crystal violet solution (0.1% in 4% formalin) was added to each well and kept for 20 min on the bench rocker. Cells were washed in a gentle stream of tap water to remove excess reagent. After washing, the plate was inverted on a filter paper to remove remaining water and was kept for drying at room temperature overnight. 500 µL of 10% acetic acid was added to each well and kept on the bench rocker for 20 min. The solution was diluted 10 times and 200 µL of the diluted solution was transferred to a 96 well plate. The absorbance was measured at 590 nm using a microplate reader (Thermo Scientific Varioscan) to estimate cell viability.

4.5 Spectral Charts

^{1}H NMR of **41** ($CDCl_3$, 400 MHz)

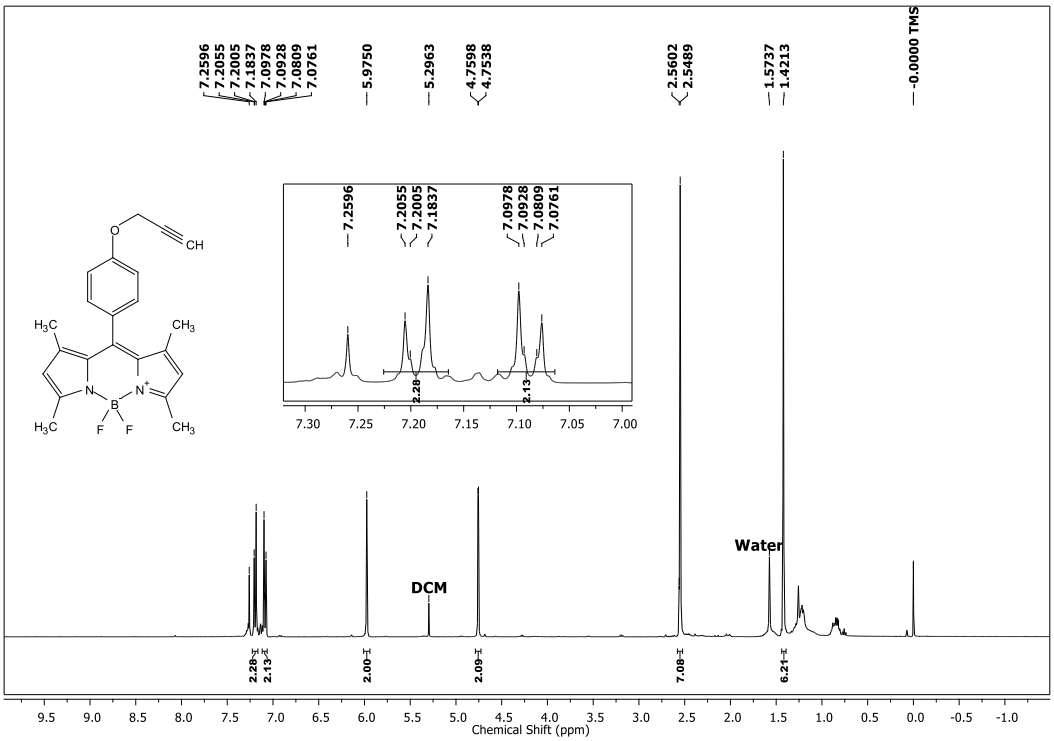

^{1}H NMR of 43 ($CDCl_3$, 400 MHz)

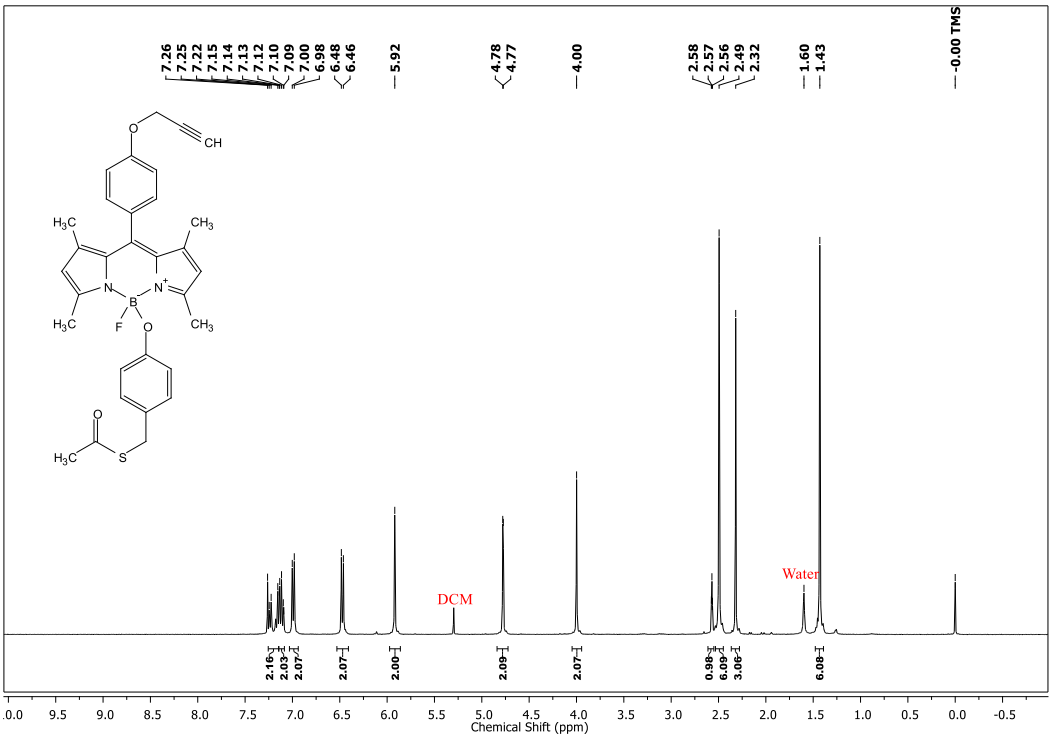

^{1}H NMR of **45** ($CDCl_3$, 400 MHz)

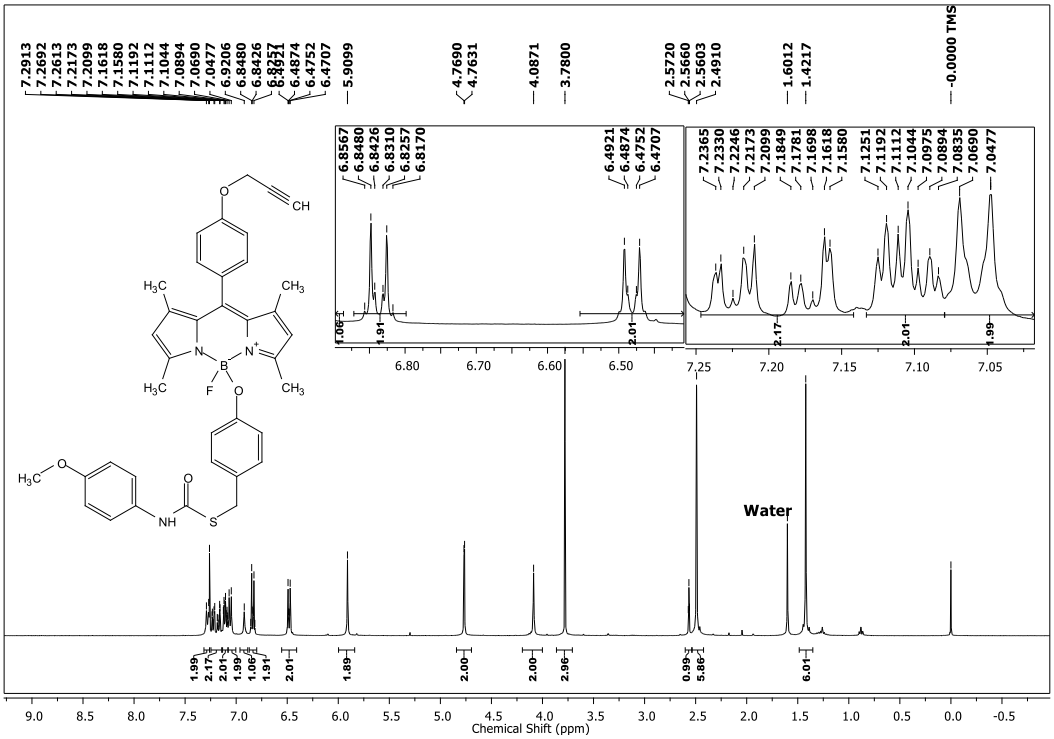

^{13}C NMR of **45** ($CDCl_3$, 125 MHz)

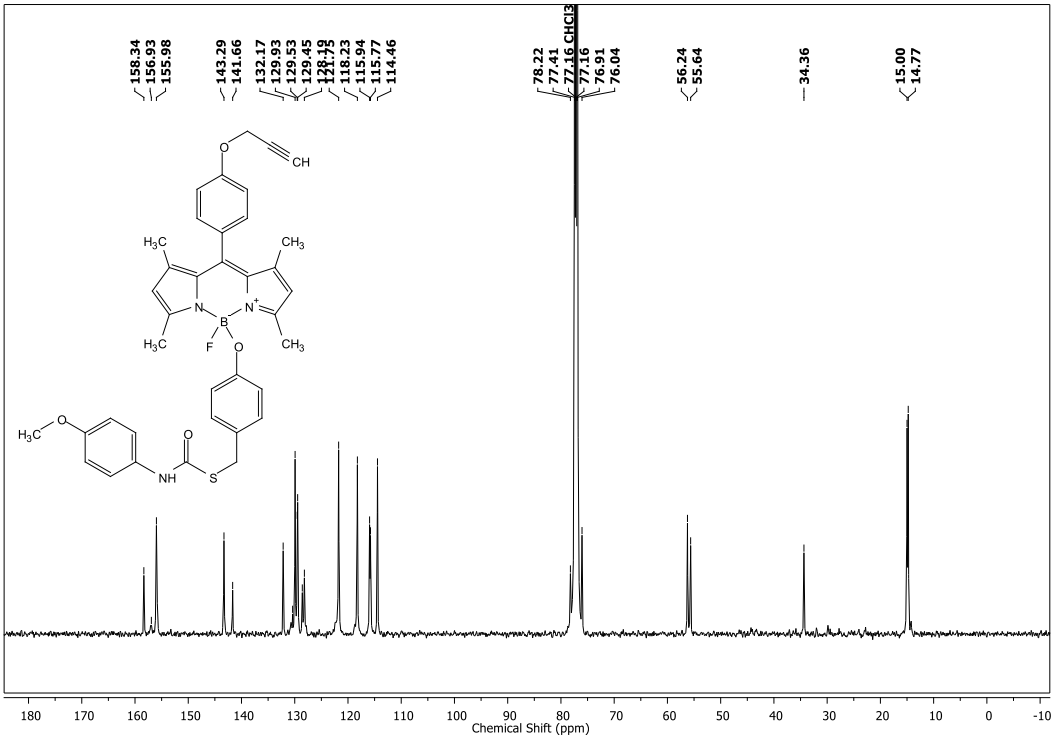

^{1}H NMR of **47** ($CDCl_3$, 400 MHz)

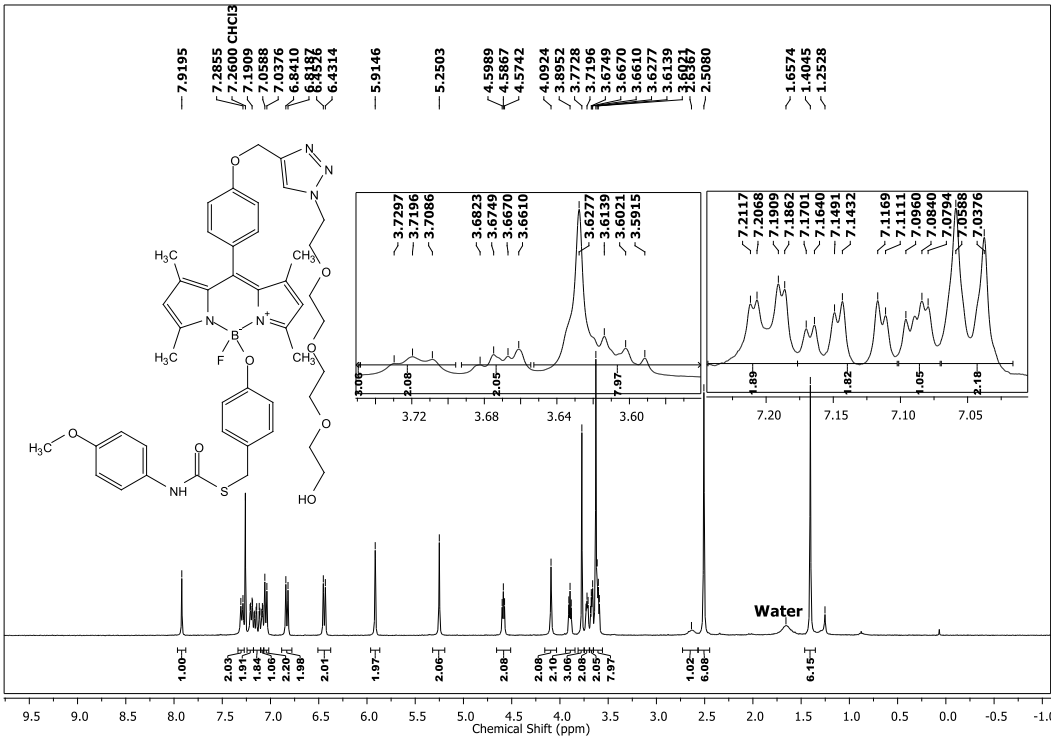

^{13}C NMR of **47** ($CDCl_3$, 150 MHz)

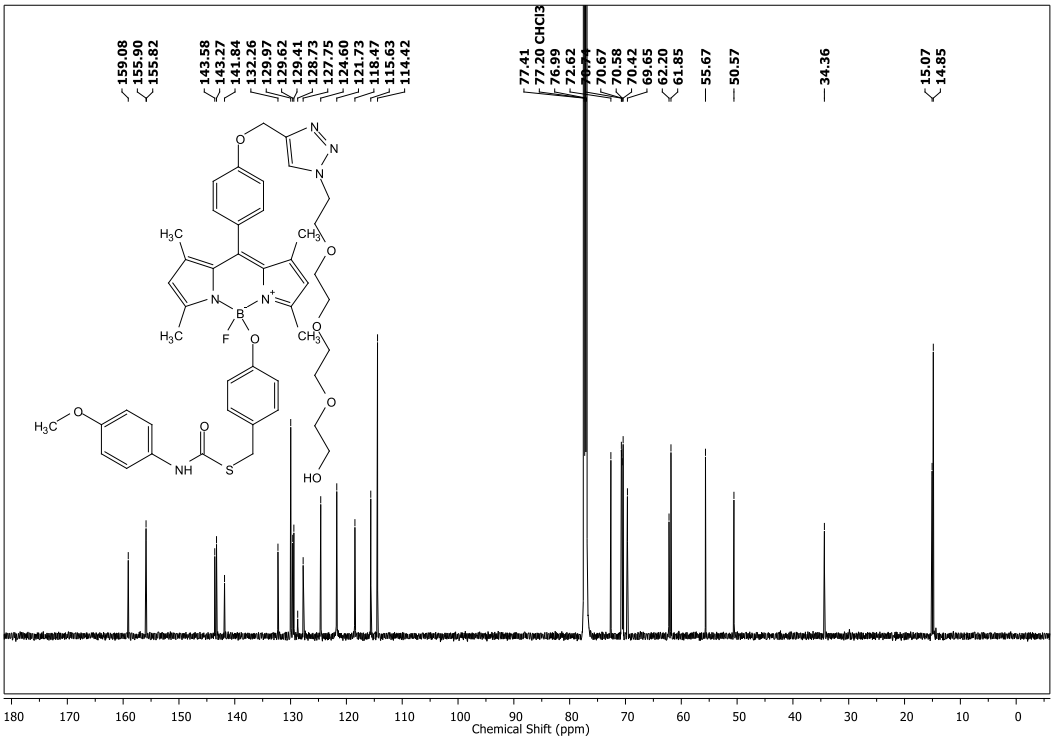

^{1}H NMR of **49** ($CDCl_3$, 400 MHz)

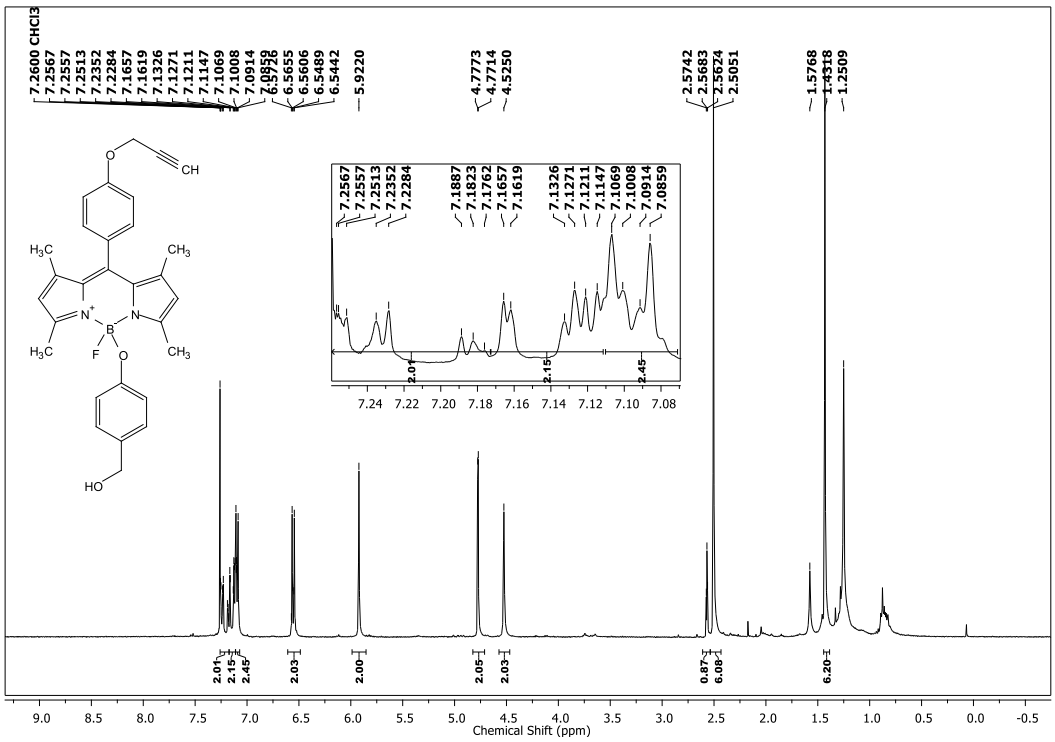

^{1}H NMR of **50** ($CDCl_3$, 400 MHz)

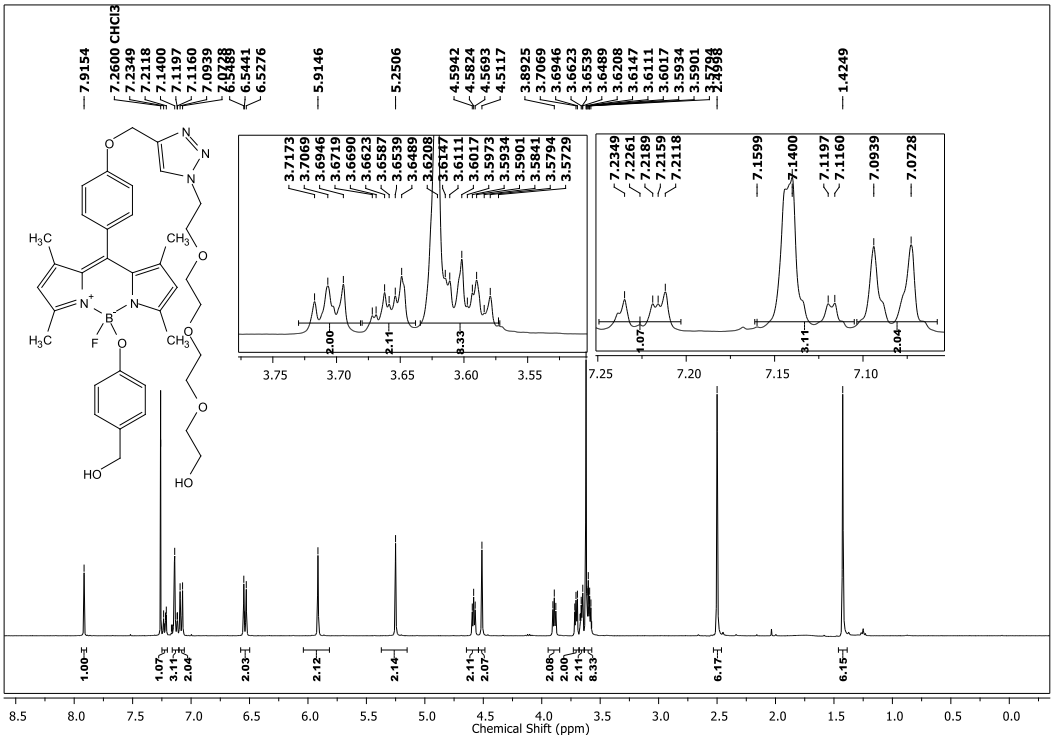

^{13}C NMR of **50** ($CDCl_3$, 400 MHz)

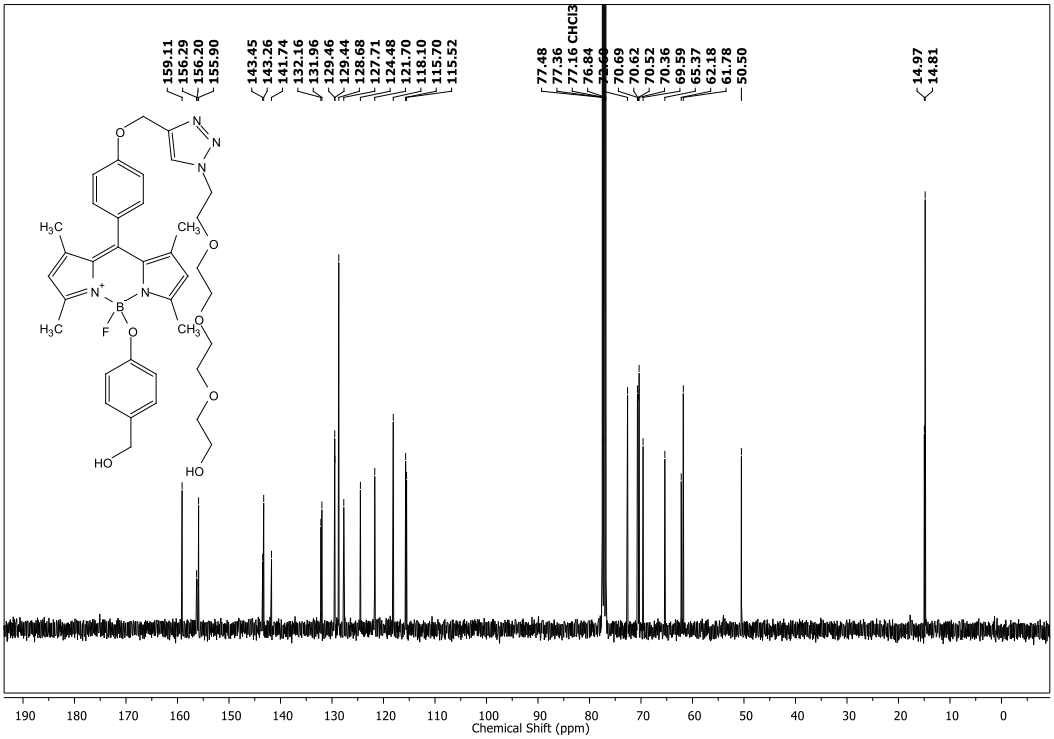

4.6 References

(1) Marino, S. M.; Gladyshev, V. N. A Structure-Based Approach for Detection of Thiol Oxidoreductases and Their Catalytic Redox-Active Cysteine Residues. *PLoS Comput. Biol.* **2009**, *5* (5), e1000383.

(2) Poole, L. B. The Basics of Thiols and Cysteines in Redox Biology and Chemistry. *Free Radic. Biol. Med.* **2015**, *80*, 148–157.

(3) Paulsen, C. E.; Carroll, K. S. Cysteine-Mediated Redox Signaling: Chemistry, Biology, and Tools for Discovery. *Chem. Rev.* **2013**, *113* (7), 4633–4679.

(4) Dickinson, D. A.; Forman, H. J. Glutathione in Defense and Signaling: Lessons from a Small Thiol. *Ann. N. Y. Acad. Sci.* **2002**, *973*, 488–504.

(5) Lu, J.; Holmgren, A. The Thioredoxin Antioxidant System. *Free Radic. Biol. Med.* **2014**, *66*, 75–87.

(6) Holmgren, A. Antioxidant Function of Thioredoxin and Glutaredoxin Systems. *Antioxid. Redox Signal.* **2000**, *2* (4), 811–820.

(7) Roh, J.-L.; Jang, H.; Kim, E. H.; Shin, D. Targeting of the Glutathione, Thioredoxin, and Nrf2 Antioxidant Systems in Head and Neck Cancer. *Antioxid. Redox Signal.* **2017**, *27* (2), 106–114.

(8) Collet, J.-F.; Messens, J. Structure, Function, and Mechanism of Thioredoxin Proteins. *Antioxid. Redox Signal.* **2010**, *13* (8), 1205–1216.

(9) Shimizu, T.; Huang, D.; Yan, F.; Stranava, M.; Bartosova, M.; Fojtíková, V.; Martínková, M. Gaseous O_2, NO, and CO in Signal Transduction: Structure and Function Relationships of Heme-Based Gas Sensors and Heme-Redox Sensors. *Chem. Rev.* **2015**, *115* (13), 6491–6533.

(10) Dennery, P. A. Signaling Function of Heme Oxygenase Proteins. *Antioxid. Redox Signal.* **2014**, *20* (11), 1743–1753.

(11) Kobayashi, A.; Ishikawa, K.; Matsumoto, H.; Kimura, S.; Kamiyama, Y.; Maruyama, Y. Synergetic Antioxidant and Vasodilatory Action of Carbon Monoxide in Angiotensin II–Induced Cardiac Hypertrophy. *Hypertension* **2007**, *50* (6), 1040–1048.

(12) Rahman, F. U.; Park, D.-R.; Joe, Y.; Jang, K. Y.; Chung, H. T.; Kim, U.-H. Critical

Roles of Carbon Monoxide and Nitric Oxide in Ca $^{2+}$ Signaling for Insulin Secretion in Pancreatic Islets. *Antioxid. Redox Signal.* **2019**, *30* (4), 560–576.

(13) Piantadosi, C. A. Biological Chemistry of Carbon Monoxide. *Antioxid. Redox Signal.* **2002**, *4* (2), 259–270.

(14) Wang, M.; Liao, W. Carbon Monoxide as a Signaling Molecule in Plants. *Front. Plant Sci.* **2016**, *7*, 572.

(15) Ryter, S. W.; Otterbein, L. E. Carbon Monoxide in Biology and Medicine. *BioEssays* **2004**, *26* (3), 270–280.

(16) Tomasian, D.; Keaney, J. F.; Vita, J. A. Antioxidants and the Bioactivity of Endothelium-Derived Nitric Oxide. *Cardiovasc. Res.* **2000**, *47* (3), 426–435.

(17) Wink, D. A.; Miranda, K. M.; Espey, M. G.; Pluta, R. M.; Hewett, S. J.; Colton, C.; Vitek, M.; Feelisch, M.; Grisham, M. B. Mechanisms of the Antioxidant Effects of Nitric Oxide. *Antioxid. Redox Signal.* **2001**, *3* (2), 203–213.

(18) Hummel, S. G.; Fischer, A. J.; Martin, S. M.; Schafer, F. Q.; Buettner, G. R. Nitric Oxide as a Cellular Antioxidant: A Little Goes a Long Way. *Free Radic. Biol. Med.* **2006**, *40* (3), 501–506.

(19) Kojšová, S.; Jendeková, L.; Zicha, J.; Kuneš, J.; Andriantsitohaina, R.; Pecháňová, O. The Effect of Different Antioxidants on Nitric Oxide Production in Hypertensive Rats. *Physiol. Res* **2006**, *55*, 3–16.

(20) Lane, P.; Gross, S. S. Cell Signaling by Nitric Oxide. *Semin. Nephrol.* **1999**, *19* (3), 215–229.

(21) Ignarro, L. J.; Cirino, G.; Casini, A.; Napoli, C. Nitric Oxide as a Signaling Molecule in the Vascular System: An Overview. *J. Cardiovasc. Pharmacol.* **1999**, *34* (6), 879–886.

(22) Groß, F.; Durner, J.; Gaupels, F. Nitric Oxide, Antioxidants and Prooxidants in Plant Defence Responses. *Front. Plant Sci.* **2013**, *4*, 419.

(23) Ishigami, M.; Hiraki, K.; Umemura, K.; Ogasawara, Y.; Ishii, K.; Kimura, H. A Source of Hydrogen Sulfide and a Mechanism of Its Release in the Brain. *Antioxid. Redox Signal.* **2009**, *11* (2), 205–214.

(24) Szabó, C. Hydrogen Sulphide and Its Therapeutic Potential. *Nat. Rev. Drug Discov.*

2007, *6* (11), 917–935.

(25) Bannenberg, G. L.; Vieira, H. LA. Therapeutic Applications of the Gaseous Mediators Carbon Monoxide and Hydrogen Sulfide. *Expert Opin. Ther. Pat.* **2009**, *19* (5), 663–682.

(26) Qu, K.; Lee, S. W.; Bian, J. S.; Low, C.-M.; Wong, P. T.-H. Hydrogen Sulfide: Neurochemistry and Neurobiology. *Neurochem. Int.* **2008**, *52* (1–2), 155–165.

(27) Geng, B.; Yang, J.; Qi, Y.; Zhao, J.; Pang, Y.; Du, J.; Tang, C. H2S Generated by Heart in Rat and Its Effects on Cardiac Function. *Biochem. Biophys. Res. Commun.* **2004**, *313* (2), 362–368.

(28) Whiteman, M.; Armstrong, J. S.; Chu, S. H.; Jia-Ling, S.; Wong, B.-S.; Cheung, N. S.; Halliwell, B.; Moore, P. K. The Novel Neuromodulator Hydrogen Sulfide: An Endogenous Peroxynitrite "Scavenger"? *J. Neurochem.* **2004**, *90* (3), 765–768.

(29) Chang, L.; Geng, B.; Yu, F.; Zhao, J.; Jiang, H.; Du, J.; Tang, C. Hydrogen Sulfide Inhibits Myocardial Injury Induced by Homocysteine in Rats. *Amino Acids* **2008**, *34* (4), 573–585.

(30) Li, L.; Rose, P.; Moore, P. K. Hydrogen Sulfide and Cell Signaling. *Annu. Rev. Pharmacol. Toxicol.* **2011**, *51* (1), 169–187.

(31) Kolluru, G. K.; Shen, X.; Bir, S. C.; Kevil, C. G. Hydrogen Sulfide Chemical Biology: Pathophysiological Roles and Detection. *Nitric Oxide* **2013**, *35*, 5–20.

(32) Panthi, S.; Chung, H.-J.; Jung, J.; Jeong, N. Y. Physiological Importance of Hydrogen Sulfide: Emerging Potent Neuroprotector and Neuromodulator. *Oxid. Med. Cell. Longev.* **2016**, *2016*, 1–11.

(33) Li, L.; Rose, P.; Moore, P. K. Hydrogen Sulfide and Cell Signaling. *Annu. Rev. Pharmacol. Toxicol.* **2011**, *51* (1), 169–187.

(34) Chauhan, P.; Bora, P.; Ravikumar, G.; Jos, S.; Chakrapani, H. Esterase Activated Carbonyl Sulfide/Hydrogen Sulfide (H2S) Donors. *Org. Lett.* **2017**, *19* (1), 62–65.

(35) Umeda, N.; Takahashi, H.; Kamiya, M.; Ueno, T.; Komatsu, T.; Terai, T.; Hanaoka, K.; Nagano, T.; Urano, Y. Boron Dipyrromethene As a Fluorescent Caging Group for Single-Photon Uncaging with Long-Wavelength Visible Light. *ACS Chem. Biol.* **2014**,

9 (10), 2242–2246.

(36) Zhao, Y.; Bolton, S. G.; Pluth, M. D. Light-Activated COS/H2S Donation from Photocaged Thiocarbamates. *Org. Lett.* **2017**, *19* (9), 2278–2281.

(37) Zhao, Y.; Pluth, M. D. Hydrogen Sulfide Donors Activated by Reactive Oxygen Species. *Angew. Chem. Int. Ed.* **2016**, *55* (47), 14638–14642.

(38) Steiger, A. K.; Pardue, S.; Kevil, C. G.; Pluth, M. D. Self-Immolative Thiocarbamates Provide Access to Triggered H2S Donors and Analyte Replacement Fluorescent Probes. *J. Am. Chem. Soc.* **2016**, *138* (23), 7256–7259.

(39) Steiger, A. K.; Yang, Y.; Royzen, M.; Pluth, M. D. Bio-Orthogonal "Click-and-Release" Donation of Caged Carbonyl Sulfide (COS) and Hydrogen Sulfide (H 2 S). *Chem. Commun.* **2017**, *53* (8), 1378–1380.

(40) Steiger, A. K.; Zhao, Y.; Pluth, M. D. Emerging Roles of Carbonyl Sulfide in Chemical Biology: Sulfide Transporter or Gasotransmitter? *Antioxid. Redox Signal.* **2017**.

(41) Sharma, A. K.; Nair, M.; Chauhan, P.; Gupta, K.; Saini, D. K.; Chakrapani, H. Visible-Light-Triggered Uncaging of Carbonyl Sulfide for Hydrogen Sulfide (H2S) Release. *Org. Lett.* **2017**, *19* (18), 4822–4825.

(42) Patil, N. G.; Basutkar, N. B.; Ambade, A. V. Visible Light-Triggered Disruption of Micelles of an Amphiphilic Block Copolymer with BODIPY at the Junction. *Chem. Commun.* **2015**, *51* (100), 17708–17711.

(43) Bugaut, A.; Jantos, K.; Wietor, J.-L.; Rodriguez, R.; Sanders, J. K. M.; Balasubramanian, S. Exploring the Differential Recognition of DNA G-Quadruplex Targets by Small Molecules Using Dynamic Combinatorial Chemistry. *Angew. Chemie Int. Ed.* **2008**, *47* (14), 2677–2680.

(44) Sankar, R. K.; Kumbhare, R. S.; Dharmaraja, A. T.; Chakrapani, H. A Phenacrylate Scaffold for Tunable Thiol Activation and Release. *Chem. Commun.* **2014**, *50* (97), 15323–15326.

(45) DeForest, C. A.; Tirrell, D. A. A Photoreversible Protein-Patterning Approach for Guiding Stem Cell Fate in Three-Dimensional Gels. *Nat. Mater.* **2015**, *14* (5), 523–531.

(46) Moest, R. R. Hydrogen Sulfide Determination by the Methylene Blue Method. *Anal.*

Chem. **1975**, *47* (7), 1204–1205.

(47) P. Jeroschewski, C. Steuckart, A.; Kühl, M. An Amperometric Microsensor for the Determination of H2S in Aquatic Environments. *Anal. Chem.* **1996**, *68* (24), 4351–4357.

(48) Steiger, A. K.; Pardue, S.; Kevil, C. G.; Pluth, M. D. Self-Immolative Thiocarbamates Provide Access to Triggered H_2S Donors and Analyte Replacement Fluorescent Probes. *J. Am. Chem. Soc.* **2016**, *138* (23), 7256–7259.

(49) Nakashima, Y.; Ohta, S.; Wolf, A. M. Blue Light-Induced Oxidative Stress in Live Skin. *Free Radic. Biol. Med.* **2017**, *108*, 300–310.

Synopsis

Synthesis and Evaluation of Light Triggerable Redox-Active Species Generators

Chapter 1. Introduction

In living organism, several molecules undergo oxidation-reduction reaction to facilitate cellular processes. These molecules play crucial role in the different metabolic pathways of cells, which are mediated by several enzymatic and non-enzymatic mechanisms. These mechanisms exploit the use of either an intracellular redox sensitive metal[1,2] or a redox active organic molecule.[3,4]. Apart from these, there are certain short-lived species formed during normal metabolism which are also known to participate in redox processes of cells. These species are termed as redox-active species and majorly were classified in three categories based on the reactive atom (Figure 1).

1. Reactive oxygen species (ROS)
2. Reactive sulfur species (RSS)
3. Reactive nitrogen species (RNS)

Figure 1. Classification of different redox active species

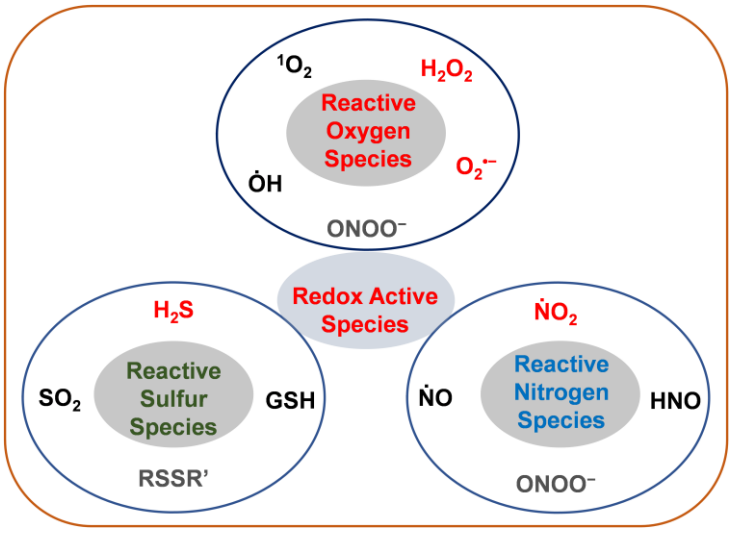

All these redox species are synthesized endogenously and help in maintaining the integrity of cell by regulating the several signaling pathways. The physiology of these species is dependent on the concentration and location of generation. At the homeostatic level, where concentration of antioxidant and oxidants are balanced, these species mediate several pathways

such as cell signaling, immune response, inflammatory response, cellular adhesion, differentiation, proliferation, metabolism, autophagy, senescence, vascular diameter regulation apoptosis, cell cycle, protein misfolding and endoplasmic reticulum-associated degradation of proteins (Figure 2), which are beneficial to the cell.[5–8] However, at the elevated levels, these species can irreversibly oxidize essential biomolecules like proteins, lipids and nucleic acids which result into dysfunction of cellular machinery, leading to cell death.[7,8] The elevated levels of these species are also associated with several pathophysiological conditions[9–13] such as cancer, Alzheimer's disease, Parkinson's disease, aging, diabetes, inflammation *etc*. To counter the over production of reactive species, the cell evolved a powerful machinery which regulates the generation of these species and maintain the integrity of cells to carry out the normal functions.

Figure 2. Physiological role of redox active species

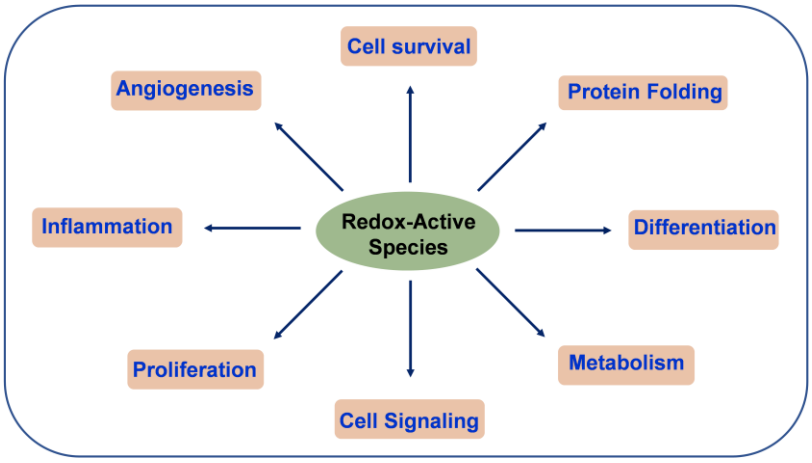

It may be stated that all species that are highly reactive may indiscriminately interact with several biomolecules and this may lead to the activation of non-specific cellular processes. For instance, NO interacts with $O_2^{\bullet-}$ to form $ONOO^-$ which differs from NO and $O_2^{\bullet-}$ alone. Likewise, H_2S also interacts with ROS to form polysulfides or sulfite. Further, RNS interact with thiols to form *S*-nitrosothiols.[14–21] In order to reduce the cross talk and off-site reactivity of the generated reactive species, one needs to develop molecules which can be activated under highly specific conditions to produce the desired species without any complications to cellular metabolic pathways. There are several tools reported to generate different reactive species in cellular system. Some of these tools can generate these species in spontaneous manner, without any control; however, some tools are activated with metabolic stimuli such as thiols, bioreduction, esterase, nitroreductase enzyme (NTR). Thiol and bioreductive mediated

approaches do not provide the selectivity over generation because of their ubiquitous nature and also slow metabolism of NTR limits the use of NTR mediated approach. Here, to overcome the problem of non-specific delivery, light may be used as a stimulus, since the localization and intensity of light can be controlled externally thus providing spatio-temporal control over the delivery of reactive species. This photo-triggered approach may minimize any off-site generation of reactive species and may, further, be utilized for gaining valuable insights into understanding redox-mediated signaling pathways.

Our aim is to design, synthesize and evaluate molecules which can produce reactive species in a localized manner. This can be achieved by using light as an external stimulus, where a spatio-temporal control over the generation of reactive species is possible. Here, in this thesis, we present light triggered strategies to release ROS and H_2S.

In **Chapter 1**, background about the generation, regulation and physiological roles of the redox active species is discussed. In **Chapter 2**, an ROS generator coupled with 2-nitrobenzyl as a photo-responsive moiety is proposed, which may release the ROS generator upon UV light irradiation. Such a UV light activatable ROS generator can also be examined for being a potential candidate for a cancer-targeted approach, since ROS can inhibit the growth of cancer cells. As it is known that UV light-based methods have several drawbacks, rendering them unsuitable in studying ROS-mediated biological processes. To overcome these problems, in **Chapter 3**, a visible light triggered release of an ROS generator is developed, while making use of a BODIPY-based photo-responsive group. Finally, in **Chapter 4**, the BODIPY-based photo-cleavable linker is further utilized to release H_2S upon visible light activation.

The different types of reactive species present in a cell are known to cross-talk with each other. Furthermore, these species can interact with different sites in cells and hence complicate the interpretation of results. Hence, the development of light activatable tools may find an application in delivering these highly reactive species to a particular site in a localized manner, followed by the study of the effect(s) of these species. The proposed tools might be activated under mild conditions, which may not be responsible for any non-specific results.

Chapter 2. UV Light Triggerable ROS Generators

ROS are reduced forms of oxygen and play vital roles in biology. To study the ROS mediated effects, here, the concept of increasing ROS in cells by generating superoxide ($O_2^{\bullet-}$) is explored. $O_2^{\bullet-}$ can form hydrogen peroxide (H_2O_2) followed by hydroxyl radical (ȮH) which may lead to cell death. These species can be generated by several methods using different metabolic stimuli of cells e.g. bioreduction,[22] thiol activation,[23] esterase enzymatic activation,[24] *etc*. These are very good approaches to generate ROS; however, few limitations such as ubiquitous nature or slow metabolism of trigger(s), hinder their use in studying signaling pathways. To overcome such limitations, alternatively, light can be employed as a stimulus where spatio-temporal generation of ROS is possible. The light triggered approach has gained a lot of interest in drug delivery systems where spatiotemporally controlled delivery can be achieved by a photoactivatable prodrug concept.[25–31] For instance, photodynamic therapy (PDT),[32–34] a photosensitizer that produces singlet oxygen upon irradiation is used thereby leading to an increase in the ROS levels which damages essential biomolecules in cellular system and thereupon resulting in cell death. The levels of ROS can be increased by generation of either $^1O_2$ or $O_2^{\bullet-}$. However, the $^1O_2$ generation may not be relevant to study ROS mediated pathways because endogenous production of $^1O_2$ is low and hence is not known to contribute much to ROS physiology.[32] Whereas $O_2^{\bullet-}$, is the major contributing pathway in the ROS physiology. Hence, the generation of $O_2^{\bullet-}$ is desired. The efforts of releasing $O_2^{\bullet-}$ using light as a trigger, has been made by Chang and co-workers[35]. They used the 2-nitrobenzyl group as a photoactivable moiety and 1,2,4-trihydroxybenzene as ROS generator. But certain limitations such as cytotoxicity induced by 304 nm UV light, less efficient ROS generation and thiol reactivity with quinone byproduct are associated with this approach. These shortcomings hinder the use of the above approach to study ROS-mediated signaling pathways.

Therefore, a molecule needs to be designed which may release ROS generator upon irradiation and should have following properties:

1. Stable in buffer
2. Efficient in generating ROS
3. ROS donor or its end product should not react with thiols

In most of the ROS generators, either a 1,4- or 1,2-quinone functionality is present which bioreductively converted to its hydroquinone counterpart.[36–39] These electron rich

hydroquinones react with molecular oxygen and revert back to quinones, concomitantly generating ROS. These quinones, for example, juglone and menadione have an α,β-unsaturated site where thiols can react in a 1,4-Michael fashion to form thiol adducts.[40] These thiol adducts can either be effluxed out of the cells as a detoxification mechanism[40] or can further generate ROS. Furthermore, important cysteine residues can be covalently modified by quinones and crucial pathways can eventually be affected *in situ*.[40] In such scenario, the observed phenotype may not be due to ROS generation alone. Therefore, to overcome the problems due to off-site reactivity of ROS generators, a suitable molecule is chosen such that it would not react with cellular thiols thereby obtained results may only be due to the ROS generation.

Thiol reactivity with juglone and menadione could be due to easy accessibility to the less hindered α, β-unsaturated site. Here, rationale is to design a ROS donor having relatively more hindered α, β-unsaturated site which may be inaccessible by thiols. As known in the literature that compound **1**, a Diels-Alder adduct of juglone[41] converts to compound **2,** a quinone derivative after ROS generation. In compound **2,** α, β-unsaturated site of quinone is more hindered and may not accessible to thiols while, compound **1** is not a candidate for thiol attack in the absence of α, β-unsaturated site.[24]

As it is known that compound **1** generate ROS in buffer, only when its hydroxyl group is in free from, if this hydroxy is protected, the resulting scaffold shows diminished ROS generating capacity.[41] Furthermore utilizing this concept, the phenolic group of compound **1** was masked with 4-nitro benzyl moiety, a substrate of nitroreductase (NTR) and ester moiety which upon activation with NTR[42] and esterase,[24] respectively, release compound **1** to generate ROS (Scheme 1).

Scheme 1. Activation methods to release compound **1**

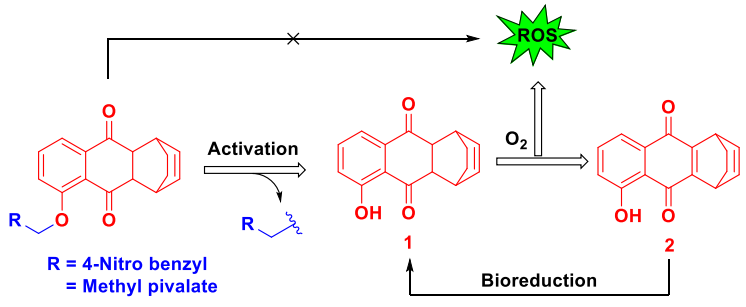

Inspired by these approaches, phenolic group of compound **1** can be protected with light triggerable linker, 2-nitrobenzyl which should release the compound **1** in the presence of light to generate ROS. [53] Apart from this, a biotin moiety can also be incorporated to facilitate the

accumulation of this molecule selectively in the cancer cells over normal cells (Scheme 2).[43–46] As cancer cells are known to overexpress vitamin receptors which may facilitate the enhanced accumulation of this vitamin molecules.[43] In addition, this biotin moiety may also increase the buffer solubility of the compound.

Scheme 2. Design of Light activatable ROS Generator

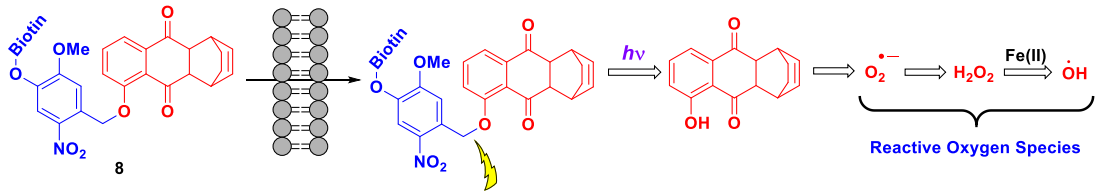

In order to do this, biotinylated compound **8** was synthesized in multiple steps, having 2-nitrobenzyl as a photo-cleavable linker coupled with a ROS generator **1**. Next, a photocleavage study was performed by HPLC analysis. In the HPLC trace, a peak corresponds to the compound **8** was completely disappeared upon irradiation with 365 nm light within 15 min to form a new peak that corresponds to compound **1** (Figure 3). However, there was no cleavage observed in the absence of light. This experiment suggests that the compound **8** is stable in dark and upon irradiation, photo-cleave to release compound **1**.

Figure 3. HPLC traces of photolysis study with compound **8** (50 µM) in the presence and absence of Light

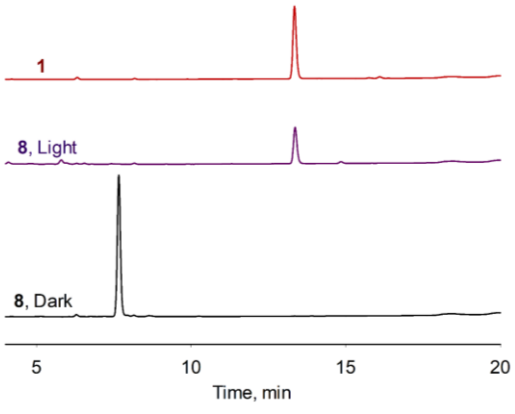

After photolysis of compound **8**, it releases compound **1** which should react with molecular oxygen to generate ROS. To test the ROS generation, a DHE assay was conducted, where DHE (dihydroethidium) dye was independently incubated with irradiated and non-irradiated sample of compound **8** and injected in HPLC. In the irradiated sample, two new

peaks were observed in HPLC trace and further an independent experiment was performed, wherein irradiated sample was treated with SOD, a known quencher of $O_2^{\bullet-}$, resulting in disappearance of one peak corresponding to superoxide adduct, 2-hydroxyethidium (2-OH-E^+). However, no peak was observed in the dark sample, suggests the compound **8** generate superoxide only after irradiation (Figure 4).

Figure 4. HPLC traces of DHE assay for $O_2^{\bullet-}$ detection with biotinylated compound **8**

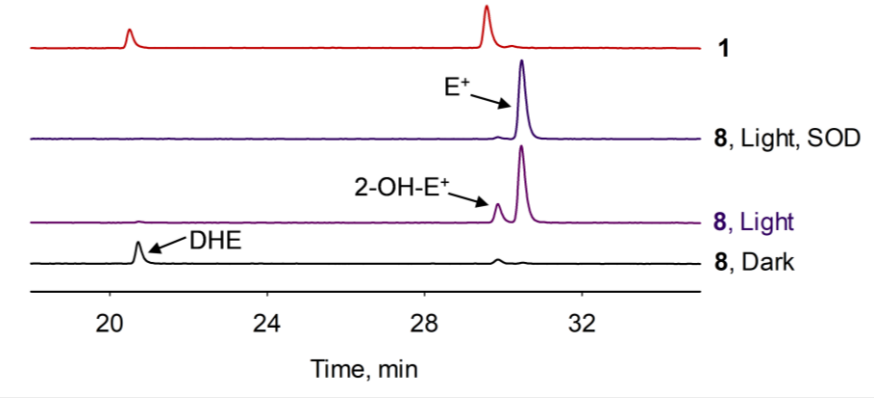

Further, to test the ROS enhancement in cellular system, H_2DCF-DA, a weakly fluorescent and cell permeable dye was used for intracellular detection of ROS, which produced an intense fluorescent signal only in cells which are exposed with compound **8** and light (Figure 5). However, no fluorescent signal was observed in light alone and dark. This suggests that light alone did not enhance the ROS level in cells. In contrast, an enhanced ROS level was observed in the cells pretreated with compound on exposure to light.

Figure 5. Intracellular ROS detection using H_2DCF-DA dye; A) Cellular images and B) Relative intensity graph of intracellular ROS level; Data represent the mean ± s.e.m. for 3 technical replicates per group.

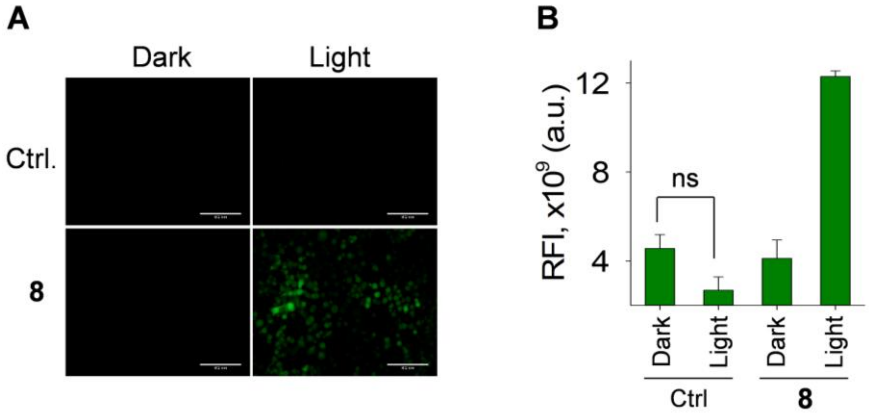

As described, compound **8** is cell permeable and photo-cleave to release **1**, which generates ROS intracellularly which further can damage essential biomolecules leading to inhibition of cellular proliferation. To test the effect of the compound **8**, MTT assay was carried out where inhibition in cellular growth was not observed in absence of light with compound **8** and light alone; however; nearly complete inhibition in growth was found upon irradiation with 10 µM of compound **8** (Figure 6).

Figure 6. Cell growth inhibition assay with 10 µM of compound using A549 cells; Data represent the mean ± s.e.m. for 3 technical replicates per group.

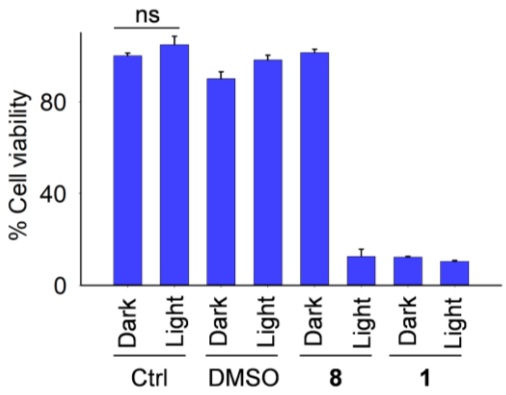

In Chapter 2, the unique photoactivable ROS generators were developed which produced ROS only in the presence of light and might be explored as cancer therapeutics. However, there are few shortcomings associated with the UV triggered approach e.g., UV light induced oxidative stress[47–51] and its lower tissue penetration. Owing to such limitations, *in vivo* experiments are more challenging to perform with the compound **8**. To overcome these drawbacks, there is need to develop a molecule which can get activated under visible light to produce ROS.

Chapter 3.1. Synthesis and Evaluation of a Triggerable Hydroquinone Based ROS Releasing Molecule

Chapter 2, described the development of UV light activatable ROS generators which cleave under 365 nm light to release molecule **1**, which then reacts with oxygen to generate ROS. To overcome the limitations associated with UV light based strategy,[47–51] a scaffold which would cleave upon irradiation with visible light to release ROS generating moiety is desired. In order

to achieve the visible light triggered release of ROS, a well-known fluorescent molecule, boron-dipyrromethene (BODIPY)[52,53] was chosen as the photolabile moiety.

Scheme 3. Design of Visible light triggered ROS generating molecules

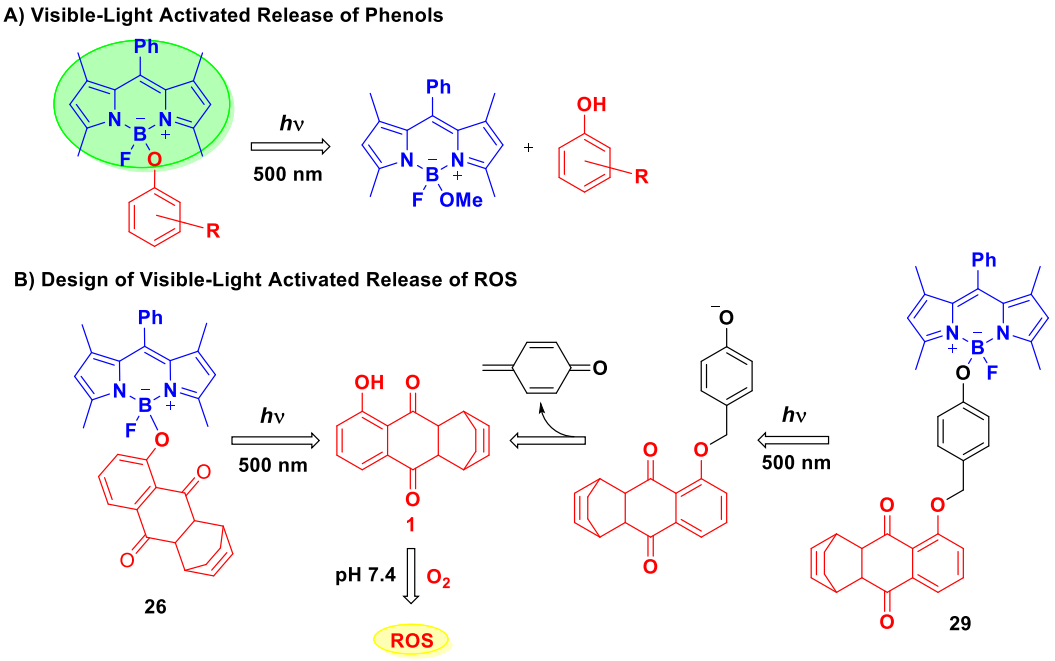

Release of several BODIPY-masked bioactive molecules under visible light has been demonstrated in literature.[27,31,54–61] However, we were particularly inspired by the work carried out by Urano and co-workers, wherein a phenolic group attached to the boron atom of BODIPY was shown to uncage under visible light (Scheme 3).[55] BODIPY moieties are typically fluorescent in nature, but the presence of an electron rich aryloxy substituent on the boron atom can result in the quenching of fluorescence, as a result of photoinduced electron transfer (PET). These BODIPY derivatives form a charge-separation intermediate upon irradiation, with a partial negative charge on the boron atom and a partial positive charge on the oxygen atom of the aryloxy group. The intermediate further undergoes solvolysis to release the aryloxy group. As described previously, compound **1** (which generates ROS) can be attached with the boron atom of BODIPY; the adduct, then, cleaves with visible light to release compound **1** (Scheme 3). Here, two possibilities of attaching compound **1** with BODIPY were described. First, where the phenolic group can be directly attached to the boron of BODIPY and in another alternative, a 4-hydroxybenzyl group can be used as a self-immolative linker between compound **1** and the boron atom of BODIPY. These designed compounds should photocleave under visible light to release compound **1**, which is known to generate superoxide ($O_2^{\bullet-}$) under ambient aerobic

conditions. But despite of several attempts, we could not succeed in synthesizing the derivatives of compound **1** which may cleave under visible light condition. The reason for failure in synthesizing designed compounds could be few synthetic challenges such as less stability under acidic and basic reaction conditions and limited scope of derivatization, are associated with the ROS generator **1**.

To surmount these limitations, a scaffold for ROS generation need to be developed, which would have a site to functionalize, for making it selective towards a particular organelle in a cell or towards one cell type, without compromising the ability to generate ROS. Further, the scaffold should be stable in mild acidic and basic conditions and also should be compatible with a range of electrophiles of different triggers. To do this, we inspired by a study where the derivatives of 1,4-hydroquinone (1, 4-HQ) were used as ROS generating molecules. Where both the hydroxy group should be free for generating ROS, thus protecting any one of the hydroxyl group of 1,4-HQ should diminish its ROS generating ability. Here, as a proof of concept, a compound was designed where one of hydroxyl group is masked with an ether linkage and further linked with an ester group. The ester moiety should hydrolyzed with an esterase enzyme to release 1,4-HQ, which should further react with molecular oxygen to produce ROS (Scheme 4).

Scheme 4. Design of Esterase activated ROS generator

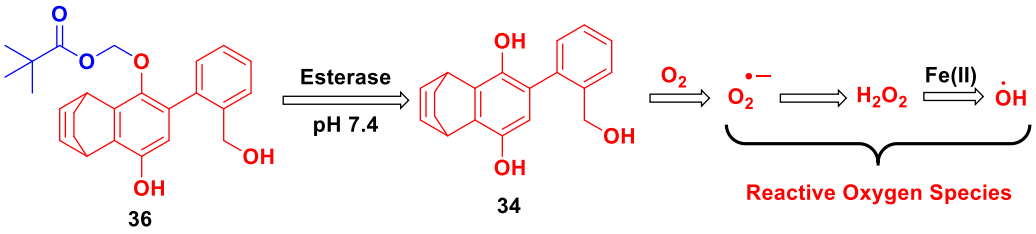

An esterase activated ROS generator **36** and its unmasked 1,4-hydroquinone derivative **34** were synthesized in multiple steps. Further, it was studied for possible ester hydrolysis in the presence of esterase by HPLC, where **36** was incubated with esterase for 30 min and injected in HPLC. It was found that the peak corresponds to **36,** completely disappeared and new peak was observed which corresponds to **34**, underwent oxidation to form quinone derivative **37** (Figure 7).

Figure 7. HPLC traces of ester hydrolysis of **36** in the presence and absence of esterase enzyme

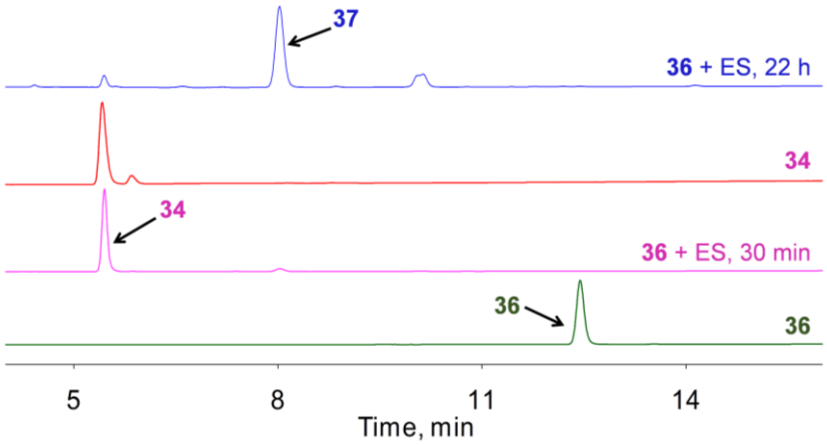

After ester hydrolysis of compound **36**, compound **34** was formed which should react with molecular oxygen to generate ROS. To test the generation of ROS, a DHE assay was carried out to look for $O_2^{\bullet-}$ generation, where DHE (dihydroethidium) dye was independently incubated with compound **36** in the absence and presence of esterase and injected in HPLC. In the esterase treated sample, a new intense peak at 29.8 min in HPLC trace was observed and disappeared in SOD treated samples, suggests that the peak at 29.8 min corresponds to $O_2^{\bullet-}$ adduct, 2-hydroxyethidium (2-OH-E^+). However, no peak was observed in the absence of esterase, confirmed that the compound **36** generate $O_2^{\bullet-}$ only in the presence of esterase enzyme. (Figure 8).

Figure 8. Superoxide detection using DHE assay with compound **36**

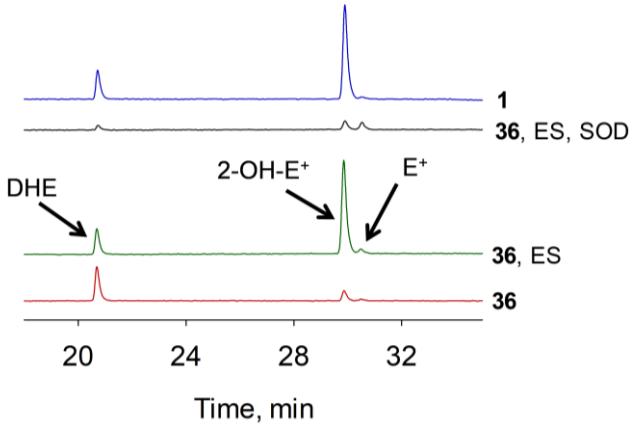

The ROS generating scaffold **36** does not offer selectivity to particular types of cells over others, owing to the ubiquity of the trigger: esterase. Apart from selectivity, the esterase possibly quenches the generated H_2O_2 and hence, interferes with the *in vitro* detection of H_2O_2. Taken together, a new triggerable ROS-generating scaffold has been developed.

Chapter 3.2. Synthesis and Evaluation of Visible Light Triggerable ROS Generator

To solve the problems encountered in the chapter 3.1, a different class of ROS releasing scaffolds were developed based on the 1,4-hydroquinone (1,4-HQ)[62] moiety masked with an ester moiety. It was established that ester-protected 1,4-HQ molecule hydrolyzes in the presence of esterase to release 1,4-HQ, which produces ROS. Here, a molecule was designed where one of the hydroxyl groups of 1,4-HQ derivative was masked with BODIPY,[55] a visible light responsive moiety and the other hydroxyl group, with an esterase cleavable moiety (Scheme 5) which, upon visible light irradiation and esterase treatment, should free up both the hydroxyl groups of 1,4-HQ and the released molecule may react with molecular oxygen to produce ROS.

Scheme 5. Revised design of Visible light activated ROS generation

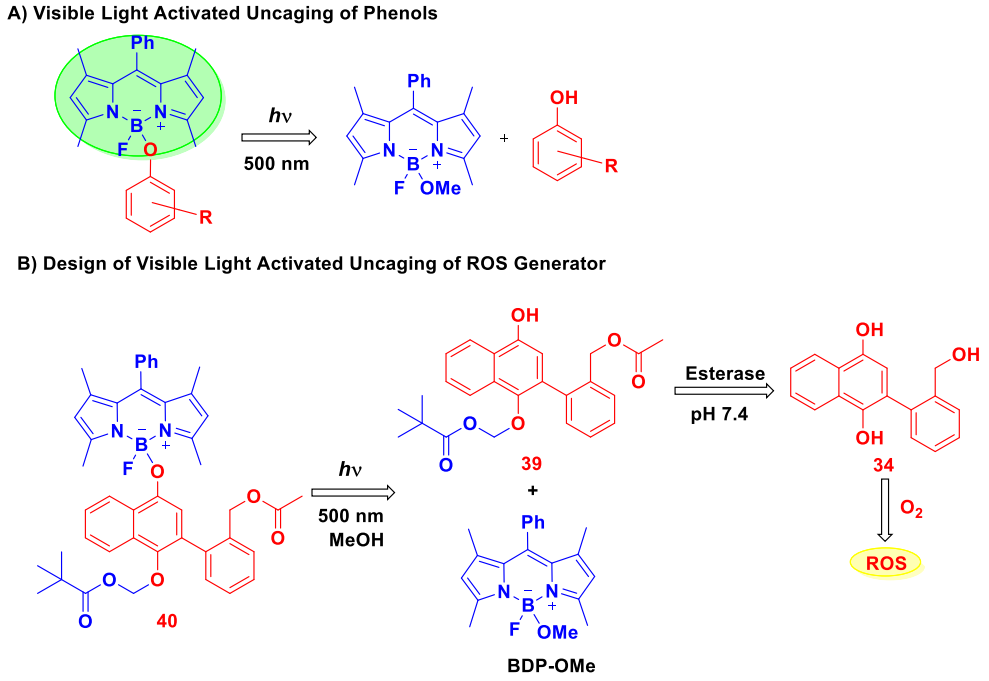

Here, a triggerable ROS donor **40** was synthesized, using BODIPY as a photolabile linker and 1,4-hydroquinone derivative as a ROS generating moiety. To investigate the cleavage under visible light, compound **40** was irradiated using 500 nm light and injected in HPLC where two new peaks were appeared in the HPLC trace. One of the peaks corresponds to compound **39** and another peak possibly for the BODIPY photo-product BDP-OMe (Figure

9). However, **40** was stable in absence of light. This study demonstrates that compound **40** releases the compound **39**, upon activation with visible light.

Figure 9. Photocleavage study of compound **40** in visible light, HPLC was operated using 250 nm detector

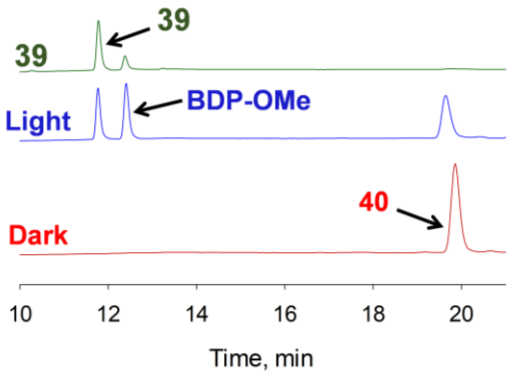

When $O_2^{\bullet-}$ detection was performed with compound **40** using DHE assay, as expected, high intense peak for 2-OH-E^+ was observed in the presence of light and esterase enzyme and this signal was diminished when reaction mixture was treated with superoxide dismutase (SOD), a known quencher of $O_2^{\bullet-}$, suggests that the observed intense signal in HPLC is attributable to $O_2^{\bullet-}$ (Figure 10). However, signal for $O_2^{\bullet-}$ was very weak in dark, only esterase treated and only light irradiated samples.

Figure 10. Superoxide detection using DHE assay

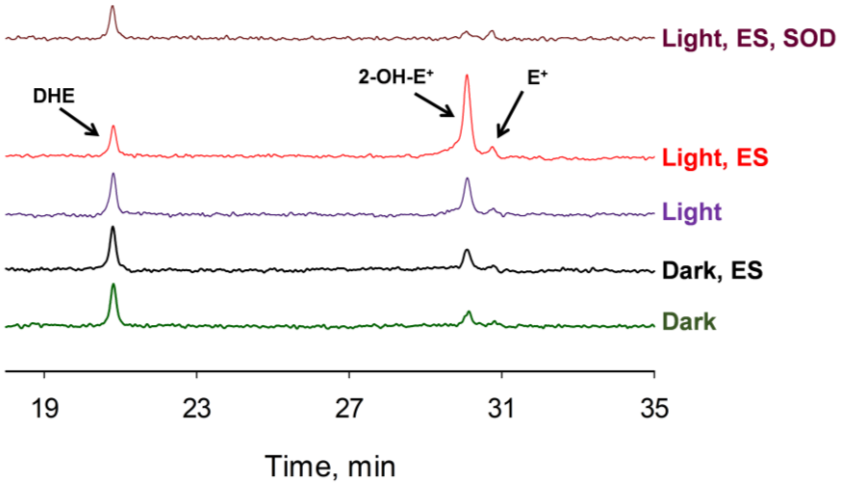

As this compound activates under mild visible conditions and may find application in studying the ROS mediated signaling pathways in spatiotemporally controlled manner.

Chapter 4. Visible Light Triggered Uncaging of COS/H_2S

Chapter 3 deals with the synthesis and evaluation of a potential BODIPY-based 1,4-hydroquinone derivative, which produces ROS after visible light activation. Here, releasing another redox active species, H_2S, using a BODIPY-based visible light uncaging group is attempted. Our group has previously reported a scaffold which is activated by esterase to release a phenolate intermediate.[63] This phenolate intermediate subsequently self-immolates to release carbonyl sulfide (COS), a gaseous molecule which produces H_2S, upon hydrolysis with carbonic anhydrase (CA), a widely prevalent enzyme. To generate H_2S in a spatio-temporally controlled manner under ambient conditions, a phenolate (linked with a carbamothioate moiety) can be masked with BODIPY, such that the phenolate can be released upon irradiation with visible light.[55] The phenolate should self-immolate to release a carbamothioate intermediate which, then, should release COS to produce H_2S upon hydrolysis with CA (Scheme 6).[29,63–67] This method may generate H_2S in a spatio-temporally controlled manner under ambient conditions.

Scheme 6. Rational design for visible light triggered uncaging of H_2S

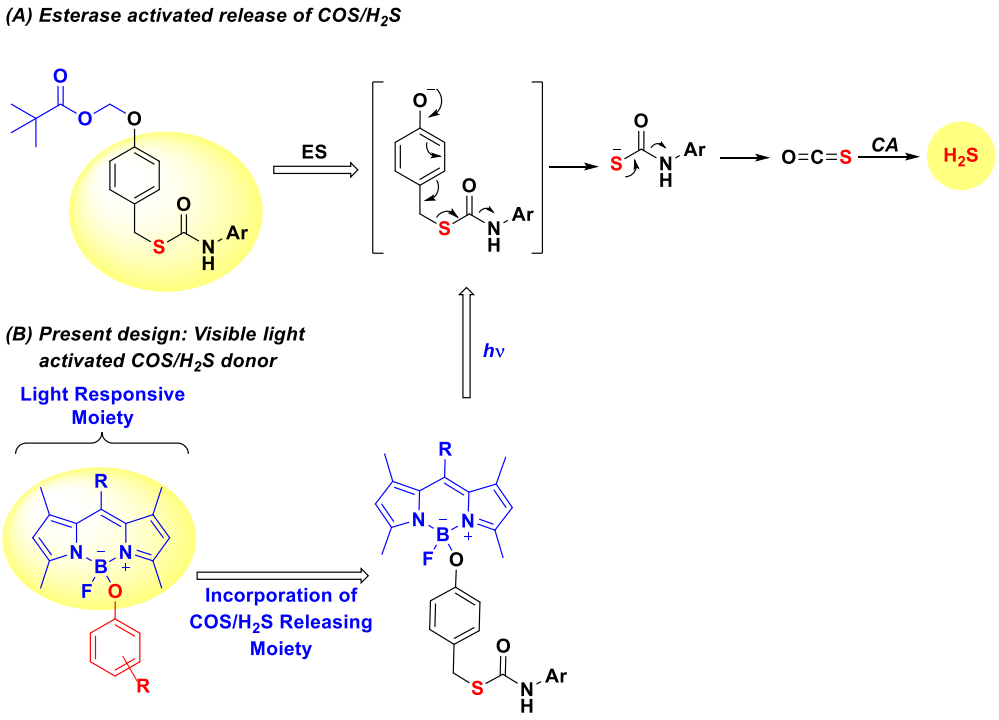

Here, a BODIPY based visible light activated H_2S donor, **47** was synthesized in multiple steps. Next, photo-cleavage study was performed, where compound **47** was irradiated with 470 nm light and injected in HPLC where two new peaks were observed in the HPLC

trace (Figure 11). One of the peaks corresponds to a highly fluorescent BODIPY photoproduct **51**. Another peak could be for phenolate intermediate **52**. The phenolate intermediate **52** may undergoes self-immolation to release COS which upon hydrolysis in the presence of CA to generate H_2S.

Figure 11. Photo-cleavage study with **47**

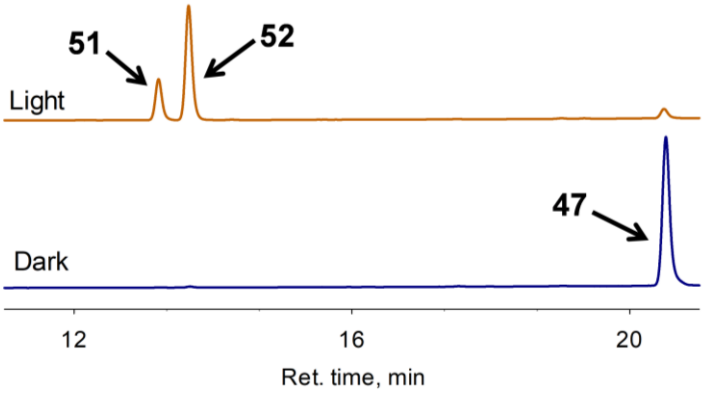

Next, H_2S detection was performed with compound **47** using methylene blue formation assay as H_2S is known to form methylene blue complex in the presence of *N*,*N*-dimethyl-*p*-phenylenediamine and $FeCl_3$ in acidic medium which can be estimated calorimetrically at 676 nm wavelength. When this assay was carried out with compound **47**, a significant enhancement at 676 nm was observed only in the irradiated sample; however, no enhancement in signal was found in the absence of light (Figure 12). This experiment confirmed the generation of H_2S by compound **47** only in the presence of light. The compound **47** was well tolerated by cells and protect cells from ROS-induced damage, assessed by MTT assay (Figure 13).

Figure 12. H_2S detection by Methylene blue assay (A) compound **47** was irradiated with 470 nm light for 25 min followed by incubation with carbonic anhydrase in pH 7.4 buffer for predetermined time points; (B) Curve fitting for first order kinetics give rate constant = 0.03 min^{-1}(R^2 = 0.995).

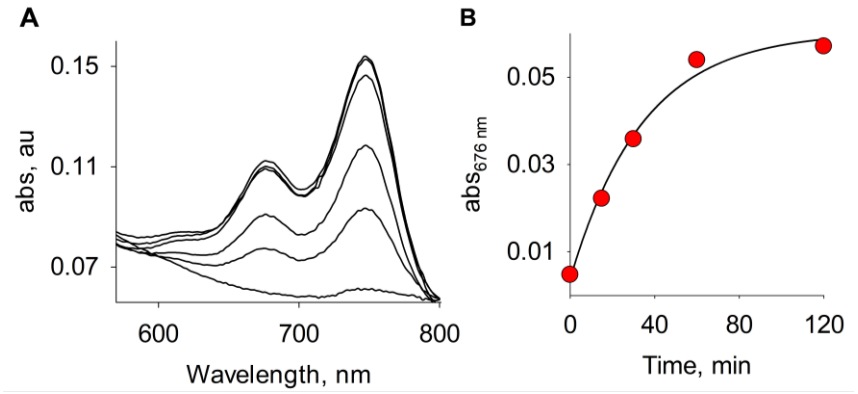

Figure 13. Cytoprotective effect of **47** against H_2O_2 induced damage: A549 cells with increasing doses of **47** followed by irradiation with 470 nm light for 5 min (24 h incubation, MTT assay).

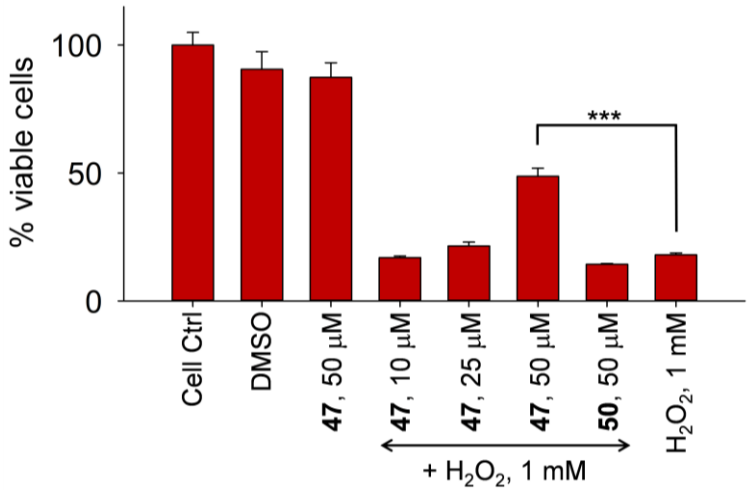

These tools may provide an opportunity to understand the H_2S mediated signaling pathways of cell in spatiotemporally controlled manner as being activated under visible light conditions which may not complicate the other cellular machinery.

In this thesis, presented light activated tools may solve few problems such as lack of controlled and localized delivery of highly reactive species which were associated with the existing methods. In addition, the visible light may not generate unwanted free radicals in cells that may provide a better opportunity to understand the ROS and H_2S mediated physiology. However, these methods have few limitations such as, poor tissue penetration of 500 nm that hinder their use in *in vivo* experiments. This opens the floor for the development of new tools which may get activated under the conditions where low tissue penetration may not be a barrier in probing the physiology of reactive species *in vivo*.

References

(1) Leonard, S. S.; Harris, G. K.; Shi, X. Metal-Induced Oxidative Stress and Signal Transduction. *Free Radic. Biol. Med.* **2004**, *37* (12), 1921–1942.

(2) Dizdaroglu, M.; Rao, G.; Halliwell, B.; Gajewski, E. Damage to the DNA Bases in Mammalian Chromatin by Hydrogen Peroxide in the Presence of Ferric and Cupric Ions. *Arch. Biochem. Biophys.* **1991**, *285* (2), 317–324.

(3) Minteer, S. D.; Giroud, F.; Milton, R. D.; Tan, B. Quinone Electrochemistry: From the Electron Transport Chain to Electron Mediators and Orientational Moieites. *Meet. Abstr.* **2015**, *MA2015-01* (45), 2307–2307.

(4) ZIEGLER, D. M. The Role of Quinones in the Mitochondrial Electron Transport System. *Am. J. Clin. Nutr.* **1961**, *9* (4), 43–49.

(5) D'Autréaux, B.; Toledano, M. B. ROS as Signalling Molecules: Mechanisms That Generate Specificity in ROS Homeostasis. *Nat. Rev. Mol. Cell Biol.* **2007**, *8* (10), 813–824.

(6) Finkel, T. Signal Transduction by Reactive Oxygen Species. *J. Cell Biol.* **2011**, *194* (1), 7–15.

(7) Fruehauf, J. P.; Meyskens, F. L. Reactive Oxygen Species: A Breath of Life or Death? *Clin. Cancer Res.* **2007**, *13* (3), 789–794.

(8) Schieber, M.; Chandel, N. S. ROS Function in Redox Signaling and Oxidative Stress. *Curr. Biol.* **2014**, *24* (10), R453–R462.

(9) Lando, D.; Peet, D. J.; Whelan, D. A.; Gorman, J. J.; Whitelaw, M. L. Asparagine Hydroxylation of the HIF Transactivation Domain: A Hypoxic Switch. *Science (80-.).* **2002**, *295* (5556), 858–861.

(10) Hoshikawa, Y.; Nana-Sinkam, P.; Moore, M. D.; Sotto-Santiago, S.; Phang, T.; Keith, R. L.; Morris, K. G.; Kondo, T.; Tuder, R. M.; Voelkel, N. F.; et al. Hypoxia Induces Different Genes in the Lungs of Rats Compared with Mice. *Physiol. Genomics* **2003**, *12* (3), 209–219.

(11) Michiels, C. Physiological and Pathological Responses to Hypoxia. *Am. J. Pathol.* **2004**, *164* (6), 1875–1882.

(12) Obin, M.; Shang, F.; Gong, X.; Handelman, G.; Blumberg, J.; Taylor, A. Redox Regulation of Ubiquitin-Conjugating Enzymes: Mechanistic Insights Using the Thiol-Specific Oxidant Diamide. *FASEB J.* **1998**, *12* (7), 561–569.

(13) Kwak, Y.-D.; Wang, B.; Li, J. J.; Wang, R.; Deng, Q.; Diao, S.; Chen, Y.; Xu, R.; Masliah, E.; Xu, H.; et al. Upregulation of the E3 Ligase NEDD4-1 by Oxidative Stress

Degrades IGF-1 Receptor Protein in Neurodegeneration. *J. Neurosci.* **2012**, *32* (32), 10971–10981.

(14) Di Simplicio, P.; Franconi, F.; Frosalí, S.; Di Giuseppe, D. Thiolation and Nitrosation of Cysteines in Biological Fluids and Cells. *Amino Acids* **2003**, *25* (3–4), 323–339.

(15) Winterbourn, C. C.; Hampton, M. B. Thiol Chemistry and Specificity in Redox Signaling. *Free Radic. Biol. Med.* **2008**, *45* (5), 549–561.

(16) Zheng, N.; Liu, L.; Liu, W.; Li, F.; Hayashi, T.; Tashiro, S.; Onodera, S.; Ikejima, T. Crosstalk of ROS/RNS and Autophagy in Silibinin-Induced Apoptosis of MCF-7 Human Breast Cancer Cells in Vitro. *Acta Pharmacol. Sin.* **2017**, *38* (2), 277–289.

(17) Bubici, C.; Papa, S.; Dean, K.; Franzoso, G. Mutual Cross-Talk between Reactive Oxygen Species and Nuclear Factor-Kappa B: Molecular Basis and Biological Significance. *Oncogene* **2006**, *25* (51), 6731–6748.

(18) Gordeeva, A. V; Zvyagilskaya, R. A.; Labas, Y. A. Cross-Talk between Reactive Oxygen Species and Calcium in Living Cells. *Biochemistry. (Mosc).* **2003**, *68* (10), 1077–1080.

(19) Lindermayr, C. Crosstalk between Reactive Oxygen Species and Nitric Oxide in Plants: Key Role of S-Nitrosoglutathione Reductase. *Free Radic. Biol. Med.* **2018**, *122*, 110–115.

(20) Kolbert, Z.; Feigl, G. Cross-Talk of Reactive Oxygen Species and Nitric Oxide in Various Processes of Plant Development. In *Reactive Oxygen Species in Plants*; John Wiley & Sons, Ltd: Chichester, UK, 2017; pp 261–289.

(21) Zhao, J. Interplay among Nitric Oxide and Reactive Oxygen Species: A Complex Network Determining Cell Survival or Death. *Plant Signal. Behav.* **2007**, *2* (6), 544–547.

(22) Khodade, V. S.; Sharath Chandra, M.; Banerjee, A.; Lahiri, S.; Pulipeta, M.; Rangarajan, R.; Chakrapani, H. Bioreductively Activated Reactive Oxygen Species (ROS) Generators as MRSA Inhibitors. *ACS Med. Chem. Lett.* **2014**, *5* (7), 777–781.

(23) Dharmaraja, A. T.; Dash, T. K.; Konkimalla, V. B.; Chakrapani, H. Synthesis, Thiol-Mediated Reactive Oxygen Species Generation Profiles and Anti-Proliferative Activities of 2,3-Epoxy-1,4-Naphthoquinones. *Med. Chem. Commun.* **2012**, *3* (2), 219–224.

(24) Kelkar, D. S.; Ravikumar, G.; Mehendale, N.; Singh, S.; Joshi, A.; Sharma, A. K.; Mhetre, A.; Rajendran, A.; Chakrapani, H.; Kamat, S. S. A Chemical–Genetic Screen Identifies ABHD12 as an Oxidized-Phosphatidylserine Lipase. *Nat. Chem. Biol.* **2019**,

15 (2), 169–178.

(25) Carling, C.-J.; Viger, M. L.; Nguyen Huu, V. A.; Garcia, A. V; Almutairi, A. In Vivo Visible Light-Triggered Drug Release from an Implanted Depot. *Chem. Sci.* **2015**, *6* (1), 335–341.

(26) Venkatesh, Y.; Das, J.; Chaudhuri, A.; Karmakar, A.; Maiti, T. K.; Singh, N. D. P. Light Triggered Uncaging of Hydrogen Sulfide (H2S) with Real-Time Monitoring. *Chem. Commun.* **2018**, *54* (25), 3106–3109.

(27) Sharma, A. K.; Nair, M.; Chauhan, P.; Gupta, K.; Saini, D. K.; Chakrapani, H. Visible-Light-Triggered Uncaging of Carbonyl Sulfide for Hydrogen Sulfide (H2S) Release. *Org. Lett.* **2017**, *19* (18), 4822–4825.

(28) Wong, P. T.; Tang, S.; Cannon, J.; Mukherjee, J.; Isham, D.; Gam, K.; Payne, M.; Yanik, S. A.; Baker, J. R.; Choi, S. K. A Thioacetal Photocage Designed for Dual Release: Application in the Quantitation of Therapeutic Release by Synchronous Reporter Decaging. *ChemBioChem* **2017**, *18* (1), 126–135.

(29) Zhao, Y.; Bolton, S. G.; Pluth, M. D. Light-Activated COS/H2S Donation from Photocaged Thiocarbamates. *Org. Lett.* **2017**, *19* (9), 2278–2281.

(30) Linsley, C. S.; Wu, B. M. Recent Advances in Light-Responsive on-Demand Drug-Delivery Systems. *Ther. Deliv.* **2017**, *8* (2), 89–107.

(31) Patil, N. G.; Basutkar, N. B.; Ambade, A. V. Visible Light-Triggered Disruption of Micelles of an Amphiphilic Block Copolymer with BODIPY at the Junction. *Chem. Commun.* **2015**, *51* (100), 17708–17711.

(32) Agostinis, P.; Berg, K.; Cengel, K. A.; Foster, T. H.; Girotti, A. W.; Gollnick, S. O.; Hahn, S. M.; Hamblin, M. R.; Juzeniene, A.; Kessel, D.; et al. Photodynamic Therapy of Cancer: An Update. *CA. Cancer J. Clin.* **2011**, *61* (4), 250–281.

(33) DeRosa, M. C.; Crutchley, R. J. Photosensitized Singlet Oxygen and Its Applications. *Coord Chem Rev* **2002**, *233–234*, 351–371.

(34) Onyango, A. N. Endogenous Generation of Singlet Oxygen and Ozone in Human and Animal Tissues: Mechanisms, Biological Significance, and Influence of Dietary Components. *Oxid. Med. Cell. Longev.* **2016**, *2016*, 2398573.

(35) Miller, E. W.; Taulet, N.; Onak, C. S.; New, E. J.; Lanselle, J. K.; Smelick, G. S.; Chang, C. J. Light-Activated Regulation of Cofilin Dynamics Using a Photocaged Hydrogen Peroxide Generator. *J. Am. Chem. Soc.* **2010**, *132* (48), 17071–17073.

(36) Chaudhuri, L.; Sarsour, E. H.; Goswami, P. C. 2-(4-Chlorophenyl)Benzo-1,4-Quinone Induced ROS-Signaling Inhibits Proliferation in Human Non-Malignant Prostate

Epithelial Cells. *Environ. Int.* **2010**, *36* (8), 924–930.

(37) Cassagnes, L.-E.; Perio, P.; Ferry, G.; Moulharat, N.; Antoine, M.; Gayon, R.; Boutin, J. A.; Nepveu, F.; Reybier, K. In Cellulo Monitoring of Quinone Reductase Activity and Reactive Oxygen Species Production during the Redox Cycling of 1,2 and 1,4 Quinones. *Free Radic. Biol. Med.* **2015**, *89*, 126–134.

(38) Fato, R.; Bergamini, C.; Leoni, S.; Lenaz, G. Mitochondrial Production of Reactive Oxygen Species: Role of Complex I and Quinone Analogues. *Biofactors* **2008**, *32* (1–4), 31–39.

(39) Bolton, J. L.; Dunlap, T. Formation and Biological Targets of Quinones: Cytotoxic versus Cytoprotective Effects. *Chem. Res. Toxicol.* **2017**, *30* (1), 13–37.

(40) Wang, X.; Thomas, B.; Sachdeva, R.; Arterburn, L.; Frye, L.; Hatcher, P. G.; Cornwell, D. G.; Ma, J. Mechanism of Arylating Quinone Toxicity Involving Michael Adduct Formation and Induction of Endoplasmic Reticulum Stress. *Proc. Natl. Acad. Sci. U. S. A.* **2006**, *103* (10), 3604–3609.

(41) Dharmaraja, A. T.; Alvala, M.; Sriram, D.; Yogeeswari, P.; Chakrapani, H. Design, Synthesis and Evaluation of Small Molecule Reactive Oxygen Species Generators as Selective Mycobacterium Tuberculosis Inhibitors. *Chem. Commun.* **2012**, *48* (83), 10325–10327.

(42) Dharmaraja, A. T.; Chakrapani, H. A Small Molecule for Controlled Generation of Reactive Oxygen Species (ROS). *Org. Lett.* **2014**, *16* (2), 398–401.

(43) Chen, S.; Zhao, X.; Chen, J.; Chen, J.; Kuznetsova, L.; Wong, S. S.; Ojima, I. Mechanism-Based Tumor-Targeting Drug Delivery System. Validation of Efficient Vitamin Receptor-Mediated Endocytosis and Drug Release. *Bioconjug. Chem.* **2010**, *21* (5), 979–987.

(44) Ren, W. X.; Han, J.; Uhm, S.; Jang, Y. J.; Kang, C.; Kim, J.-H.; Kim, J. S. Recent Development of Biotin Conjugation in Biological Imaging, Sensing, and Target Delivery. *Chem. Commun.* **2015**, *51* (52), 10403–10418.

(45) Kim, T.; Jeon, H. M.; Le, H. T.; Kim, T. W.; Kang, C.; Kim, J. S. A Biotin-Guided Fluorescent-Peptide Drug Delivery System for Cancer Treatment. *Chem. Commun.* **2014**, *50* (57), 7690.

(46) Luo, S.; Kansara, V. S.; Zhu, X.; Mandava, N. K.; Pal, D.; Mitra, A. K. Functional Characterization of Sodium-Dependent Multivitamin Transporter in MDCK-MDR1 Cells and Its Utilization as a Target for Drug Delivery. *Mol. Pharm.* **2006**, *3* (3), 329–339.

(47) Jackson, D. A.; Hassan, A. B.; Errington, R. J.; Cook, P. R. Oxidative Stress Is Involved in the UV Activation of P53. *J. Cell Sci.* **1996**, *107* (7), 1753–1760.

(48) Zhang, X.; Rosenstein, B. S.; Wang, Y.; Lebwohl, M.; Wei, H. Identification of Possible Reactive Oxygen Species Involved in Ultraviolet Radiation-Induced Oxidative DNA Damage. *Free Radic. Biol. Med.* **1997**, *23* (7), 980–985.

(49) Heck, D. E.; Vetrano, A. M.; Mariano, T. M.; Laskin, J. D. UVB Light Stimulates Production of Reactive Oxygen Species. *J. Biol. Chem.* **2003**, *278* (25), 22432–22436.

(50) Bossi, O.; Gartsbein, M.; Leitges, M.; Kuroki, T.; Grossman, S.; Tennenbaum, T. UV Irradiation Increases ROS Production via PKCδ Signaling in Primary Murine Fibroblasts. *J. Cell. Biochem.* **2008**, *105* (1), 194–207.

(51) de Jager, T. L.; Cockrell, A. E.; Du Plessis, S. S. Ultraviolet Light Induced Generation of Reactive Oxygen Species; Springer, Cham, 2017; pp 15–23.

(52) Ulrich, G.; Ziessel, R.; Harriman, A. The Chemistry of Fluorescent Bodipy Dyes: Versatility Unsurpassed. *Angew. Chemie Int. Ed.* **2008**, *47* (7), 1184–1201.

(53) and, A. L.; Burgess, K. BODIPY Dyes and Their Derivatives: Syntheses and Spectroscopic Properties. *Chem. Rev.* **2007**, *107* (11), 4891–4932.

(54) Palao, E.; Slanina, T.; Muchová, L.; Šolomek, T.; Vítek, L.; Klán, P. Transition-Metal-Free CO-Releasing BODIPY Derivatives Activatable by Visible to NIR Light as Promising Bioactive Molecules. *J. Am. Chem. Soc.* **2016**, *138* (1), 126–133.

(55) Umeda, N.; Takahashi, H.; Kamiya, M.; Ueno, T.; Komatsu, T.; Terai, T.; Hanaoka, K.; Nagano, T.; Urano, Y. Boron Dipyrromethene As a Fluorescent Caging Group for Single-Photon Uncaging with Long-Wavelength Visible Light. *ACS Chem. Biol.* **2014**, *9* (10), 2242–2246.

(56) Kumari, P.; Kulkarni, A.; Sharma, A. K.; Chakrapani, H. Visible-Light Controlled Release of a Fluoroquinolone Antibiotic for Antimicrobial Photopharmacology. *ACS omega* **2018**, *3* (2), 2155–2160.

(57) Goswami, P. P.; Syed, A.; Beck, C. L.; Albright, T. R.; Mahoney, K. M.; Unash, R.; Smith, E. A.; Winter, A. H. BODIPY-Derived Photoremovable Protecting Groups Unmasked with Green Light. *J. Am. Chem. Soc.* **2015**, *137* (11), 3783–3786.

(58) Rubinstein, N.; Liu, P.; Miller, E. W.; Weinstain, R. Meso-Methylhydroxy BODIPY: A Scaffold for Photo-Labile Protecting Groups. *Chem. Commun.* **2015**, *51* (29), 6369–6372.

(59) Sitkowska, K.; Feringa, B. L.; Szymański, W. Green-Light-Sensitive BODIPY Photoprotecting Groups for Amines. *J. Org. Chem.* **2018**, *83* (4), 1819–1827.

(60) Štacko, P.; Muchová, L.; Vítek, L.; Klán, P. Visible to NIR Light Photoactivation of Hydrogen Sulfide for Biological Targeting. *Org. Lett.* **2018**, *20* (16), 4907–4911.

(61) Blangetti, M.; Fraix, A.; Lazzarato, L.; Marini, E.; Rolando, B.; Sodano, F.; Fruttero, R.; Gasco, A.; Sortino, S. A Nonmetal-Containing Nitric Oxide Donor Activated with Single-Photon Green Light. *Chem. - A Eur. J.* **2017**, *23* (38), 9026–9029.

(62) Dharmaraja, A. T.; Jain, C.; Chakrapani, H. Substituent Effects on Reactive Oxygen Species (ROS) Generation by Hydroquinones. *J. Org. Chem.* **2014**, *79* (19), 9413–9417.

(63) Chauhan, P.; Bora, P.; Ravikumar, G.; Jos, S.; Chakrapani, H. Esterase Activated Carbonyl Sulfide/Hydrogen Sulfide (H2S) Donors. *Org. Lett.* **2017**, *19* (1), 62–65.

(64) Zhao, Y.; Pluth, M. D. Hydrogen Sulfide Donors Activated by Reactive Oxygen Species. *Angew. Chem. Int. Ed.* **2016**, *55* (47), 14638–14642.

(65) Steiger, A. K.; Pardue, S.; Kevil, C. G.; Pluth, M. D. Self-Immolative Thiocarbamates Provide Access to Triggered H2S Donors and Analyte Replacement Fluorescent Probes. *J. Am. Chem. Soc.* **2016**, *138* (23), 7256–7259.

(66) Steiger, A. K.; Yang, Y.; Royzen, M.; Pluth, M. D. Bio-Orthogonal "Click-and-Release" Donation of Caged Carbonyl Sulfide (COS) and Hydrogen Sulfide (H 2 S). *Chem. Commun.* **2017**, *53* (8), 1378–1380.

(67) Steiger, A. K.; Zhao, Y.; Pluth, M. D. Emerging Roles of Carbonyl Sulfide in Chemical Biology: Sulfide Transporter or Gasotransmitter? *Antioxid. Redox Signal.* **2017**.

List of Figures

List of Schemes

Copyright permits from Royal Society of Chemistry for reusing data in Chapter 2:

Author reusing their own work published by the Royal Society of Chemistry

You do not need to request permission to reuse your own figures, diagrams, etc, that were originally published in a Royal Society of Chemistry publication. However, permission should be requested for use of the whole article or chapter except if reusing it in a thesis. If you are including an article or book chapter published by us in your thesis please ensure that your co-authors are aware of this.

Copyright permits from American Chemical Society for reusing data in Chapter 4:

Copyright Clearance Center RightsLink® Home Create Account Help LIVE CHAT

ACS Publications Most Trusted. Most Cited. Most Read.

Title:	Visible-Light-Triggered Uncaging of Carbonyl Sulfide for Hydrogen Sulfide (H2S) Release
Author:	Ajay Kumar Sharma, Mrutyunjay Nair, Preeti Chauhan, et al
Publication:	Organic Letters
Publisher:	American Chemical Society
Date:	Sep 1, 2017

LOGIN

If you're a copyright.com user, you can login to RightsLink using your copyright.com credentials.

Already **a RightsLink user** or want to learn more?

PERMISSION/LICENSE IS GRANTED FOR YOUR ORDER AT NO CHARGE

This type of permission/license, instead of the standard Terms & Conditions, is sent to you because no fee is being charged for your order. Please note the following:

- Permission is granted for your request in both print and electronic formats, and translations.
- If figures and/or tables were requested, they may be adapted or used in part.
- Please print this page for your records and send a copy of it to your publisher/graduate school.
- Appropriate credit for the requested material should be given as follows: "Reprinted (adapted) with permission from (COMPLETE REFERENCE CITATION). Copyright (YEAR) American Chemical Society." Insert appropriate information in place of the capitalized words.
- One-time permission is granted only for the use specified in your request. No additional uses are granted (such as derivative works or other editions). For any other uses, please submit a new request.

If credit is given to another source for the material you requested, permission must be obtained from that source.

BACK CLOSE WINDOW

List of Publications

1. **Sharma, A. K**., Singh, H., Chakrapani, H. Photocontrolled Endogenous Reactive Oxygen Species (ROS) Generation, *Chem. Commun.*, **2019**, *55* (36), 5259-5262.
2. Kelkar, D. S.; Ravikumar, G.; Mehendale, N.; Singh, S.; Joshi, A.; **Sharma, A. K**.; Mhetre, A.; Rajendran, A.; Chakrapani, H.; Kamat, S. S. A Chemical–genetic Screen Identifies ABHD12 as an Oxidized-Phosphatidylserine Lipase. *Nat. Chem. Biol*. **2019**, *15* (2), 169–178.
3. Kulkarni, A.; **Sharma, A. K**.; Chakrapani, H. Redox-Guided Small Molecule Antimycobacterials. *IUBMB Life* **2018**, *70* (9), 826–835.
4. Kumari, P.; Kulkarni, A.; **Sharma, A. K**.; Chakrapani, H. Visible-Light Controlled Release of a Fluoroquinolone Antibiotic for Antimicrobial Photopharmacology. *ACS omega* **2018**, *3* (2), 2155–2160.
5. **Sharma, A. K**.; Nair, M.; Chauhan, P.; Gupta, K.; Saini, D. K.; Chakrapani, H. Visible-Light-Triggered Uncaging of Carbonyl Sulfide for Hydrogen Sulfide (H_2S) Release. *Org. Lett*. **2017**, *19* (18), 4822–4825.

ChemComm

COMMUNICATION

View Article Online
View Journal

Cite this: DOI: 10.1039/c9cc01747j

Received 3rd March 2019,
Accepted 3rd April 2019

DOI: 10.1039/c9cc01747j

rsc.li/chemcomm

Photocontrolled endogenous reactive oxygen species (ROS) generation†

Ajay Kumar Sharma, Harshit Singh and Harinath Chakrapani *

A cell-permeable small molecule for light-triggered generation of endogenous reactive oxygen species (ROS) is reported.

Oxygen and its reduced forms such as superoxide ($O_2^{\bullet -}$), hydrogen peroxide (H_2O_2) and hydroxyl radicals are generated during the normal functioning of cells (Fig. 1).[1] A number of intrinsic mechanisms have evolved to attenuate these reactive oxygen species (ROS) levels.[2,3] Elevated levels of ROS generated in cells are associated with numerous pathophysiological conditions including cancer, inflammation, diabetes and several neurodegenerative disorders.[4–6] ROS are also deployed in immune response to counter pathogens.[7] Elevation of endogenous ROS levels has been associated with inhibition of cancer growth both *in vitro* and in animal models.[8–12] For example, piperlongumine has been shown to enhance ROS within cells[13–18] but the precise mechanism by which this occurs is yet unclear and would be critical to determine. Due to its short life, $O_2^{\bullet -}$ must be produced *in situ* by reaction with oxygen and an electron donor.[19] Either small organic molecules that spontaneously react with oxygen or enzymatic methods that turn over a substrate to generate $O_2^{\bullet -}$ are frequently used. A combination of hypoxanthine and xanthine oxidase (X + XO), where hypoxanthine is metabolized by XO to produce $O_2^{\bullet -}$, predominantly produces $O_2^{\bullet -}$ in the proximity of cells. Any $O_2^{\bullet -}$ that is produced must diffuse across a lipid bilayer to exert its effects. However, $O_2^{\bullet -}$ is not highly permeable at neutral pH, and hence, this protocol and other small-molecule based methods may not be useful for enhancing intracellular ROS levels. A number of bioreductively-activated ROS generators are known and they have been evaluated previously for their cancer therapeutic potential.[20–23] Although triggered by a bioreductive enzyme, these compounds have little spatiotemporal control over ROS production. Paraquat, a quaternary amine or menadione, which require bioactivation for $O_2^{\bullet -}$ production,[20,21] have often been used but at elevated concentrations that can potentially complicate mechanistic interpretations. Furthermore, their reactivity with biological thiols leading to covalent modification is also a major concern. Hartley and coworkers developed a mitochondria-specific ROS generator, MitoPQ, a paraquat derivative.[24] This strategy allows for organelle-specific generation of ROS. Since light as a tool for activation offers spatiotemporal control,[25–33] photocleavable ROS generators are expected to have significant advantages. Chang and co-workers reported a light-triggerable ROS generator that is based on hydroxyquinol.[30] This compound responds to light at a wavelength of 305 nm, which is not desirable. Furthermore, the yield of hydrogen peroxide from this compound was somewhat diminished. Here, we report the design, synthesis and evaluation of a light-triggered endogenous ROS generator.

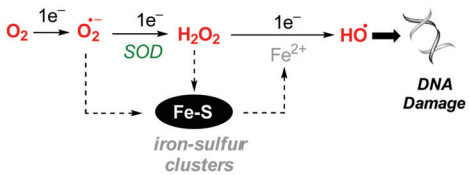

Fig. 1 Endogenous ROS and some of their effects within cells.

Our laboratory has previously reported **1**,[34] which is a derivative of juglone, as a ROS generator (Scheme 1). The proposed mechanism for ROS generation was enolization of the carbonyl as the first step, followed by generation of a 1,4-diol. Its diolate is electron-rich and is known to produce superoxide. We found that attaching a 4-nitrobenzyl group resulted in diminished ROS generation.[35] We also found that triggering with nitroreductase, an enzyme that is present in bacteria, enhanced ROS generation.[35] Thus, this strategy enabled triggerable and localized ROS production.[36] Recently, we reported an esterase-activated ROS generator that was able to elevate ROS levels within mammalian cells (Scheme 1).[36] Here, we report the design, synthesis and evaluation of a light-triggerable ROS generator.

Department of Chemistry, Indian Institute of Science Education and Research Pune, Pune 411 008, Maharashtra, India. E-mail: harinath@iiserpune.ac.in

† Electronic supplementary information (ESI) available. See DOI: 10.1039/c9cc01747j

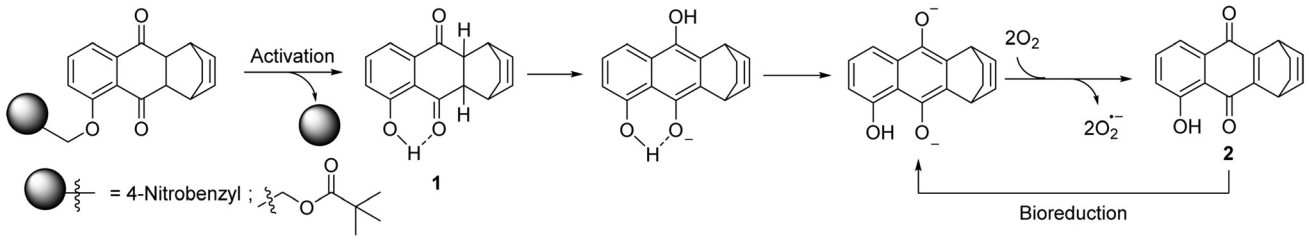

Scheme 1 General strategy for generation of compound **1** after photocleavage. Compound **1** generates superoxide during incubation in buffer under ambient aerobic conditions to produce quinone **2**, which can further generate ROS through redox cycling. The 4-nitrobenzyl derivative is a substrate for nitroreductase, while the pivaloyloxymethyl compound is triggered by esterase. The proposed substrate for photocleavage has a 2-nitroaryl functional group, which is expected to undergo deprotection to produce the ROS generator **1** (see Table 1).

The 2-nitrobenzyl functional group has been widely used as a protective group for alcohols.[26–28,37] Upon irradiation, this photo-cleavable group releases an alcohol (Scheme 1). This strategy was used by Chang and co-workers to release the 1,4-diol.[30] The yields of ROS were low possibly due to the poor efficiency of cleavage and, perhaps, low ROS generation capability. Lastly, aqueous solubility and cancer cell uptake may play major roles in determining the efficiency of ROS generation within cells. Thus, the ROS generator must have a synthetic handle to incorporate additional functional groups (such as biotin).[38–40]

Bromides **5a** and **5b** were commercially obtained and independently reacted with **1**, resulting in the formation of compounds **4a** and **4b** (Table 1, entries 1 and 2). In the case of the reaction of the dimethoxy electrophile **5b**, the formation of the *C*-alkylated product (**6**) was observed. It is likely that a phenolate intermediate is formed, which can then react *via* the oxygen or the carbon to produce the *O*-alkylated or *C*-alkylated products. We next synthesized bromide **5c**, which has a propargyl group. This alkyne should provide opportunities to conjugate biotin through the copper-catalyzed alkyne–azide click reaction. However, under the conditions we used, we found no reaction between **5c** and **1** (Table 1, entry 3). Activation of the bromide by silver ions is an important step in the substitution reaction. It is likely that the alkyne coordinates with the silver ions and competes with activation of the bromide. We therefore revised our strategy and we first synthesized bromide **5d**, which has an azide that can be utilized for orthogonal conjugation (Scheme S1 in the ESI†), and it was reacted with **1** to afford the corresponding azide **4d** in 25% yield. The desired conjugate **4e** was next synthesized by reacting **4d** with the biotin-alkyne derivative **12** (Fig. 2A and Scheme S2 in the ESI†).

Next, the stability of the derivatives was evaluated. In the dark, we found no evidence for the decomposition of these compounds in a pH 7.4 buffer. To evaluate the photocleavage efficiency, **4a**, **4b** and **4e** were irradiated with 365 nm light and HPLC analysis revealed complete cleavage within 15 min. This cleavage resulted in the formation of **1**, a known ROS generator (Fig. 3A and Fig. S2 in the ESI†). As previously reported, **1** reacts with oxygen and produces $O_2^{\bullet-}$, which disproportionates to form H_2O_2,[34] another ROS. To validate the generation of $O_2^{\bullet-}$ during the incubation of **4e**, this compound was irradiated and a dihydroethidium (DHE, see the ESI†) assay was used. The DHE dye reacts with $O_2^{\bullet-}$ and other ROS (H_2O_2, OH) to form 2-hydroxy ethidium (2-OH-E^+) and ethidium (E^+), respectively (Scheme S4 in the ESI†), which can be detected by HPLC analysis.[41] When **4e** was incubated in the presence of light under the assay conditions, HPLC analysis revealed a peak at 29.5 min, which corresponds to 2-hydroxy ethidium (2-OH-E^+). This signal decreased when the solution was treated with superoxide dismutase, a known quencher of $O_2^{\bullet-}$. When this experiment was conducted in the dark, no peak for 2-OH-E^+ was observed (Fig. 3B). This observation supports the generation of $O_2^{\bullet-}$ by **4e** only in the presence of light. This assay was also performed with **4a** and **4b** and similar results were obtained (Fig. S3 in the ESI†).

Table 1 Reaction of bromides with **1**

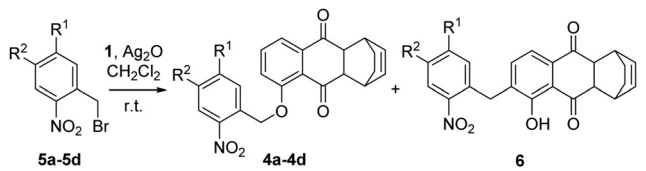

Entry	Bromide	R^1	R^2	Product(s)	Yield(s) (%)
1	**5a**	H	H	**4a**	55
2	**5b**	OMe	OMe	**4b** & **6**	30 & 11
3	**5c**	OMe	*O*-Propargyl	**4c**	—
4	**5d**	OMe	$OCH_2CH_2N_3$	**4d**	25

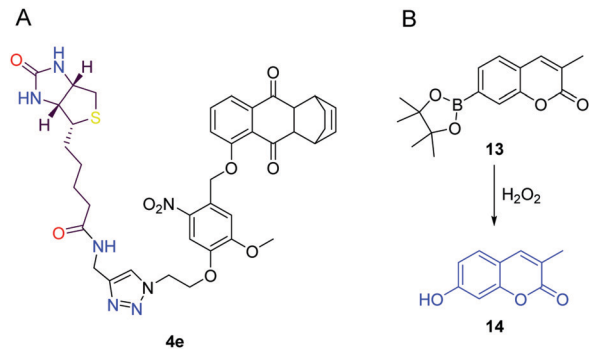

Fig. 2 (A) Structure of biotinylated adduct **4e**. (B) Reaction of hydrogen peroxide with coumarin boronate-ester dye **13**. The boronate ester **13** is weakly fluorescent, and upon oxidation, a turn on fluorescence is observed due to the formation of **14**.

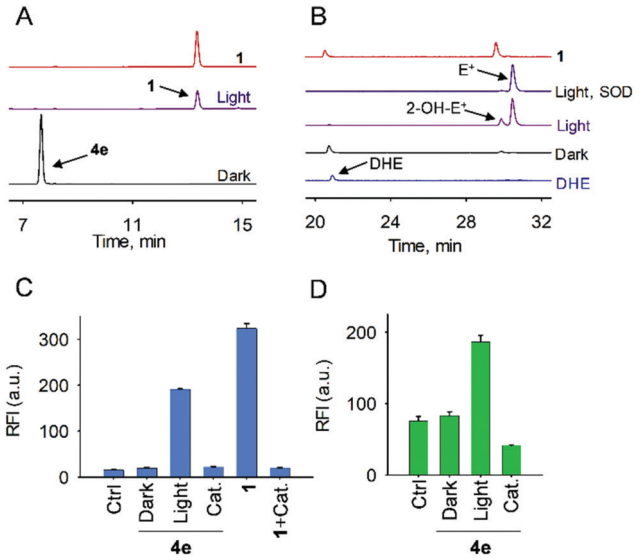

Fig. 3 Photolysis and ROS analysis of **4e**. (A) HPLC traces of **4e** (50 μM) in the presence and absence of light. Light irradiation was performed with 365 nm light for 15 min with 30 mW cm^{-2} intensity. (B) HPLC traces of DHE assay for superoxide detection; **4e** (25 μm) was irradiated with 30 mW cm^{-2} 365 nm light for 15 min followed by addition of DHE and incubated for 1 h; as a control, SOD was used for quenching the superoxide. (C) Hydrogen peroxide detection using the dye coumarin-boronate ester **13** as a probe (excitation 320 nm; emission 460 nm). (D) Hydrogen peroxide detection using Amplex Red assay; **4e** (25 μM) was irradiated with 365 nm light for 15 min and incubated for 2 h (cat. = catalase enzyme). Data represent the means ± s.d. for 3 technical replicates per group.

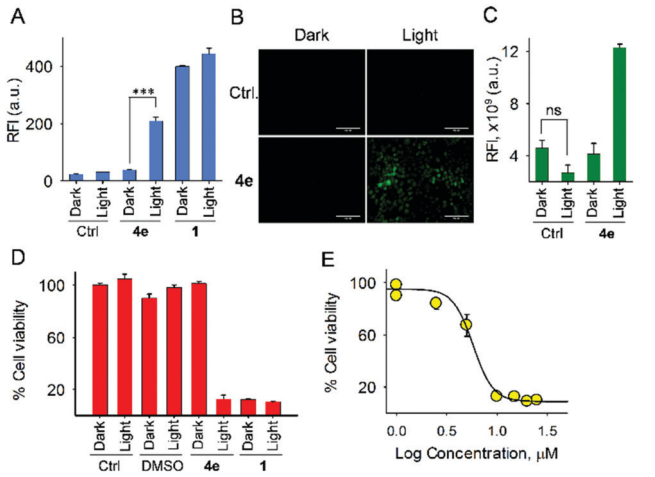

Fig. 4 Cellular assays. (A) Extracellular hydrogen peroxide detection by Amplex Red assay (excitation 550 nm; emission 590 nm; ***$p < 0.0001$). (B and C) Intracellular ROS detection using H_2DCF-DA as a probe; scale bar = 200 μm and ns = not significant. (D) Cell viability assay using A549 cells with 10 μM compounds. (E) Growth inhibition curve after irradiation with **4e** and IC_{50} was found to be 5.8 μM. Data represent the means ± s.e.m. for 3 technical replicates per group.

The radical anion $O_2^{\bullet-}$ disproportionates to form H_2O_2. We next assessed the production of H_2O_2 using two independent assays. First, the oxidation of fluorogenic boronic acids/esters has been frequently used to detect the presence of hydrogen peroxide.[42,43] The non-fluorescent coumarin based dye **13** reacts with H_2O_2 to form umbelliferone derivative **14**, a highly fluorescent molecule (Fig. 2B).

Irradiated and non-irradiated samples of **4e** were independently incubated with dye **13** and fluorescence enhancement was found only in the irradiated sample (Fig. 3C). This fluorescence signal was diminished in the presence of catalase, a known quencher of H_2O_2. This study was also performed with compounds **4a** and **4b**, and as expected, fluorescence enhancement was observed in the irradiated samples (Fig. S4 in the ESI†). These results suggest that the production of H_2O_2 by **4e** occurred only in the presence of light. Next, an Amplex Red assay was used to infer the production of H_2O_2. Again, irradiated and non-irradiated samples of **4e** were independently treated with Amplex Red solution containing horseradish peroxidase (HRP) enzyme and it was found that an enhanced fluorescence signal was observed only in the irradiated sample. This signal was diminished in the presence of catalase (Fig. 3D). Taken together, our results support the ability of **4e** to undergo photocleavage to produce ROS.

Next, this compound was evaluated as an endogenous ROS generator in cells after activation with light. First, generation of extracellular H_2O_2 was assessed using coumarin based dye **13** and Amplex Red in lung carcinoma A549 cells, and it was found that **4e** was able to generate H_2O_2 extracellularly only in the presence of light. However, no ROS enhancement was observed in cells only in the presence of light and cells treated with **4e** in the dark (Fig. 4A and Fig. S5 in the ESI†).

Further evaluation of intracellular ROS was also done using a cell permeable weakly fluorescent ROS responsive dye, 2′,7′-dichlorodihydrofluorescein diacetate (H_2DCF-DA), which upon reaction with ROS forms a highly fluorescent molecule, 2′,7′-dichlorodihydrofluorescein (DCF), and its fluorescence intensity can be measured using a well plate reader. This assay was performed in A549 cells and it was found that cells treated with **4e** had enhanced ROS levels in the presence of light when compared with a similar treatment in the dark (Fig. 4B and C). In addition, ROS enhancement was not observed when cells without **4e** were irradiated, suggesting that 365 nm UV light alone does not enhance the ROS level in cells. This study suggests that **4e** is cell permeable and elevates the ROS level only after irradiation with light.

Elevated levels of ROS can damage essential biomolecules, leading to oxidative stress, which in turn can result in cell death. In order to test the hypothesis, cell viability assay was conducted using A549 and DLD-1 cell lines. Under the assay conditions, in the presence of **4e**, no significant inhibition of growth was observed in the dark even at 50 μM (Fig. S7 and S9 in the ESI†). When this experiment was conducted with cells that were irradiated (30 mW cm^{-2} intense 365 nm light, 5 min), nearly complete inhibition of growth of these cells was observed at 10 μM (Fig. 4D and Fig. S8 in the ESI†). The inhibitory concentration 50% (IC_{50}) of **4e** in the presence of light was found to be 5.8 μM (Fig. 4E). Similarly, in DLD-1 cells, no significant inhibition was observed in the dark, while potent inhibitory effects were observed during irradiation (IC_{50} = 5.3 μM) (Fig. S8 and S9 in the ESI†).

Recently, the ROS generation capability of **1** was compared with those of various other probes. A major drawback of several ROS generators is their inherent reactivity with thiols. For example, menadione and Juglone react with glutathione (Fig. S10 in the ESI†). However, with **1** and the oxidized form of **1**, *i.e.* **2**, we found no evidence for reaction with glutathione even after incubation for several hours (Fig. S10 in the ESI†). The reason for negligible reactivity with glutathione might be the absence of an α,β-unsaturated site in **1**, whereas this site could be sterically inaccessible in **2**. Hence, this ROS generator has advantages over other ROS generators such as menadione since it allows us to study the effects of ROS without complications associated with covalent modification. Furthermore, the improved aqueous solubility of **4e** presents opportunities for the wide applicability of this compound as a ROS generator.

Taken together, our results suggest the use of this compound for photolabile ''turn on'' ROS generation and overexpression of biotin receptors in cancer cells may provide an opportunity to selectively target tumour cells.[38–40] As a cancer therapeutic, singlet oxygen has been used;[44] however, examples of the use of other biological ROS are fewer.[45] The ability to conjugate this ROS generator with directing groups enhances the versatility of this tool.

This work was supported by the Department of Biotechnology, India (Grant number: BT/PR17514/BRB/10/1615/2017), and the Council for Scientific and Industrial Research (Fellowship award number: 09/936(0110)/2014-EMR-I). The authors thank Ms Preeti Chauhan, IISER Pune, for help with setting up cellular assays and Mr Rafeeque Mavoor, Science media Centre, IISER Pune, for support with the table of content image.

Conflicts of interest

There are no conflicts to declare.

Notes and references

1 M. Schieber and N. S. Chandel, *Curr. Biol.*, 2014, **24**, R453–R462.
2 S. B. Nimse and D. Pal, *RSC Adv.*, 2015, **5**, 27986–28006.
3 J.-M. Lü, P. H. Lin, Q. Yao and C. Chen, *J. Cell. Mol. Med.*, 2010, **14**, 840–860.
4 B. Uttara, A. Singh, P. Zamboni and R. Mahajan, *Curr. Neuropharmacol.*, 2009, **7**, 65–74.
5 Z. Liu, T. Zhou, A. C. Ziegler, P. Dimitrion and L. Zuo, *Oxid. Med. Cell. Longev.*, 2017, 1–11.
6 G. H. Kim, J. E. Kim, S. J. Rhie and S. Yoon, *Exp. Neurobiol.*, 2015, **24**, 325.
7 Y. Yang, A. V. Bazhin, J. Werner and S. Karakhanova, *Int. Rev. Immunol.*, 2013, **32**, 249–270.
8 J. Wang and J. Yi, *Cancer Biol. Ther.*, 2008, **7**, 1875–1884.
9 J. P. Fruehauf and F. L. Meyskens, *Clin. Cancer Res.*, 2007, **13**, 789–794.
10 S. Suzuki, M. Higuchi, R. J. Proske, N. Oridate, W. K. Hong and R. Lotan, *Oncogene*, 1999, **18**, 6380–6387.
11 D. J. Adams, Z. V. Boskovic, J. R. Theriault, A. J. Wang, A. M. Stern, B. K. Wagner, A. F. Shamji and S. L. Schreiber, *ACS Chem. Biol.*, 2013, **8**, 923–929.
12 A. T. Dharmaraja, *J. Med. Chem.*, 2017, **60**, 3221–3240.
13 J.-L. Roh, E. H. Kim, J. Y. Park, J. W. Kim, M. Kwon and B.-H. Lee, *Oncotarget*, 2014, **5**, 9227–9238.
14 K. Karki, E. Hedrick, R. Kasiappan, U.-H. Jin and S. Safe, *Cancer Prev. Res.*, 2017, **10**, 467–477.
15 H. Dhillon, S. Chikara and K. M. Reindl, *Toxicol. Rep.*, 2014, **1**, 309–318.
16 X. Xu, X. Fang, J. Wang and H. Zhu, *Bioorg. Med. Chem. Lett.*, 2017, **27**, 1325–1328.
17 W.-J. Yan, Q. Wang, C.-H. Yuan, F. Wang, Y. Ji, F. Dai, X.-L. Jin and B. Zhou, *Free Radical Biol. Med.*, 2016, **97**, 109–123.
18 L.-H. Gong, X.-X. Chen, H. Wang, Q.-W. Jiang, S.-S. Pan, J.-G. Qiu, X.-L. Mei, Y.-Q. Xue, W.-M. Qin, F.-Y. Zheng, Z. Shi and X.-J. Yan, *Oxid. Med. Cell. Longev.*, 2014, 906804.
19 M. Hayyan, M. A. Hashim and I. M. AlNashef, *Chem. Rev.*, 2016, **116**, 3029–3085.
20 D. N. Criddle, S. Gillies, H. K. Baumgartner-Wilson, M. Jaffar, E. C. Chinje, S. Passmore, M. Chvanov, S. Barrow, O. V. Gerasimenko, A. V. Tepikin, R. Sutton and O. H. Petersen, *J. Biol. Chem.*, 2006, **281**, 40485–40492.
21 D. M. Frank, P. K. Arora, J. L. Blumer and L. M. Sayre, *Biochem. Biophys. Res. Commun.*, 1987, **147**, 1095–1104.
22 V. S. Khodade, M. Sharath Chandra, A. Banerjee, S. Lahiri, M. Pulipeta, R. Rangarajan and H. Chakrapani, *ACS Med. Chem. Lett.*, 2014, **5**, 777–781.
23 M. A. Silvers, S. Deja, N. Singh, R. A. Egnatchik, J. Sudderth, X. Luo, M. S. Beg, S. C. Burgess, R. J. DeBerardinis, D. A. Boothman and M. E. Merritt, *J. Biol. Chem.*, 2017, **292**, 18203–18216.
24 E. L. Robb, J. M. Gawel, D. Aksentijević, H. M. Cochemé, T. S. Stewart, M. M. Shchepinova, H. Qiang, T. A. Prime, T. P. Bright, A. M. James, M. J. Shattock, H. M. Senn, R. C. Hartley and M. P. Murphy, *Free Radical Biol. Med.*, 2015, **89**, 883–894.
25 P. Klán, T. Šolomek, C. G. Bochet, A. Blanc, R. Givens, M. Rubina, V. Popik, A. Kostikov and J. Wirz, *Chem. Rev.*, 2013, **113**, 119–191.
26 S. Chalmers, S. T. Caldwell, C. Quin, T. A. Prime, A. M. James, A. G. Cairns, M. P. Murphy, J. G. McCarron and R. C. Hartley, *J. Am. Chem. Soc.*, 2012, **134**, 758–761.
27 M. J. Hansen, W. A. Velema, M. M. Lerch, W. Szymanski and B. L. Feringa, *Chem. Soc. Rev.*, 2015, **44**, 3358.
28 Y. V. Il'ichev, M. A. Schwö and J. Wirz, *J. Am. Chem. Soc.*, 2004, **126**, 4581–4595.
29 A. K. Sharma, M. Nair, P. Chauhan, K. Gupta, D. K. Saini and H. Chakrapani, *Org. Lett.*, 2017, **19**, 4822–4825.
30 E. W. Miller, N. Taulet, C. S. Onak, E. J. New, J. K. Lanselle, G. S. Smelick and C. J. Chang, *J. Am. Chem. Soc.*, 2010, **132**, 17071–17073.
31 Y. Li, Y. Shu, M. Liang, X. Xie, X. Jiao, X. Wang and B. Tang, *Angew. Chem., Int. Ed.*, 2018, **57**, 12415–12419.
32 Y. Iwamoto, M. Kodera and Y. Hitomi, *Chem. Commun.*, 2015, **51**, 9539–9542.
33 X. Xie, J. Fan, M. Liang, Y. Li, X. Jiao, X. Wang and B. Tang, *Chem. Commun.*, 2017, **53**, 11941–11944.
34 A. T. Dharmaraja, M. Alvala, D. Sriram, P. Yogeeswari and H. Chakrapani, *Chem. Commun.*, 2012, **48**, 10325–10327.
35 A. T. Dharmaraja and H. Chakrapani, *Org. Lett.*, 2014, **16**, 398–401.
36 D. S. Kelkar, G. Ravikumar, N. Mehendale, S. Singh, A. Joshi, A. K. Sharma, A. Mhetre, A. Rajendran, H. Chakrapani and S. S. Kamat, *Nat. Chem. Biol.*, 2019, **15**, 169–178.
37 A. Patchornik, B. Amit and R. B. Woodward, *J. Am. Chem. Soc.*, 1970, **92**, 6333–6335.
38 S. Luo, V. S. Kansara, X. Zhu, N. K. Mandava, D. Pal and A. K. Mitra, *Mol. Pharmaceutics*, 2006, **3**, 329–339.
39 W. X. Ren, J. Han, S. Uhm, Y. J. Jang, C. Kang, J.-H. Kim and J. S. Kim, *Chem. Commun.*, 2015, **51**, 10403–10418.
40 T. Kim, H. M. Jeon, H. T. Le, T. W. Kim, C. Kang and J. S. Kim, *Chem. Commun.*, 2014, **50**, 7690.
41 H. Zhao, J. Joseph, H. M. Fales, E. A. Sokoloski, R. L. Levine, J. Vasquez-Vivar and B. Kalyanaraman, *Proc. Natl. Acad. Sci. U. S. A.*, 2005, **102**, 5727–5732.
42 E. W. Miller, A. E. Albers, A. Pralle, E. Y. Isacoff and C. J. Chang, *J. Am. Chem. Soc.*, 2005, **127**, 16652–16659.
43 V. S. Khodade, A. Kulkarni, A. Sen Gupta, K. Sengupta and H. Chakrapani, *Org. Lett.*, 2016, **18**, 1274–1277.
44 P. Agostinis, K. Berg, K. A. Cengel, T. H. Foster, A. W. Girotti, S. O. Gollnick, S. M. Hahn, M. R. Hamblin, A. Juzeniene, D. Kessel, M. Korbelik, J. Moan, P. Mroz, D. Nowis, J. Piette, B. C. Wilson and J. Golab, *Ca-Cancer J. Clin.*, 2011, **61**, 250–281.
45 A. N. Onyango, *Oxid. Med. Cell. Longevity*, 2016, 2398573.

Organic LETTERS

Letter

pubs.acs.org/OrgLett

Visible-Light-Triggered Uncaging of Carbonyl Sulfide for Hydrogen Sulfide (H_2S) Release

Ajay Kumar Sharma,[†] Mrutyunjay Nair,[†] Preeti Chauhan,[†] Kavya Gupta,[‡] Deepak K Saini,[‡] and Harinath Chakrapani*[,†]

[†]Department of Chemistry, Indian Institute of Science Education and Research Pune, Dr. Homi Bhabha Road, Pashan, Pune 411 008, Maharashtra, India

[‡]Department of Molecular Reproduction, Development and Genetics, Indian Institute of Science, Bangalore, Karnataka, India

Supporting Information

ABSTRACT: Generation of hydrogen sulfide (H_2S) is challenging and few methods are capable of localized delivery of this gas. Here, a boron dipyrromethene-based carbamothioate (BDP-H_2S) that is uncaged by visible light of 470 nm to generate carbonyl sulfide (COS), which is rapidly hydrolyzed to H_2S in the presence of carbonic anhydrase, a widely prevalent enzyme, is reported.

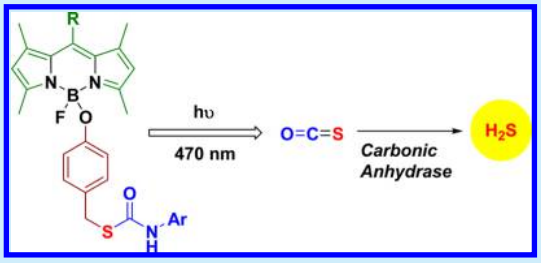

Gaseous species derived from carbon, nitrogen, and sulfur are emerging as major mediators of cellular processes. Some have been termed as "gasotransmitters", which are small gaseous molecules that can act as signal transmitting agents within cells as well as across cells. For example, hydrogen sulfide (H_2S) is known to mediate a number of physiological processes.[1] Due to its highly diffusible nature and multiple targets within cells, cell signaling by H_2S is often complex and can depend on local concentrations of this species.[2,3] This underscores the need for spatiotemporally controlled generation of this gas under ambient conditions. A number of donors of H_2S with varying degrees of control over release of H_2S are known.[4,5] Among these, light-triggered donors have distinct advantages for localized delivery.[6−8] On account of the ability to direct the light source, generation of H_2S in a spatially controlled manner is possible. Although small molecule-based light-triggered H_2S generation methodologies are known, they all are based on ultraviolet light. For example, Xian and co-workers have reported a 2-nitrobenzyl-based donor that when exposed to 365 nm light produces a geminal dithiol, which undergoes hydrolysis to generate H_2S (Figure 1a). Nakagawa and co-workers have reported two scaffolds based on thioethers that are triggered by UV light to produce H_2S (Figure 1a).[7,8] More recently, Connal and co-workers have reported photogenerated thiobenzaldehydes as H_2S donors.[9] While these methods offer excellent spatiotemporal control, the phototoxicity associated with UV light is a major limitation.[10] Thus, a method for photouncaging of a H_2S source under ambient visible light conditions is yet unavailable.

Recently, 4-arylalkoxy-boron dipyrromethene (4-OAr-BODIPY)[11] has been used to deliver histamine, an important mediator of inflammation and allergy.[12] Our group[13] and others[14−17] have shown that carbonyl sulfide (COS)[18] is an excellent donor of H_2S. The gas COS is known to undergo rapid hydrolysis in the presence of the widely occurring enzyme carbonic anhydrase (CA),[19] to produce H_2S. Pluth and co-workers have recently reported a UV light activated COS/H_2S

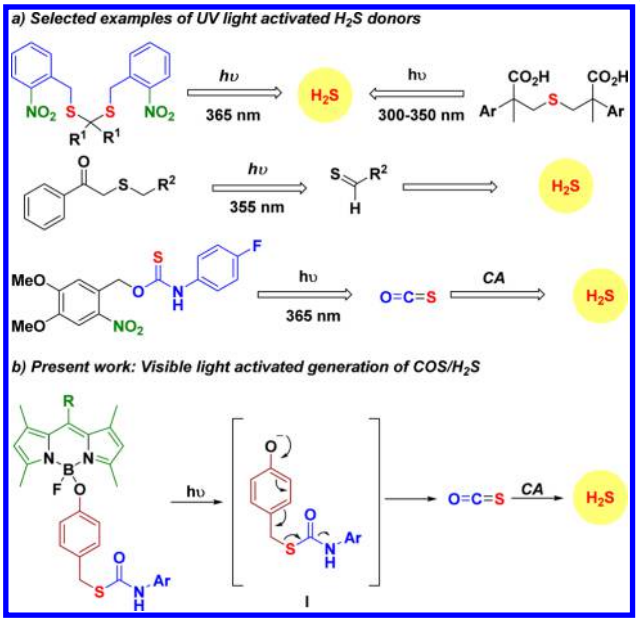

Figure 1. (a) Selected UV-light-activated methodologies for H_2S generation R^1 = various alkyl groups; Ar = PhCOPh; R^2 = aryl group. (b) Design of a visible light-triggered COS/H_2S donor. Visible-light-mediated cleavage of the B−O bond produces an intermediate **I** that undergoes self-immolation to generate COS that undergoes hydrolysis in the presence of CA to generate H_2S.

Received: July 23, 2017
Published: September 5, 2017

DOI: 10.1021/acs.orglett.7b02259
Org. Lett. 2017, 19, 4822−4825

Scheme 1. Synthesis of H_2S Donor 1

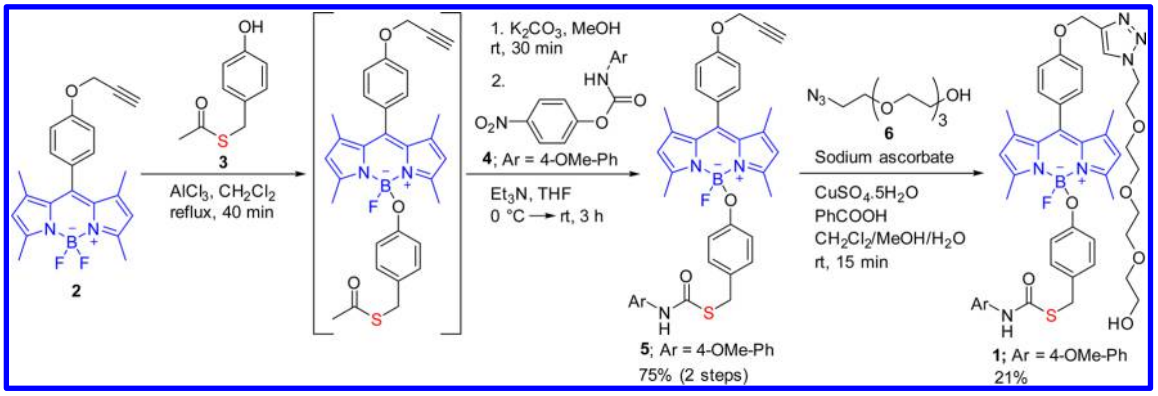

donor (Figure 1a).[20] Again, the potential for phototoxicity due to prolonged UV exposure may be a limitation of this method. Therefore, masking COS in the form of a carbamothioate with attachment of this functional group to a BODIPY-based photolabile group was considered (Figure 1b). Upon exposure to visible light, this compound is expected to undergo cleavage to produce COS/H_2S.

Compound **2** (Scheme 1) was first synthesized using a reported methodology (see Supporting Information (SI)).[21] Next, 4-*S*-(hydroxybenzyl) ethanethioate **3** was prepared, and reaction of **3** with **2** in the presence of a Lewis acid $AlCl_3$ gave a thioacetate (crude) as an intermediate, which was subsequently hydrolyzed to the corresponding thiol (not isolated). Reaction of the crude thiol with the 4-nitrophenylcarbamate **4** gave **5** in 75% yield over two steps. Due to the increased hydrophobicity associated with BODIPY derivatives, incorporation of a short oligo-ethylene glycol functional group that should increase aqueous solubility was considered. Using a copper-mediated click reaction, the desired compound, BDP-H_2S **1**, was prepared in 21% yield.

Using a reported method, BDP-H_2S was incubated in MeOH and exposed to 470 nm light for 20 min. HPLC analysis (detection wavelength, 500 nm) revealed nearly complete decomposition of **1** (Figure 2a; also see Figure S1, SI). Urano and co-workers have reported that uncaging of the 4-aryloxy-BODIPY derivative[12] is accomplished by a photoinduced electron transfer (PeT)[22,23] process that results in the formation of a charge-separated intermediate, involving a cation radical of the aryloxy group and the anion radical of BODIPY. This results in the cleavage of the B−O bond by solvolysis, and the expected product in methanol is the B−OMe derivative. The time course of decomposition of **1** was studied, and a first-order rate constant of 0.16 min^{-1} was obtained (Figure 2b). During photolysis of **1**, HPLC analysis revealed the formation of a new product (Figure 2a), which was characterized by mass spectrometry as the methoxy-derivative **7** (Figure 2d, Figure S5, SI). The time course for formation of **7** gave a first order rate constant of 0.20 min^{-1} (Figure 2b). Together, these data suggest cleavage of **1** is accompanied by rapid solvolysis to produce **7**.

When photolysis of **1** was monitored by HPLC attached with a fluorescence detector, a distinct peak attributable to **7** was formed (see SI, Figure S2). Thus, photocleavage of **1**, a weakly fluorescent compound, in methanol produces **7**, which is highly fluorescent (excitation 470 nm, emission 540 nm).

This enhancement in fluorescence is attributable to the differences in the quenching ability of the O-aryl group in **1**

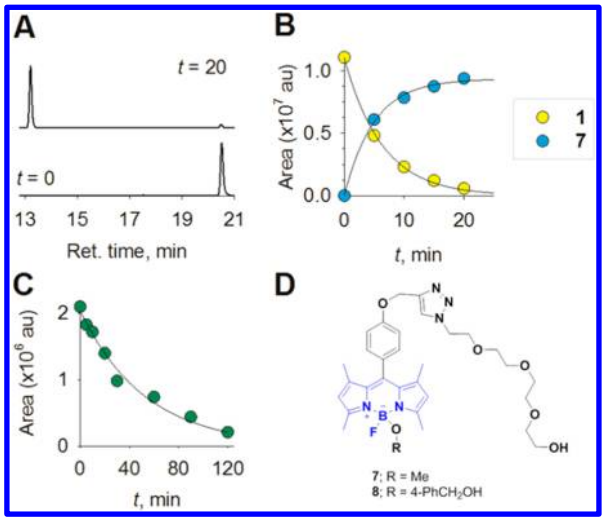

Figure 2. (a) HPLC traces for **1** before and after irradiation with 470 nm light (30 mW/cm^2) for 20 min in MeOH showed nearly complete disappearance of **1** with concomitant formation of an intermediate at retention time of 13.2 min, which was later identified by mass spectrometry analysis as BDP-OMe (**7**). (b) Time course of disappearance of **1** and formation of intermediate **7** during the same time period was determined by HPLC analysis. Curve fitting yielded first-order rate constants for disappearance of **1** as 0.16 min^{-1} and formation of **7** as 0.20 min^{-1}. (c) Time course of disappearance of intermediate **I** was followed by HPLC analysis. The rate constant for decomposition was found as 0.02 min^{-1}, (d) Proposed structure of the intermediate **7** produced during photolysis of **1** in methanol and the negative control **8**.

when compared with the OMe group in **7**. In a separate experiment, the fluorescence enhancement was monitored by a microwell plate reader and the fluorescence enhancement after irradiation was >20-fold (Figure 3a). In order to test whether this fluorescence enhancement also occurred within cells, human cervical cancer HeLa cells were incubated with **1** for 2 min followed by imaging using a fluorescence microscope. A small fluorescence signal at 540 nm (excitation 470 nm) was seen under these conditions (Figure 3b, dark). However, when HeLa cells pretreated with **1** were irradiated with a 470 nm light source for 2 min, and subsequent fluorescence enhancement was studied by microscopy, a significant enhancement in fluorescence signal was recorded (Figure 3b and 3c, light versus dark).

A cell viability assay was next conducted to assess the cytotoxicity during photocleavage of **1**. HeLa cells were independently incubated with **1** at various concentrations,

DOI: 10.1021/acs.orglett.7b02259
Org. Lett. 2017, 19, 4822−4825

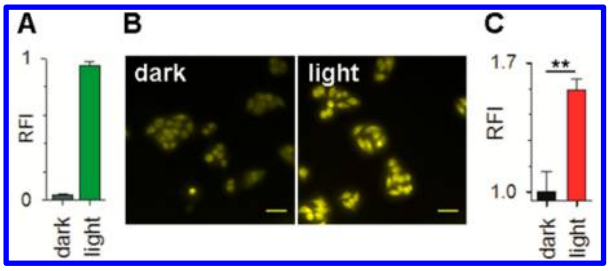

Figure 3. (a) Enhancement in fluorescence (excitation 470 nm, emission 540 nm) when **1** (50 μM) was irradiated with 470 nm light; (b) HeLa cells pretreated with **1** (10 μM) were irradiated for 2 min by 470 nm light and imaging showed increased fluorescence signal (YFP channel); Scale bar = 50 μm (c) Fluorescence enhancement data for the cellular experiment. **p-value = 0.002.

and these cells were exposed to 470 nm light for 5 min. We found no evidence for inhibition of proliferation of HeLa cells by **1** during photocleavage suggesting that this compound was not cytotoxic (Figure 4). The compound itself was not toxic in the dark (Figure S9a), and the absorbance at 570 nm from this compound was not significant (Figure S9b).

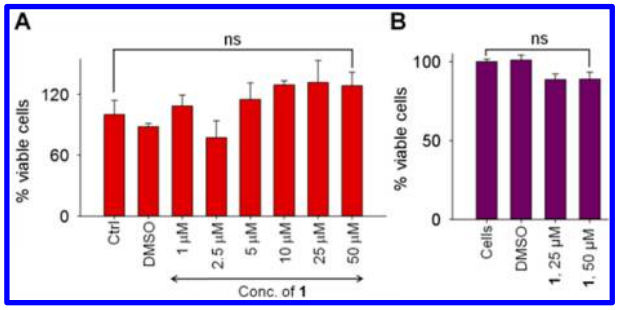

Figure 4. Effect of **1** on cell viability was determined by two independent assays: (a) HeLa cells with increasing doses of **1** followed by irradiation with 470 nm light for 5 min (24 h incubation, MTT assay). (b) A549 cells with increasing doses of **1** followed by irradiation with 470 nm light for 5 min (24 h incubation, crystal violet assay). The differences in viability are not significant (ns) as determined by Student's t-test.

A crystal violet assay was independently conducted using the A549 human lung cancer cell line to validate our results: the compound was not significantly cytotoxic (Figure 4b). Together, these results indicate that **1** is nontoxic, is cell permeable, and can be cleaved by a visible light source within cells to generate a fluorescence signal.

Cleavage of the B−O bond results in the formation of a phenolate-intermediate **I**, which has been previously reported to generate COS (Scheme 2).[13] The time course of decomposition of **I** was monitored in pH 7.4 buffer (see Figure S3, SI), and this intermediate disappeared within 2 h (Figure 2c). The rate constant for decomposition was found to be 0.02 min^{-1}. In the presence of carbonic anhydrase (CA), COS is known to generate H_2S (Scheme 2). In order to test this hypothesis, **1** was irradiated using visible light at 470 nm in methanol and the resulting mixture was incubated in pH 7.4 buffer in the presence of CA. The formation of H_2S was monitored by a methylene blue assay. If H_2S were produced, a characteristic UV−visible absorption spectrum with absorption maxima at 676 nm would be expected.

When this experiment was conducted, as predicted, an increase in absorption at 676 nm confirming the ability of **1** to

Scheme 2. Proposed Mechanism for H_2S Generation during Photocleavage of BDP-H_2S 1 in Methanol Followed by Incubation in pH 7.4 Buffer[a]

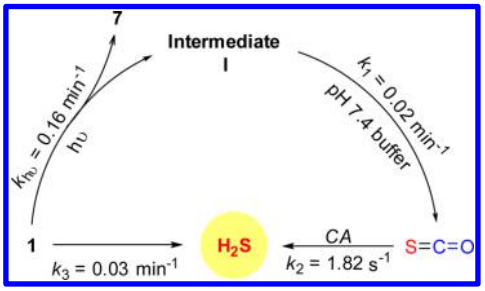

[a]For further details, see Scheme S2, SI.

produce H_2S was observed (Figure 5a). In the absence of CA or when incubated in the dark, **1** was incapable of generating H_2S

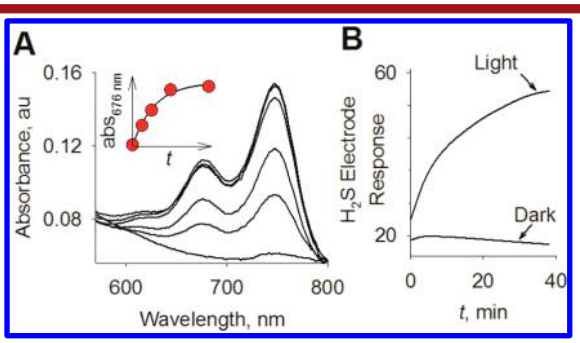

Figure 5. (a) A methylene blue formation assay was used to determine H_2S release from **1** when irradiated with 470 nm light for 25 min followed by exposure to carbonic anhydrase in pH 7.4 buffer. Inset, time course of increase in absorbance at 676 nm during 2 h. Curve fitting to a pseudo-first-order release gave a rate constant of 0.03 min^{-1} (see SI). (b) H_2S generation during incubation of **1** after irradiation with visible light followed by exposure to CA in pH 7.4 buffer was assessed by a H_2S-sensitive electrode. Dark: A similar experiment was conducted in the absence of light.

in 2 h (Figure S6, SI). The time course of H_2S release showed a gradual increase over 2 h (Figure 5a, inset). The rate constant for H_2S release was found to be 0.03 min^{-1}, which is comparable with the disappearance of intermediate **I** (Figure 2c). The yield of H_2S was found to be in the range 30%−40%; this efficiency is comparable with the previously reported photouncaging of histamine that produced a similar yield of the amine.[12]

Next, a H_2S-sensitive electrode was used to independently verify the generation of H_2S from **1**. Here, the irradiated sample of **1** in methanol was incubated in pH 7.4 buffer in the presence of CA and H_2S generation was monitored by the electrode. As expected, a distinct signal attributable to H_2S was recorded (Figure 5b). No detectable signal was observed when the donor was incubated under similar conditions in the absence of light. BDP-H_2S **1** was found to be stable in pH 7.4 buffer during 2.5 h incubation in the dark as determined by HPLC analysis (see SI, Figure S4). Together, these data confirm the ability of **1** to generate H_2S only when exposed to visible light of 470 nm.

Compound **8** was next synthesized (see Figure 2d, Scheme S1, SI) and was similarly irradiated with 470 nm light in methanol. The resultant reaction mixture was incubated in pH 7.4 buffer and was analyzed for H_2S production by a methylene

DOI: 10.1021/acs.orglett.7b02259
Org. Lett. 2017, 19, 4822−4825

blue assay. As expected, no evidence for the formation of H_2S under these conditions was found (see SI, Figure S7).

Much like the other biological gases nitric oxide (NO),[24−30] carbon monoxide (CO),[31] and sulfur dioxide (SO_2),[32−37] both chemical and biological tools to generate and detect H_2S are necessary. The ability to effectively localize H_2S presents numerous opportunities to study the biology of this gas as well as progress toward site-directed delivery of H_2S for therapeutic purposes.[38−41] Again, BDP-H_2S that we report herein has distinct advantages over the existing class of UV-activated H_2S donors. Although blue light can cause moderate oxidative stress in cells,[10] the short irradiation times and low intensity of light required for H_2S release do not compromise cell viability (Figure 4). The formation of a quinone-methide intermediate may be a limitation for therapeutic use of this compound. However, to our knowledge, this is the first example of a visible light activated H_2S donor, and it is anticipated that this tool will lay the platform for delivery of this gas under ambient conditions.

■ ASSOCIATED CONTENT

Supporting Information

The Supporting Information is available free of charge on the ACS Publications website at DOI: 10.1021/acs.orglett.7b02259.

Compound characterization data, spectra, and assay protocols (PDF)

■ AUTHOR INFORMATION

Corresponding Author

*E-mail: harinath@iiserpune.ac.in.

ORCID

Harinath Chakrapani: 0000-0002-7267-0906

Notes

The authors declare no competing financial interest.

■ ACKNOWLEDGMENTS

The authors thank the Department of Science and Technology (DST, Grant No. EMR/2015/000668) and Council for Scientific and Industrial Research (CSIR) for financial support.

■ REFERENCES

(1) Szabo, C. *Nat. Rev. Drug Discovery* **2007**, *6*, 917.
(2) Li, L.; Rose, P.; Moore, P. K. *Annu. Rev. Pharmacol. Toxicol.* **2011**, *51*, 169.
(3) Shukla, P.; Khodade, V. S.; SharathChandra, M.; Chauhan, P.; Mishra, S.; Siddaramappa, S.; Pradeep, B. E.; Singh, A.; Chakrapani, H. *Chem. Sci.* **2017**, *8*, 4967.
(4) Zhao, Y.; Biggs, T. D.; Xian, M. *Chem. Commun.* **2014**, *50*, 11788.
(5) Wallace, J. L.; Wang, R. *Nat. Rev. Drug Discovery* **2015**, *14*, 329.
(6) Devarie-Baez, N. O.; Bagdon, P. E.; Peng, B.; Zhao, Y.; Park, C.-M.; Xian, M. *Org. Lett.* **2013**, *15*, 2786.
(7) Fukushima, N.; Ieda, N.; Kawaguchi, M.; Sasakura, K.; Nagano, T.; Hanaoka, K.; Miyata, N.; Nakagawa, H. *Bioorg. Med. Chem. Lett.* **2015**, *25*, 175.
(8) Fukushima, N.; Ieda, N.; Sasakura, K.; Nagano, T.; Hanaoka, K.; Suzuki, T.; Miyata, N.; Nakagawa, H. *Chem. Commun.* **2014**, *50*, 587.
(9) Xiao, Z.; Bonnard, T.; Shakouri-Motlagh, A.; Wylie, R.; Collins, J.; Heath, D.; Hagemeyer, C.; Connal, L. *Chem. - Eur. J.* **2017**, *23*, 11294.
(10) Nakashima, Y.; Ohta, S.; Wolf, A. M. *Free Radical Biol. Med.* **2017**, *108*, 300.
(11) Ulrich, G.; Ziessel, R.; Harriman, A. *Angew. Chem., Int. Ed.* **2008**, *47*, 1184.
(12) Umeda, N.; Takahashi, H.; Kamiya, M.; Ueno, T.; Komatsu, T.; Terai, T.; Hanaoka, K.; Nagano, T.; Urano, Y. *ACS Chem. Biol.* **2014**, *9*, 2242.
(13) Chauhan, P.; Bora, P.; Ravikumar, G.; Jos, S.; Chakrapani, H. *Org. Lett.* **2017**, *19*, 62.
(14) Powell, C. R.; Foster, J. C.; Okyere, B.; Theus, M. H.; Matson, J. B. *J. Am. Chem. Soc.* **2016**, *138*, 13477.
(15) Yang, G.; Zhao, K.; Ju, Y.; Mani, S.; Cao, Q.; Puukila, S.; Khaper, N.; Wu, L.; Wang, R. *Antioxid. Redox Signaling* **2013**, *18*, 1906.
(16) Steiger, A. K.; Pardue, S.; Kevil, C. G.; Pluth, M. D. *J. Am. Chem. Soc.* **2016**, *138*, 7256.
(17) Zhao, Y.; Pluth, M. D. *Angew. Chem., Int. Ed.* **2016**, *55*, 14638.
(18) Steiger, A. K.; Zhao, Y.; Pluth, M. D. *Antioxid. Redox Signaling* **2017**, https://doi.org/10.1089/ars.2017.7119.
(19) Tanc, M.; Carta, F.; Scozzafava, A.; Supuran, C. T. *ACS Med. Chem. Lett.* **2015**, *6*, 292.
(20) Zhao, Y.; Bolton, S. G.; Pluth, M. D. *Org. Lett.* **2017**, *19*, 2278.
(21) Patil, N. G.; Basutkar, N. B.; Ambade, A. V. *Chem. Commun.* **2015**, *51*, 17708.
(22) Sunahara, H.; Urano, Y.; Kojima, H.; Nagano, T. *J. Am. Chem. Soc.* **2007**, *129*, 5597.
(23) Miura, T.; Urano, Y.; Tanaka, K.; Nagano, T.; Ohkubo, K.; Fukuzumi, S. *J. Am. Chem. Soc.* **2003**, *125*, 8666.
(24) Maciag, A. E.; Saavedra, J. E.; Chakrapani, H. *Anti-Cancer Agents Med. Chem.* **2009**, *9*, 798.
(25) Chakrapani, H.; Maciag, A. E.; Citro, M. L.; Keefer, L. K.; Saavedra, J. E. *Org. Lett.* **2008**, *10*, 5155.
(26) Chakrapani, H.; Showalter, B. M.; Kong, L.; Keefer, L. K.; Saavedra, J. E. *Org. Lett.* **2007**, *9*, 3409.
(27) Dharmaraja, A. T.; Ravikumar, G.; Chakrapani, H. *Org. Lett.* **2014**, *16*, 2610.
(28) Sharma, K.; Iyer, A.; Sengupta, K.; Chakrapani, H. *Org. Lett.* **2013**, *15*, 2636.
(29) Keefer, L. K. *ACS Chem. Biol.* **2011**, *6*, 1147.
(30) Khodade, V. S.; Kulkarni, A.; Gupta, A. S.; Sengupta, K.; Chakrapani, H. *Org. Lett.* **2016**, *18*, 1274.
(31) Wu, L.; Wang, R. *Pharmacol. Rev.* **2005**, *57*, 585.
(32) Malwal, S. R.; Chakrapani, H. *Org. Biomol. Chem.* **2015**, *13*, 2399.
(33) Malwal, S. R.; Gudem, M.; Hazra, A.; Chakrapani, H. *Org. Lett.* **2013**, *15*, 1116.
(34) Malwal, S. R.; Sriram, D.; Yogeeswari, P.; Konkimalla, V. B.; Chakrapani, H. *J. Med. Chem.* **2012**, *55*, 553.
(35) Malwal, S. R.; Sriram, D.; Yogeeswari, P.; Chakrapani, H. *Bioorg. Med. Chem. Lett.* **2012**, *22*, 3603.
(36) Day, J. J.; Yang, Z.; Chen, W.; Pacheco, A.; Xian, M. *ACS Chem. Biol.* **2016**, *11*, 1647.
(37) Wang, W.; Ji, X.; Du, Z.; Wang, B. *Chem. Commun.* **2017**, *53*, 1370.
(38) Zhao, Y.; Kang, J.; Park, C.-M.; Bagdon, P. E.; Peng, B.; Xian, M. *Org. Lett.* **2014**, *16*, 4536.
(39) Kang, J.; Li, Z.; Organ, C. L.; Park, C.-M.; Yang, C.-t.; Pacheco, A.; Wang, D.; Lefer, D. J.; Xian, M. *J. Am. Chem. Soc.* **2016**, *138*, 6336.
(40) Zhao, Y.; Wang, H.; Xian, M. *J. Am. Chem. Soc.* **2011**, *133*, 15.
(41) Zheng, Y.; Yu, B.; Ji, K.; Pan, Z.; Chittavong, V.; Wang, B. *Angew. Chem., Int. Ed.* **2016**, *55*, 4514.

DOI: 10.1021/acs.orglett.7b02259
Org. Lett. 2017, 19, 4822−4825